INFORMATION TO USERS

This manuscript has been reproduced from the microfilm master. UMI films the text directly from the original or copy submitted. Thus, some thesis and dissertation copies are in typewriter face, while others may be from any type of computer printer.

The quality of this reproduction is dependent upon the quality of the copy submitted. Broken or indistinct print, colored or poor quality illustrations and photographs, print bleedthrough, substandard margins, and improper alignment can adversely affect reproduction.

In the unlikely event that the author did not send UMI a complete manuscript and there are missing pages, these will be noted. Also, if unauthorized copyright material had to be removed, a note will indicate the deletion.

Oversize materials (e.g., maps, drawings, charts) are reproduced by sectioning the original, beginning at the upper left-hand corner and continuing from left to right in equal sections with small overlaps.

Photographs included in the original manuscript have been reproduced xerographically in this copy. Higher quality 6" x 9" black and white photographic prints are available for any photographs or illustrations appearing in this copy for an additional charge. Contact UMI directly to order.

Bell & Howell Information and Learning
300 North Zeeb Road, Ann Arbor, MI 48106-1346 USA
800-521-0600

NOTE TO USERS

The diskette is not included in this original manuscript. It is available for consultation at the authors graduate school library.

Page(s) not included in the original manuscript are unavailable from the author or university. The manuscript was microfilmed as received.

222

This reproduction is the best copy available.

UMI

MECHANICAL PROPERTIES OF FIBER REINFORCED CONCRETE WITH ACM APPLICATIONS

by

Mehdi Zanganeh

A thesis submitted in conformity with the requirements
for the degree of Master of Applied Science
Graduate Department of Civil Engineering
University of Toronto

Abstract

This thesis presents an experimental study of the mechanical response of various types of fiber reinforced concrete, tested under triaxial compression and bending. The objective was to characterize the constitutive properties of these materials, with respect to fiber type and content, load path, condition at testing, and size. A total of 256 tests were performed, on specimens made of concrete with the following fiber types and contents (volumetric ratio): steel micro-fibers 1% and 2%, mix of steel micro-fibers and steel fibers 1% and 2%, polypropylene fibers 1.5% and 4%, and mix of steel micro-fibers and polypropylene fibers 2.5% and 5%.

Triaxial stresses were applied either by hydraulic pressure, or by means of passive confinement, which was provided by means of carbon fiber wraps. The results were used to quantify the influences induced by the various fiber components, and provide insight on the effectiveness of confinement provided by carbon fiber wraps.

Acknowledgments

The author wishes to thank Professor S.J. Pantazopoulou for her support and guidance over the extended period of accomplishing this work. The contribution of Professor R.H. Mills, particularly at the beginning of research, is greatly appreciated.

The author would also like to thank the personnel of The Structural Lab and Machine Shop, especially Mr. John Mc Donald, for their contributions to the development and success of this experimental program.

The financial support provided by ISIS Canada and NSERC for this study is greatly appreciated.

Finally, the author would like to thank his wife Julie for her support and encouragement in completing the thesis.

Table of Contents

List of Tables

List of Figures

Notation

b	Breadth of the prismatic specimens (mm)
D	Deflection in the bending test (mm)
E	Elasticity Modulus; average of E_{ave} of all identical specimens (MPa)
E_{ave}	Average of E_{20} and E_{30} (MPa)
E_{20}	The slope of a line passing through 10% and 20% of the peak stress on the ascending branch of stress-strain curve (MPa)
E_{30}	The slope of a line passing through 10% and 30% of the peak stress on the ascending branch of stress-strain curve (MPa)
f_c'	Compressive strength (MPa)
f_{cc}'	Average compressive strength of all identical specimens (MPa)
f_c	Axial stress at the last point of stress-strain curve (MPa)
h	Depth of the prismatic specimens (mm)
R	Modulus of Rupture; maximum tensile stress (MPa)
P	Total load in the bending test (kN)
P_c	The strength for a unit length of carbon fiber sheet
S_{50}	The slope of a line passing through the peak stress and 50% of it on the descending branch of stress-strain curve (MPa)
S_{85}	The slope of a line passing through the peak stress and 85% of it on the descending branch of stress-strain curve (MPa)
S'	The slope of a line passing through the peak stress and the last point of the descending branch of stress-strain curve (MPa)
VR	Void Ratio (%)
ε_1	Axial strain; in loading direction ($\mu\varepsilon$)
$\varepsilon_{1\,min}$	Axial strain corresponding to $\varepsilon_{v\,min}$ ($\mu\varepsilon$)

ε_3	Circumferential strain; perpendicular to loading direction (με)
$\varepsilon_{3\,max}$	Maximum value of ε_3; corresponding to the last point of stress-strain curve (με)
ε_{10}	Axial strain at 10% of the peak load on the ascending branch of stress-strain curve (με)
ε_{20}	Axial strain at 20% of the peak load on the ascending branch of stress-strain curve (με)
ε_{30}	Axial strain at 30% of the peak load on the ascending branch of stress-strain curve (με)
ε_{50}	Axial strain at 50% of the peak load on the descending branch of stress-strain curve (με)
ε_{85}	Axial strain at 85% of the peak load on the descending branch of stress-strain curve (με)
ε_c	Axial strain corresponding to the peak stress on stress-strain curve (με)
ε_{cc}	Axial strain at the peak; average of ε_c of all identical specimens (με)
ε_R	Tensile strain corresponding to R (με)
ε^*	Axial strain corresponding to zero volumetric strain (με)
ε_{min}	Axial strain corresponding to the last point of stress-strain curve (με)
ε_{v10}	Volumetric strain at 10% of the peak stress (on loading part) (με)
ε_{v20}	Volumetric strain at 20% of the peak stress (on loading part) (με)
ε_{v30}	Volumetric strain at 30% of the peak stress (on loading part) (με)
$\varepsilon_{v\,min}$	The minimum value of volumetric strain (με)
ν	Poisson's Ratio; average of ν_{ave} of all identical specimens
ν_{20}	Poisson's ratio based on strains at 10% and 20% of the peak load
ν_{30}	Poisson's ratio based on strains at 10% and 30% of the peak load
ν_{ave}	Average of ν_{20} and ν_{30}
ν	Average of ν_{ave} of all identical specimens

σ_1	Axial stress; in loading direction (MPa)
σ_3	Circumferential stress; perpendicular to loading direction (MPa)
σ'_3	Effective lateral stress (MPa)

1. Introduction

1.1. Background

Concrete can compete with other structural materials in many aspects, such as: cost, formability, availability, and compressive strength. However, its value in civil engineering applications is diminished by certain mechanical characteristics such as low tensile strength and brittleness. Both of these drawbacks may be alleviated through the use of fiber reinforcement (Ramakrishnan, 1988).

The use of fibers in brittle materials has a history of at least 3500 years when sun baked bricks reinforced with straw were used to build high structures near Baghdad (Hannant, 1995). In cement products, asbestos fibers have been used for the last 100 years, cellulose fibers for at least 50 years, and metal, polypropylene, and glass fibers for the past 30 years (Hannant, 1995). Ramakrishnan (1988) states that the interest in reinforcing Portland cement based materials with randomly distributed fibers was spurred by pioneering research on steel fiber reinforced concrete conducted in the United States in the 1960s.

Fiber Reinforced Concrete (FRC) is produced by adding fibers to the fresh concrete mix. The improvement in cement properties with increase in fiber content is subject to practical limitations. Firstly, mixing and compacting become more difficult with increased fiber content (Soroushian and Bayasi, 1991), and the resultant incomplete compaction leads to poor quality fiber concrete. Secondly, the price of fiber is much higher than that of concrete and even low volume addition of fiber substantially increase the cost of fiber concrete (Hannant, 1995).

Although adding fibers to concrete is not a new concept, the use of combinations of different fiber types has not been extensively researched. Each fiber type contributes

certain beneficial functions to the concrete, and it has been suggested that further improvement may be achieved by mixing fiber types (Banthia et al, 1995; Mindess, 1995).

Parallel to the development of fiber concrete, the use of other Fiber Reinforced Plastics (FRP) in civil engineering applications has gained momentum. Development of FRP composites essentially began in the early 1940's, for military and aerospace applications (Ballinger, 1992). These materials, which are also known as Advanced Composite Materials (ACM), have been mainly used in repair of concrete structures damaged by earthquakes. Recently, many researchers have worked on the application of FRP to strengthen concrete structural members (Sheikh et al, 1996; Picher and Labossière, 1995; Slattery, 1992).

Basically, fibers contribute to the tensile strength and deformability of concrete, whereas concrete itself provides the compressive strength. This mechanism can be provided by either internally (FRC), or externally (FRP) placement of fibers. In the literature, the first one is known as fiber concrete and the second one is known as composite concrete.

1.2. Fiber Reinforced Concrete (FRC)

In this method fibers are added to the fresh concrete mix. A variety of fibers with different material, shape, length, and thickness have been used in fiber concrete. The fibers may be either continuous and aligned in the desired direction, or discrete and randomly scattered. Most fibers do not absorb water, but water is needed to wet their surface areas. This may cause some difficulties in the workability of the mix. Besides, during mixing, the fibers may get together and form fiber balls (ACI Committee 544, 1993; Soroushian and Bayasi, 1991). Addition of fibers may require special mixing procedure for that fiber type.

The tensile strength that the fibers contribute to concrete produces increase in ductility for the concrete member. Besides, fibers provide a crack-arrest mechanism which

resists the progressive connection of micro cracks and formation of large cracks (Kuilman, 1988). This results in raising the flexural strength of concrete and improving its resistance to spalling, abrasion, heat, cavitation, and impact. Hannant (1995) mentioned that a low fiber volume generally does not increase the tensile or bending strength of concrete appreciably, but the main benefit stems from the resulting increase in toughness, impact resistance, abrasion resistance, and control of crack width. The most commonly used fiber types in concrete mixes are steel fibers, steel micro-fibers, and polypropylene fibers.

1.2.1. Steel Fibers in Concrete

Steel fibers have been studied extensively by many researchers. A number of studies have been done on the improvement of their bonding and anchorage to concrete matrix and on the mixing process. To overcome the problem of formation of fiber balls in the fresh-mix, a method involving the use of a water-soluble adhesive to glue a number of fibers together has been developed (Soroushian and Bayasi, 1991). Ramakrishnan (1988) mentioned that this glue also increases the bond and anchorage parameters of the fibers, however, there is no experimental indication for this notion. Steel fibers have modulus of elasticity varying from 276 to 2413 Mpa (Soroushian and Bayasi, 1991). A variety of commercially available fibers are illustrated in Figure 1-1.

1.2.2 Steel Micro Fibers in Concrete

Micro fibers have been developed in recent years to provide both closer spacing between fibers and a high volume fraction that can be incorporated in the matrix (Mindess, 1995). The length of these fibers is within a millimeter, and their diameter is within micrometer. Therefore, they produce a very large relative surface area which not only requires a considerable amount of water for wetting, but also makes the fibers susceptible to binding impurities. Addition of theses fibers, at high volume fractions, increases strength and stiffness of concrete (Banthia et al, 1995).

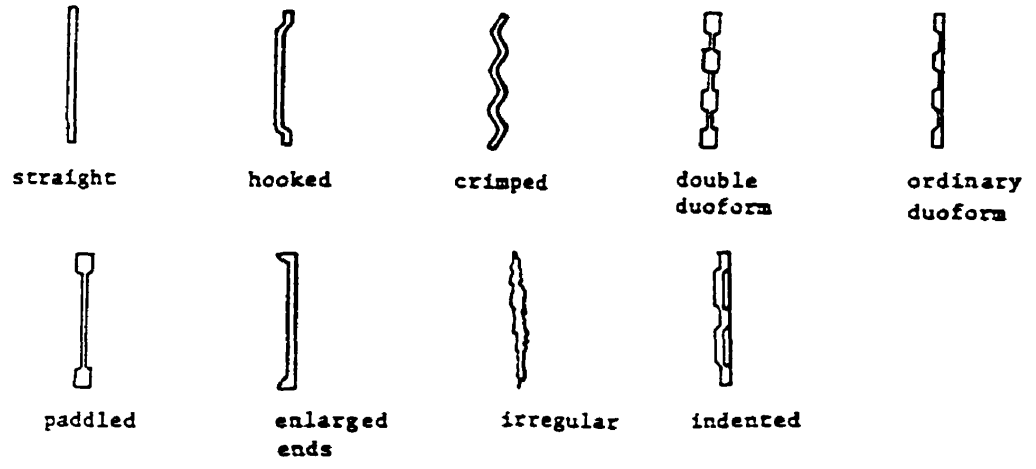

(a) Steel fiber shapes

(b) Steel fiber cross sections

(c) Fibers glued together into a bundle

Figure 1-1: Various available shapes of steel fibers
(taken from Soroushian and Bayasi, 1991)

1.2.3 Polypropylene Fibers in Concrete

A number of studies have been published on polypropylene fibers. This product is available not only in different shapes, but also with different mechanical properties. The fibers are light weight and have low modulus of elasticity. They are inert in alkaline and corrosive environments, and also improve such properties of fresh concrete as bleeding and plastic shrinkage cracking (Hannant, 1995; Bayasi and Zeng, 1993). Therefore, they have been used widely in construction of industrial slabs. Figure 1-2 illustrates a few types of polypropylene fibers.

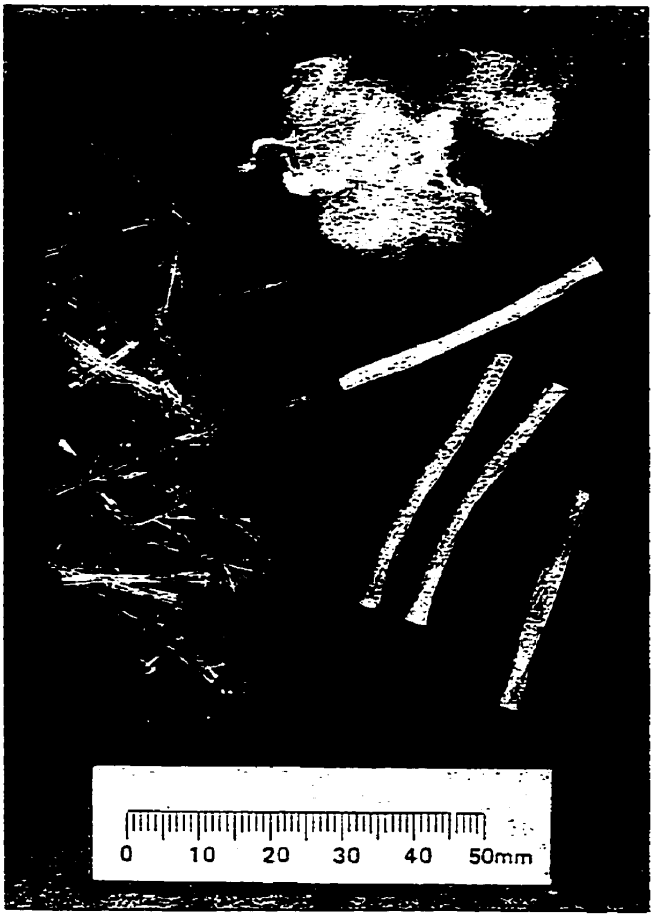

Figure 1-2: A few types of polypropylene fibers
(taken from Hannant, 1995)

1.3. Composite Concrete (FRP)

In this method FR sheets are attached to the surface of hardened concrete at the tensile zone. The fibers improve the tensile strength of concrete, and increase the overall capacity of the structural member. In case of cylinders (columns) under concentric compression, the tensile stresses develop on the lateral surface perpendicular to the loading direction. Therefore, the fiber sheets are wrapped around the cylinders (fibers in tensile direction) to provide hoop tensile stresses, which results in passive confinement action for concrete.

The fiber plastics commonly available are carbon, glass, and aramid. Sheets are manufactured with the main fibers oriented in the longitudinal direction. The sheet is

soaked in a resin when it is installed on the concrete member. This resin not only acts as an adhesive, but also makes the fibers work together and uniformly. The combination of the fibers and the resin is referred to as Advanced Composite Material (ACM).

Since ACM in composite concrete works in tension, the continuity of fibers is of great importance. Hence, a proper overlapping, based on the required full stress developing length, is essential at the seams. The required overlapping length depends on the type and thickness of sheet (Forca catalog, Appendix B). Furthermore, it has been suggested by Karbhari and Ecker (1995) and Picher and Labossière (1995) that it is possible to control the sequence of failure, so as to maximize the amount of energy absorption, by installing the sheets at different angles with respect to the tensile direction.

Part of this study is concerned with the use of carbon fiber sheets for providing passive confinement. Carbon fibers have a high tensile strength and modulus of elasticity, and their behavior is mainly elastic with a brittle failure (Forca catalog, Appendix B). The fibers are held in the sheet by an attached string net. Because of the high strength, the sheet is very thin and it is supported by a paper backing which is peeled off at installation. Figure 1-3 illustrates the details of the sheet. This product is quite expensive, however, it is expected that by increase in consumption the production cost will decrease (Hannant, 1995; Collins, 1995).

1.4. Objectives

In this research, an extensive experimental study has been carried out to evaluate the effects of certain design variables on the mechanical properties of various Fiber Reinforced Concretes (FRCs) with and without layers of Fiber Reinforced Plastics (FRP). A high strength concrete mix (f'_c more than 50 MPa) was intended to be used as the concrete matrix for all the batches. Specimens of this plain concrete, were also tested in order to provide the reference in determining the benefits resulting from the addition of fibers.

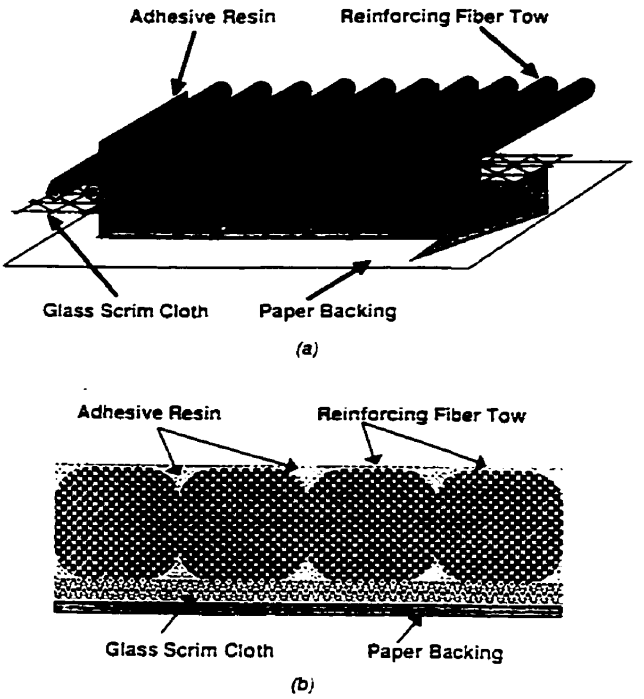

(a) Schematic of the tow sheet system. (b) Cross-section of the tow sheet

Figure 1-3; Common carbon fiber sheet
(taken from Howie and Kaebhari, 1995)

Axial and circumferential deformations of the prepared specimens were measured under different conditions of loading, and stresses and strains were calculated. The mechanical parameters and the degree of internal damage were obtained from the stress-strain relationships. The degree of internal damage, which is determined by volumetric or area strains, is known to be a consistent indication of the residual resistance (Pantazopoulou and Mills, 1995; Pantazopoulou, 1995; Imran and Pantazopoulou, 1995). The primary interests that motivated this research can be classified as follows:

- **Effects of Fiber Type and Content:** Each fiber type has distinct mechanical properties, and hence, very specific effects on the fiber reinforced concrete behavior. The volume ratio of the added fibers controls the intensity of these effects. Therefore,

various volume ratios for some favorable types of fibers were examined, and the benefits were determined by comparison to the response of plain concrete.

- **Effects of Mixing Fiber Types:** The majority of the research studies reported in the literature are concerned with FRC mixes containing a single type of fibers. Mixing different types might combine the benefits which would be obtained from individual fiber types, and could improve further the mechanical properties of FRC. In this study, combinations of different fiber types were examined, but the volumetric ratio of the fiber types (relative to each other) remained constant.

- **Effects of Saturation:** When a wet specimen is loaded, absorbed water in the pores develops considerable amount of pressure due to the contraction of the specimen, thereby weakening the concrete from inside (Imran and Pantazopoulou, 1994; Mills, 1966). The specimens were examined in dry and saturated conditions in order to investigate this phenomenon on fiber concrete.

- **Effects of Size:** The failure mechanism of concrete structural members are influenced by their dimensions and the aggregate size. Hatanaka et al (1994) have mentioned that the size effect on the compressive strength of concrete is not so remarkable as that on the tensile, flexural, and shearing strength. This issue will be discussed later in greater detail. In this study, the mechanical properties of each batch were studied with different size specimens, to quantify this influence.

- **Effects of Active and Passive Confinement:** The effectiveness of confinement in increasing the strength of concrete has been studied in the literature over the years. The original work, which belongs to Richart et al (1928), indicates that there is a linear relationship between strength and lateral pressure. In this study the effects of

confinement on the mechanical properties of FRC have been investigated using two mechanisms: active pressure (provided by encasing the specimen in a special hydraulic chamber), and passive confinement (provided by ACM wraps in the circumferential direction of cylinders).

- **Effects of ACM Wraps:** The concept of using ACM wraps for confinement of concrete structural members is gaining popularity. These materials have been used successfully to provide ductility for earthquake applications, in the past. The effectiveness of ACM wraps in increasing the strength of concrete structures have been studied recently (Erki and Agarwal, 1995; Picher and Labossière, 1995). In this experimental program different numbers of ACM layers have been considered, in order to measure their effective degrees of confinement.

2. Literature Review

This experimental study is concerned with the improvements on the mechanical properties of high strength concrete resulting from the use of fiber reinforcement and fiber reinforced plastic wraps. Both of these cases have been studied extensively and many research articles have been published. A review of the literature is essential to establish the state of art and to reveal the issues of importance to this research.

2.1. Fiber Reinforced Concrete (FRC)

The types of fibers which were mixed with the concrete matrix in this experiment were: steel fibers, steel micro fibers, and polypropylene fibers. A number of articles which are relevant to different aspects of using these fiber types in concrete are reviewed in this section.

2.1.1. Steel Fibers

2.1.1.1. Fresh Concrete

A study on the effects of steel-fiber types on the properties of freshly mixed and hardened concrete was performed by Soroushian and Bayasi (1991). The fiber types studied were straight-round, crimped-round, crimped rectangular, hooked single, and hooked collated. A constant fiber volume fraction of 2% was used for all the mixes. The workability of fresh concrete was characterized by its slump, inverted slump-cone time, and subjective workability which was scaled from 1 for poor to 4 for excellent condition. The study showed that the inclusion of fibers decreased the workability of fresh concrete, particularly for fibers with high aspect ratio, but this effect was generally independent of the fiber type. However, crimped fibers resulted in slightly higher slump value. Besides,

hooked fibers were more effective than straight and crimped ones in enhancing the post-peak energy absorption of concrete under compression, but the effect of fibers on the compression strength was relatively small.

The workability of the fresh mix of steel fiber concrete was also studied by Bayasi and Soroushian (1992). In this study, the investigators used the same fiber types as in the previous paper, but the workability was measured by slump, inverted slump cone and Vebe times, and subjective workability scaled from 0 to 4. The air content was also determined for each mix. In addition to fiber type, the effect of fiber reinforcement index, which is the product of fiber volume fraction and fiber aspect ratio, on workability was assessed. The study showed that the workability of fresh mix differed slightly for various fiber types, and it decreased with increasing value of the fiber reinforcement index at a rate which was compatible with different fiber types. Air content increased with decrease in fiber length. Also, the use of deformed (hooked or crimped) fibers resulted in increasing the air content of the fresh mix. Furthermore, relatively large values of air content were noted in mixes with low workability.

2.1.1.2. Bond to Concrete

A comprehensive experimental study on bond-slip mechanisms of steel fibers in concrete was presented by Naaman and Najm (1991). The parameters studied in this experiment included three types of fibers (straight, deformed, and hooked), three different mortar matrices (low, medium, and high strength), and additives (latex, fly ash, and micro-silica). The fiber volume fraction, fiber diameter, and its embedded length were, also, varied. Special emphasis was placed on obtaining accurate records of the pullout load versus end-slip response, and a number of different responses were obtained. Hooked and deformed fibers behaved differently, but both types showed higher resistance to pullout than smooth fibers. However, the slip at maximum load for hooked and deformed fibers

was up to two orders of magnitude that of a smooth fiber. As a result, the pullout work up to the peak load for hooked and deformed fibers could be as high as one hundred times that of a smooth fiber. On the other hand, an increase in the matrix strength raised the bond of fibers. The addition of latex to the matrix improved the peak load significantly (up to four times), but had no effect on post-peak response. The addition of fly ash resulted in very small improvement of overall response, and the addition of micro-silica did not have any effect on the bond strength. The authors also proposed that the mechanical bond component was not likely to influence the composite first cracking strength.

Interface properties between a straight steel fiber and mortar were investigated by Mandel et al (1987). Two types of mortar were used: with and without polymer. They found that addition of polymer to mortar significantly increased the steel fiber bond; with 10% polymer (by weight of cement) doubling the average interface bond strength. The authors also developed a procedure to determine the coefficient of adhesion, the energy release rate per unit area of crack surface at the crack front required for unstable growth of a crack along the fiber-matrix interface. This procedure used the results of a fiber pullout test in a finite element analysis model.

2.1.1.3. Distribution of Fibers

Measurements on the distribution and orientation of fibers in steel fiber concrete were made by Soroushian and Lee (1990). They derived theoretical expressions for 2-D and 3-D fiber orientation, and compared them to the actual values. Counting the number of fibers per unit area was performed on the fractured cross section of steel fiber reinforced concrete beams which were tested in flexure, at 28 days of age. The dimensions of the beams were 152×152×457 mm, and they contained fly ash and super plasticizer. The W/C ratio was equal to 0.4. The fiber volume fractions were 0.5, 1.0, 1.5, and 2.0 percent, and the fibers were 51 mm, straight and hooked types. The vibration

was done externally. The experiment showed that the type of the steel fiber and the location in cross section, with respect to the casting direction, did not have any significant effect on the number of fibers per unit area. Also, vibration of steel fiber reinforced concrete tended to orient the fibers towards horizontal planes. The comparison indicated that the number of fibers per unit cross section area after vibration was between the theoretical values obtained from 3-D and 2-D orientation formulas, due to boundary effects.

2.1.1.4. Uniaxial Compression

Hsu and Hsu (1994) performed a series of uniaxial compression tests on high strength steel-fiber concrete with fiber volume fractions of 0, 0.5, 0.75, and 1 percent. The steel fibers were of collated hooked type. They observed that increasing the fiber volume fraction caused an increase in the slope of the descending part of the stress-strain curve, but the ascending part changed slightly. Also, the addition of steel fibers increased the strain corresponding to the peak stress, but did not produce any significant changes in the compressive strength. The authors proposed that the reason may be attributed to the reduced workability caused by adding fibers, or to the effect of aggregates on orienting the fibers. It was shown that the toughness index increased by increasing the fiber content, and the failure mode changed from cracks parallel to the loading for plain concrete cylinders to irregular crack pattern near the middle zone for fiber concrete cylinders. The parallel study on the cylindrical specimens with tie confinement showed that compressive strength and its corresponding strain increased with decreasing tie spacing, and also lateral reinforcement became effective with the lateral expansion of concrete and after considerable axial deformation had taken place. Finally, analytical equations were proposed for a complete stress-strain curve of a concrete with different fiber contents, expressed in terms of the maximum compressive strength and fiber volume fraction:

$$\eta = \frac{n\beta x}{n\beta - 1 + x^{n\beta}} \qquad \text{for } 0 \le x < x_d \tag{2-1}$$

where $\eta = \frac{f_c}{f'_c}$ $\qquad x = \frac{\varepsilon}{\varepsilon_o}$

and $\beta = \frac{1}{1 - \frac{f'_c}{\varepsilon_o E_{it}}}$ $\qquad$ for $\beta \ge 1.0$

In the above equations, β and n are the material parameters, η is the normalized stress, x is normalized strain, f'_c is the peak stress of concrete, f_c is the stress in general, ε_o is the strain corresponding to the peak stress, ε is the strain in general, E_{it} is the slope at the origin, and x_d is the strain at $0.6f'_c$ on the descending branch of stress-strain curve. Equation 2-1 was modified and corrected for the unconfined high strength concrete:

$$\eta = \eta_d e^{[-k_d(x-x_d)^a]} \quad \text{for } x_d \le x \tag{2-2}$$

where, for high strength fiber reinforced concrete, η_d was equal to 0.6 which corresponds to $0.6f'_c$ on the descending branch, $k_d = 0.7$, and $a = 0.8$.

The descending part of the compressive stress-strain curve of high-strength concrete is difficult to attain, and proper controlling of the loading machine is essential. Taerwe (1992) improved the previous testing technique and obtained the descending branch of plain concrete with typical characteristics consisting of a fairly steep slope followed by a general snap-back (a non-desired behavior). The system which was used is shown in Figure 2-1, where the axial displacement was controlled by the lateral deformation. In Figure 2-2, HS-11 is the behavior of a High Strength Concrete (HSC), NS-3 is the response of Normal Strength Concrete (NSC), MS-3 was obtained from a Medium Strength Concrete (MSC), and SF-14 is the behavior of FRC (0.76% steel fibers). The addition of steel fibers improved the descending branch of stress-strain curve. The steel fibers that used in this experiment were hooked, drawn-wire type with two

different dimensions (60 mm long with 0.80 mm diameter, and 50 mm long with 0.5 mm diameter), and their volume fractions were 0.51 and 0.76 percent. He showed that addition of rather small quantities of steel fibers to high strength concrete resulted in a strain-softening behavior, similar to that of normal strength concrete. Also, due to fiber addition to high strength concrete the toughness increased significantly, and the toughness index more than doubled and approached that of normal strength concrete. Furthermore, it was illustrated that the fracture surface no longer predominantly ran through the aggregates, as opposed to explosively failed specimens.

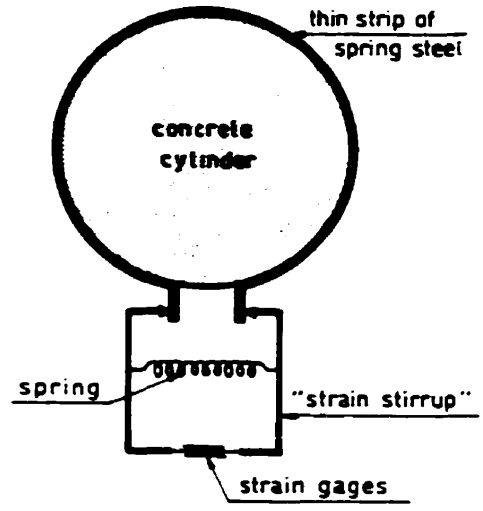

Figure 2-1: The system used by Taerwe (1992) for measuring circumferential strain

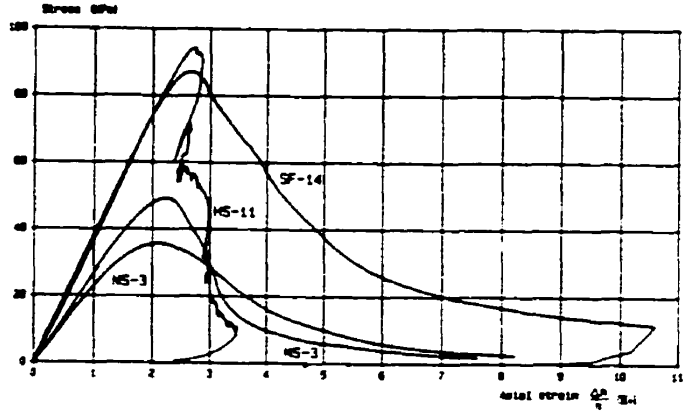

Figure 2-2; The stress-strain curves for different concretes (Taerwe, 1992)
HS is high strength, MS is medium strength, NS is normal strength, and SF is steel fiber concrete

2.1.1.5. Analytical Models

Lee et al (1987) developed an analytical model for the tensile behavior of steel fiber concrete (SFC). The model predicted the elastic and post-cracking behavior of SFC by considering the tensile-extension behavior of an uncracked and pre-cracked SFC specimen. The specimens, which were made with 0.5, 1.0, and 1.5 percent volume fractions of hooked and straight steel fibers with 30 and 50 mm length, confirmed good predictions of the model. The study showed that the fiber-slip values, obtained for a mix with particular type and length of fibers, could be applied to all similar mixes having fiber volume fractions within 0 to 1.5 percent, which is the common range of fiber fraction in the industry. An idealized elastic perfectly plastic stress strain curve was also suggested.

In a French research paper, Rossi (1994) classifies the effects of adding steel fibers to concrete in two scales. At the material scale fibers work in knitting together the

microcracks and delaying crack localization, where as at the scale of structure fibers effectively transfer the forces across the macrocracks created. He suggested the study of mechanical behavior of Steel Fiber Reinforced Concrete (SFRC) must clearly distinguish the influence of the fibers on these two scales. The author also argued that the microstructure of SFRC depends not only on the type of fiber used, but also on the type of structure, and on the technology of placement of the material chosen. Hence, any study of SFC composition must be conducted according to the intended application. To develop simple design rules for SFRC structures, the author illustrated an introductory computation attempt for substituting the stirrups of a concrete reinforced beam with metal fibers. It was concluded that the development of powerful numerical models that reflect the cracking of this material on a fine scale is essential for constructing design rules. In addition, the paper discussed increase in air content due to addition of fibers in concrete. This mechanism is shown in Figure 2-3, where circles represent sand, gravel and cement powder, whereas straight line indicates a fiber. The fiber walls disturb the optimal packing which can be obtained for plain concrete; so called local wall effect.

2.1.2.6. Bending

An extensive study on bending of steel fiber reinforced concrete prisms was performed by de Loock (1988) under four-point loading. Six mixes with the same concrete matrix but different fiber types and content were used. The steel fibers were hooked-collated galvanized with two aspect ratios, and the contents were 30, 55, and 80 kg/m^3. The experiment showed that the cracks developed in the section of the beams between the two middle loads. For low fiber contents, there was one major crack, sometimes splitting up into minor related cracks forming a crack band. In the beams with high fiber content, there were two distinct cracks within the central section, one of them staying quite small. No direct relation was found between the cracking pattern and the load-deflection graph.

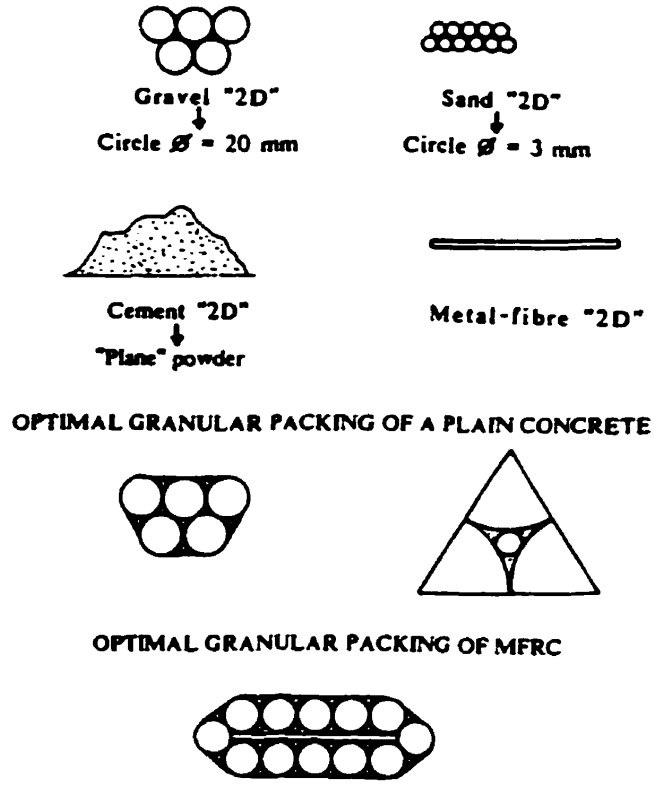

Figure 2-3; Schematic diagram of 2D packing of concrete with and without fibers
(taken from Rossi, 1994)

2.1.1.7. Corrosion of Fibers

In an attempt to protect steel fibers from corrosion, and in order to improve their adherence to cement paste, Sugama et al (1992) deposited a zinc phosphate (ZnPh) conversion coating at 150°C on the surface of the crimped-round steel fibers. They found that at the interfacial contact zones, between the cement paste and ZnPh, alkali-induced dissolution caused the dissociation of abundant PO_4^{3-} ions from ZnPh. These ions interacted with Ca^{2+} ions from the paste and led to the formation of hydroxyapatite and brushite in the vicinity of the dissolved ZnPh surface. The intermediate calcium phosphate compounds played important roles in improving the cement-fiber interfacial bonds, and

repairing back the damage of the ZnPh surface dissolved by alkali. Their experiment showed that these processes protected the steel fibers from corrosion.

Kosa and Naaman (1990) investigated the accelerated corrosion of steel fiber reinforced concrete. The effects of corrosion on steel fiber mortar, and the effects of using pre-corroded fibers in mortar were studied on 1200 specimens. Hooked steel fibers with 2% volume fraction were used throughout. Combinations of different conditions for the specimens (carbonated, cracked, and highly permeable), testing temperature, test type (tension, compression, bending), and period of exposure were applied, with a total of 35 variables. In these series of tests, no crack was detected on the specimens subjected to corrosion, but substantial changes of coloring was observed at their surface due to rust products. Also, a small change in modulus of elasticity was seen after exposure. The corrosion reduced the fiber diameter and changed the failure mode from typical fiber pullout to fiber breakage before pullout. Severe corrosion could lead to noticeable reduction in the peak strength in tension and bending, and significant reduction in toughness. The group of specimens with pre-corroded fibers produced similar results as the first group. Hence, the mechanical properties of steel fiber concrete exhibited great dependence on the value of the reduction in the fiber diameter, caused by corrosion. Furthermore, a simplified analytical model was developed to predict the tensile stress-strain response of steel fiber concrete influenced by corrosion:

$$\frac{\sigma}{\sigma_{max}} = \left[1 - \frac{x}{kL_f / 4}\right]^2 \qquad (2\text{-}3)$$

where σ is the stress at the crack, σ_{max} is peak-stress, x is crack width, L_f is length of the fiber, and k is a modifier.

2.1.1.8. Fatigue

Fatigue behavior of steel fiber reinforced concrete under biaxial compression was examined by Yin and Hsu (1995). They used 1% volume fraction of 25 mm long, straight steel fibers. The deformations in all three principal directions were measured, and Stress level versus Number of cycles (S-N) curves were obtained for 0 (uniaxial), 0.2, 0.5, and 1.0 stress ratios. The curves for fiber concrete in biaxial compression were similar to those of plain concrete. Furthermore, it was concluded that the fatigue strength of fiber concrete in biaxial compression was greater than that in uniaxial compression. Addition of fibers did not increase the fatigue endurance limit of concrete, but increased its strength for fatigue loads in the low-cycle region, and significantly increased the ductility of the specimen. The fatigue failure mode changed from splitting for plain concrete to faulting (crack redistribution) for fiber concrete. Lastly, fatigue strength envelopes for biaxial compression were produced for design of fiber reinforced concrete structure (Figure 2-4).

2.1.1.9. Cyclic Load

Naaman and Otter (1988) investigated the behavior of steel fiber reinforced concrete under cyclic compressive loading. Three different volume fractions were used. The fibers were either straight with three different aspect ratios, or hooked. The applied loading was either cyclic with three different regimes, or monotonic. The envelope curves of monotonic loading showed that hey govern the cyclic responses. Besides, it was found that the toughness under monotonic loading provides a lower bound to the amount of energy absorption that can be achieved under a general cyclic load history, and the behavior of fiber reinforced concrete under cyclic load, when normalized by its monotonic behavior, is very similar to that of plain concrete. Hence, it was concluded that the existing models for the cyclic loading of plain concrete can be applied to fiber reinforced concrete.

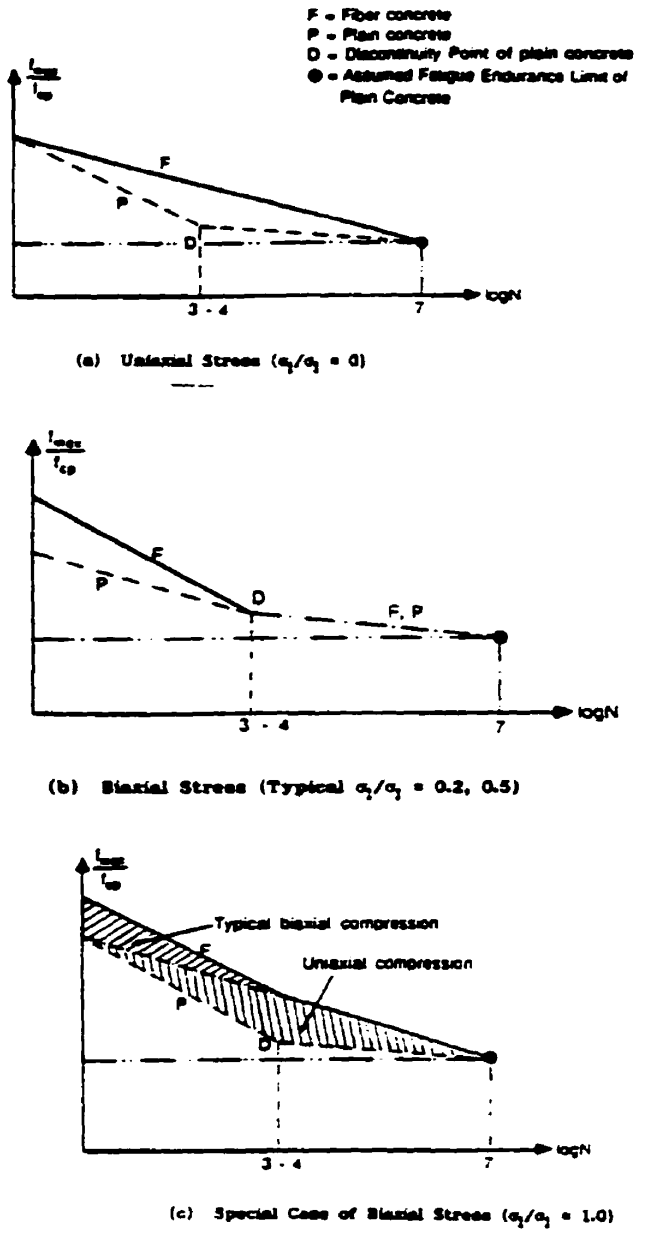

Figure 2-4: Idealized fatigue curves for plain (P) and fiber concrete (F) produced by Yin and Hsu (1995)

2.1.2. Micro Fibers

Micro fibers have been developed in recent years (Mindess, 1995) to increase the number of fibers in the mix, and reduce the fiber-fiber spacing (Banthia et al, 1995). The dimensions of these fibers are very small (length within millimeters, and thickness within micrometers). The fine size of the fibers allows large volume fractions to be mixed easily and dispersed uniformly in the matrix (Banthia et al, 1995). These fibers are made of various materials, hence, they have different mechanical properties.

The uniaxial tensile behaviors of cement paste and mortar containing high volume fractions of micro fibers (1% to 3%) were investigated by Banthia et al (1995). Carbon, steel and polypropylene micro fibers were used individually (mono) and in combinations (hybrid). The study showed that significant improvements on the mechanical properties of cement matrices were achieved by the addition of these fibers at high quantities. Steel fibers provided better strengthening and stiffness, carbon fibers contributed better ductility, and polypropylene fibers implemented better toughening at large crack openings. The tests on hybrid composites showed that different fiber types acted as additive phases, i.e. they maintained their individual reinforcing capabilities. The specimens also were subjected to impact tensile loads, and exhibited stronger and tougher responses. These improvements were greater at higher fiber volume fractions.

Banthia and Sheng (1995) studied the flexural response of micro-fiber reinforced cement paste and mortar. Both notched and unnotched specimens were tested by four-point flexure. It should be noted that the test setup provided free rotation for neither of supports, and a yoke was mounted on the beams to eliminate the spurious deformations arising due to support settlements. The fiber types were: 6 mm long carbon fibers, 3 mm long steel fibers, and 6 mm long polypropylene fibers. Steel fiber reinforcement led to an improvement in the strength of matrix, but had less effect on the toughness than carbon

fiber reinforcement. The notched steel reinforced specimens, which were tested for crack propagation, showed less brittleness than unnotched beams.

2.1.3. Polypropylene Fibers

This type of fibers are made of organic materials with complex molecular structure. They are available with different mechanical properties, but generally their modulus of elasticity is low compared to that of steel. These fibers can be found in shapes of individual needles, or fibrilated nets.

2.1.3.1. Fresh and Hardened Mix

The properties of fibrillated polypropylene fiber reinforced concrete were investigated in fresh and hardened states by Bayasi and Zeng (1993). Fiber lengths were 12 and 18 mm, and volume fractions were 0.1, 0.3, and 0.5%. Fresh concrete slump, inverted slump cone time, and air content were measured. The hardened specimens behaviors were assessed by compressive and flexural strength, impact resistance, rapid chloride permeability, and volume percent of permeable voids. In this experiment, fibrillated polypropylene fibers had no detectable effect on the workability and air content of fresh concrete at volumes below 0.3 percent, but adverse effect on workability and increase in air content resulted from the application of fibers at 0.5 percent volume. It was also found that for volumes less than 0.3 percent the 18 mm long fibers were more effective in enhancing the post peak resistance, whereas for 0.5 percent volume the 12 mm long fibers had better effects.

2.1.3.2. Compressive Strength

Compressive strength of polypropylene fiber reinforced concrete was experimented by Tavakoli (1994). The fibers were 70 mm long, and their volume fractions were: 0, 0.5,

1, 1.5, and 2 percent. The results showed that the strength of concrete decreased slightly with increasing the fiber fraction. Higher fiber ratio also had declining effect on the specific gravity of mix. Furthermore, the author found that the tensile strength of FRC increased almost linearly with raising fiber percentage up to a ratio of about 1.5%, and then decreased.

2.1.3.3. Fire Effects

The effect of fire on polypropylene (PP) fiber mortar has been investigated by Raivio and Sarvaranta (1994). The aggregates expand with rising temperature, while the cement paste shrank due to water loss. Hence, thermal incompatibility caused degradation of concrete. In addition, synthetic organic fibers had a tendency to shrink at around 100°C due to entropic heat relaxation. On the other hand, fibers affected the release of moisture from the fiber mortar. Hence, local pressures caused by water vaporization, due to rapid heating from fire, could be reduced by incorporating fibers. The spalling tendency of fiber concrete at the early stage of rapid heat exposure also was related to the extend to which the matrix was able to withstand the vapor pressure of the pore water. The polypropylene fibers melted around 160-170°C. Therefore, this fiber type can no longer contribute tensile strength to the FRC at higher temperatures. Besides, it was observed that the use of fibers increased the air-void in mortar when traditional mixing methods were used. The Back Scattered Electron (BSE) images indicated that porosity was higher around the fibers.

2.2. Concrete Confined by Fiber Wrap

An experimental study was performed at University of Toronto on rehabilitation of concrete columns which were damaged by corrosion process (Sheikh et al, 1996). In this study a fiber sheet made of E-glass and Kevlar fibers was used for wrapping the

specimens. The wrapping was accompanied by a number of repair techniques, to evaluate the most effective procedure. The specimens which were repaired by placing expansive grout between a plastic sheet and concrete, prior to wrapping, produced false results due to strain concentration at the seam of the plastic sheet. The half scale columns which were repaired with fiber reinforced mortar showed that FRP could fully recover the strength of corroded columns. Additionally, ductility of the repaired columns was significantly higher than that of undamaged one. These repair techniques were also applied on small size cylinders (300×150 mm) and their effects on slowing down the corrosion process was studied.

The confinement of concrete by carbon fiber wraps was examined by Slattery and Harmon (1992). The experiment was based on 100×50 mm concrete cylinders with compressive strength ranging from 41 to 103 MPa, and composite reinforcement ratios from 0% to 5%. The compression tests showed that the axial stress-strain curves were bilinear with a yield point somewhat higher than the failure stress of the corresponding un-wrapped specimen. Reinforcement ratio had slight effect on the ascending portion of the curve, but considerably increased the slope of the second portion. Increasing the fiber ratio increased the ultimate stress, but had a minor effect on the yield stress. Also, the transverse strains increased dramatically at some point after the failure stress of the unconfined cylinder, and decreased as the circumferential fiber ratio increased. However, it was not possible to quantify this variation due to difficulties in measuring the strains. Besides, the increase in failure stress was approximately 39 MPa per each percent increase in confinement carbon fiber ratio. The authors suggested that the strength efficiency could be increased with better fabrication. In addition, the effect of cyclic loading was experimented briefly. The results suggested that cyclic loading had little degradation effect on the wrapped cylinders.

2.2.1. Orientation Effects

Karbhari et al (1995) investigated the use of carbon-fiber-reinforced jackets applied to 300×150 mm concrete cylinders through the use of tow-sheet-type fabrics. The primary interest in this study was to investigate the effects of orientation and thickness of the composite wraps on the load carrying efficiency and enhanced ductility of concrete. It was hypothesized that although fibers at the hoop direction would produce the most confinement and strength, the other orientations could potentially increase the ductility and prevent catastrophic failure. Therefore, fiber sheets were installed at combinations of orientations of 0°, ± 45°, and 90°. The overlap on a given layer was about 90° of the circumference of the cylinder. It was observed that the addition of each layer in the hoop direction led to an increase of about 33% in load carrying capacity. The experiment showed that the specimens with the layers aligned only along the shear planes (± 45°) gave the worst results. However, these jackets did not show extensive damage, and rather the damage was seen in mis-orientation of the layers from their original positions. The axial load-deformation curves had a change in slope, a so called "kink point", occurring at about the point where the unconfined concrete exhibits failure. Figure 2-5 shows the findings of this experimental study.

The effect of variation of the angle of carbon fiber wraps on the strength of cylindrical specimens was investigated by Picher and Labossière (1995). The 300×150 mm cylinders were wrapped by a layer of fiber sheet in the hoop direction and two layers in 0°, ± 6°, ± 9°, ± 12°, ± 18°, and ± 24° (in respect to the hoop direction). The obtained stress-strain curves exhibited bilinear shape, the first part indicating the elastic behavior up to a kink-point (Figure 2-6). The location of the kink-point did not vary considerably with increasing the number of wrapping layers, where as the slope of the second part of the curve had increase.

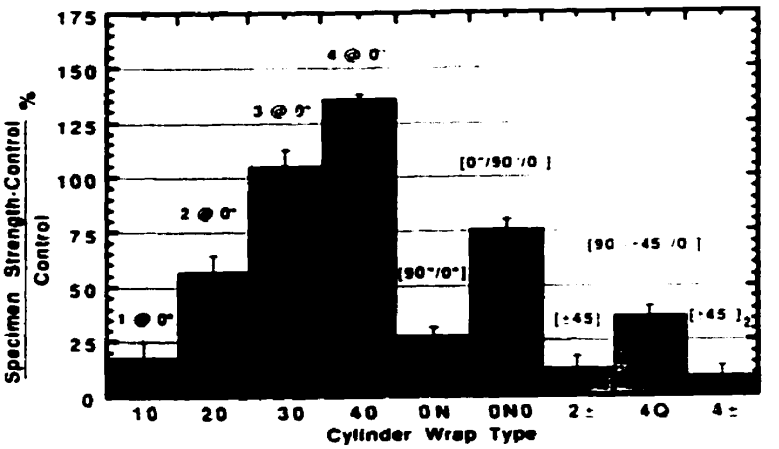

Percentage increase in compressive strength of jacketed specimens

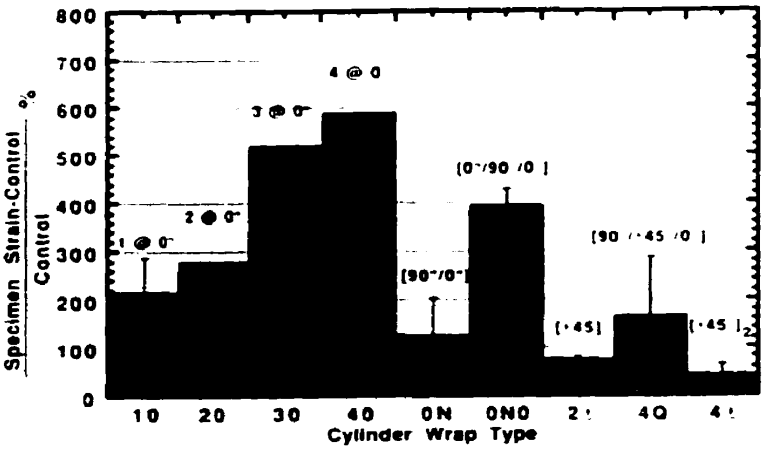

Percentage increase in axial strain of jacketed specimens over the concrete con-

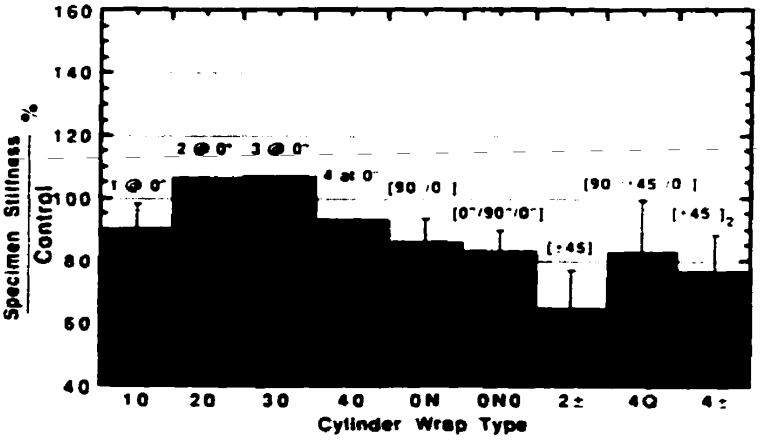

Ratio of structural stiffness of jacketed specimens to that of the concrete control.

Figure 2-5: The effects of wrapping orientation on compressive response produced by Howie and Karbhari (1995)

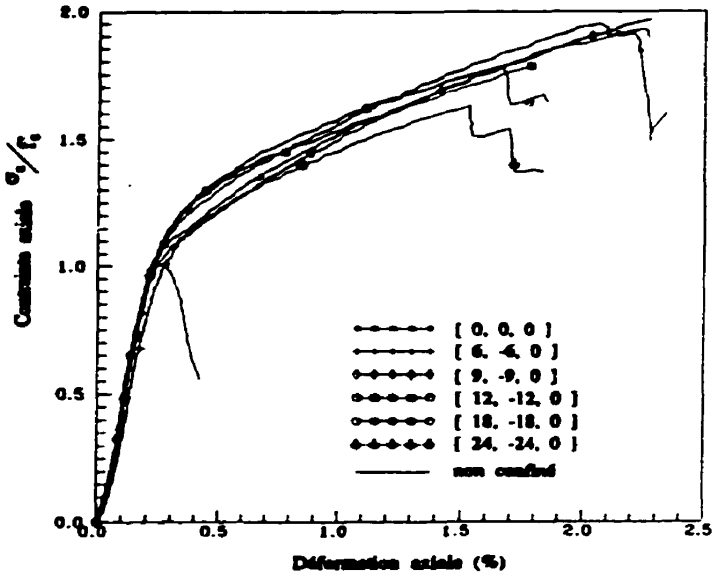

Figure 2-6; The normalized stress-strain of wrapping systems with various orientations produced by Picher and Labossiere (1995)

Picher and Labossière (1995) concluded that angles greater than 12° had less strengthening effect than smaller ones. The angles of 6° and 9° resulted in the most deformation and doubled the strength of concrete. Tests on 200×100 mm wrapped cylinders showed that their strength is 10% more than similar 300×150 mm cylinders. This study was accompanied by developing a mathematical model for multilayer concrete composites based on linear-elastic theory at rupture which obeys the Hooke's general law. The average stress in all layers can be define as:

$$\overline{\sigma}_i = \frac{1}{t}\int_{-t/2}^{t/2} \sigma_i . dz = \frac{1}{t} \int Q_{ij} . dz . \varepsilon_j \qquad \text{for} \quad i, j = 1, 2, 6 \tag{2-4}$$

The stress-strain relationship of multi-layer composite can be obtained from:

$$\begin{Bmatrix}\bar{\sigma}_1\\ \bar{\sigma}_2\\ \bar{\sigma}_3\end{Bmatrix}=\frac{1}{t}\begin{bmatrix}A_{11}A_{12}A_{16}\\ A_{21}A_{22}A_{26}\\ A_{61}A_{62}A_{66}\end{bmatrix}\begin{Bmatrix}\varepsilon_1\\ \varepsilon_2\\ \varepsilon_3\end{Bmatrix} \qquad \text{where } A_{ij}=\int Q_{ij}dz \tag{2-5}$$

The inverse relationship of the above equation permits to evaluate the modulus of elasticity for multi-layer composite based on individual layers:

$$\begin{Bmatrix}\varepsilon_1\\ \varepsilon_2\\ \varepsilon_3\end{Bmatrix}=\begin{bmatrix}a_{11}a_{12}a_{16}\\ a_{21}a_{22}a_{26}\\ a_{61}a_{62}a_{66}\end{bmatrix}\begin{Bmatrix}\bar{\sigma}_1\\ \bar{\sigma}_2\\ \bar{\sigma}_3\end{Bmatrix}t \tag{2-6}$$

where $E_1=\frac{1}{a_{11}t}$, $E_2=\frac{1}{a_{22}t}$, $E_6=\frac{1}{a_{66}t}$, $\nu_{21}=-\frac{a_{21}}{a_{11}}$

2.2.2. Environmental Effects

Karbhari and Eckel (1995) studied the effects of short-term environmental exposure on the axial strength capacity of composite jacketed concrete. Concrete cylinders with the nominal size of 300×150 mm, and average strength of 52 MPa were cured for 28 days. Then, they were wrapped with 2 layers of ACM, and placed in a vacuum bag in room temperature for 36 hours to cure the resin. Then, the specimens were subjected to one of four environmental conditions: ambient, water, sea water, and -18°C, for 60 days. The authors have discussed that the main environmental deterioration can take place in the potentially weak interfacial zone of the wrap and concrete. After exposure, the cylinders were tested in axial compression. The failure was defined as a 15% drop in load capacity. The specimens subjected to -18°C had brittle failure, but increased stiffness. Sea water was found to have deterioration effects on the fiber-matrix interface, whereas fresh water had insignificant effects on the strength. In this study glass, carbon, and aramid fiber sheets were examined. Furthermore, the need for long term and accelerated environmental study was mentioned.

3. Parametric Dimensions of The Experimental Program

3.1. Objective

The objective of this experimental study was to evaluate and quantify the effects of various types and contents of fibers on the mechanical properties of High Strength Concrete (HSC). Combinations of favorable fibers such as steel micro fibers, steel fibers and polypropylene fibers were also examined during the series of tests. Additional variables of the experimental program were the condition at testing (degree of saturation), the load path, and the specimen size.

Table 3-1 summarizes the number of specimens and test variables for this experimental study. Rows represent the fiber combination used for each batch, whereas columns represent the type of testing. The number in each cell indicates the number of identical specimens for that experiment. A total of 9 different batches (including the plain concrete used as the matrix), 19 different types of testing conditions, and 258 specimens constitute this research. The outcomes of the experiments are discussed in the following sub-sections; nomenclature refers to Table 3-1.

3.1.1. Fiber Type and Content

The behavior of fiber concrete varies depending on the type and content of mixed fibers. The design of concrete batches were intended to provide extensive knowledge of the improvements effected by various types, contents, and combinations of fibers on the behavior of plain concrete. Batch 1 is the plain concrete which was used as the matrix for all subsequent fiber concrete batches. Batches 2 and 3 contained 1% and 2% steel micro-fibers by volume, respectively.

The Bat. No.	Combinations of Fiber Types / Test Type	Active Confinement									Toothpaste	Passive Confinement (wrapped)						Uniaxial Saturated		Flexural Testing Prism
		100 mm Saturated					100 mm Dry				100 mm Saturated	200 mm Saturated			100 mm Saturated					
		0%	20%	40%	60%	80%	0%	20%	40%	60%		1Layer	2Layer	3Layer	1Layer	2Layer	3Layer	200	300	
		A	B	C	D	E	F	G	H	I	J	K	L	M	N	O	P	Q	R	S
1	Plain Concrete	3	2	2	2	2	2	2	2	2	2	2	2	2	2	2	2	3	3	3
2	Microfibre 1%	3	-	-	-	-	-	-	-	-	-	2	2	2	-	-	-	3	3	3
3	Microfibre 2%	3	2	2	2	2	2	2	2	2	2	2	2	2	2	2	2	3	3	3
4	(Micro+Steel)Fibre 1%	3	-	-	-	-	-	-	-	-	-	2	2	2	-	-	-	3	3	3
5	(Micro+Steel)Fibre 2%	3	2	2	2	2	2	2	2	2	2	2	2	2	2	2	2	3	3	3
6	Polypropylene 4%	3	-	-	-	-	-	-	-	-	-	2	2	2	-	-	-	3	3	3
7	(Poly+Micro)Fiber 2.5%	3	2	2	2	2	2	2	2	2	2	2	2	2	2	2	2	3	3	3
8	(Poly+Micro)Fibre 5%	3	-	-	-	-	-	-	-	-	-	2	2	2	-	-	-	3	3	3
9	Polypropylene 1.5%	3	-	-	-	-	-	-	-	-	-	2	2	2	-	-	-	3	3	3

Table 3-1: The overall layout of the experimental program

Rows present batches, Columns present test types, and
Numbers in cells present the number of identical specimens

The total volume fractions of fibers for Batches 4 and 5 were 1% and 2% respectively, which consisted of 40% steel micro-fibers and 60% steel fibers (by volume). Batch 6 contained 4% polypropylene fibers by volume. The total volume fractions for Batches 7 and 8 were 2.5% and 5%, respectively. The fibers were combination of 40% steel micro-fibers and 60% polypropylene fibers (by volume). Batch 9 had 1.5% polypropylene fibers. For the purpose of comparison, the fiber content of Batch 7 is equal to the sum of those of Batches 2 and 9. The volume of micro-fibers of Batch 8 is equal to that of Batch 3.

3.1.2. Active Confinement

It is known that lateral pressure improves considerably the mechanical properties of concrete. These improvements were examined for fiber concrete in a triaxial hydraulic cell (Hoek Cell) under various degrees of confinement. The relative tests are listed in columns A through I of Table 3-1. In this experiment, lateral pressure was increased up to its final value prior to the application of axial load. The degree of confinement was defined as the ratio of the lateral pressure to the average uniaxial compressive strength of saturated 100×50 mm cylindrical specimens. For saturated specimens these ratios were 0, 20, 40, 60, and 80%, and for dried ones they were 0, 20, 40, and 60%. The tests on dry specimens were designed to determine the changes in fiber concrete response in the absence of pore water pressure.

3.1.3. Passive Confinement

Except in cases of prestressing, stress states in concrete structures seldom involve conditions of active confining pressure. Usually, passive confining stresses arise in reaction to concrete expansion in one direction resulting from damage under load in the orthogonal direction. Hence, it is possible that the mechanical properties of passively confined concrete might be different from those obtained under active confining pressure.

In this study, passive confinement was provided by means of carbon fiber wraps. The fibers act against the lateral deformation of concrete, and provide passive confinement. Relevant tests are listed in columns K through P of Table 3-1. The fiber wraps were applied in 1, 2, and 3 independent layers to produce different degrees of passive confinement. The magnitude of confining pressure depends on the number of layers, lateral strain, and modulus of elasticity of the wrap.

3.1.4. Moisture

Previous findings (discussed in section 5.5.1) indicated that pore water pressure counteracts lateral confinement in concrete, thereby weakening the compressive strength of the material. Batches 1, 3, 5, and 7 were examined to assess the influence of water held in the pores at the time of testing on the mechanical properties of fiber concrete. Similar tests were performed on the specimens in columns A to D which were saturated, and those in columns F to I which were dried. Saturated condition was achieved after subjecting the specimens to 100% humidity for 3 days, whereas dry condition was achieved by placing them in a 60°C oven for 3 days. Comparison of the responses of the two groups would determine the effects of moisture on fiber concretes.

3.1.5. Effects of Size

An extensive number of research studies have shown that the response of concrete varies with the size of specimen (discussed in section 5.4.1). In this study, it was intended to assess and quantify the effects of specimen size on the compressive mechanical properties of fiber concrete. For this reason cylindrical specimens were cast in three different sizes while maintaining the ratio of height to diameter equal to two. The nominal specimen sizes were 100×50, 200×100 and 300×150 mm, and the relative tests are shown

in columns A, Q and R of Table 3-1, respectively. However, in performing the data reduction, the actual dimensions were used for each specimen.

3.1.6. The "Toothpaste" Test

The so called "toothpaste test" is an indirect splitting test. This series of tests was performed in the triaxial cell (Hoek Cell). With no axial load, lateral pressure was increasingly applied to the specimens up to splitting along the circumference. The behavior of the specimens under these conditions is of particular interest in order to complete the overall failure envelope (yields failure data for the tension regime), and also to describe the performance of concrete in the absence of axial compression. This test was applied to Batches 1, 3, 5, and 7, which are presented on column J of Table 3-1.

3.1.7. Prism Bending Test

The behavior of fiber concrete in tension was studied by performing bending tests on prismatic beam specimens, listed in column S of Table 3-1. The nominal dimensions of the beams were 420×150×80 mm, and the actual dimensions of each specimen were recorded for related data reduction purposes (Appendix A). Four-point loading with three equal spans was applied to the simply supported beam specimens. The tensile parameters were obtained through relevant calculations.

3.2. Concrete-Matrix Design

A high strength concrete (over 50 MPa, 28 days strength) was intended to be used as the reference batch and the matrix for the fiber concrete batches. In designing the mix, it was intended to omit gravel, due to small size of the specimens. The mix design was selected through a series of trial and error experiments with a constant water/ cement ratio of 0.45. The 200×100 mm cylindrical specimens were tested after 7 days curing, and the

average of compressive strengths of three specimens were measured. The moisture content for gravel was negligible, and for sand was 2%. Hence, this value increased the actual W/C ratio.

Initially, two mix designs were considered, referred to as mix I and mix II in Table 3-2. Mix I, which contained rock flour (as a substitution for gravel) and wet sand had an average 7-day compressive strength of 34.5 MPa. The workability of this mix was very low, due to its dryness. Mix II had sand, gravel and 2% (by the weight of cement) superplasticizer (Lomar-D) with a 7-day strength of 19.4 MPa. This concrete resulted in vast bleeding and segregation. Consequently, mix III, which is the same as mix II but without superplasticizer, was examined. The strength of this concrete was 27.4 MPa at 7 days, and it was too fluid. The W/C ratio for the above mixes was practically 0.47 by considering the moisture content of sand. For mix IV dried aggregates were used which led to 36.8 MPa compressive strength. Finally, gravel was omitted from the latter mix and its weight was replaced by sand, and mix V was produced (Table 3-2). The 7 day compressive strength of 200×100 mm cylindrical specimens for this mix was 34.3 MPa which was adequate for the intended experiments.

The materials which were used as the composition of the different batches in this research are described in detail in the following sub-sections.

3.2.1. Concrete Matrix

The mortar mix V of Table 3-2 formed the concrete matrix of all the subsequent fiber reinforced batches. The composition of this mortar for 1 m^3 was:

- type 10 Ordinary Portland Cement 660 kg
- tap water 297 kg
- sand: washed crushed lime stone with maximum grain size 2.5 mm 1320 kg

The Constituents of Trial Mixes; Values Are in kg/m^3

Constituents of trial mixes	Mix I (wet agg.)	Mix II (wet agg.)	Mix III (wet agg.)	Mix IV (dry agg.)	Mix V (dry agg.)
Cement	660	660	660	660	660
Water	297	297	297	297	297
Sand	990	990	990	990	1320
Gravel	---	330	330	330	---
Rock Flour	330	---	---	---	---
Lomar-D	---	13	---	---	---

The Compressive Strength of 200×100 mm Cylinders at 7 Days Age; Values Are in MPa

Specimen 1	35.66	18.66	28.81	36.76	32.92
Specimen 2	35.66	20.03	26.06	35.66	34.84
Specimen 3	32.10	19.48	27.4	37.86	35.12
Average	34.5	19.4	27.4	36.8	34.3

Table 3-2; The trial mixes for the concrete matrix

3.2.2. Fibers

The following three types of fibers were used in construction of FRC batches:

- **Micro Fibers:** Steel micro-fibers, with specific gravity of 7.85, 1 mm long and 25 μm thick, and high modulus of elasticity.
- **Steel Fibers:** Rounded 25 mm long, hooked-collated fibers (Figure 1-1) with water soluble adhesive. The specific gravity is 7.85, and modulus of elasticity is high.
- **Polypropylene Fibers:** Fibrilated 25 mm long polypropylene fibers with specific gravity of 0.9. Each group of the collated fibers were woven together by internal fibers, so that after opening during the mixing process, they formed a fiber mesh (Figure 3-1). The modulus of elasticity is 3.5×10^3 MPa.

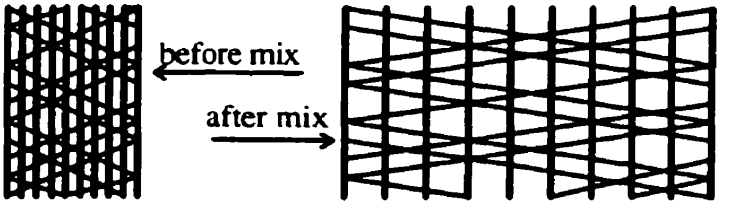

Figure 3-1; Type of Polypropylene Fibers

3.2.3. Super-Plasticiser

The superplasticiser used in this series of experiments was Lomar-D, which was a dry powder. It is generally assumed that this product does not affect the W/C ratio.

3.3 Casting

Mixing and casting of each batch had particular characteristics and problems which are explained in this section. The saturated unit weight for each batch was obtained by averaging the weight of three 200×100 specimens divided by their volumes, in saturated condition. These values are presented in Table 3-3 (they will be discussed in section 5.1).

Bat. No.	Batch Compositions	Measured Unit-Weight	Calculated Unit-Weight	Percent of Compaction
1	Plain Concrete	2320	2277	102%
2	Microfibers 1%	2298	2333	98%
3	Microfibers 2%	2307	2388	97%
4	(Micro+Steel)Fiber 1%	2375	2333	102%
5	(Micro+Steel) Fiber 2%	2328	2388	97%
6	Polypropylene 4%	2183	2222	98%
7	(Poly+Micro)Fiber 2.5%	2260	2312	98%
8	(Poly+Micro)Fiber 5%	2252	2347	96%
9	Polypropylene 1.5%	2265	2256	100%

Table 3-3: Saturated Unit Weight of Different Batches

- **Plain Concrete:** This mix was described in section 3.2.1, and was cast by using a vibrating table.

- **Microfiber 1%:** The mix contained 1% microfibre by total volume. The fibers were mixed with sand and cement at dry stage. This batch, which was cast twice, was a workable mix with a slump of 180. The mix was compacted the first time by a vibrating table externally, and the second time by a vibrating hose internally for a longer period, but the expected density was not achieved.

- **Microfiber 2%:** This batch contained 2% steel microfibres by total volume. The mix was expected to be too stiff, because the high surface area of the microfiber would absorb considerable amount of water. In the first trial, it was mixed with 1% Lomar-D (of the cement weight), but bleeding and segregation occurred. In the second trial, when it was mixed with 0.5% Lomar-D, the same behavior in smaller scale was observed. Finally, in the third trial, no plasticizer was used and a slump of 45 mm was obtained.

- **Micro + Steel fibers 1%:** A total of 1% of the volume of mix was occupied by micro and steel fibers. The ratio of steel fibers to micro fibers was 60% to 40% respectively. The fibers were mixed with sand and cement before adding water. A slump of 200 mm was measured for this mix.

- **Micro + Steel fibers 2%:** This mix was similar to the latter mix, but the volumetric fraction of the fibers in the concrete was double. Despite of the high ratio of fibers, the workability of this mix was good. No superplasticizer was used, and a slump of 180 was obtained. A vibrating table was used for compaction of the molds.

- **Polypropylene fibers 4%:** The mix contained 4% of polypropylene fibers by total volume. The fibers were added gradually to the wet mix. Rapid adding would result in clogging. After mixing with concrete, the fibers opened up and connected with each other. The resulting mix was very stiff with zero slump. Compaction was done by using internal vibration and hand tamping in layers of about 5 centimeters.

- **Polypropylene + Micro fibers 2.5%:** The mix contained 2.5% polypropylene and steel micro fibers by total volume. The ratio of polypropylene to steel fibers was 60%

to 40% respectively. The microfibres were mixed with concrete at dry stage, and polypropylene fibers were added gradually to the wet concrete. The same method as in the previous section was used for compaction.

- **Polypropylene + Micro fibers 5%:** This mix was similar to that of the latter section, but contained twice the volume of fibers. Because of the high ratio of fibers and the high surface area of the microfibres 0.4% Lomar-D (by weight of the cement) was added to the mix to improve its workability. The slump was still zero, but it allowed the cement paste to cover the aggregates. The compaction was done by means of internal vibration and hand tamping in layers of about 50 mm.

- **Polypropylene 1.5%:** The mix contained 1.5% polypropylene fibers by total volume. No superplasticizer was added, and the slump remained zero. The method of compaction of the previous section was used. Despite of zero slump, the workability and compactability of this mix was satisfactory.

3.4. Curing

The specimens were covered with wet burlap after casting, and were striped the next day. Then they were kept in the curing room at 100% relative humidity and 30°C temperature, for a minimum of forty days. Since the concrete matrix did not contain fly ash or slag, it was assumed that its strength would not vary considerably after this age. The specimens were taken out for preparation after this period, and returned to the room until the time of test (for dry and wet definitions and related procedures refer to section 3.1.4).

3.5. Sample Preparation

All the batches were cast in four different sizes, and the following tailorings were performed to make the specimen sizes into required dimensions.

- **Prisms:** The prisms were cast in 410×150×80 mm dimensions. For those batches which contained polypropylene fibers, the molds were overfilled to cover the aggregates and fibers by cement paste. The extra top was saw cut after hardening. In addition, the soft walls of the molds were curved due to the necessary severe compaction for polypropylene fiber concrete. Therefore, these concrete prisms were slightly out of shape.

- **The 300 mm Cylinders:** The batches were cast in standard 300×150 mm nominal size cylinders. For those batches which contained polypropylene fibers, the molds were over filled. The ends of all the cylinders were ground after hardening.

- **The 200 mm Cylinders:** Standard cylinders with nominal size of 200×100 mm were cast, with the similar procedure of the previous section.

- **The 100 mm Cylinders:** Concrete was cast in blocks with 345×260×160 mm dimensions. The 100×50 mm nominal size cylinders were cored from these blocks. The inside diameter of the core drill was 53.5 mm. The cylinders did not have a unique diameter due to the vibration of the drill. In order to eliminate the end effects, the cored cylinders were, then, saw cut to within 1 mm longer than the required length (remaining length about twice that of their diameters). Both end-faces of each specimen were ground (within fractions of a millimeter) till the grinding blade could touch the entire surface area, so that the end surfaces were smooth and orthogonal to the longitudinal axis.

3.6 Strain-Gauge Installation

Strain-gauges were installed on the 100 mm cylinder which would be used in the triaxial testing device . All the gauges were 60 mm long to be able to average the strains on a long length. Two gauges were installed at mid-height of each specimen: in the circumferential and axial directions. Ordinary gauges were used for the low confinement ($\sigma_3 \leq 20\%\ f'_c$) tests, and high strain capacity (post-yielding) ones were used for the other tests including the "toothpaste" series.

Since the surface of the concrete specimens were rough and porous, a first layer of the adhesive (AE-10) was applied and sanded after hardening. Then, the second layer was applied and the strain-gauge with its terminal were installed. They were clamped to the concrete by scotch tape and placed in front of a heat lamp for about an hour. After hardening of the adhesive and stripping the tapes, a protective coat (M-coat) was applied in three layers.

According to the Intertechnology (1995) catalog, the applied adhesive (AE-10) is highly resistant to moisture. A trial experiment also showed that the above procedure is sufficient to protect the strain-gauge against water or moisture. However, if the specimen is in direct contact with water, the water would penetrate into the concrete and destroy the bond between the adhesive and concrete. Intertechnology (1995) suggested to apply wax (strain gauge accessory) on the surface of concrete at the installation location and blow it into the pores by a heat gun, till the rough surface of the concrete is visible. This would seal off the pores underneath the adhesive. Then, the surface is sanded and the other steps of gauge installation, as the above, should be followed .

3.7 Wiring

The wires which extended out of the terminals should be thin to be accommodated in the Hook cell without interfering with the alignment of the specimen in the cell. For the

triaxial tests, #32 magnet wire was used. Because of the high lateral pressure, if the wires pass on each other they would create a short circuit, and if they pass over holes they would break during the test. Therefore, the paths of wires were carefully determined and taped to the specimens. Plastic tape was wrapped around the wires at the location of passing the edge of the concrete to the top platen, otherwise, they would snap at that edge (Figure 3-2). At high degrees of confinement, the lateral pressure could break the wires where they were passing over even small size pores, or at the edge of specimens, and often, the test should be repeated. For the toothpaste tests, in particular, the lateral pressure was extremely high and the possibility of wire breakage would increase, hence, a slightly thicker wire was used.

3.8 Wrapping Carbon Fiber Sheets on Specimens

Sheets of carbon fibers were used to wrap some of the specimens (Table 3-1) in order to provide passive confinement. The procedure followed the steps suggested by the manufacturer (Forca catalog, Appendix B).

1. Apply prime-coat (consisting of solvent and hardener) by a roller brush to the surfaces of specimens, and leave them in the room temperature for one day.
2. Apply resin (consisting of solvent and hardener) by a roller brush to the carbon fiber sheet.
3. Put the sheet on the specimen's surface and push it hard to soak the fibers in the resin and eliminate any existing air bubbles.
4. Apply resin on the exterior of the fiber sheet to cover all the fibers.
5. The catalog requires a 100 mm overlapping in general. However, because of the small perimeter of the specimens, shorter overlappings were used. For specimens with one layer wrap the overlapping used was 80 mm for the 200 mm diameter cylinders, and 50 mm for the 100 mm diameter cylinders. For specimens with two or three wraps the

overlapping used was 50 mm for the 200 mm diameter cylinders, and 30 mm for the 100 mm diameter cylinders.

6. For the cylinders with two and three layers of wrap, steps 2 to 5 were repeated after one day of curing.

Figure 3-2: Typical wiring for strain gauges

The specimens were cured in room temperature for two weeks. The cylinders were ground after hardening of the wraps to restore their smooth ends. According to the catalog, water would not cause damage after the resin is hardened.

3.9. "Toothpaste" Specimens

In this series of tests, extremely high lateral pressure without any axial force was applied. The lack of axial force produced particular problems which necessitated additional preparation. Since the length of the specimens were shorter than the membrane's, platens were added to the specimens. The lateral pressure would squeeze the membrane between the specimen and the platens and separate them, which would result in membrane failure. Strong glues could not overcome this problem.

Eventually, thin steel straps were wrapped around the seams to prevent the membrane from squeezing in the junction (Figure 3-3). The diameter of the platens should be equal to the concrete cylinder diameter. Otherwise, the bump which would be formed at the junction would produce axial force. The top platen was covered by plastic tape at the location where the wires were passing to prevent potential short circuit. The wire, which was used in this experiment, was one number thicker than the one which was used for the active confinement tests. The high applied pressure could break the wire at the locations that it was passing over even small size pores. The paths of the wires were carefully determined and they were taped to the concrete. Still, occasionally the pores which were hidden under a thin layer of concrete were opened up by applying pressure, and the test should be repeated.

The large size pores which were more observed on the specimens with microfibers, created additional problem. The membrane could be squeezed into these holes and generate tension at that location. This led to tension failure where the pores were on a plane. To overcome this problem, gypsum (plaster of paris) was applied to the surface of

the specimens to fill up the holes (Figure 3-2). Filling the holes also helped to prevent the wire breakage.

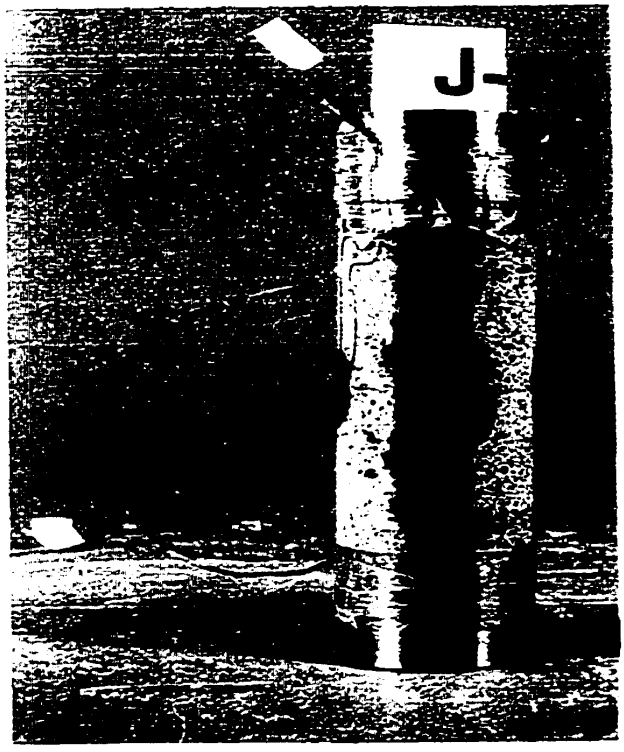

Figure 3-3: A prepared specimen for "Toothpaste" test

4. Testing and Results

4.1. Background

It is known that the mechanical response of concrete is determined or controlled in a consistent way by the physical properties of the material micro-structure, and the imposed boundary conditions (Pantazopoulou and Mills, 1995). The components which form the micro structure of concrete consist of cement paste, aggregate (and fibers), and voids (pores). The system of voids in the micro structure of concrete (porosity) weakens the mechanical response, since it has no contribution towards interparticle bonding but nevertheless occupies space in the material mass (Imran and Pantazopoulou, 1995).

The initial slope of the stress-strain curve represents the stiffness of undamaged concrete. As the imposed axial strain increases, damage starts to accumulate in the material structure, which can be detected by deviation from the linear elastic response in the stress-strain plot (Figure 4-1a) (Pantazopoulou and Mills, 1995). This nonlinearity is accompanied by a simultaneous deviation in the plot of volumetric strain (ε_v) versus axial strain (ε_1) from linear elastic response (Figure 4-1b). This means that the transverse strains increase at a faster rate than what the theory of elasticity would predict, due to internal micro-cracking . The idealized linear elastic response indicates a net contraction that would increase linearly at the rate of 1-2ν (ν is Poisson's ratio). Note that the post peak range of the stress-strain response is accompanied by reversal of the ε_v-ε_1 curve into the range of volumetric expansion (dilation). The axial Strain which corresponds to zero volumetric strain (ε^*) marks the onset of a dramatic loss of resistance, and uncontrolled crack growth and propagation (Pantazopoulou and Mills, 1995). The post-peak response is a phase where cracks widen, separating the concrete mass into slender chunks, and due to their slenderness these chunks buckle outward, reducing the resistance of the member (Pantazopoulou, 1995).

(a)

(b)

(c)

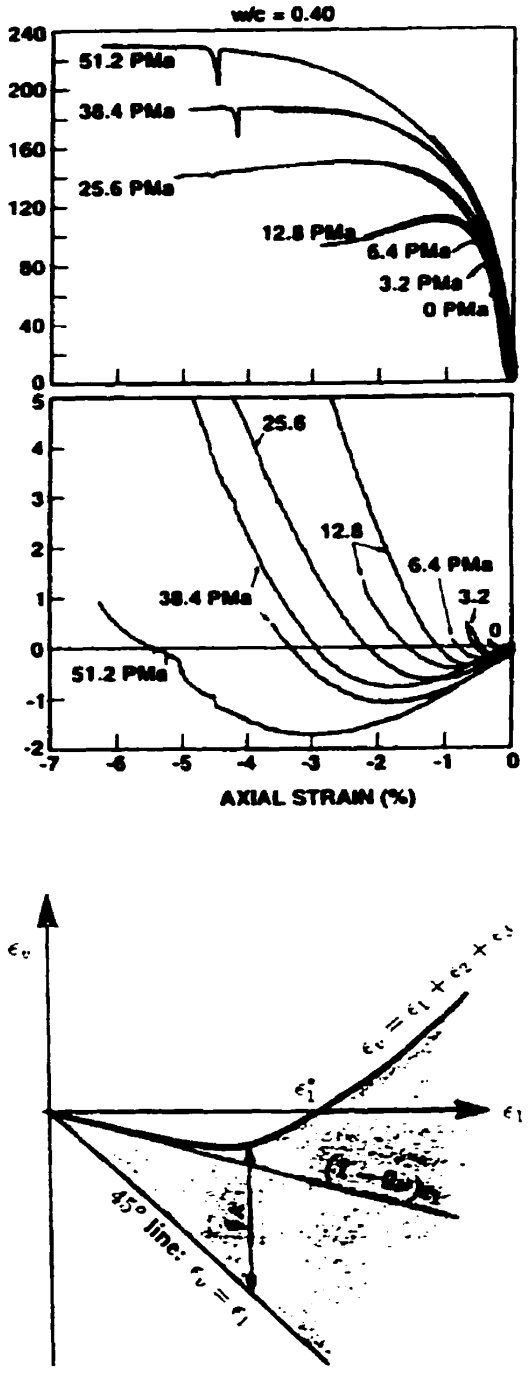

Figure 4-1: Typical behavior of plain concrete

a. stress versus axial strain (taken from Imran and Pantazopoulou, 1995)

b. volumetric strain versus axial strain (taken from Imran and Pantazopoulou, 1995)

c. presentation of area strain (taken from Pantazopoulou and Mills ,1995)

The shaded area in Figure 4-1c, which is bound between the ε_v-ε_1 curve and a 45° line, presents the area increase per unit area of the cross section supporting the load. This area strain coordinate, denoted by ε_A, is a measure of the crack (cross-sectional) sizes developing in the material in response to the mechanical load. Resistance of concrete is sustained as long as the increase in ε_A is controlled, and initiation of the descending branch in the stress-strain curve is directly associated with a drastic increase in the rate of ε_A growth (Pantazopoulou and Mills, 1995).

Generally, the lower the porosity of a given material, the closer the packing of particles, and thus the higher the density of the interparticle bonds and the more resilient the material to deformation. Cracking can be interpreted as mechanically induced form of porosity, and its impact on material resistance is similar to that caused by natural porosity. Based on this idealization, softening of resistance is seen as a consequence of increase in centent of voids in the micro structure (i.e. pores and cracks)(Pantazopoulou and Mills, 1995). Increase in voids causes volumetric expansion in concrete, and it has been shown that the loss of strength and stiffnesscan can be quantified consistently by using the volumetric expansion as a state variable, along with the applied boundary conditions (Pantazopoulou, 1995).

Confinement is known to delay loss of stiffness and strength, increase the deformability of material, and decelerate softening rate in the post peak region of concrete (Figure 4-1). In tests under very high confining stresses, it has been shown that the ε_v-ε_1 diagram may not even cross the ε_1 axis. It has been suggested that confinement provides lateral kinematic restraint that prevents volumetric dilation and keeps the concrete fragments together, to the extend that failure can be delayed and even altered, resembling plastic flow (Pantazopoulou and Mills, 1995). At high intensity of confinement stress, the area strain becomes smaller for a particular axial strain. Therefore, it can be concluded that the presence of confinement imposes a kinematic restraint against separating the compressive struts supporting the axial load. It has been shown that the variation of

secant stiffness of concrete is closely related to the amount of area strain that is developed in the cross section of the compressed struts (Imran and Pantazopoulou, 1995).

At low range of confinement (up to 40% of uniaxial strength) the failure is associated with tensile cracking and subsequent volume expansion, whereas at higher confinements the failure is closer to plastic flow. At the stage of plastification, damage is no longer a result of unstable crack propagation, and failure is associated with alteration in micro-structure of concrete by means of compaction and collapse of pores. By assuming that the total maximum space available for concrete compaction is the net volume of initially occupied by capillary pores, Pantazopoulou and Mills estimated this damage component based on the physical characteristics of the concrete mix, such as water/cement ratio, air content, and fraction of aggregates.

The importance of volumetric expansion in determining the degree of micro-structural damage, which is an indication for existing resistance, have been established for plain concrete. In this research, the significance of this strain is investigated for FRCs, as well as composites wrapped by carbon fiber fabric. Hence, throughout the compressive tests, the axial and circumferential deformations were measured for the purpose of development of the relationship of volumetric strain with the mechanical behavior of FRC.

4.2. Data Reduction

The recorded dimensions and weight of each specimen are listed in Appendix A. The test results, which are presented in Tables 4-1 and 4-2, required analysis and data reduction process in order to establish the relationships of the important variables with the mechanical properties of FRC. The analysis procedures for determining each parameter are described in the following sections, and the outcomes are presented in Table 4-3 for compression and Table 4-4 for bending.

No.	f_c	ε_{10}	ε_{20}	ε_{30}	ε_c	ε_{85}	ε_{50}	ε_{min}	f_c	$\varepsilon_{3\,max}$	ε^*	$\varepsilon_{v\,min}$	$\varepsilon_{1\,min}$	ε_{v10}	ε_{v20}	ε_{v30}
1A1	56.1	-277	-570	-841	-3954	-4268	-4851	-5659	6.1		-4229	-1970	-3470	-293	-514	-702
1A2	NOT A RELIABLE SPECIMEN															
1A3	56.1	-272	-569	-843	-4058	-4724		-4788	39.7		-4428	-2140	-3620	-274	-479	-584
1B1	105.6	-700	-1186	-1725	-14083	-24490	-27140	-28473	79.5		-18293	-5566	-10787			
1B2	103.8	-1487	-2191	-2731	-15588	-29900		-29866	89.4		-18865	-6046	-10882			
1C1	127.7	-371	-963	-1599	-36377	-39100		-39052	127.6							
1C2	122.5	-585	-1133	-1717	-22865	-32900		-41438	118.6		-25968	-4370	-13270			
1D1	NOT RELIABLE RESULTS															
1D2	162.0	-548	-1260	-2000	-43596	-45400		-45352	161.8			-16238	-32151			
1E1	187.4	-166	-1023	-1975	-42111			-42290	187.4			-24876	-42111			
1E2	184.0	-529	-1416	-2388	-45118			-45118	184.0			-20058	-42021			
1F1	66.7	-531	-877	-1215	-4692			-5290	62.3		-5049	-2477	-3769	-474	-753	-1012
1F2	64.8	-632	-995	-1127	-4634			-5119	59.8		-5031	-2432	-3948	-352	-661	-929
1G1	106.2	-631	-1164	-1671	-13206	-20627	-27396	-28449	73.1		-16579	-4902	-9020			
1G2	107.4	-596	-1215	-1768	-13427	-22144	-26025	-26740	69.1		-15561	-4211	-9336			
1H1	157.6	53.8	-794	-1670	-22145	-21666		-22287	156.8							
1H2	140.1	-692	-1442	-2163	-28729	-35121	-35930	-36142	51.3		-35427	-8145	-15231			
1I1	176.0	-691	-1582	-2499	-37094	-37527		-38556	176.1			-16078	-29774			
1I2	177.3	-373	-1177	-2033	-38035			-38050	173.0			-11390	-22792			
1K1	67.6	-168	-370	-576	-3551	-4451		-6935	51.0	8791	-3678	-1247	-2465			
1K2	69.1	-179	-375	-607	-3698	-5126		-5890	55.7	7334	-4289	-1779	-3321			
1L1	70.7	-195	-405	-622	-3864	-4590		-7859	64.9	5931	-5843	-3635	-4115			
1L2	70.1	-198	-409	-618	-3739	-5080		-6120	60.4	5818	-5005	-2814	-3739			
1M1	NOT RELIABLE RESULTS															
1M2	71.1	-177	-386	-308	-2987	-3863		-8710	73.9	7585	-4099	-2739	-3175			
1N1	74.9	-520	-884	-1234	-5433	-7072		-17745	62.6	9464	-7748	-3589	-5195			
1N2	69.1	-563	-886	-1205	-4687	-5807		-7608	56.0	4492	-6432	-3546	-4934			
1O1	73.5	-1176	-1748	-2228	-7495			-27003	97.3	9586		-5603	-7264			
1O2	75.1	-707	-1114	-1473	-6013			-38212	122.9	9918						
1P1	76.3	-825	-1294	-1661	-6241			-34202	123.8	6985						
1P2	102.4	43.9	-212	-454	-2668			-44887	143.7	8415						
1Q1	53.3	-133	-292	-464	-2739	-3223	-3905	-4615	16.7		-2744	-1320	-2220	-161	-181	-260
1Q2	56.4	-137	-310	-491	-2885			-2995	53.4		-2970	-1450	-2550	-74	-121	-148
1Q3	NOT RELIABLE RESULTS															
1R1	56.8	-107	-244	-391	-2358			-2409	56.8			-839	-1972	-79	-161	-243
1R2	55.9	-132	-277	-431	-2467			-2743	50.0		-2586	-948	-2559	26.6	-36	-118
1R3	51.2	-139	-273	-415	-2091			-2579	48.8		-2571	-750	-2056	14	-44	-115

Table 4-1; Compression test results for cylindrical specimens

No.	f_c'	ε_{10}	ε_{20}	ε_{30}	ε_c	ε_{85}	ε_{50}	ε_{min}	f_r	$\varepsilon_{3\,max}$	ε^*	$\varepsilon_{v\,min}$	$\varepsilon_{1\,min}$	ε_{v10}	ε_{v20}	ε_{v30}
2A1	58.4	-435	-724	-987	-4145	-5103	-5660	-6598	18.1		-4566	-2036	-3431	-380	-605	-797
2A2	60.7	-548	-811	-1096	-4377	-5143	-6086	-6447	25.0		-4677	-3589	-3589	-447	-647	-843
2A3	57.3	-503	-808	-1056	-4246	-5313	-6365	-6961	23.0		-4680	-2120	-3228	-464	-712	-904
2K1	65.6	-186	-392	-611	-4073			-9128	61.3	11002	-4639	-1717	-3050			
2K2	62.9	-184	-370	-573	-3640			-10533	56.8	11431	-4218	-1555	-2741			
2L1	65.0	-170	-360	-551	-3426			-9191	63.3	8979	-5232	-2356	-3269			
2L2	65.1	-186	-406	-629	-3749			-11363	64.0	8032	-6675	-2637	-3749			
2M1	67.4	-171	-375	-578	-3948			-16094	83.1	10356	-7242	-2835	-3718			
2M2	62.1	-175	-377	-585	-4261			-11948	62.7	7362	-9977	-3829	-5446			
2Q1	47.8	-138	-304	-460	-2847	-3623		-3852	28.1		-3461	-1500	-2700	-143	-141	-270
2Q2	48.0	-155	-304	-445	-2617	-2922		-2923	41.3		-2779	-1370	-1970	-154	-270	-377
2Q3	47.6	-122	-267	-424	-2589	-3161		-3952	35.1		-2884	-1280	-1980	-152	-232	-368
2R1	47.2	-105	-240	-386	-2272			-2389	46.4			-1025	-1888	-81	-187	-298
2R2	44.0	-85.6	-193	-298	-1497			-1561	43.2		-818	-450	-781	-64	-120	-208
2R3	46.0	-120	-247	-385	-2141			-2254	45.3		-2251	-761	-1640	-88	-173	-261

Table 4-1: Compression test results for cylindrical specimens

No.	f_c	ε_{10}	ε_{20}	ε_{30}	ε_c	ε_{85}	ε_{50}	ε_{min}	f_c	$\varepsilon_{3\,max}$	ε^*	$\varepsilon_{v\,min}$	$\varepsilon_{1\,min}$	ε_{v10}	ε_{v20}	ε_{v30}
3A1	49.3	-558	-824	-1042	-4128	-5470	-6764	-9302	13.8		-4661	-2137	-3336	-509	-711	-884
3A2	49.2	-258	-505	-753	-3676	-4408	-5973	-8681	14.8		-4056	-1799	-3161	-218	-405	-588
3A3	49.0	-741	-1052	-1324	-4243	-5224	-6568	-7370	19.0		-4640	-2315	-3692	-669	-931	-1139
3B1	87.4	-239	-461	-660	-10321	-22328		-27962	70.4		-12846	-4000	-6361			
3B2	88.9	-318	-749	-1184	-11664	-23401		-28196	72.4		-14534	-5189	-9312			
3C1	104.8	-417	-982	-1507	-23127			-27603	98.6			-11347	-26484			
3C2	103.8	-326	-820	-1305	-18801			-27358	100.0			-17536	-27358			
3D1	137.0	-441	-1132	-1845	-40842			-44871	135.9			-17674	-33595			
3D2	144.0	-199	-868	-1604	-44001			-44001	144.0			-13120	-32815			
3E1	147.4	130	-601	-1363	-44378			-44378	147.4			-21162	-35234			
3E2	148.1	-165	-930	-1719	-43849			-44094	147.9							
3F1	60.4	-457	-813	-1143	-5384	-6484	-7832	-10263	9.1		-5646	-2502	-3685	-406	-692	-935
3F2	52.9	-581	-906	-1190	-4821	-5617	-6487	-10505	12.9		-4975	-2314	-3359	-533	-796	-1019
3G1	93.7	-724	-1183	-1659	-12001	-28289		-34668	75.2		-14689	-4118	-7397			
3G2	75.8	-388	-812	-1217	-7932	-14440		-14432	66.6							
3H1	120.2	-367	-983	-1628	-17309	-35467	-36275	-36961	40.2		-32956	-7045	-12653			
3H2	130.0	-336	-1005	-1673	-23725			-34678	125.7		-18193	-4935	-9228			
3I1	136.2	-324	-985	-1697	-18549			-36064	132.2		-23960	-7691	-11458			
3I2	150.7	-256	-977	-1727	-27329			-37620	146.6			-9329	-19322			
3K1	62.0	-184	-377	-587	-3911			-10632	61.8	11278	-4228	-1467	-2611			
3k2	59.0	-167	-351	-557	-3875			-9023	59.3	7985	-4568	-1521	-2945			
3L1	59.6	-178	-355	-594	-3723			-13237	66.3	7119	-11147	-2858	-4392			
3L2	58.2	-166	-349	-539	-3509			-11885	60.4	8143	-6645	-2651	-3802			
3M1	73.1	-136	-322	-507	-3655			-10245	81.0	8145	-6445	-2702	-3655			
3M2	57.3	-155	-348	-524	-2841			-13670	69.2	8254	-6291	-1682	-2277			
3N1	65.1	-409	-729	-1046	-5591			-15977	68.5	9337	-8178	-2714	-4430			
3N2	59.3	-375	-686	-980	-4691			-12172	60.5	8592	-6515	-2836	-3819			
3O1	62.1	-826	-1185	-1498	-5284			-22505	84.6	8084	-26117	-3746	-5761			
3O2	69.3	-463	-822	-1161	-5994			-37215	112.6	9837						
3P1	63.1	-515	-833	-1135	-5358			-40556	109.3	8985						
3P2	67.0	-518	-851	-1171	-4991			-44587	128.5	8838						
3Q1	48.9	-137	-279	-427	-2879	-3981	-6406	-6953	22.2		-3079	-936	-2039	-106	-189	-274
3Q2	46.0	-153	-307	-468	-2792	-4453	-6473	-6602	21.6		-2763	-820	-1757	-108	-205	-299
3Q3	46.9	-155	-307	-468	-2960	-4923	-6291	-6621	20.1		-3009	-926	-2073	-119	-223	-310
3R1	46.5	-162	-323	-490	-2910	-3963	-5410	-6047	20.6		-3190	-1022	-2260	-112	-213	-315
3R2	46.3	-157	-319	-487	-3106	-4252	-4445	-4631	21.3		-3209	-1030	-2009	-125	-246	-356
3R3	48.2	-151	-300	-465	-2869	-3873	-4411	-4502	22.7		-3033	-977	-2049	-104	-205	-314

Table 4-1: Compression test results for cylindrical specimens

No.	f_c	ε_{10}	ε_{20}	ε_{30}	ε_c	ε_{85}	ε_{50}	ε_{min}	f_r	$\varepsilon_{3\,max}$	ε^*	$\varepsilon_{v\,min}$	$\varepsilon_{l\,min}$	ε_{v10}	ε_{v20}	ε_{v30}
4A1	53.1	-639	-1033	-1355	-4706	-5551	-6499	-7487	19.9		-5137	-2503	-3812	-593	-925	-1181
4A2	53.8	-753	-1085	-1362	-4499	-5853	-7317	-7776	23.7		-5040	-2377	-3715	-711	-989	-1195
4A3	55.5	-409	-685	-977	-4246	-5164	-6129	-7380	18.2		-4917	-2120	-3405	-358	-570	-793
4K1	69.0	-195	-408	-630	-3885			-7305	63.4	8696	-4270	-1662	-3112			
4K2	69.1	-206	-421	-632	-3822			-8647	60.4	10664	-4443	-1664	-3112			
4L1	67.7	-185	-394	-606	-3802			-8689	66.0	7933	-5546	-2579	-3509			
4L2	66.4	-216	-428	-629	-3676			-8637	68.9	7220	-5331	-2361	-3426			
4M1	72.1	-192	-413	-604	-4183			-13384	85.8	12294	-5185	-1944	-3206			
4M2	70.8	-189	-387	-608	-3943			-7671	72.3	9337	-4924	-2300	-3363			
4Q1	54.2	-136	-288	-458	-2820	-3409	-4724	-6539	18.6		-3016	-874	-2143	-90	-162	-250
4Q2	56.8	-155	-337	-530	-3260	-4036		-4358	42.9		-3394	-1056	-2310	-107	-205	-320
4Q3	56.6	-173	-330	-500	-3006	-3842		-4158	37.3		-3093	-887	-2202	-97	-177	-266
4R1	54.1	-134	-291	-461	-2829	-3564		-3754	43.0		-3011	-885	-2066	-86	-174	-269
4R2	43.8	-97	-207	-327	-1647	-2077		-2307	32.4		-414	-269	-402	-75	-154	-228
4R3	50.2	-145	-295	-458	-2473			-2518	49.6			-1009	-2148	-113	-222	-337

Table 4-1: Compression test results for cylindrical specimens

No.	f_c	ε_{10}	ε_{20}	ε_{30}	ε_c	ε_{85}	ε_{50}	ε_{min}	f_r	$\varepsilon_{3\,max}$	ε^*	$\varepsilon_{v\,min}$	$\varepsilon_{1\,min}$	ε_{v10}	ε_{v20}	ε_{v30}
5A1	49.0	-260	-543	-819	-3701	-5064	-8646	-11306	19.4		-4240	-1713	-2916	-185	-400	-608
5A2	43.6	-843	-1325	-1683	-4996	-6221	-10306	-10464	21.2		-5799	-2745	-3945	-820	-1238	-1526
5A3	47.5	-406	-688	-949	-3714	-4387		-6797	24.5		-4066	-1890	-3298	-344	-561	-747
5B1	81.6	-923	-1492	-1935	-9398			-28188	70.9		-12686	-3552	-7411			
5B2	84.0	-1041	-1549	-2002	-10900			-31857	73.4		-29527	-8006	-14942			
5C1	94.1	-284	-802	-1314	-35234			-38528	93.6							
5C2	104.6	-484	-1143	-1844	-36629			-42305	104.4			-22819	-37830			
5D1	123.7	-260	-911	-1551	-42098			-42827	123.4		-35258	-4731	-20033			
5D2	125.8	-136	-923	-1557	-41007			-41284	125.5							
5E1	141.7	58.6	-681	-1428	-42239			-44463	139.3			-13487	-35284			
5E2	139.6	-278	-1103	-1877	-43878			-43878	139.6							
5F1	56.4	-489	-822	-1186	-5020	-6764		-12439	29.2		-5324	-2220	-3777	-424	-681	-966
5F2	59.3	-610	-974	-1318	-5296	-6990	-11379	-12153	27.1		-6066	-2779	-4144	-577	-874	-1148
5G1	92.4	-698	-1222	-1733	-12597	-29630		-38080	75.0		-15897	-5375	-8921			
5G2	89.7	-491	-970	-1449	-9231	-20794		-35682	71.9		-20555	-6593	-19585			
5H1	NOT RELIABLE RESULTS															
5H2	112.0	-659	-1276	-1884	-13575			-18173	109.9		-12004	-4211	-6519			
5I1	144.4	-333	-1079	-1807	-36572			-37532	144.3		-23960					
5I2	140.7	-395	-1161	-1882	-23885			-38711	136.8			-16614	-36238			
5K1	61.5	-211	-415	-632	-4318			-9974	59.2	9312	-4201	-1562	-2835			
5K2	57.9	-170	-354	-543	-3258			-7802	55.3	9711	-3521	-1355	-2501			
5L1	60.1	-182	-370	-611	-3441			-11493	70.8	8062	-5471	-2136	-3300			
5L2	61.7	-176	-378	-593	-3572			-8731	60.9	7050	-5918	-2697	-3702			
5M1	65.3	-214	-418	-615	-3713			-17133	86.2	8984	-11730	-2350	-3091			
5M2	63.2	-191	-396	-611	-3660			-16641	81.2	8164	-17122	-2299	-3514			
5N1	64.1	-423	-759	-1105	-5220			-18043	70.0	10835	-6816	-2653	-3768			
5N2	58.2	-624	-914	-1256	-5010			-17655	57.3	10721	-6679	-2679	-3825			
5O1	63.1	-777	-1264	-1711	-6499			-36912	99.8	11078						
5O2	58.6	-443	-741	-1049	-4926			-34198	93.4	7299						
5P1	63.5	-676	-1103	-1434	-5233			-38900	104.5	8046						
5P2	72.1	-443	-793	-1139	-5792			-41576	126.3	7188						
5Q1	48.0	-150	-306	-472	-2423	-2616		-2878	30.7		-2539	-866	-1885	-109	-196	-292
5Q2	48.5	-103	-213	-323	-1554	-1672	-4515	-4770	22.7		-1406	-370	-983	-80	-144	-187
5Q3	46.9	-174	-325	-490	-2572	-3314		-3717	32.4		-2770	-966	-1914	-142	-261	-377
5R1	45.3	-157	-316	-484	-2631	-3202	-3784	-3823	21.1		-2702	-911	-1943	-98	-191	-296
5R2	45.5	-143	-296	-461	-2519	-3041		-4191	27.9		-2640	-958	-2091	-143	-212	-320
5R3	46.3	-144	-302	-463	-2551	-2605		-3901	25.6		-2696	-872	-1929	-87	-177	-269

Table 4-1: Compression test results for cylindrical specimens

No.	f_c	ε_{10}	ε_{20}	ε_{30}	ε_c	ε_{85}	ε_{50}	ε_{min}	f_r	$\varepsilon_{3\,max}$	ε^*	$\varepsilon_{v\,min}$	$\varepsilon_{1\,min}$	ε_{v10}	ε_{v20}	ε_{v30}
6A1	NOT RELIABLE TEST															
6A2	28.1	-53	-256	-437	-4833			-9356	26.6		-3734	-1526	-2328	-38	-208	-366
6A3	26.5	-232	-441	-577	-5589			-9470	25.8		-3572	-1326	-2399	-296	-382	-478
6K1	23.9	-92	-200	-326	-2021			-13535	42.8	8736	-3843	-1119	-1875			
6K2	22.3	-98	-200	-334	-2078			-17599	42.7	11502	-4434	-1335	-2240			
6L1	20.5	-119	-235	-351	-2538			-21556	46.5	5500						
6L2	22.8	-99	-218	-339	-2402			-17357	46.9	6732						
6M1	18.6	-83	-184	-292	-2339			-28700	54.9	10328		-9009	-25462			
6M2	20.9	-98	-214	-320	-2277			-26632	56.9	8866		-9053	-23081			
6Q1	20.8	-70	-162	-260	-3588			-7320	19.7		-1744	-522	-1049	-50	-118	-170
6Q2	23.3	-98	-203	-316	-3679			-5303	22.0		-2044	-574	-1304	66.7	-17	-98
6Q3	23.9	-118	-217	-325	-3373			-6710	22.4		-1996	-620	-1230	-91	-165	-230
6R1	25.3	-84	-189	-304	-2962			-5247	24.1		-1777	-531	-1030	-70	-148	-230
6R2	25.7	-114	-224	-345	-2883			-5298	24.5		-1785	-502	-1132	-88	-163	-234
6R3	24.6	-97	-205	-325	-2812	-5069		-5069	20.9		-1777	-495	-1114	-73	-151	-224

Table 4-1; Compression test results for cylindrical specimens

No.	f_c'	ε_{10}	ε_{20}	ε_{30}	ε_c	ε_{85}	ε_{50}	ε_{min}	f_r	$\varepsilon_{3\,max}$	ε^*	$\varepsilon_{v\,min}$	$\varepsilon_{1\,min}$	ε_{v10}	ε_{v20}	ε_{v30}
7A1	44.7	-325	-547	-783	-3653	-5689		-8817	27.0		-4005	-1737	-2805	-280	-464	-645
7A2	42.2	-409	-648	-866	-3542	-5698		-7669	28.8		-3936	-1806	-2576	-385	-590	-769
7A3	38.5	-249	-476	-676	-3298	-5384		-6987	26.2		-3127	-1302	-2286	-212	-386	-537
7B1	78.6	-539	-977	-1399	-11758			-28967	68.9		-12136	-3731	-6015			
7B2	77.3	-381	-815	-1212	-12438			-27689	69.9		-19516	-6822	-10296			
7C1	94.4	-266	-770	-1276	-22045			-38446	93.0							
7C2	96.9	-388	-887	-1400	-25384			-40130	94.5		-22330	-3503	-14395			
7D1	120.5	-346	-831	-1479	-41529			-41529	120.5							
7D2	122.2	-149	-765	-1423	-42865			-42865	122.2			-12818	-28818			
7E1	139.0	-401	-1085	-1899	-42050			-42050	139.0			-16644	-27569			
7E2	138.5	-53	-803	-1628	-44520			-44520	138.5			-21638	-43338			
7F1	44.9	-411	-706	-980	-4217	-6594		-8121	31.1					-410	-704	-976
7F2	47.9	-469	-796	-1077	-4494	-6693		-8666	29.7					-468	-794	-1074
7G1	79.2	-847	-1312	-1773	-13400	-33497		-38128	65.1		-12527	-4239	-6616			
7G2	80.0	-865	-1421	-1904	-11064	-24744		-31480	64.2		-19875	-5040	-8956			
7H1	107.0	-289	-878	-1473	-16989			-24370	105.0		-17483	-5608	-9310			
7H2	NOT RELIABLE RESULTS															
7I1	130.4	-269	-970	-1721	-24266			-37402	127.0			-9814	-24266			
7I2	132.0	-363	-1091	-1893	-26590			-38535	128.5		-24694	-7481	-12971			
7K1	51.2	-154	-327	-507	-3305			-10188	55.5	10558	-3401	-1158	-1875			
7K2	51.2	-153	-345	-537	-3196			-10553	55.6	11858	-3442	-1313	-2214			
7L1	49.3	-161	-324	-497	-2653			-17140	68.7	9754	-7780	-2118	-3488			
7L2	47.4	-167	-319	-494	-2553			-14679	63.5	8085	-9756	-2534	-3681			
7M1	50.0	-143	-296	-454	-2449			-15490	75.1	8984	-10578	-2141	-3091			
7M2	49.5	-148	-318	-480	-2611			-17024	76.0	10778	-6027	-1590	-2392			
7N1	45.3	-328	-568	-819	-3519			-15776	55.7	10243	-6328	-2331	-3042			
7N2	43.1	-255	-500	-726	-3124			-14078	55.3	8498	-7484	-2598	-3579			
7O1	52.7	-480	-779	-1041	-4000			-34531	101.2	10550						
7O2	57.5	-335	-638	-945	-4907			-31898	102.7	9398						
7P1	51.3	-467	-735	-990	-4356			-36044	100.3	6685						
7P2	45.7	-452	-796	-1046	-3678			-47516	119.3	7453						
7Q1	37.1	-107	-240	-373	-2376	-4017	-8658	-8697	18.2		-2410	-785	-1632	-97	-203	-278
7Q2	40.0	-145	-274	-417	-2436	-4216		-7717	23.6		-2283	-690	-1506	-80	-144	-187
7Q3	37.8	-138	-277	-418	-2392	-3417	-5074	-5277	17.7		-2326	-752	-1481	-105	-198	-285
7R1	38.6	-117	-247	-389	-2389	-3396		-5487	22.5		-2389	-748	-1658	-83	-178	-274
7R2	39.3	-159	-306	-458	-2700	-4332		-5377	27.7		-2542	-809	-1651	-139	-222	-310
7R3	41.7	-135	-276	-421	-2640	-3814		-4488	28.3		-2491	-815	-1738	-97	-192	-297

Table 4-1; Compression test results for cylindrical specimens

No.	f_c'	ε_{10}	ε_{20}	ε_{30}	ε_c	ε_{85}	ε_{50}	ε_{min}	f_c	$\varepsilon_{3\,max}$	ε^*	$\varepsilon_{v\,min}$	$\varepsilon_{1\,min}$	ε_{v10}	ε_{v20}	ε_{v30}
8A1	33.3	-457	-658	-877	-5002	-9300		-9315	27.9		-4142	-1652	-2745	-417	-578	-749
8A2	36.2	-472	-699	-931	-5463			-10267	33.0		-4511	-1701	-2704	-425	-606	-789
8A3	32.6	-252	-471	-678	-4488			-9489	29.4		-3659	-1373	-2260	-208	-389	-544
8K1	34.8	-195	-278	-437	-2590			-14882	53.5	10145	-5065	-1405	-2715			
8K2	34.8	-136	-309	-481	-2950			-12766	48.1	8790	-4180	-1086	-1990			
8L1	34.9	-137	-276	-428	-2538			-18059	59.0	6919		-4803	-15650			
8L2	33.9	-121	-266	-422	-2506			-18339	62.2	7820		-2856	-17074			
8M1	37.1	-147	-302	-453	-2668			-23248	71.5	8892		-5635	-22177			
8M2	32.9	-112	-255	-394	-2506			-24606	65.7	7878		-9261	-23540			
8Q1	31.2	-113	-236	-381	-3762			-9719	27.7		-2851	-889	-1621	-99	-198	-302
8Q2	29.0	-122	-246	-383	-4178			-6609	27.9		-2291	-642	-1265	-101	-198	-287
8Q3	29.1	-123	-255	-409	-5297			-9658	27.5		-1954	-452	-1069	-84	-170	-258
8R1	26.9	-112	-237	-366	-4265			-7073	26.2		-2259	-607	-1321	-84	-160	-239
8R2	26.7	-110	-226	-355	-4610			-6513	25.5		-1890	-485	-1132	-87	-159	-237
8R3	27.5	-110	-235	-365	-4517			-6494	26.0		-2072	-600	-1210	-87	-182	-280

Table 4-1: Compression test results for cylindrical specimens

No.	f_c	ε_{10}	ε_{20}	ε_{30}	ε_c	ε_{85}	ε_{50}	ε_{min}	f_r	$\varepsilon_{3\,max}$	ε^*	$\varepsilon_{v\,min}$	$\varepsilon_{1\,min}$	ε_{v10}	ε_{v20}	ε_{v30}
9A1	45.4	-766	-1074	-1309	-3935	-5208		-8185	24.4		-4682	-2378	-3534	-701	-951	-1130
9A2	49.6	-343	-594	-837	-3531	-4209	-5261	-8821	12.7		-3743	-1635	-2997	-281	-475	-649
9A3	51.2	-413	-695	-930	-3470	-4341	-5943	-7068	21.7		-3822	-1739	-2860	-353	-571	-733
9K1	53.2	-161	-335	-514	-2491			-8627	57.9	10236	-3537	-1373	-2318			
9K2	58.7	-170	-350	-547	-3070	-4990		-5932	47.4	11543	-3277	-1518	-2501			
9L1	49.2	-166	-354	-529	-2522			-10021	66.1	10041	-4416	-1768	-2522			
9L2	54.8	-151	-333	-522	-2632			-10632	67.7	7734	-4713	-1941	-2856			
9M1	55.7	-171	-340	-532	-2632			-11760	66.6	11032	-5602	-2141	-2778			
9M2	57.1	-172	-332	-501	-2527			-12595	74.8	11748	-3849	-1421	-2115			
9Q1	47.8	-123	-255	-391	-1905	-2406	-4977	-5439	21.9		-1690	-408	-1047	-92	-171	-234
9Q2	42.7	-101	-238	-390	-2272	-2927	-5241	-5302	21.0		-2408	-826	-1676	-67	-160	-260
9Q3	47.5	-170	-321	-485	-2543	-3151		-3899	24.0		-2657	-890	-1910	-116	-211	-302
9R1	43.0	-131	-263	-403	-2171	-2797	-4337	-4393	21.2		-2351	-736	-1775	-77	-146	-216
9R2	42.7	-101	-238	-393	-2272	-2927	-5241	5302	21.0		-2408	-826	-1676	-67	-160	-261
9R3	44.4	-134	-278	-431	-2407	-2856	-4148	-5026	18.8		-2454	-863	-1853	-102	-184	-268

Table 4-1: Compression test results for cylindrical specimens

No.	P1 (Kn)	D1 (mm)	P2 (kN)	D2 (mm)	P3 (kN)	D3 (mm)	P4 (kN)	D4 (mm)	Pmin (kN)	Dmin (mm)
1S1	18.1	0.46								
1S2	18.2	0.41								
1S3	17.5	0.4								
2S1	17.5	0.44								
2S2	18.1	0.42								
2S3	17.6	0.41								
3S1	17.8	0.41								
3S2	18.8	0.43								
3S3	18.3	0.43								
4S1	17.5	0.4	10.5	0.6	9.9	1.05	5.7	2.3	3.4	4.3
4S2	19.8	0.45	12.7	0.6	12	1.15	7.1	3.3	4.3	5.8
4S3	18.4	0.4	12.7	0.6	12.2	1.1	4.7	3.6	2.8	6.35
5S1	17	0.47	15.3	0.65	16.5	0.95	10.4	2.9	6.3	5.75
5S2	17.6	0.6	15.2	0.7	14.8	0.9	6.9	3.2	3.5	5.7
5S3	18.4	0.5	14.6	0.8	12.6	1.74	7.4	4.26	4.3	8
6S1	14.3	0.5	14	0.5	15.6	1.76	8.8	6.25	6.7	7.65
6S2	13.4	0.4	13.25	0.5	15	2	6.25	6	3.3	8.2
6S3	13.8	0.35	13.6	0.4	15	1	6.75	5.25	3.6	8.1
7S1	16.5	0.5	9.2	0.8	8.9	1.8	5.1	3.9	3.4	5.55
7S2	17.85	0.44	8.6	0.75	8.9	1.3	3.8	3.5	2.1	5.23
7S3	15.6	0.35	8.15	0.56	8.5	1.16	3.6	3	1.45	5.4
8S1	16.5	0.53	15.1	0.7	16	1.28	7.1	3.75	5.7	5.68
8S2	18.5	0.6	15.9	0.77	16.6	1.72	11	3.85	7.4	4.94
8S3	17.5	0.58	15.6	0.97	16.15	1.35	8.1	3.8	4.7	5.4
9S1	13.6	0.35	6.95	0.58	8.6	1.65	4.4	4.6	3.7	5.3
9S2	12.9	0.3	4.7	0.65	5.5	1.75	3.2	4	2.3	5.23
9S3	13.8	0.3	6.7	0.6	8	1.65	4.4	4.7	3.3	6.08

No.	P1 (Kn)	D1 (mm)	P2 (kN)	D2 (mm)	P3 (kN)	D3 (mm)	P4 (kN)	D4 (mm)	Pmin (kN)	Dmin (mm)
1S	17.93	0.42								
2S	17.73	0.42								
3S	18.30	0.42								
4S	18.57	0.42	11.97	0.60	11.37	1.10	5.83	3.07	3.50	5.48
5S	17.67	0.52	15.03	0.72	14.63	1.20	8.23	3.45	4.70	6.48
6S	13.83	0.42	13.62	0.47	15.20	1.59	7.27	5.83	4.53	7.98
7S	16.65	0.43	8.65	0.70	8.77	1.42	4.17	3.47	2.32	5.39
8S	17.50	0.57	15.53	0.81	16.25	1.45	8.73	3.80	5.93	5.34
9S	13.43	0.32	6.12	0.61	7.37	1.68	4.00	4.43	3.10	5.54

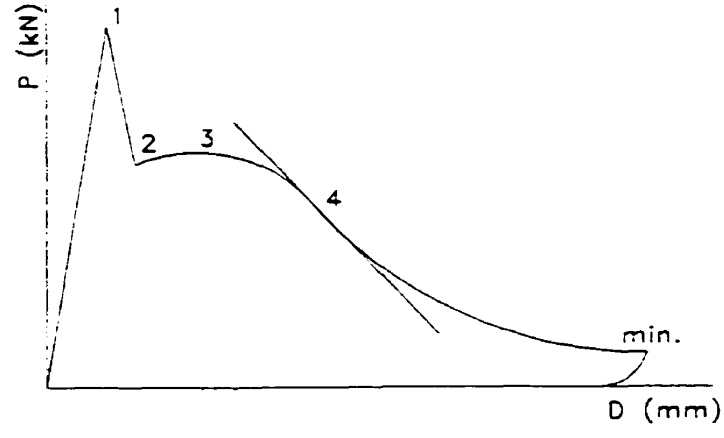

Table 4-2; Summary of Bending test results for prism specimens

Top: for each specimen; Bottom: average values

No.	f_c	f_{cc}	E_{20}	E_{30}	E_{avg}	E (Mpa)	ν_{20}	ν_{30}	ν_{avg}	ν	S_{33} (MPa)	S_{11} (MPa)	S' (MPa)	σ_3/f_c	σ_3/f_{cc}
1A1	56.1		19147	19894	19520		0.123	0.137	0.130		-31271	-26799	-29326	0.00%	0.00%
1A2		56.1				19395				0.161					0.00%
1A3	56.1		18889	19650	19269		0.155	0.229	0.192			-12635	-22466	0.00%	0.00%
1B1	105.6	104.7	21728	20605	21167	18440					-4044	-1522	-1814	20.00%	18.90%
1B2	103.8		14741	16685	15713							-1088	-1007	20.00%	18.90%
1C1	127.7	125.1	21568	20795	21181	21586						-7033	-30	40.00%	37.79%
1C2	122.5		22347	21636	21991							-1830	-208	40.00%	37.79%
1D1		162.0				22533									0.00%
1D2	162.0		22753	22314	22533							-13470	-114	60.00%	56.69%
1E1	187.4	185.7	21867	20719	21293	20781							0	80.00%	75.58%
1E2	184.0		20744	19796	20270								---	80.00%	75.58%
1F1	66.7	65.8	19277	19503	19390	20703	0.097	0.107	0.102	0.088			-7358	0.00%	0.00%
1F2	64.8		17851	26182	22017		0.074		0.074				-10309	0.00%	0.00%
1G1	106.2	106.8	19925	20423	20174	19007					-3742	-2147	-2171	20.00%	18.90%
1G2	107.4		17351	18328	17839						-4263	-1848	-2877	20.00%	18.90%
1H1	157.6	148.9	18589	18285	18437	18651							-5634	40.00%	37.79%
1H2	140.1		18680	19048	18864						-9728	-3288	-11984	40.00%	37.79%
1I1	176.0	176.7	19753	19469	19611	20659						-60970	68	60.00%	56.69%
1I2	177.3		22052	21361	21707								-286667	60.00%	56.69%
1K1	67.6	68.4	33465	33137	33301	33537						-11267	-4905	7.84%	7.40%
1K2	69.1		35255	32290	33772							-7258	-6113	6.54%	6.18%
1L1	70.7	70.4	33667	33115	33391	33346						-14607	-1452	10.58%	9.99%
1L2	70.1		33223	33381	33302							-7841	-4074	10.37%	9.80%
1M1		71.1				71284									0.00%
1M2	71.1		34019	108550	71284							-12175	489	20.29%	19.17%
1N1	74.9	72.0	20577	20980	20779	21119						-6855	-999	15.88%	15.00%
1N2	69.1		21393	21526	21460							-9254	-4485	7.53%	7.12%
1O1	73.5	74.3	12850	13973	13412	16221							1220	32.16%	30.38%
1O2	75.1		18452	19608	19030								1485	33.27%	31.44%
1P1	76.3	89.4	16269	18254	17261	28918							1699	35.15%	33.21%
1P2	102.4		40016	41133	40574								978	42.35%	40.01%
1Q1	53.3		33522	32205	32864		0.437	0.350	0.394		-22856	-16519	-19510	0.00%	0.00%
1Q2	56.4	54.9	32601	31864	32233	32548	0.364	0.395	0.380	0.387	9775		-27273	0.00%	0.00%
1Q3														0.00%	0.00%
1R1	56.8		41460	40000	40730		0.201	0.211	0.206				0	0.00%	0.00%
1R2	55.9	54.6	38552	37391	37972	38786	0.284	0.258	0.271	0.251			-21377	0.00%	0.00%
1R3	51.2		38209	37101	37655		0.284	0.266	0.275				-4918	0.00%	0.00%

Table 4-3; Mechanical properties obtained from compression tests

No.	f_c	f_{cc}	E_{10}	E_{30}	E_{avg}	E (Mpa)	ν_{20}	ν_{30}	ν_{avg}	ν	S_{30} (MPa)	S_{33} (MPa)	S' (MPa)	σ_3/f_c	σ_3/f_{cc}
2A1	58.4		20208	21159	20684		0.111	0.122	0.117		-19274	-9144.1	-16429	0.00%	0.00%
2A2	60.7	58.8	23080	22153	22617	21018	0.120	0.139	0.129	0.115	-17759	-11886	-17246	0.00%	0.00%
2A3	57.3		18787	20723	19755		0.093	0.102	0.098		-13521	-8055.3	-12634	0.00%	0.00%
2K1	65.6	64.3	31845	30871	31358	32218							-850.64	9.36%	8.76%
2K2	62.9		33817	32339	33078								-884.96	9.72%	9.10%
2L1	65.0	65.1	34211	34121	34166	31828							-294.88	15.28%	14.30%
2L2	65.1		29591	29391	29491								-144.47	13.66%	12.79%
2M1	67.4	64.8	33039	33120	33080	31799							1292.61	26.43%	24.73%
2M2	62.1		30743	30293	30518								78.0539	18.79%	17.58%
2Q1	47.8		28795	29689	29242			0.303	0.303			-9239.7	-19602	0.00%	0.00%
2Q2	48.0	47.8	32215	33103	32659	31359	0.111	0.116	0.113	0.200		-23607	-21895	0.00%	0.00%
2Q3	47.6		32828	31523	32175		0.224	0.142	0.183			-12483	-9170.9	0.00%	0.00%
2R1	47.2		34963	33594	34279		0.107	0.114	0.111				-6837.6	0.00%	0.00%
2R2	44.0	45.7	40968	41431	41200	36982	0.239	0.161	0.200	0.160			-12500	0.00%	0.00%
2R3	46.0		36220	34717	35469		0.165	0.174	0.169				-6194.7	0.00%	0.00%

Table 4-3: Mechanical properties obtained from compression tests

No.	f_c	f_{cc}	E_{20}	E_{30}	E_{avg}	E (Mpa)	ν_{20}	ν_{30}	ν_{avg}	ν	S_{33} (MPa)	S_{11} (MPa)	S' (MPa)	σ_3 / f_c	σ_3 / f_{cc}
3A1	49.3		18534	20372	19453		0.120	0.113	0.116		-9351.3	-5510.4	-6861.2	0.00%	0.00%
3A2	49.2	49.2	19919	19879	19899	18545	0.121	0.126	0.124	0.109	-10710	-10082	-6873.1	0.00%	0.00%
3A3	49.0		15756	16810	16283		0.079	0.097	0.088		-10538	-7492.4	-9593.9	0.00%	0.00%
3B1	87.4	88.2	39369	41520	40445	30512						-1091.9	-963.66	20.00%	18.89%
3B2	88.9		20626	20531	20579							-1136.2	-998.06	20.00%	18.89%
3C1	104.8	104.3	18549	19229	18889	19999							-1385.2	40.00%	37.78%
3C2	103.8		21012	21205	21109								-444.08	40.00%	37.78%
3D1	137.0	140.5	19826	19516	19671	20341							-273.02	60.00%	56.67%
3D2	144.0		21525	20498	21011								---	60.00%	56.67%
3E1	147.4	147.8	20164	19745	19955	19582							---	80.00%	75.56%
3E2	148.1		19359	19060	19210								-816.33	80.00%	75.56%
3F1	60.4	56.7	16966	17609	17288	17056	0.098	0.114	0.106	0.102	-12337	-8236.4	-10514	0.00%	0.00%
3F2	52.9		16277	17373	16825		0.095	0.101	0.098		-15876	-9968.6	-7037.3	0.00%	0.00%
3G1	93.7	84.8	20414	20043	20228	19155						-862.91	-816.16	20.00%	18.89%
3G2	75.8		17877	18287	18082							-1747.1	-1415.4	20.00%	18.89%
3H1	120.2	125.1	19513	19064	19289	19364					-3168.8	-992.95	-4070.8	40.00%	37.78%
3H2	130.0		19432	19447	19439								-392.59	40.00%	37.78%
3I1	136.2	143.5	20605	19840	20222	20459							-228.38	60.00%	56.67%
3I2	150.7		20902	20489	20695								-398.41	60.00%	56.67%
3K1	62.0	60.5	32124	30769	31447	31304							-29.757	11.47%	10.84%
3k2	59.0		32065	30256	31161								58.2751	8.12%	7.67%
3L1	59.6	58.9	33672	28654	31163	31334							704.225	14.48%	13.68%
3L2	58.2		31803	31206	31505								262.655	16.57%	15.65%
3M1	73.1	65.2	39301	39407	39354	34864							1198.79	24.86%	23.48%
3M2	57.3		29689	31057	30373								1098.9	25.19%	23.79%
3N1	65.1	62.2	20344	20440	20392	19864							327.364	17.87%	16.88%
3N2	59.3		19068	19603	19335								160.406	16.44%	15.53%
3O1	62.1	65.7	17298	18482	17890	18735							1306.54	30.95%	29.23%
3O2	69.3		19304	19857	19580								1386.89	37.66%	35.57%
3P1	63.1	65.1	19843	20355	20099	20210							1312.57	51.59%	48.73%
3P2	67.0		20120	20521	20320								1553.19	50.75%	47.93%
3Q1	48.9		34437	33724	34080		0.208	0.210	0.209		-6932.2	-6656.1	-6553.8	0.00%	0.00%
3Q2	46.0	47.3	29870	29206	29538	31343	0.185	0.197	0.191	0.192	-6248.3	-4154.1	-6404.2	0.00%	0.00%
3Q3	46.9		30855	29968	30412		0.158	0.195	0.176		-7039.9	-3583.8	-7320.4	0.00%	0.00%
3R1	46.5		28882	28354	28618		0.186	0.191	0.188		-9300	-6623.9	-8256.3	0.00%	0.00%
3R2	46.3	47.0	28580	28061	28320	29488	0.127	0.150	0.138	0.163	-17289	-6060.2	-16393	0.00%	0.00%
3R3	48.2		32349	30701	31525		0.161	0.166	0.163		-15629	-7201.2	-15615	0.00%	0.00%

Table 4-3: Mechanical properties obtained from compression tests

No.	f_c	f_{cc}	E_{20}	E_{30}	E_{avg}	E (Mpa)	ν_{20}	ν_{30}	ν_{avg}	ν	S_{30} (MPa)	S_{33} (MPa)	S' (MPa)	σ_3 / f_c	σ_3 / f_{cc}
4A1	53.1		13477	14832	14155		0.079	0.089	0.084		-14808	-9426	-11938	0.00%	0.00%
4A2	53.8	54.1	16205	17668	16937	16972	0.081	0.103	0.092	0.098	-9545.8	-5960.1	-9185.2	0.00%	0.00%
4A3	55.5		20109	19542	19825		0.116	0.117	0.117		-14737	-9068.6	-11902	0.00%	0.00%
4K1	69.0	69.1	32394	31724	32059	32175							-1637.4	8.03%	7.55%
4K2	69.1		32140	32441	32290								-1803.1	9.85%	9.26%
4L1	67.7	67.1	32392	32162	32277	32007							-347.86	14.66%	13.78%
4L2	66.4		31321	32155	31738								503.931	13.34%	12.54%
4M1	72.1	71.5	32624	35000	33812	34294							1488.97	34.08%	32.04%
4M2	70.8		35758	33795	34776								402.361	25.88%	24.33%
4Q1	54.2		35658	33665	34661		0.263	0.252	0.257		-14233	-13803	-9572.5	0.00%	0.00%
4Q2	56.8	55.9	31209	30293	30751	33582	0.231	0.216	0.223	0.241		-10979	-12659	0.00%	0.00%
4Q3	56.6		36051	34618	35334		0.245	0.242	0.243			-10156	-16753	0.00%	0.00%
4R1	54.1		34459	33089	33774		0.220	0.220	0.220			-11041	-12000	0.00%	0.00%
4R2	43.8	49.4	39818	38087	38953	35166	0.141	0.167	0.154	0.171		-15279	-17273	0.00%	0.00%
4R3	50.2		33467	32077	32772		0.137	0.142	0.139				-13333	0.00%	0.00%

Table 4-3: Mechanical properties obtained from compression tests

No.	f_c	f_{cc}	E_{20}	E_{30}	E_{avg}	E (Mpa)	ν_{20}	ν_{30}	ν_{avg}	ν	S_{30} (MPa)	S_{33} (MPa)	S^* (MPa)	σ_3/f_c	σ_3/f_{cc}
5A1	49.0		17314	17531	17423		0.120	0.122	0.121		-4954.5	-5392.5	-3892.2	0.00%	0.00%
5A2	43.6	46.7	9045.6	10381	9713.3	14769	0.066	0.080	0.073	0.105	-4105.5	-5338.8	-4096.6	0.00%	0.00%
5A3	47.5		16844	17495	17170		0.115	0.129	0.122			-10587	-7460.3	0.00%	0.00%
5B1	81.6	82.8	14341	16126	15234	16121							-569.45	20.00%	18.96%
5B2	84.0		16535	17482	17009								-505.8	20.00%	18.96%
5C1	94.1	99.4	18166	18272	18219	16923							-151.79	40.00%	37.92%
5C2	104.6		15873	15382	15627								-35.236	40.00%	37.92%
5D1	123.7	124.8	19002	19163	19082	17964							-411.52	60.00%	56.87%
5D2	125.8		15985	17706	16845								-1083	60.00%	56.87%
5E1	141.7	140.7	19159	19064	19111	18151							-1079.1	80.00%	75.83%
5E2	139.6		16921	17461	17191								---	80.00%	75.83%
5F1	56.4	57.9	16937	16184	16560	16541	0.114	0.111	0.113	0.104		-4850.9	-3666.3	0.00%	0.00%
5F2	59.3		16291	16751	16521		0.092	0.097	0.094		-4874.2	-5250.9	-4695.9	0.00%	0.00%
5G1	92.4	91.1	17634	17855	17744	18235						-813.71	-682.81	20.00%	18.96%
5G2	89.7		18727	18727	18727							-1163.6	-672.94	20.00%	18.96%
5H1		112.0				18219									0.00%
5H2	112.0		18152	18286	18219								-456.72	40.00%	37.92%
5I1	144.4	142.6	19357	19593	19475	19060							-104.17	60.00%	56.87%
5I2	140.7		18368	18924	18646								-263.05	60.00%	56.87%
5K1	61.5	59.7	30147	29216	29682	30469							-406.65	9.97%	9.45%
5K2	57.9		31467	31046	31256								-572.18	10.40%	9.86%
5L1	60.1	60.9	31968	28019	29993	30031							1328.86	17.27%	16.37%
5L2	61.7		30545	29592	30068								-155.07	15.10%	14.31%
5M1	65.3	64.3	32010	32569	32289	31376							1557.38	28.87%	27.36%
5M2	63.2		30829	30095	30462								1386.64	26.23%	24.86%
5N1	64.1	61.2	19077	18798	18938	19090							460.111	21.83%	20.70%
5N2	58.2		20069	18418	19243								-71.174	21.60%	20.48%
5O1	63.1	60.9	12957	13512	13234	16368							1206.72	44.65%	42.32%
5O2	58.6		19664	19340	19502								1188.85	29.42%	27.88%
5P1	63.5	67.8	14871	16755	15813	18236							1217.81	48.64%	46.11%
5P2	72.1		20600	20718	20659								1514.64	43.45%	41.19%
5Q1	48.0		30769	29814	30291		0.221	0.216	0.218			-37306	-38022	0.00%	0.00%
5Q2	48.5	47.8	44091	44091	44091	34918	0.209	0.257	0.233	0.190	-8189.8	-61653	-8022.4	0.00%	0.00%
5Q3	46.9		31060	29684	30372		0.106	0.128	0.117			-9481.1	-12664	0.00%	0.00%
5R1	45.3		28491	27706	28098		0.208	0.197	0.202		-19644	-11900	-20302	0.00%	0.00%
5R2	45.5	45.7	29739	28616	29177	28814	0.275	0.222	0.248	0.222		-13075	-10526	0.00%	0.00%
5R3	46.3		29304	29028	29166		0.215	0.215	0.215			-128611	-15333	0.00%	0.00%

Table 4-3: Mechanical properties obtained from compression tests

No.	f_c	f_{cc}	E_{20}	E_{30}	E_{avg}	E (Mpa)	ν_{20}	ν_{30}	ν_{avg}	ν	S_{33} (MPa)	S_{11} (MPa)	S (MPa)	σ_1/f_c	σ_1/f_{cc}
6A1															0.00%
6A2	28.1	27.3	13842	14635	14239	14130	0.081	0.073	0.077	0.171			-331.64	0.00%	0.00%
6A3	26.5		12679	15362	14021		0.294	0.236	0.265				-180.37	0.00%	0.00%
6K1	23.9	23.1	22130	20427	21278	20830							1641.48	16.00%	15.02%
6K2	22.3		21863	18898	20381								1314.35	21.07%	19.78%
6L1	20.5	21.7	17672	17672	17672	18376							1367.13	20.15%	18.91%
6L2	22.8		19160	19000	19080								1611.5	24.67%	23.15%
6M1	18.6	19.8	18416	17799	18107	18265							1377.03	56.76%	53.27%
6M2	20.9		18017	18829	18423								1478.14	48.73%	45.73%
6Q1	20.8		22609	21895	22252		0.130	0.184	0.157				-294.75	0.00%	0.00%
6Q2	23.3	22.7	22190	21376	21783	22551	0.101	0.122	0.112	0.138			-800.49	0.00%	0.00%
6Q3	23.9		24141	23092	23617		0.126	0.164	0.145				-449.51	0.00%	0.00%
6R1	25.3		24095	23000	23548		0.129	0.136	0.132				-525.16	0.00%	0.00%
6R2	25.7	25.2	23364	22251	22807	22844	0.159	0.184	0.172	0.153			-496.89	0.00%	0.00%
6R3	24.6		22778	21579	22178		0.139	0.169	0.154			-1634.9	-1639.3	0.00%	0.00%

Table 4-3: Mechanical properties obtained from compression tests

No.	f_c	f_{cc}	E_{20}	E_{30}	E_{avg}	E (Mpa)	ν_{20}	ν_{30}	ν_{avg}	ν	S_{33} (MPa)	S_{33} (MPa)	S' (MPa)	σ_3/f_c	σ_3/f_{cc}
7A1	44.7		20135	19520	19827		0.086	0.102	0.094			-3293.2	-3427.6	0.00%	0.00%
7A2	42.2	41.8	17657	18468	18063	18462	0.071	0.080	0.075	0.096		-2936	-3246.9	0.00%	0.00%
7A3	38.5		16960	18033	17497		0.117	0.119	0.118			-2768.5	-3334.2	0.00%	0.00%
7B1	78.6	78.0	17945	18279	18112	18160							-563.66	20.00%	18.80%
7B2	77.3		17811	18604	18208								-485.21	20.00%	18.80%
7C1	94.4	95.7	18730	18693	18712	18998							-85.361	40.00%	37.60%
7C2	96.9		19419	19150	19285								-162.76	40.00%	37.60%
7D1	120.5	121.4	24845	21271	23058	21284							---	60.00%	56.41%
7D2	122.2		19838	19184	19511								---	60.00%	56.41%
7E1	139.0	138.8	20322	18558	19440	18733							---	80.00%	75.21%
7E2	138.5		18467	17587	18027								---	80.00%	75.21%
7F1	44.9	46.4	15220	15782	15501	15352	0.002	0.003	0.002	0.002		-2833.4	-3534.8	0.00%	0.00%
7F2	47.9		14648	15757	15202		0.002	0.002	0.002			-3267.4	-4362.4	0.00%	0.00%
7G1	79.2	79.6	17032	17106	17069	15982						-591.13	-570.2	20.00%	18.80%
7G2	80.0		14388	15399	14894							-877.19	-773.9	20.00%	18.80%
7H1	107.0	107.0	18166	18074	18120	18120							-270.97	40.00%	37.60%
7H2														40.00%	37.60%
7I1	130.4	131.2	18602	17961	18282	17988							-258.83	60.00%	56.41%
7I2	132.0		18132	17255	17693								-293.01	60.00%	56.41%
7K1	51.2	51.2	29595	29008	29302	27984							624.728	12.63%	11.88%
7K2	51.2		26667	26667	26667								598.07	14.19%	13.34%
7L1	49.3	48.4	30245	29345	29795	29941							1339.13	23.34%	21.94%
7L2	47.4		31184	28991	30088								1327.73	19.35%	18.19%
7M1	50.0	49.8	32680	32154	32417	30943							1924.7	32.25%	30.32%
7M2	49.5		29118	29819	29468								1838.62	38.69%	36.37%
7N1	45.3	44.2	18875	18452	18664	18305							848.495	23.06%	21.68%
7N2	43.1		17592	18301	17947								1113.75	19.13%	17.99%
7O1	52.7	55.1	17625	18788	18207	18561							1588.55	47.50%	44.66%
7O2	57.5		18977	18852	18915								1674.63	42.31%	39.78%
7P1	51.3	48.5	19142	19618	19380	16858							1546.33	45.15%	42.44%
7P2	45.7		13285	15387	14336								1678.91	50.34%	47.32%
7Q1	37.1		27895	27895	27895		0.102	0.160	0.131		-2952.9	-3391.2	-2990	0.00%	0.00%
7Q2	40.0	38.3	31008	29412	30210	28401	0.252	0.303	0.278	0.193		-3370.8	-3105.5	0.00%	0.00%
7Q3	37.8		27194	27000	27097		0.165	0.179	0.172		-7047	-5531.7	-6967.1	0.00%	0.00%
7R1	38.6		29692	28382	29037		0.135	0.149	0.142			-5749.8	-5196.9	0.00%	0.00%
7R2	39.3	39.9	26735	26288	26511	28305	0.218	0.214	0.216	0.171		-3612.1	-4333.2	0.00%	0.00%
7R3	41.7		29574	29161	29368		0.163	0.150	0.157			-5327.9	-7251.1	0.00%	0.00%

Table 4-3: Mechanical properties obtained from compression tests

No.	f_c	f_{cc}	E_{20}	E_{30}	E_{avg}	E (Mpa)	v_{20}	v_{30}	v_{avg}	v	S_{30} (MPa)	S_{33} (MPa)	S' (MPa)	σ_3 / f_c	σ_3 / f_{cc}
8A1	33.3		16567	15857	16212		0.1	0.1	0.1			-1162.2	-1252	0.00%	0.00%
8A2	36.2	34.0	15947	15773	15860	15723	0.1	0.1	0.1	0.100			-666.11	0.00%	0.00%
8A3	32.6		14886	15305	15096		0.09	0.11	0.1				-639.87	0.00%	0.00%
8K1	34.8	34.8	41928	28760	35344	27744							1521.31	14.91%	13.75%
8K2	34.8		20116	20174	20145								1354.93	12.92%	11.91%
8L1	34.9	34.4	25108	23986	24547	23750							1552.74	20.34%	18.75%
8L2	33.9		23379	22525	22952								1787.41	22.98%	21.20%
8M1	37.1	35.0	23935	24248	24092	23631							1671.53	39.20%	36.15%
8M2	32.9		23007	23333	23170								1484.16	34.73%	32.03%
8Q1	31.2		25366	23284	24325		0.1	0.12	0.11				-587.54	0.00%	0.00%
8Q2	29.0	29.8	23387	22222	22805	22776	0.11	0.14	0.13	0.140			-452.49	0.00%	0.00%
8Q3	29.1		22045	20350	21198		0.17	0.2	0.19				-366.89	0.00%	0.00%
8R1	26.9		21520	21181	21351		0.2	0.19	0.2				-249.29	0.00%	0.00%
8R2	26.7	27.0	23017	21796	22407	21847	0.19	0.19	0.19	0.169			-630.58	0.00%	0.00%
8R3	27.5		22000	21569	21784		0.12	0.12	0.12				-758.73	0.00%	0.00%

Table 4-3: Mechanical properties obtained from compression tests

No.	f_c	f_{cc}	E_{20}	E_{30}	E_{avg}	E (Mpa)	ν_{20}	ν_{30}	ν_{avg}	ν	S_{30} (MPa)	S_{33} (MPa)	S^* (MPa)	σ_3/f_c	σ_3/f_{cc}
9A1	45.4		14740	16722	15731		0.09	0.1	0.1			-5349.6	-4941.2	0.00%	0.00%
9A2	49.6	48.7	19761	20081	19921	18211	0.11	0.13	0.12	0.114	-14335	-10973	-6975.4	0.00%	0.00%
9A3	51.2		18156	19807	18981		0.11	0.13	0.12		-10352	-8817.5	-8199	0.00%	0.00%
9K1	53.2	56.0	30575	30142	30358	31117							765.971	10.51%	9.91%
9K2	58.7		32611	31141	31876							-4585.9	-3948.3	11.85%	11.18%
9L1	49.2	52.0	26170	27107	26639	28232							2253.63	20.61%	19.45%
9L2	54.8		30110	29542	29826								1612.5	15.87%	14.98%
9M1	55.7	56.4	32959	30859	31909	33554							1194.13	33.97%	32.06%
9M2	57.1		35688	34711	35199								1758.05	36.17%	34.14%
9Q1	47.8		36212	35672	35942		0.2	0.24	0.22		-7779.9	-14311	-7328.8	0.00%	0.00%
9Q2	42.7	46.0	31168	29550	30359	32370	0.16	0.17	0.16	0.192	-7191	-9778.6	-7161.7	0.00%	0.00%
9Q3	47.5		31457	30159	30808		0.19	0.2	0.2			-11719	-17330	0.00%	0.00%
9R1	43.0		32576	31618	32097		0.24	0.24	0.24		-9926.1	-10304	-9811	0.00%	0.00%
9R2	42.7	43.4	31168	29247	30207	30890	0.16	0.17	0.16	0.208	-7191	-9778.6	2865.06	0.00%	0.00%
9R3	44.4		30833	29899	30366		0.22	0.22	0.22		-12751	-14833	-9774.7	0.00%	0.00%

Table 4-3: Mechanical properties obtained from compression tests

No.	h (mm)	b (mm)	R (MPa)	ε_R ($\mu\varepsilon$)
1S1	80.25	152.63	6.629047	1337.5
1S2	79.75	153	6.733193	1184.692
1S3	78.88	152.13	6.655672	1143.188
2S1	79.25	157.38	6.373712	1263.406
2S2	77.63	152.88	7.072472	1181.326
2S3	78.75	151.88	6.726877	1169.837
3S1	78.75	152	6.797947	1169.837
3S2	78.13	151	7.342564	1217.243
3S3	78.25	149.88	7.178624	1219.112
4S1	79	151.13	6.679373	1144.928
4S2	80	150	7.425	1304.348
4S3	78.75	151.5	7.050283	1141.304
5S1	79.38	150.5	6.453462	1351.761
5S2	79.88	150.13	6.614112	1736.522
5S3	79.5	151.13	6.934823	1440.217
6S1	79.63	143.38	5.662348	1442.572
6S2	79.5	144.38	5.286473	1152.174
6S3	80.38	143.5	5.358382	1019.312
7S1	80.88	144.63	6.278354	1465.217
7S2	79.38	143.63	7.100246	1265.478
7S3	78.75	143.5	6.31065	998.6413
8S1	78.75	145.38	6.588411	1512.228
8S2	80.5	143.5	7.161938	1750
8S3	78.25	143.88	7.151077	1644.384
9S1	79.75	143.63	5.359631	1011.322
9S2	78.13	143.75	5.292352	849.2391
9S3	79.5	143.88	5.463197	864.1304

No.	R (MPa)	ε_R ($\mu\varepsilon$)
1S	6.67	1222
2S	6.72	1205
3S	7.11	1202
4S	7.05	1197
5S	6.67	1510
6S	5.44	1205
7S	6.56	1243
8S	6.97	1636
9S	5.37	908

Table 4-4: Modulus of Rupture and Its Corresponding Strain

Top: for each specimen; Bottom: average values

4.2.1. Initial Elastic Modulus (E)

The elastic (pre-cracked) modulus is the slope of the tangent to the stress-strain curve at its linear (beginning) part. In this investigation, the very initial part of the curves were not taken into account, because it was felt that disruptions and local nonlinearities due to adjustment of the testing system at the start of loading reduced the reliability of the data. Therefore, the E value was calculated as the average slope of two lines passing through the points of 10%-20%, and 10%-30% of the peak load on the stress-strain curve:

$$E_{20} = \frac{20\% \times f'_c - 10\% \times f'_c}{\varepsilon_{20} - \varepsilon_{10}} = \frac{0.1 f'_c}{\varepsilon_{20} - \varepsilon_{10}} \tag{4-1}$$

$$E_{30} = \frac{30\% \times f'_c - 10\% \times f'_c}{\varepsilon_{30} - \varepsilon_{10}} = \frac{0.2 f'_c}{\varepsilon_{30} - \varepsilon_{10}} \tag{4-2}$$

From the above, E_{avg} was calculated as the average of E_{20} and E_{30}, whereas the rported E is the average of E_{avg} for all the identical specimens.

4.2.2. The Poisson's Ratio (ν)

For uniaxial compression tests, Poisson's ratio is derived as the ratio of the strain in the direction of load to the strain in other directions ($\nu = -\varepsilon_3 / \varepsilon_1$). Considering that by definition the volumetric strain is $\varepsilon_v = \varepsilon_1 + 2\,\varepsilon_3$ (due to axisymmetry), it follows that:

$$\nu = \frac{1}{2}\left(1 - \frac{\varepsilon_v}{\varepsilon_1}\right) \quad \text{or} \tag{4-3}$$

$$\nu = \frac{1}{2}\left(1 - \frac{\Delta\varepsilon_v}{\Delta\varepsilon_1}\right) \tag{4-4}$$

By neglecting the initial part of the curves, for the reasons stated in the preceding, the elastic values of ν were calculated from strain values at 10%, 20% and 30% of the peak load as follows:

$$\nu_{20} = \frac{1}{2}\left(1 - \frac{\varepsilon_{v20} - \varepsilon_{v10}}{\varepsilon_{20} - \varepsilon_{10}}\right) \text{ and} \tag{4-5}$$

$$\nu_{30} = \frac{1}{2}\left(1 - \frac{\varepsilon_{v30} - \varepsilon_{v10}}{\varepsilon_{30} - \varepsilon_{10}}\right) \tag{4-6}$$

From these values, the average Poisson's ratio, ν_{avg}, was calculated as the average of ν_{30} and ν_{20}, whereas ν is taken as the average of ν_{avg} for all the identical specimens.

4.2.3. Softening (S)

Softening, in this report, is defined as the slope of descending branch of the stress-strain curve. Three softening values were calculated for each specimen. First, the slope of a line which passes through the peak and 85% of the peak load on the descending part of curve:

$$S_{85} = \frac{f_c' - 85\% f_c'}{\varepsilon_c - \varepsilon_{-85}} = \frac{0.15 f_c'}{\varepsilon_c - \varepsilon_{-85}} \tag{4-7}$$

Second, the slope of a line which passes through the peak and 50% of the peak load on the descending part of curve:

$$S_{50} = \frac{f_c' - 50\% f_c'}{\varepsilon_c - \varepsilon_{-50}} = \frac{0.5 f_c'}{\varepsilon_c - \varepsilon_{-50}} \tag{4-8}$$

Third, the slope of a line which passes through the peak and the last point on the curve:

$$S' = \frac{f_c' - f_c}{\varepsilon_c - \varepsilon_{min}} \tag{4-9}$$

The significance of any of the three softening values is that it reperesent a measure of ductility of concrete, and hence they are a means of quantifying the effectiveness of confinement or fiber admixtures in enhancing this property of the material.

4.2.4. Passive Confining Pressure (σ_3)

The passive confining pressure is calculated from the recorded circumferential strain of the wrap as (Figure 4-2):

$$\sigma_3 \times D = 2\, n\, \varepsilon_3 \times (E_c \times t) \qquad (4\text{-}10)$$

where n is the number of layers, E_c is the stiffness of the carbon fiber wrap, and t is its thickness. Forca catalogue (Appendix B) has given the value of $E_c \times t$, which here is termed P_c and is equal to 25400 kN per meter length of sheet. Therefore:

$$\sigma_3 = \frac{2\, n\, \varepsilon_c \times P_c}{D} \qquad (4\text{-}11)$$

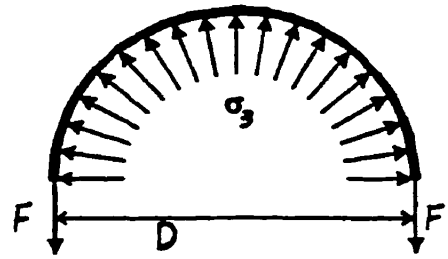

Figure 4-2: Passive Confinement Pressure

4.2.5. Modulus of Rupture

ACI Committee Report (1988) and Loock (1988) suggested extending the formulation of ASTM-C-78 (for plain concrete) to the case of FRC. The modulus of rupture was calculated from the results of prism tests, as following:

$$R = \frac{My}{I} \qquad (4\text{-}12)$$

where R is the Modulus of Rupture (tensile fracture stress), M is the moment corresponding to the peak load, I is the moment inertia, and y is half of the prism depth. In this test:

$$M = \frac{P}{2}\frac{l}{3}$$

By substituing $y = \frac{h}{2}$ and $I = \frac{bh^3}{12}$, it follows that:

$$R = \frac{Pl}{bh^2} \tag{4-13}$$

where P is the total peak load, l is the total span (360 mm), h is average depth of beam, and b is average width of beam.

The tensile strain corresponding to the fracture stress can be obtained by using virtual work. Figure 4-3 plots the actual curveture distribution along the beam under the action of four-point loading.

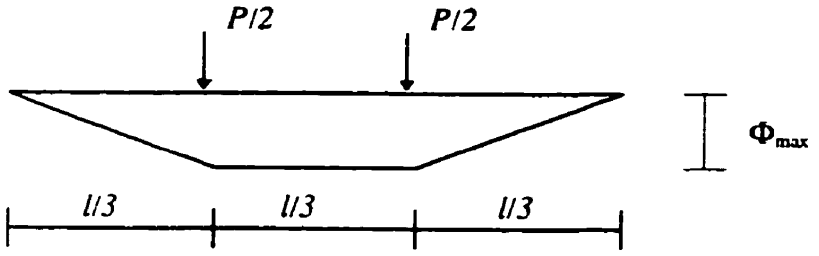

Figure 4-3; Actual Curveture Distribution for Prisms

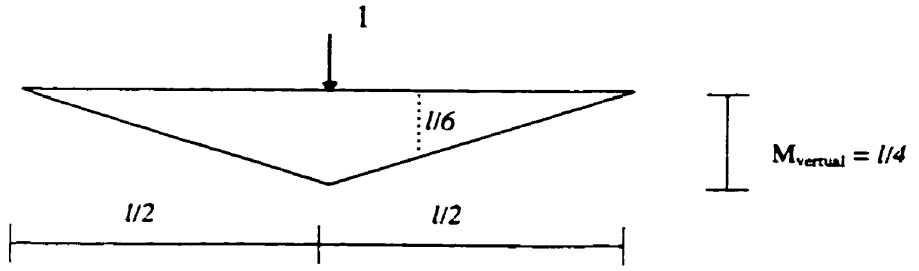

Figure 4-4; Virtual Moment Pattern for Prisms

The applied virtual force pattern is shown in Figure 4-4. Hence, the mid-span deflection δ is obtained from:

$$1 \times \delta = \left(\frac{1}{3}\frac{l}{3}\Phi_{max}\frac{l}{6}\right)2 + \left(\frac{l}{3}\Phi_{max}\frac{l}{6} + \frac{1}{2}\frac{l}{3}\Phi_{max}\frac{l}{12}\right) \tag{4-14}$$

The above simplifies to $\delta = 23/216\ \Phi_{max}\ l^2$. Considering that $\varepsilon_r = \Phi_{max}\ h/2$, the rupture strain at the extreme tension fiber is obtained as:

$$\varepsilon_R = \frac{108}{23}\frac{h}{l^2}\delta \tag{4-15}$$

4.2.6. Void Ratio (VR)

The void ratio of the specimens was calculated from their respective dry and wet weights, as Equation 4-12:

$$VR = \frac{w_w - w_d}{V} \tag{4-12}$$

where VR is void ratio, w_w is the weight of saturated specimen, w_d is the dry weight, and V is the volume of the specimen (for wet and dry definitions refer to section 3.1.4). For Batches 1, 3, 5, and 7 where both dry and wet specimens had been tested, the average void ratios were calculated (Table 4-5) from recorded data (Appendix A). For the other batches two 100×50 mm cylinders were weighted in dry and wet conditions and respective VRs were obtained (Table 4-6).

Sample No.	Length mm	Diameter mm	Volume	W (wet) gr	W (dry) gr	W water (gr)	Void Ratio	Ave. VR	1-VR
1F1	107.40	53.59	242193	541.2	527.0	14.17	5.85%		
1F2	107.44	53.58	242193	539.3	527.9	11.41	4.71%		Batch 1
1G1	107.05	53.57	241268	537.0	529.2	7.83	3.25%	5.52%	0.944804
1G2	107.97	53.62	243797	544.6	537.1	7.48	3.07%		
1H1	107.44	53.56	242057	543.6	526.9	16.71	6.90%		
1H2	107.06	53.64	241888	539.2	523.8	15.36	6.35%		
1I1	107.23	53.58	241776	540.2	523.6	16.63	6.88%		
1I2	107.27	53.59	241956	542.3	525.0	17.30	7.15%		
3F1	107.53	53.64	242984	560.4	544.3	16.07	6.61%		
3F2	107.53	53.66	243177	544.9	529.5	15.41	6.34%		
3G1	107.72	53.62	243243	550.8	539.3	11.46	4.71%		Batch 3
3G2	107.32	56.66	270585	543.8	535.2	8.59	3.17%	6.83%	0.931676
3H1	107.55	53.74	243948	550.1	531.7	18.38	7.53%		
3H2	107.41	53.63	242634	558.2	540.3	17.97	7.41%		
3I1	107.52	53.61	242701	538.9	518.3	20.63	8.50%		
3I2	107.41	53.62	242543	548.8	523.6	25.18	10.38%		
5F1	107.37	53.42	240648	536.0	524.6	11.43	4.75%		
5F2	107.40	53.39	240445	539.2	525.6	13.57	5.64%		
5G1	107.52	53.43	241029	535.5	526.0	9.48	3.93%		Batch 5
5G2	107.46	53.38	240444	529.9	521.5	8.40	3.49%	5.89%	0.941089
5H1				530.6	509.0	21.62			
5H2	107.38	53.54	241753	523.1	505.8	17.33	7.17%		
5I1	107.60	53.37	240712	541.5	519.7	21.82	9.06%		
5I2	107.71	53.46	241771	540.3	522.9	17.37	7.18%		
7F1	107.31	53.57	241809	552.3	533.0	19.34	8.00%		
7F2	107.19	53.57	241595	553.1	532.0	21.13	8.75%		
7G1	107.27	53.54	241494	538.7	530.9	7.85	3.25%		Batch 7
7G2	107.37	53.64	242634	543.7	536.3	7.45	3.07%	5.99%	0.940104
7H1	107.93	53.74	244810	547.6	532.6	14.97	6.11%		
7H2	106.78	53.59	240851	536.6	523.2	13.39	5.56%		
7I1	107.63	53.53	242225	542.4	527.3	15.06	6.22%		
7I2	107.56	53.55	242248	543.5	526.6	16.86	6.96%		

Table 4-5; Void ratios for Batches 1, 3, 5, and 7

Sample No.	Length mm	Diameter mm	Volume	W (wet) gr	W (dry) gr	W water (gr)	Void Ratio	Ave. VR	1-VR
2-1	107.19	53.59	241776	545.44	530.71	14.73	6.09%		
	107.31	53.56	241775						Batch 2
2-2	107.34	53.56	241843	550.78	534.50	16.28	6.73%	6.41%	0.93588
	107.44	53.55	241978						
4-1	107.56	53.51	241886	545.16	529.75	15.41	6.37%		
	107.51	53.49	241593						Batch 4
4-2	107.63	53.52	242134	546.64	533.06	13.58	5.61%	5.99%	0.940104
	107.57	53.48	241638						
6-1	107.48	53.63	242792	534.54	518.96	15.58	6.42%		
	107.46	53.57	242204						Batch 6
6-2	107.71	53.57	242767	542.13	527.85	14.28	5.88%	6.15%	0.938504
	107.85	53.58	243174						
8-1	107.08	53.57	241347	557.27	539.58	17.69	7.33%		
	107.06	53.65	242024						Batch 8
8-2	106.99	53.64	241775	555.71	535.81	19.90	8.23%	7.78%	0.922198
	107.02	53.63	241753						
9-1	107.55	53.59	242588	539.53	526.57	12.96	5.34%		
	107.51	53.56	242226						Batch 9
9-2	107.39	53.58	242136	539.32	525.04	14.28	5.90%	5.62%	0.943801
	107.38	53.60	242295						

Table 4-6; Void ratios for Batches 2, 4, 6, 8, and 9

4.3. Details of Testing

The tests in the following sections refer to the nomenclature given in Table 1-3. Except for nine tests (1A, 1Q and 2Q) for which the test outcomes were plotted, all test results were recorded by a data acquisition computer in spread-sheet form. The plots, also, were digitized by the help of a digitizer computer in spread-sheet form.

The dimensions of the specimens were measured at a few locations and are recorded in Appendix A. The wet weights of saturated specimens, and both dry and wet weights of dried specimens were recorded in the same appendix, as well. The wet weight was measured after the surface shine (due to water) was wiped by a piece of cloth. The testing procedures were different for various test types. All the specimens were loaded by an MTS displacement-controlled machine. The loading rate was 10 mm/ 1300 seconds, unless otherwise mentioned.

4.3.1. Active Confinement (Columns A to I in Table 3-1)

The test series A and F of Table 3-1 (0% confinement) were performed with the procedure of uniaxial compression tests (section 4.3.4). The active confinement for the remaining series was produced by a hand operated hydraulic jack in a triaxial cell. The essential features of this cell which is named after its designer, Hoek (1968), are illustrated in Figure 4-5. The body of cell consists of a stainless-steel cylinder with end caps . A cylindrical membrane sleeve, made of flexible urethane rubber, is placed inside the body, and the caps are tightened. Before applying hydraulic pressure, the concrete specimen is placed inside the membrane. The oil pressure pushes the membrane sleeve against the caps and seals off its ends. The function of the membrane is to shield the specimen from fluid penetration into its pore structure. The cell and the membrane used in this study were designed to withstand a hydraulic pressure of up to 70 MPa, and accepted only Nx-core sized specimens (cylinders with height of 108 mm and diameter of 54 mm; nominal size 100×50) (Imran et al, 1995).

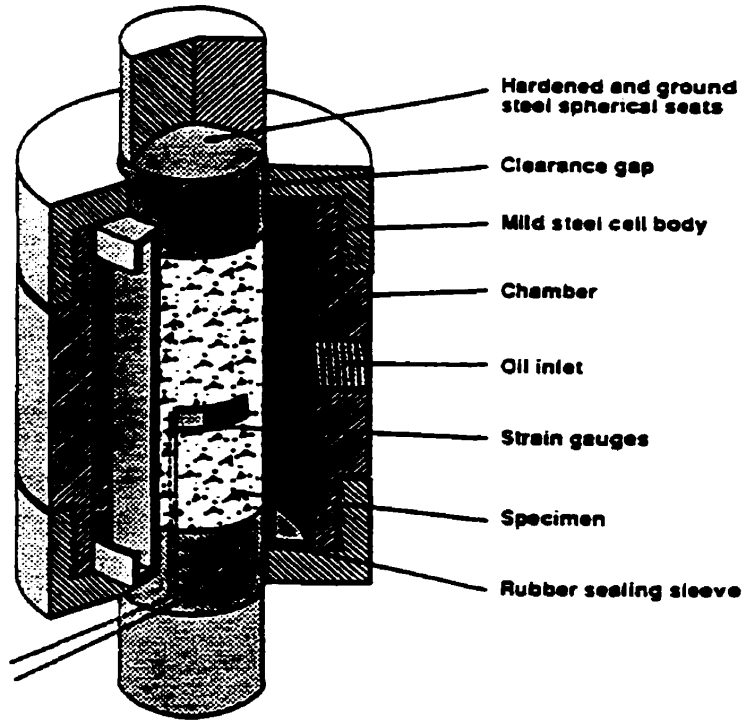

Figure 4-5: The essential features of triaxial "Hoek" cell (taken from Imran, 1995)

The applied lateral pressure was a fraction of the compressive strength of saturated 100×50 mm cylinders subjected to uniaxial compression (column A of Table 3-1). The measured parameters were lateral pressure, axial load, circumferential strain (or deformation), and axial strain. For all tests two LVDTs, which were attached to the top and bottom platens, recorded the axial deformation. To eliminate the softening effect (created by grinding the ends of specimens), the specimens were loaded to less than 10 kN (about 5 MPa) and unloaded prior to the test.

After a triaxial test was terminated, the axial load was removed first, and then the lateral pressure was released. This resulted in a distinctive point on the load-deformation curve indicating the end of the test, since deformations decreased rapidly after that point. In addition, in the absence of axial force the lateral pressure could partly recover the

cylindrical shape, and ease the removal of the specimen from the cell. For this reason the retrieved specimens do not have a barrel (bulging) shape in the Figures 4-6 to 4-13.

4.3.1.1. Saturated Condition (Columns A to E in Table 3-1)

The prepared specimens were immersed in water for three days prior to the testing. As it was explained in section 3.6, water penetrated under the adhesive and weakened the bond between the strain gauge and the concrete. During the test, the axial gauge, which was under compression, separated from the specimen at some locations and buckled. The circumferential gauge, which was under tension, performed better since even if only its ends were attached to the concrete, it still could determine the strain. Therefore, the axial deformation measurements recorded by LVDTs were used for data reduction calculations. In addition, the circumferential gauges were strengthened by a rapid strong glue at their ends prior to the testing. The procedure suggested in section 3.6 might be effective in preventing bond damage in future applications.

Figures 4-6 to 4-10 show the specimens after being tested. The failure cracks are visible on the specimens subjected to 20% f'_c lateral confinement stress(B series). The cylinders with 40% f'_c lateral pressure (C series) have slightly cracked, whereas there is no macro crack on the specimens confined with 60% and 80% lateral pressure, D and E series respectively.

4.3.1.2. Dry Condition (Columns F to I in Table 3-1)

The specimens were kept in a 60°C oven for three days. This temperature did not harm the gauges, and help to accelerate adhesive curing. Confined specimens with 20%, 40%, and 60% of f'_c lateral pressure were tested in the Hoek cell, as described in the preceding section (4.3.1.1). Although the bond between the gauges and concrete was not defected in this case, the axial LVDTs measurements were considered for the strain calculations, for consistency.

Figures 4-11 to 4-13 show the tested specimens. The cylinders with 20% f'_c confinement (G series) have cracked, where as those with 40% f'_c(H series) and 60% f'_c confinement (I series) have not.

4.3.2. The "Toothpaste" Test (Column J in Table 3-1)

In this series of tests, the saturated concrete cylinders were subjected to increasing lateral pressure with no axial load up to their failure. In order to prevent damaging the bond of the strain gauges, as was discussed in section 3.6, the specimens were kept in a covered basket in the curing room in 100% relative humidity for three days, with no direct contact with water. The bond remained in good condition after that period. This test, which was performed in the Hoek cell, was burdened with numerous difficulties, and from the total of 8 specimens half ended in premature failure. Figure 4-14 presents the specimens which had satisfactory failure. In this figure, J-1 demonstrates a typical sample with its preparations. The arrows on J-5 and J-7 indicate the crack locations.

The laboratory technicians required a minimum axial load (about 1 kN; about 0.5 MPa) for the safety of the equipments, to prevent possible explosion of the concrete. This small amount of axial load may have affected the obtained strength, and perhaps this precaution was not necessary.

4.3.3. Passive Confinement (Columns K to P in Table 3-1)

These series of tests were performed on cylindrical specimens which were wrapped prior to the test by carbon fiber sheets. All the specimens were in saturated condition. They were kept in the curing room at 100% RH until time of testing (at least for 3 days). According to the manufacturer's catalogue (Appendix B), water was not expected to damage the wrapping system (the wraps on real structures can resist rain and moisture

build up in the encased concrete). The specimens were wrapped with one, two, or three layers of carbon fiber sheet (the number of layers is a variable of the study).

Testing was done under uniaxial compression. For the measurements of axial and circumferential deformations two LVDTs and a perimeter chain were used. The cross-sectional area and length of the concrete specimens (excluding the fiber wraps) were used in the calculations of stress and axial strain, since only concrete carried the axial load. Whereas the perimeter of the whole composite (including the fiber wraps) was considered in calculation of cicumferentail strain, since the chain was wrapped over the fiber wraps.

4.3.3.1. The 200×100 mm Cylinders (Columns K to M in Table 3-1)

The two LVDTs were installed on a compressometer of a constant gauge length, which was attached to the specimen, and the chain was placed at the mid-height of the cylinder. Due to the small diameter of specimens, the overlappings were shorter than required by the manufacturer for full scale applications (section 3.8). These insufficient values led to early failure at the seam. Hence, an additional 100 mm length fiber sheet was installed over the exterior seam (50 mm on each side of the seam). Although failure was accompanied by slip at the seam, fiber breakage also occurred. Figure 4-15 illustrates the breakage of fibers for a two-layer wrapped specimen. For a few specimens of the M series, the rate of loading was reduced to 10 mm / 1700 seconds, but no significant change was observed in the behavior of specimens.

Figure 4-16 show the failed specimens which were wrapped with one layer of carbon fiber sheet. Figures 4-17 and 4-18 show the tested concrete cylinders wrapped with two and three layers of carbon fiber sheet, respectively. In general, the failure occurred at the location of the exterior seam and at the mid-height of the cylinders.

4.3.3.2. The 100×50 mm Cylinders (Columns N to P in Table 3-1)

The LVDTs were installed on the top and bottom platens, measuring deformation of the total length of specimen. The specimens were pre-loaded to eliminate the end softening effects. When the specimens were loaded, the seam of the wrap opened due to insufficient overlapping. Similar to section 4.3.3.1, a 100 mm fiber sheet was installed on the exterior seam, and satisfactory failure was subsequently obtained. Figures 4-19 to 4-21 demonstrate these series of specimens after being tested. No significant difference in the failure mode of these specimens can be seen in comparison with larger cylinders.

4.3.4. Uniaxial Compression (Columns Q and R in Table 3-1)

In these series of tests, the cylindrical specimens were loaded uniaxially. For large size specimens (300 mm and 200 mm cylinders), the axial deformation was measured for a length at midheight of the cylinders, to eliminate the softening effects of the ends of specimens due to grinding. For this reason, the LVDTs were installed on a clamping device (compressometer) with a known length (250 mm for 300×150 mm cylinders, and 153.2 mm for 200×100 mm cylinders), which was attached to the midheight of cylinders. However, for small size cylinders (100 mm), it was difficult to install the compressometer and the total deformation was measured along the length of specimens. The end softening effect was eliminated by pre-loading. The circumferential deformation was measured by the chain, which was wrapped around the cylinders at their mid heights.

Figures 4-22 and 4-23 present the 200×100 mm and 300×150 mm specimens subjected to uniaxial compression, respectively. The cracks on the specimens containing microfibers only are more scattered than those on specimens containing steel fibers. The cracks on the specimens containing polypropylene fibers are smooth and very narrow, particularly on specimens with high fiber contents (6 and 8) they are hardly visible.

4.3.5. Prism Bending (S)

The specimens were kept in the curing room until testing time. The 420×150×80 mm nominal size prisms were tested according with the ASTM-C-78 standard (1994)(Figure 4-24). The specimens were turned to their sides with respect to their position at molding. Hence, the breadth of beam was 150 mm, and its depth was 80 mm. The clear span length (L) was 360 mm. One of the supports could rotate cross-wise, and the other one could rotate longitudinal-wise. The loading lines could rotate cross-wise independently. Figures 4-25 and 4-26 show the testing setup. Since the walls of molds were not quite flat, any remaining gap between the loading lines and the specimen was filled by computer cards (Figure 4-26). When Batches 2 and 3 (very brittle) were tested, the displacement rate was decreased to 10 mm/ 3000 seconds to trace any post-peak loading curve, but no extension after the peak was observed.

Figure 4-27 shows the prisms after failure. All the failures occurred in the middle span which had maximum constant moment. The plain concrete and concrete containing only microfibers were separated in two pieces, whereas the prisms containing long fibers remained attached. The cracks on the specimens with polypropylene fibers are narrower, indicating that strain energy can be stored in this type of fiber and upon unloading of the deformed beam it can be partly recovered.

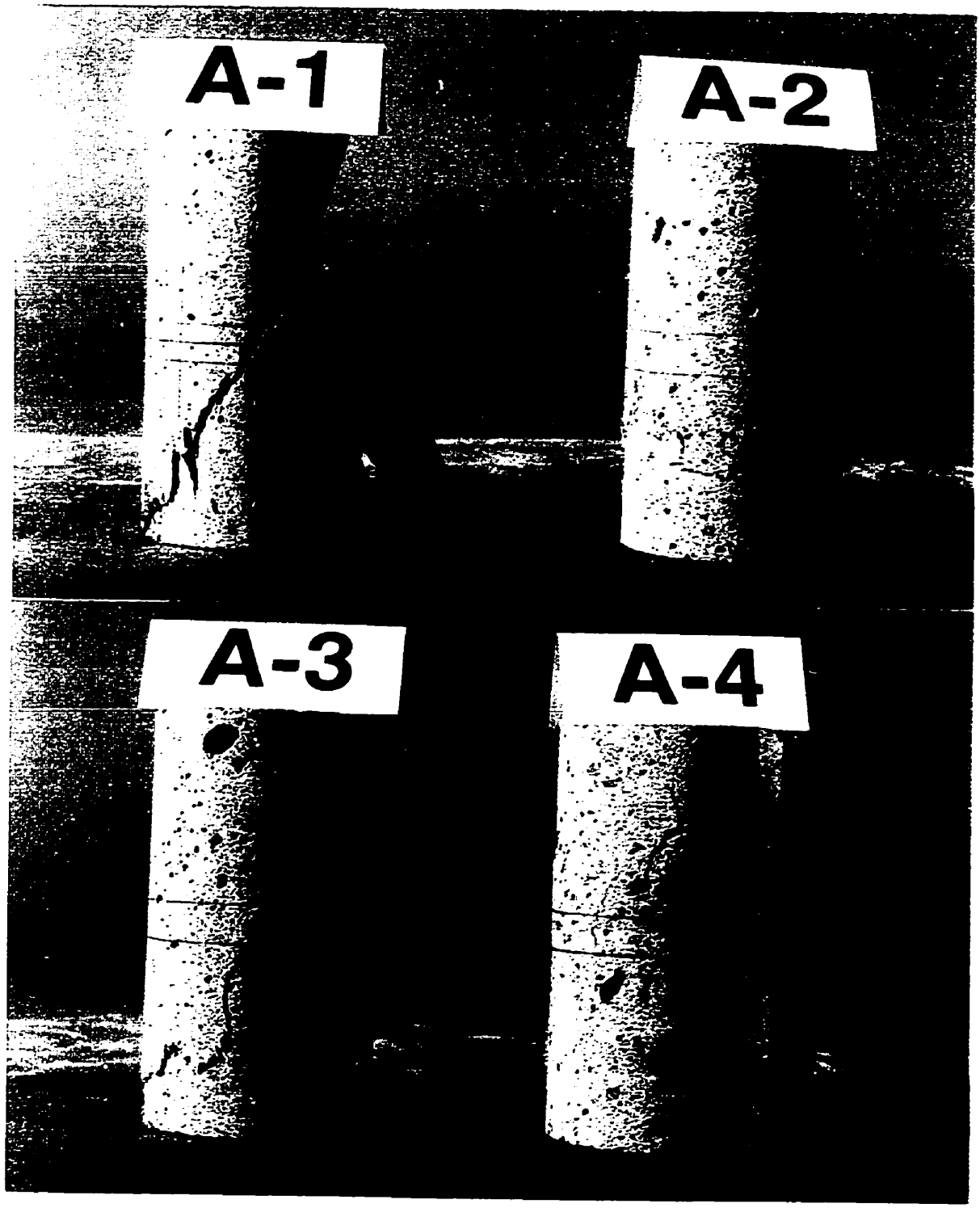

Figure 4-6: Saturated 100×50 mm cylinders subjected to 0% confinement (uniaxial)

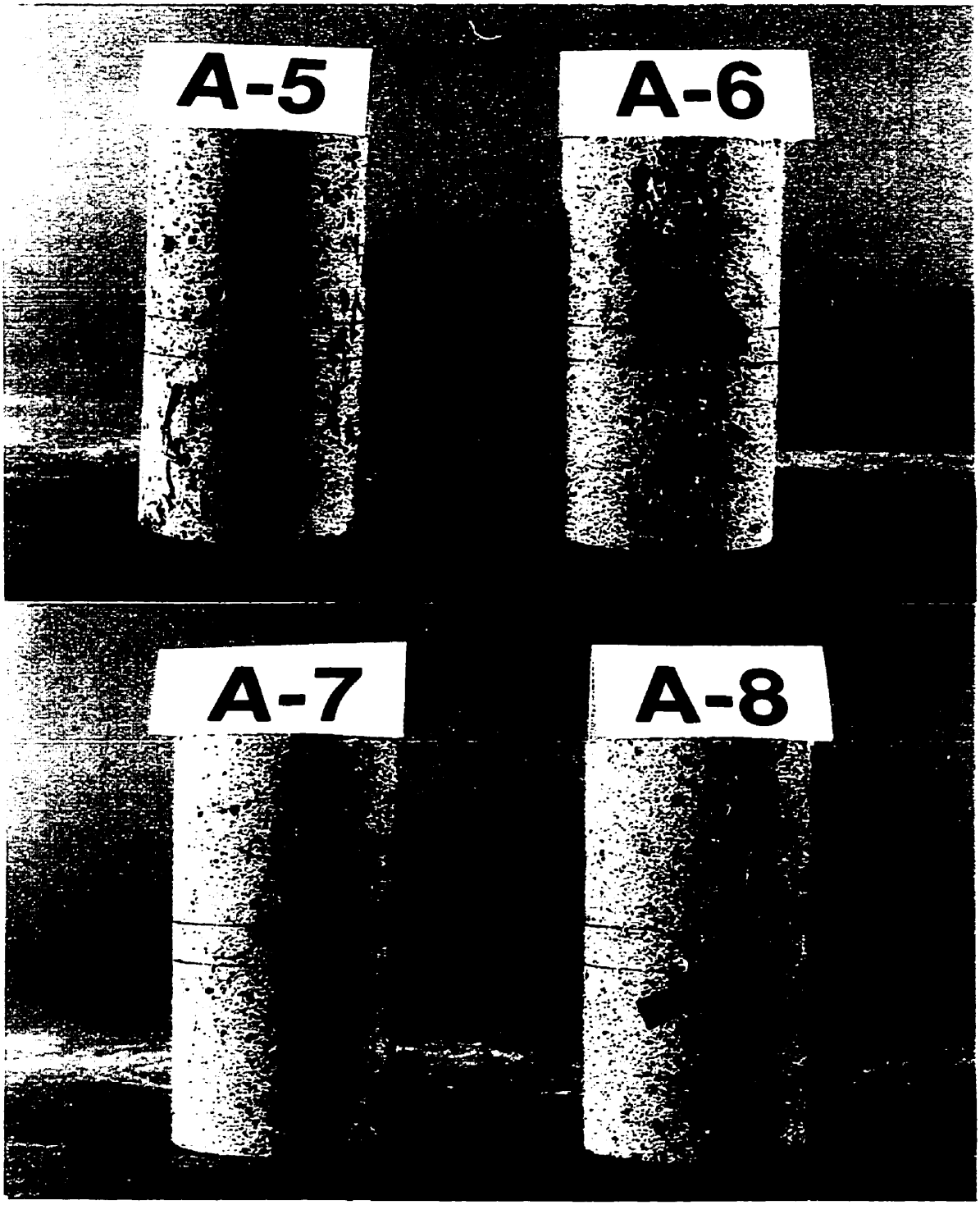

Figure 4-6: Saturated 100×50 mm cylinders subjected to 0% confinement (uniaxial)

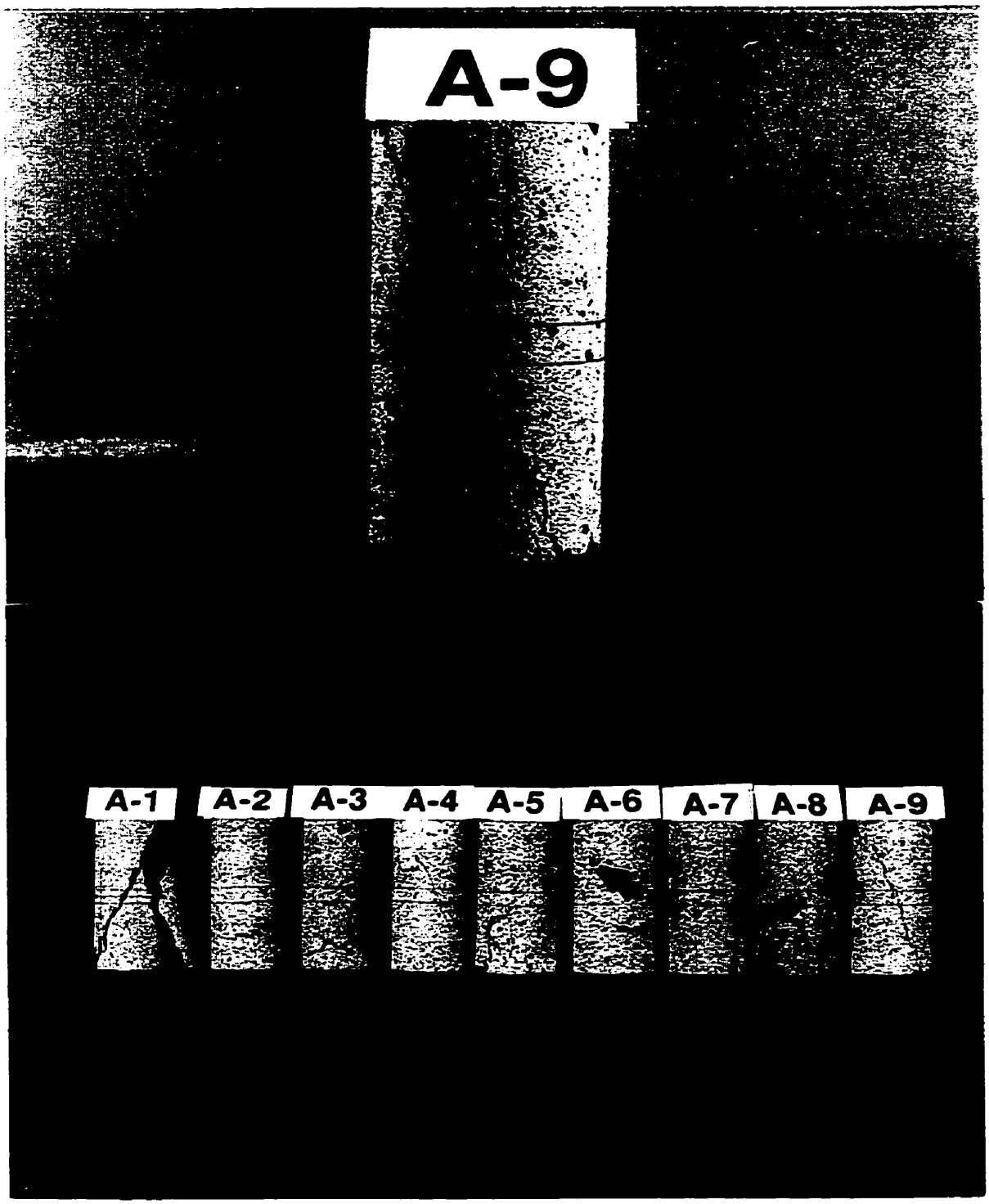

Figure 4-6: Saturated 100×50 mm cylinders subjected to 0% confinement (uniaxial)

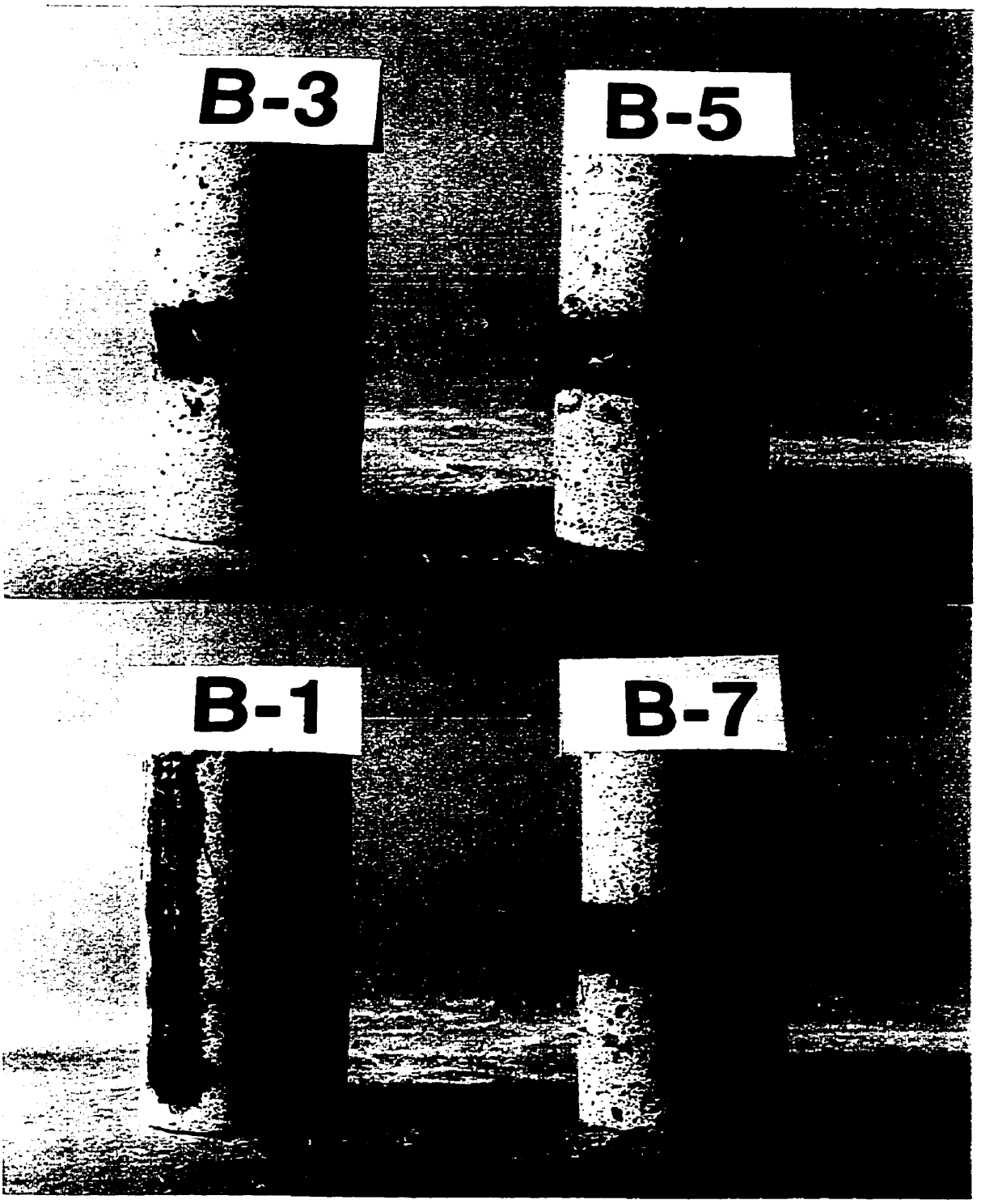

Figure 4-7: Saturated 100×50 mm cylinders subjected to 20% confinement

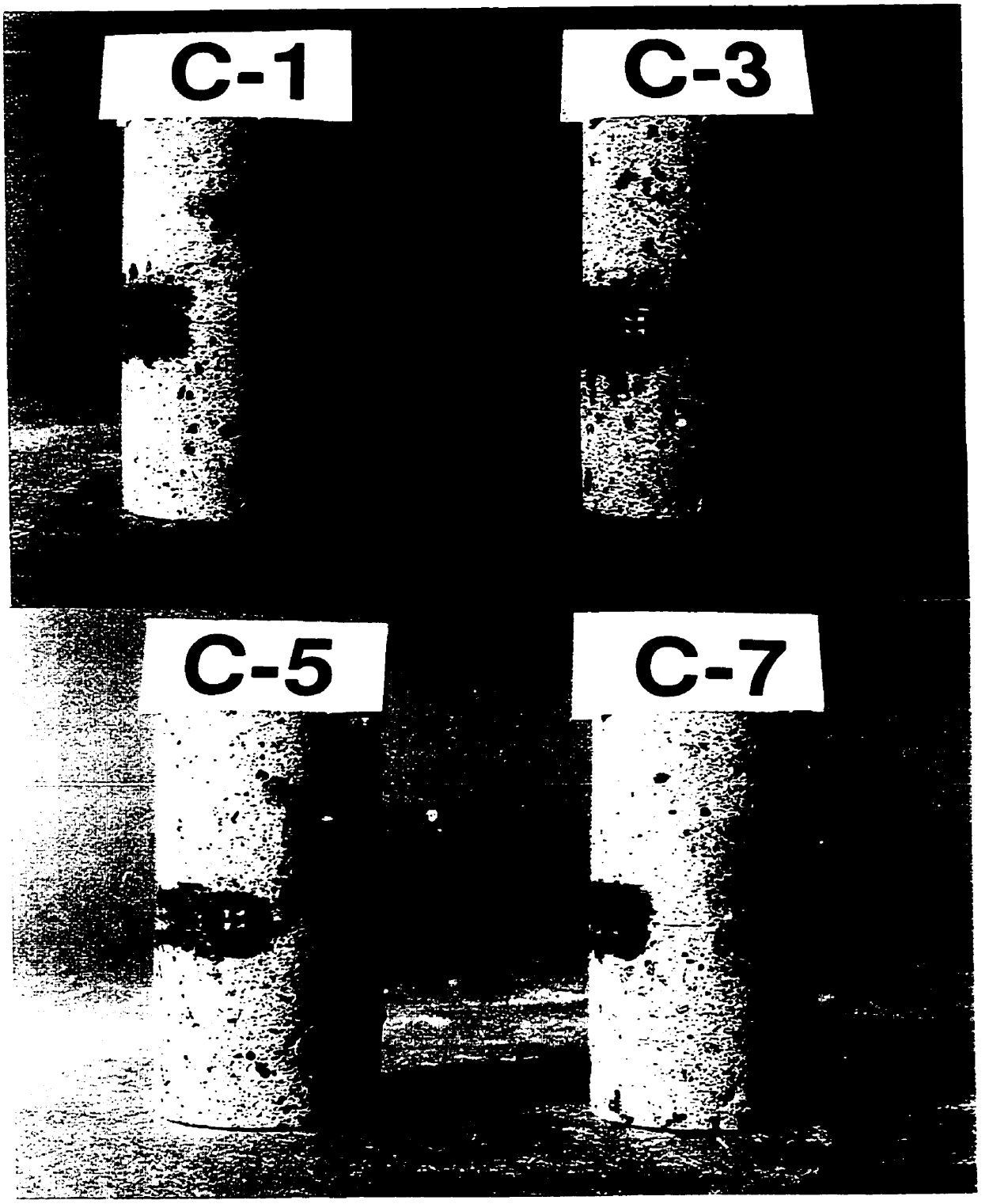

Figure 4-8: Saturated 100×50 mm cylinders subjected to 40% confinement

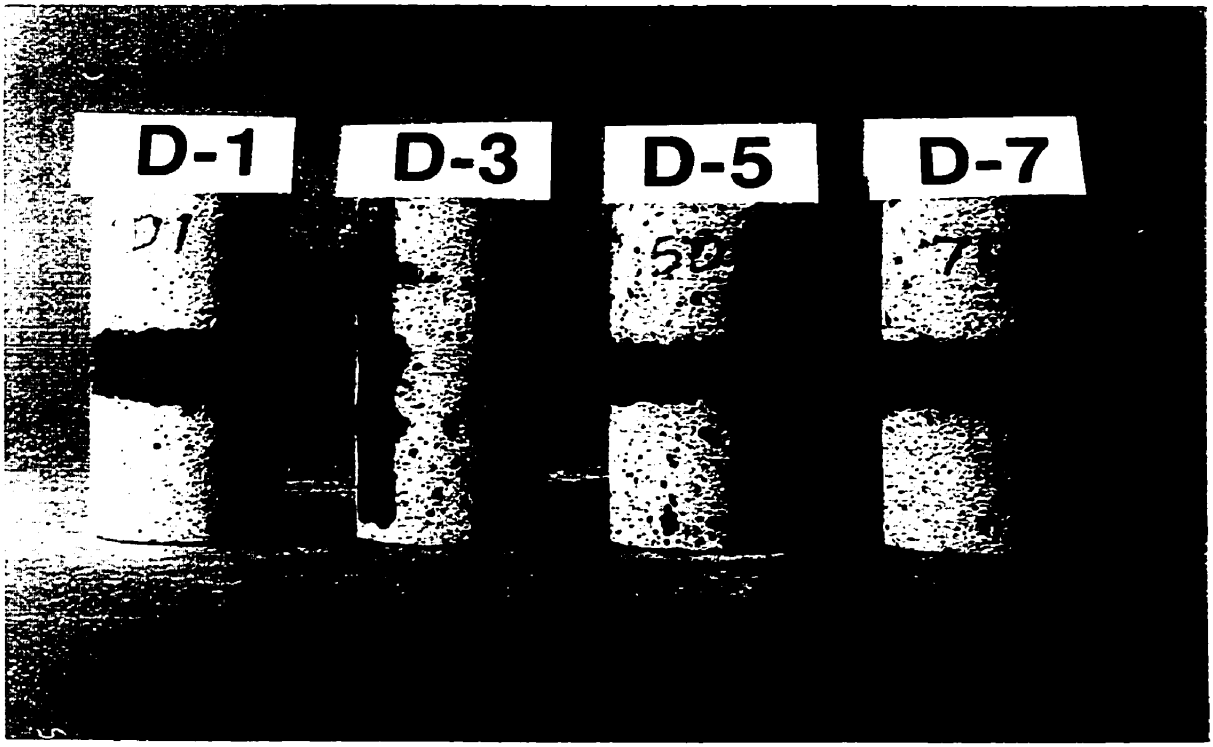

Figure 4-9: Saturated 100×50 mm cylinders subjected to 60% confinement

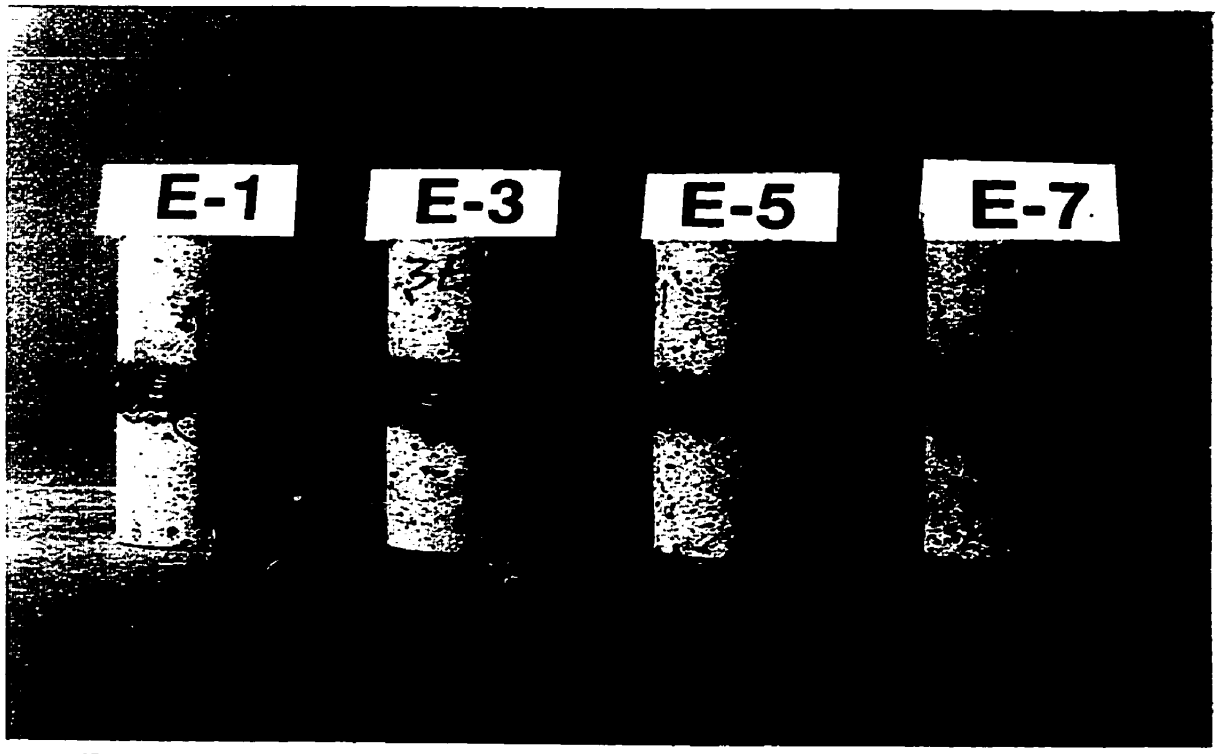

Figure 4-10: Saturated 100×50 mm cylinders subjected to 80% confinement

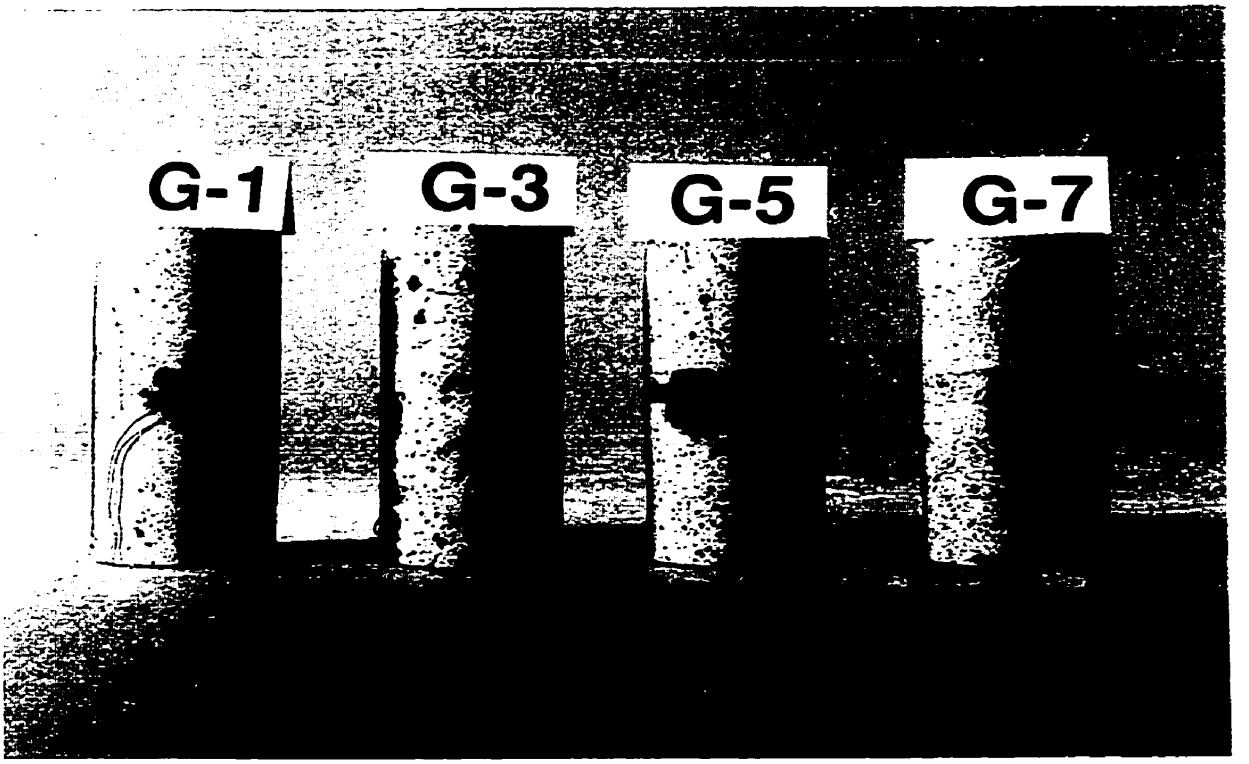

Figure 4-11: Dry 100×50 mm cylinders subjected to 20% confinement

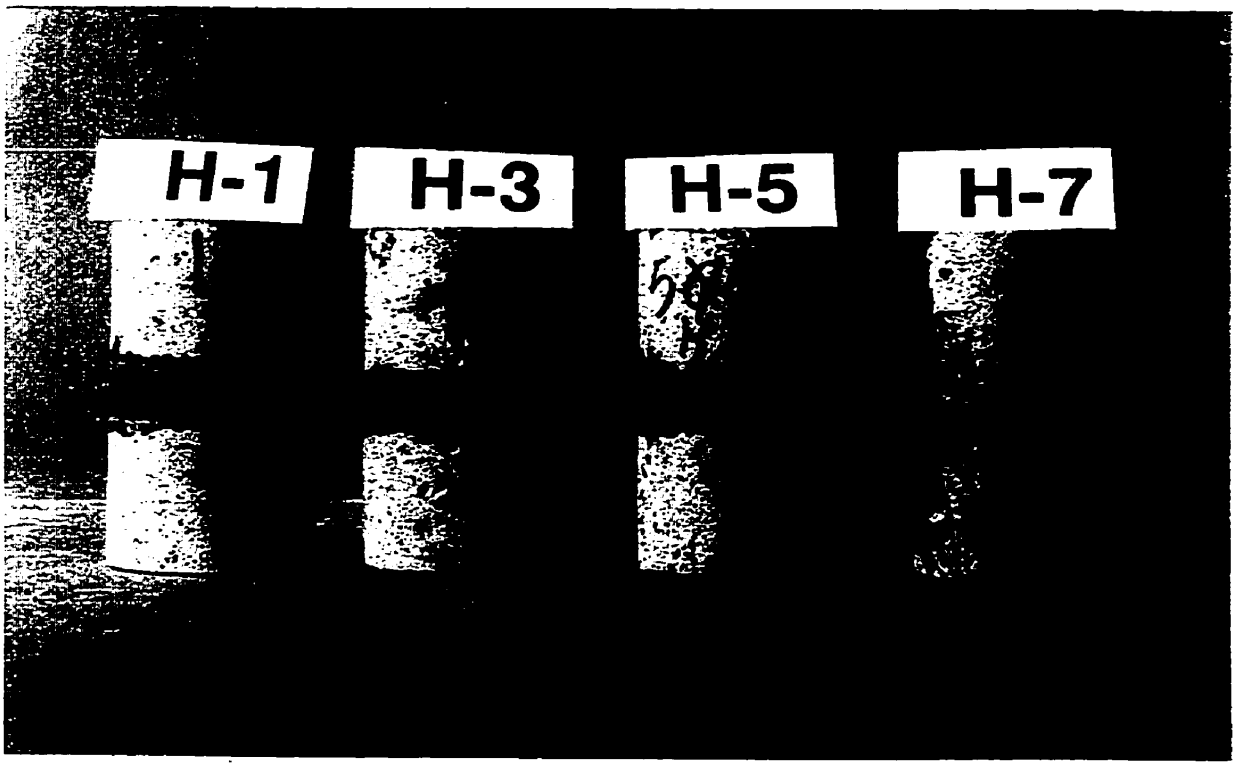

Figure 4-12: Dry 100×50 mm cylinders subjected to 40% confinement

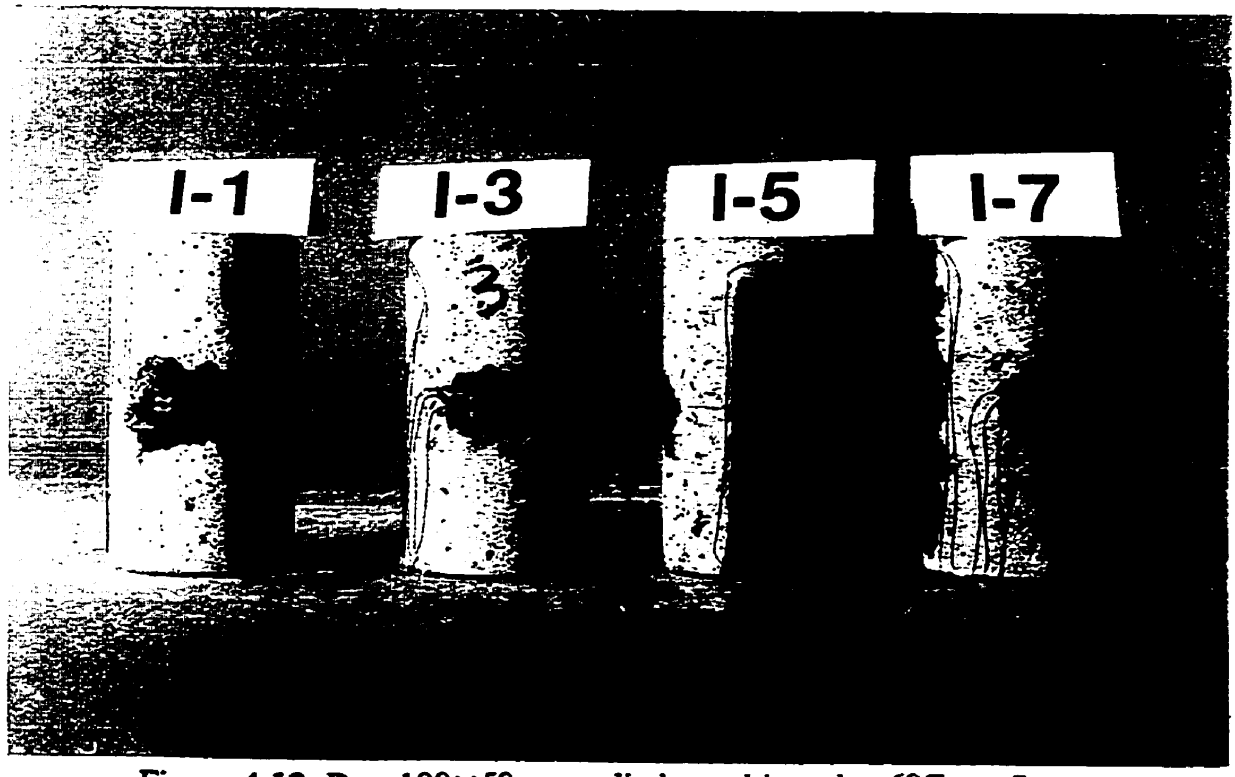

Figure 4-13: Dry 100×50 mm cylinders subjected to 60% confinement

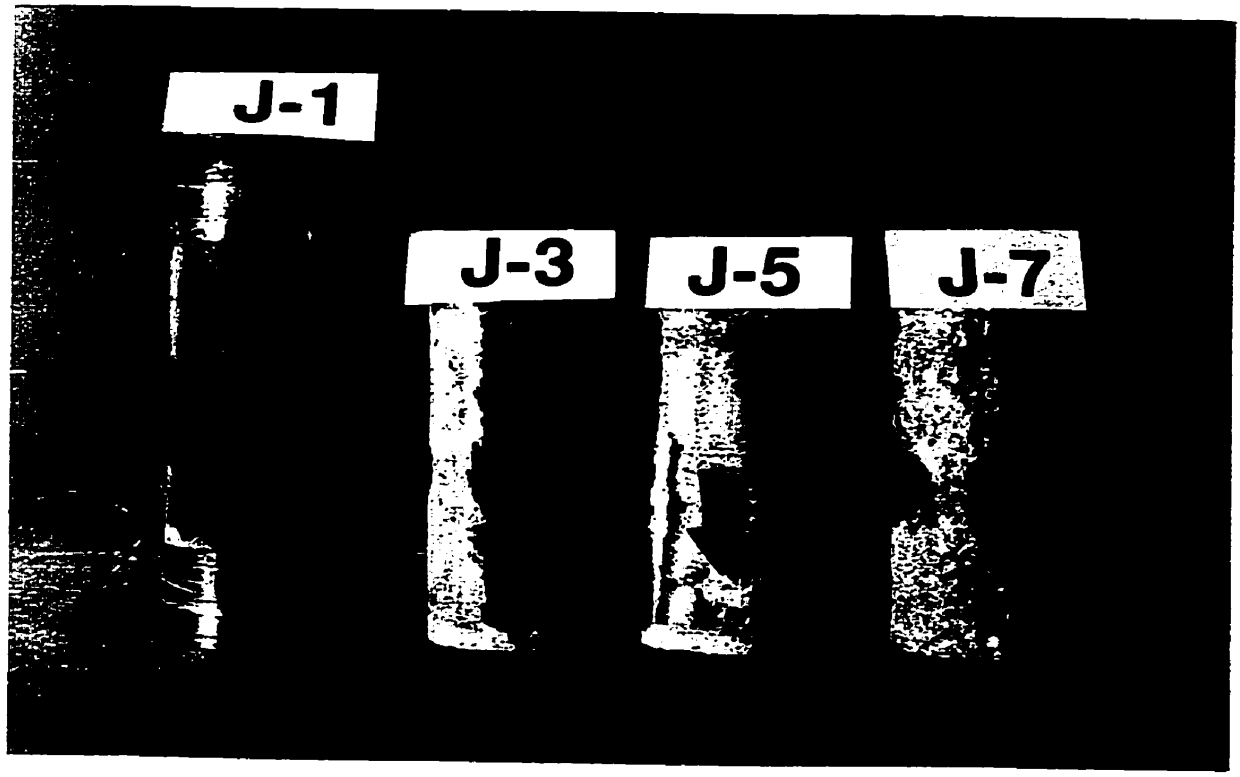

Figure 4-14: Specimens failed by Toothpaste test

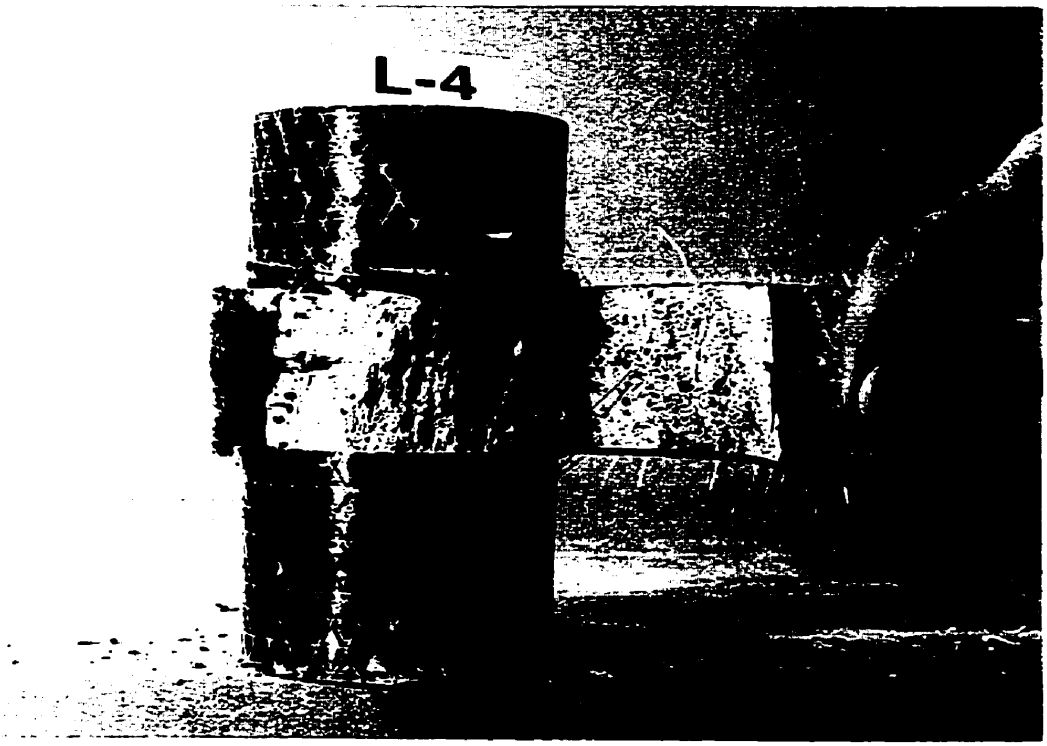

Figure 4-15: A close look at the carbon fiber sheet breakage

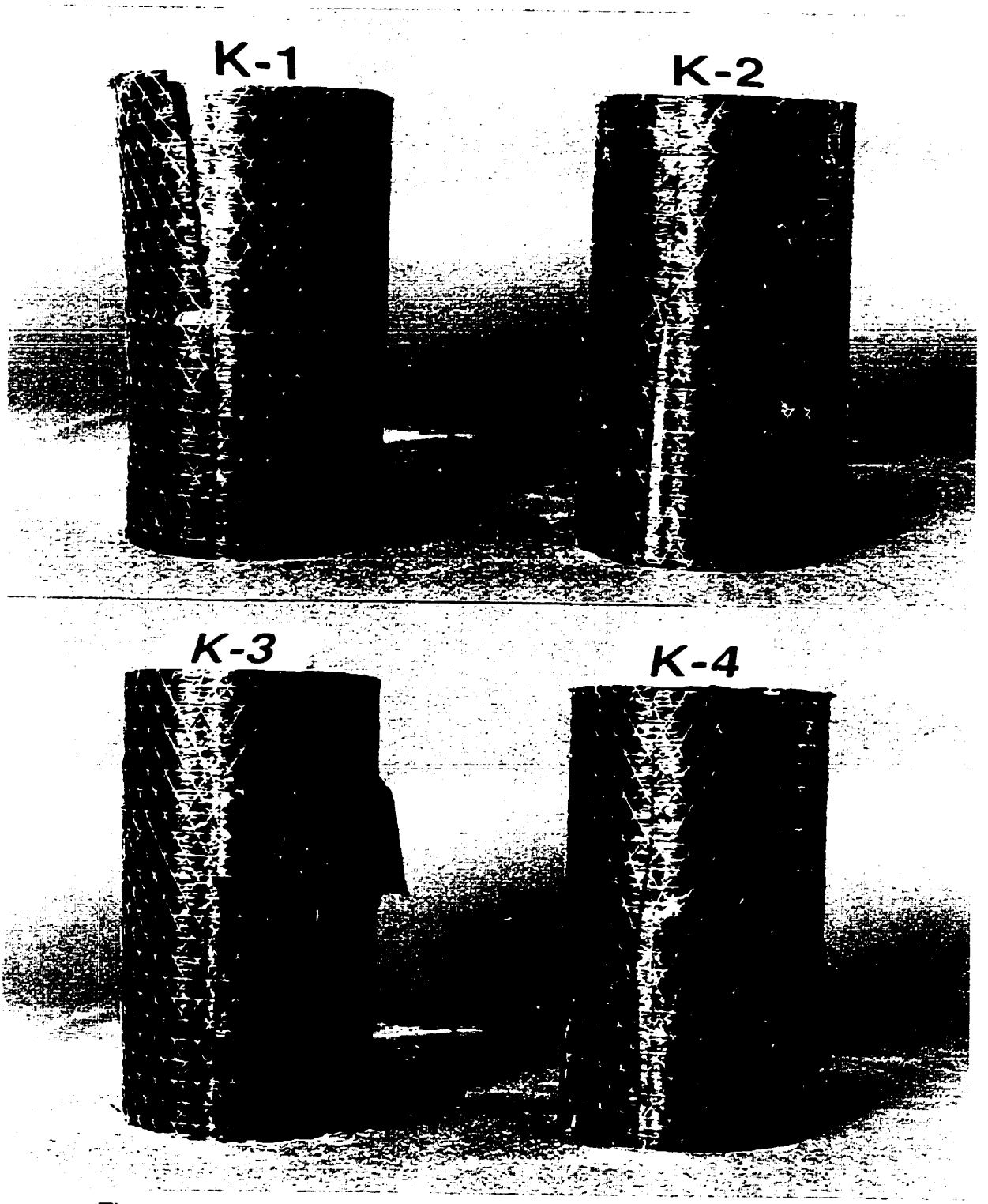

Figure 4-16: The 200×100 mm cylinders with 1 layer wrap

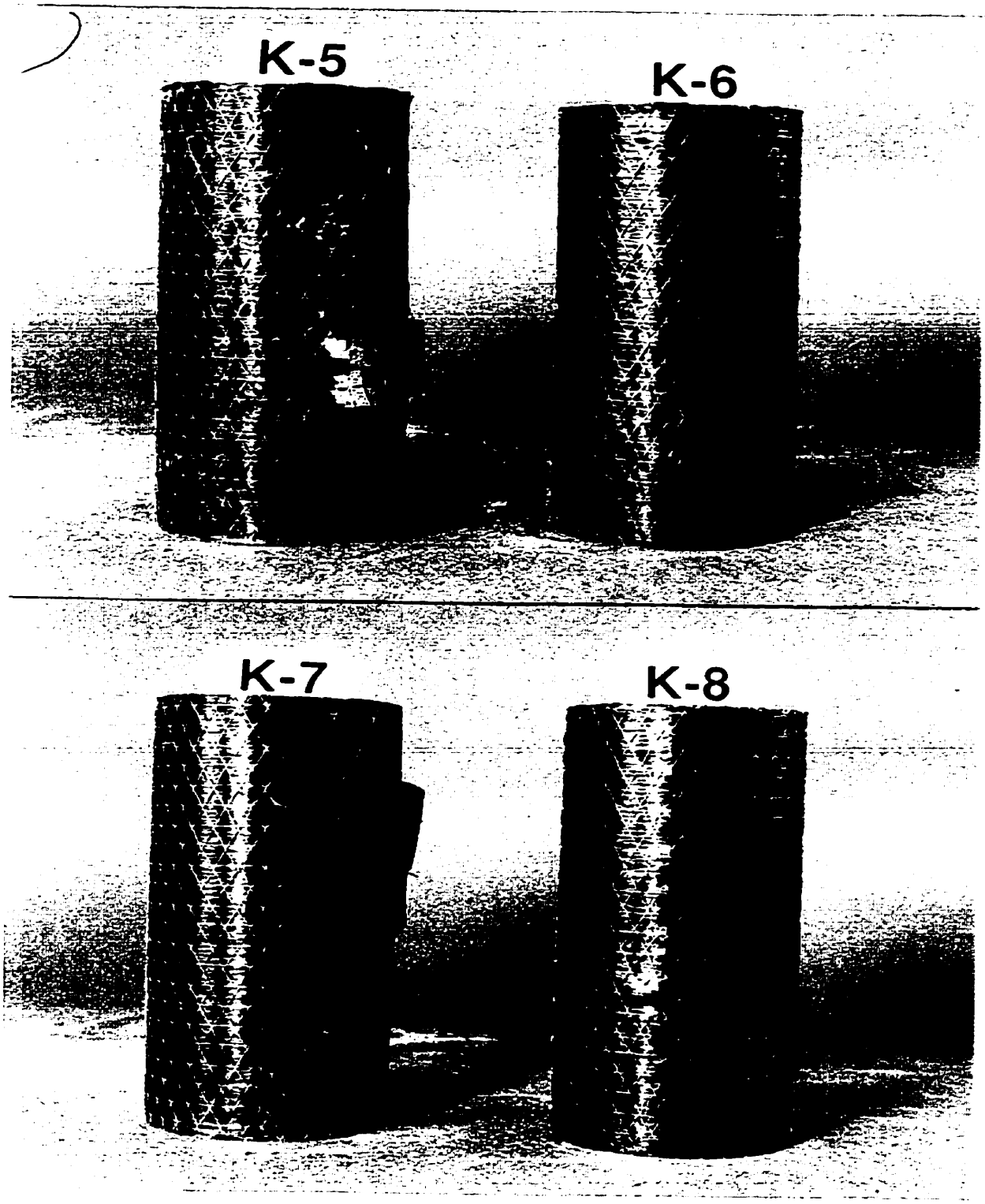

Figure 4-16: The 200×100 mm cylinders with 1 layer wrap

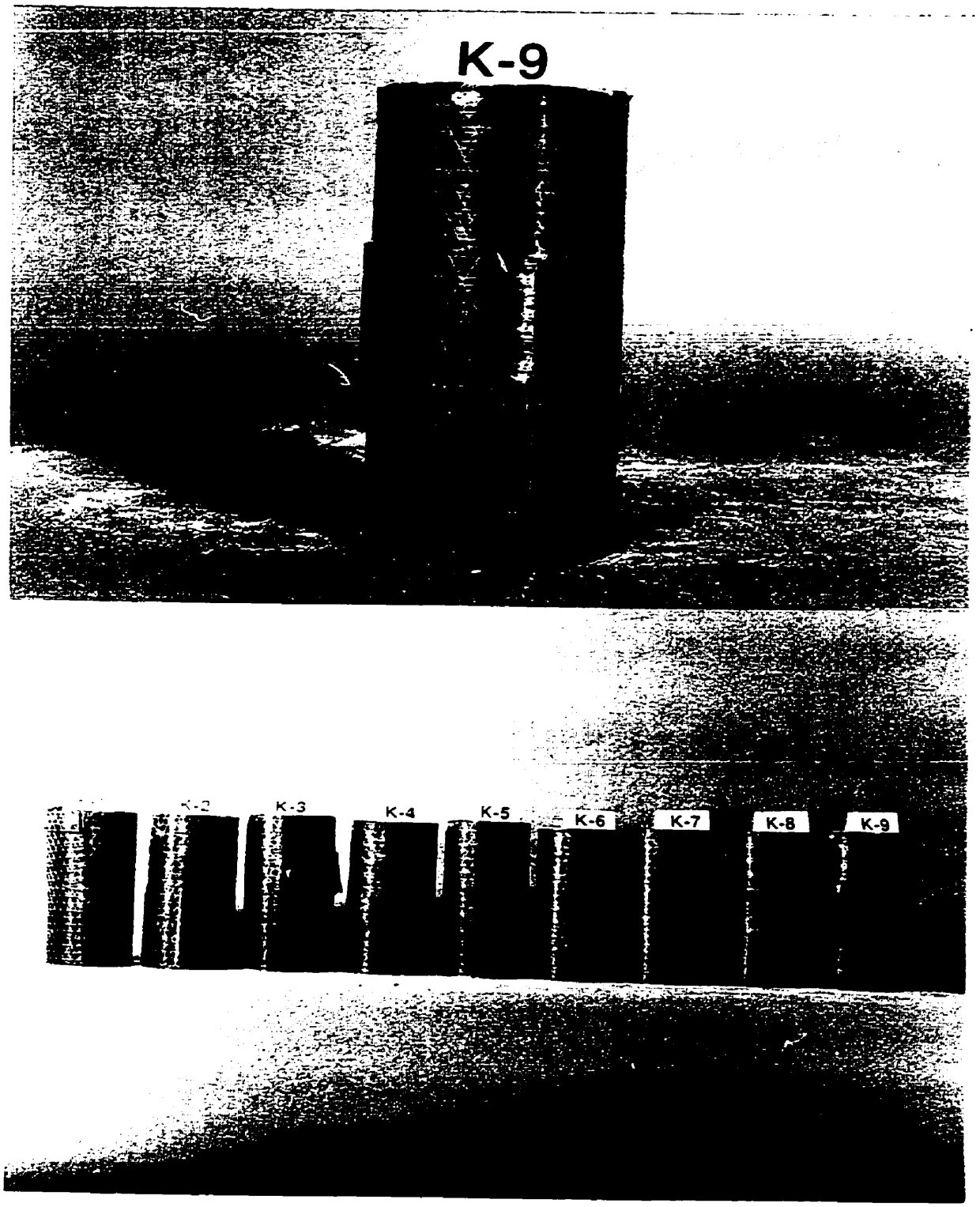

Figure 4-16: The 200×100 mm cylinders with 1 layer wrap

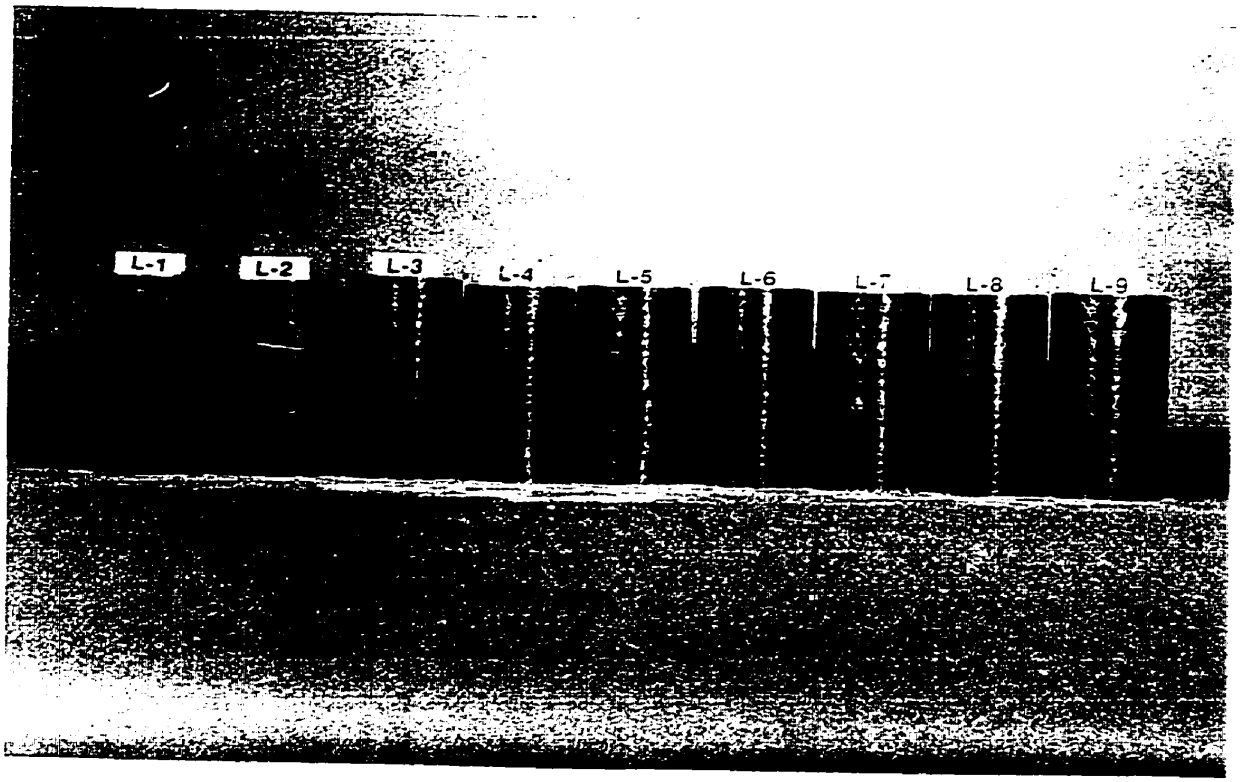

Figure 4-17: The 200×100 mm cylinders with 2 layers wrap

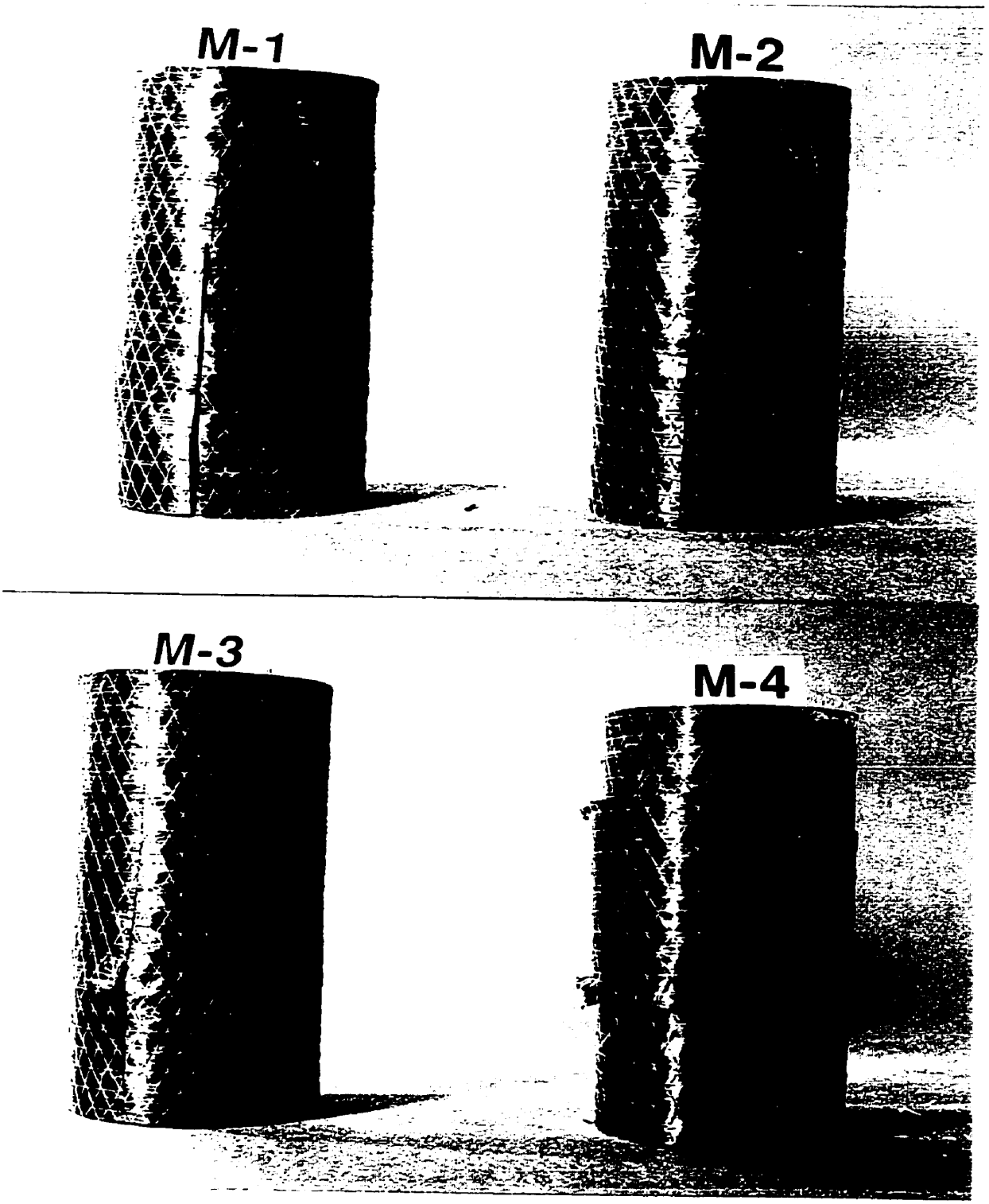

Figure 4-18: The 200×100 mm cylinders with 3 layers wrap

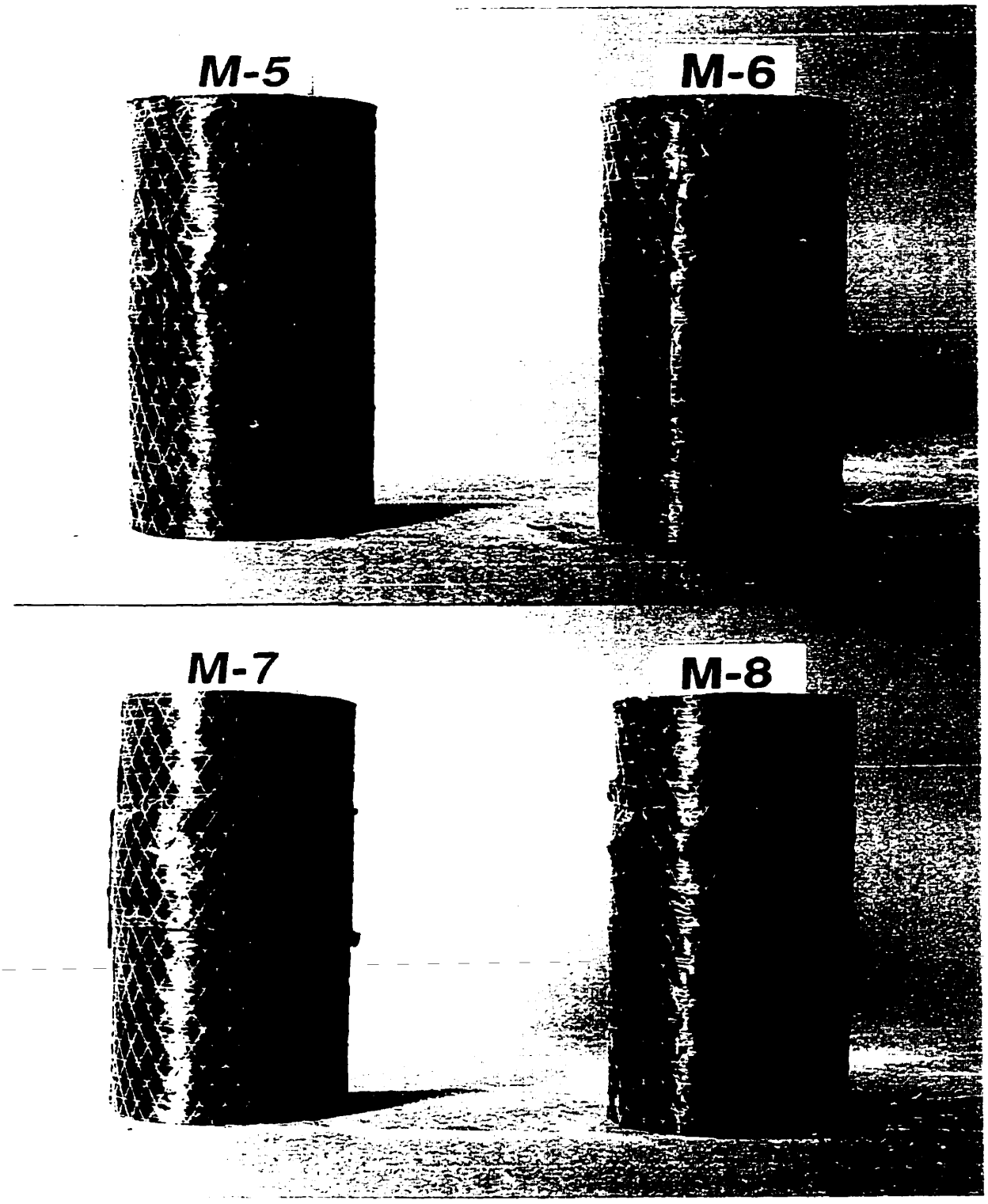

Figure 4-18: The 200×100 mm cylinders with 3 layers wrap

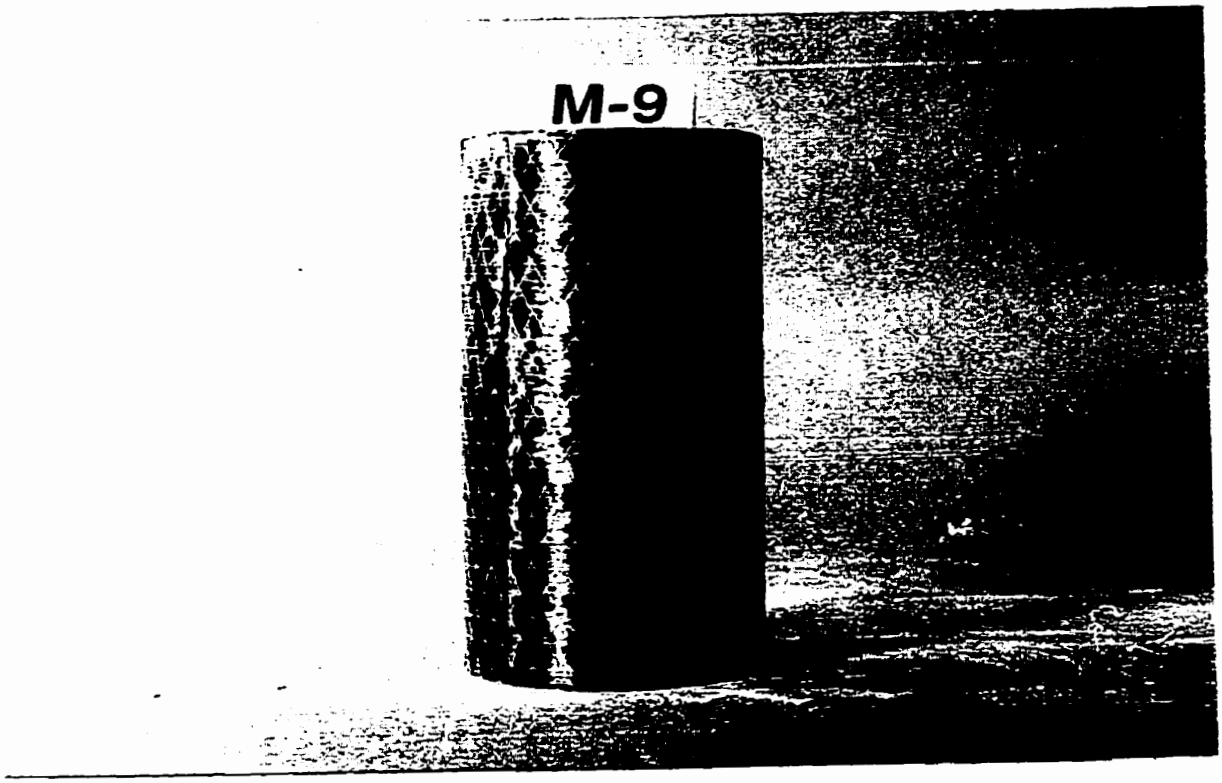

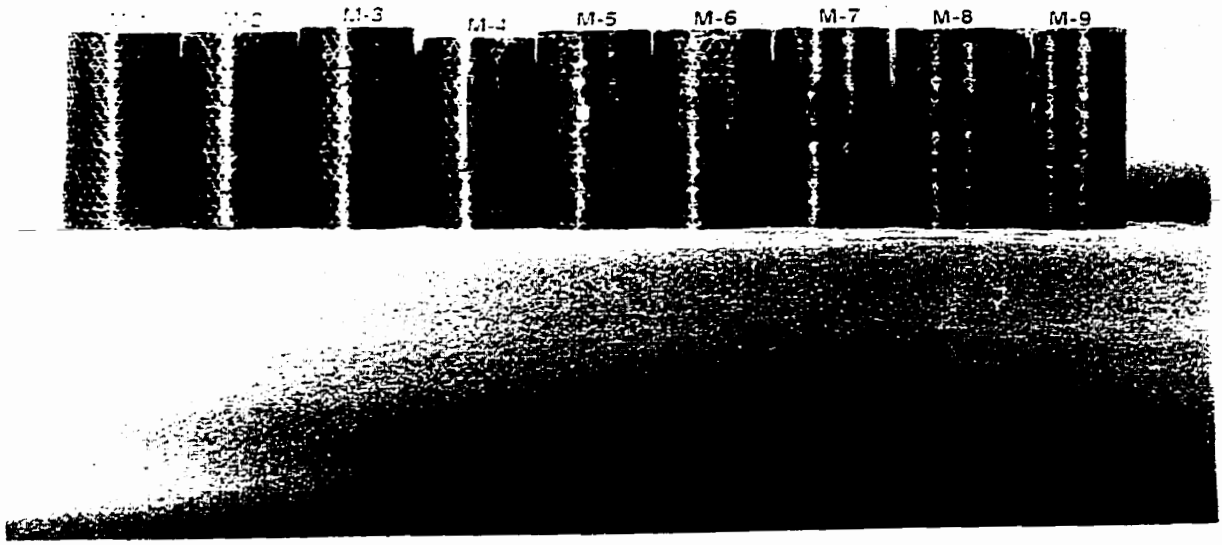

Figure 4-18: The 200×100 mm cylinders with 3 layers wrap

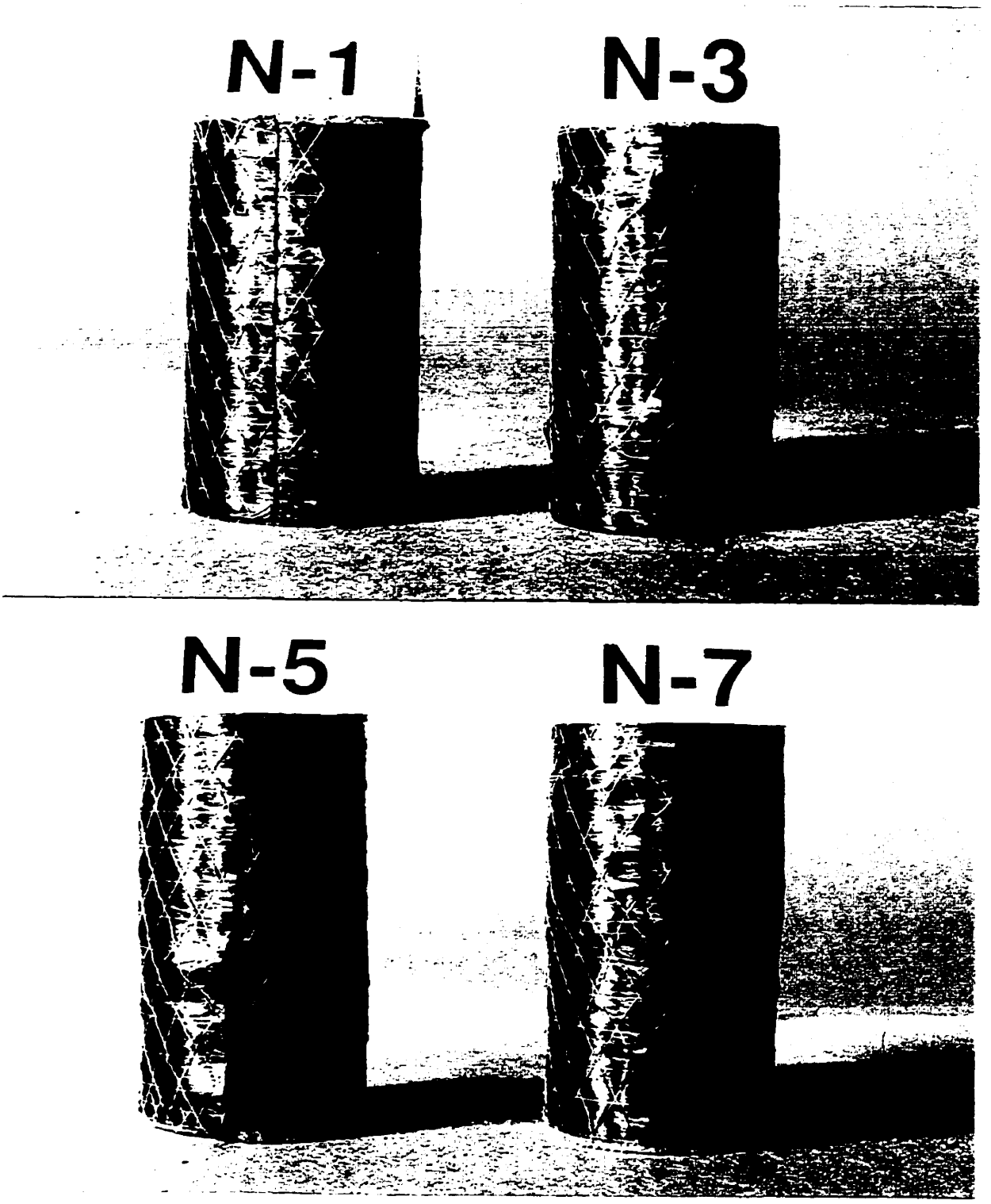

Figure 4-19: The 100×50 mm cylinders with 1 layer wrap

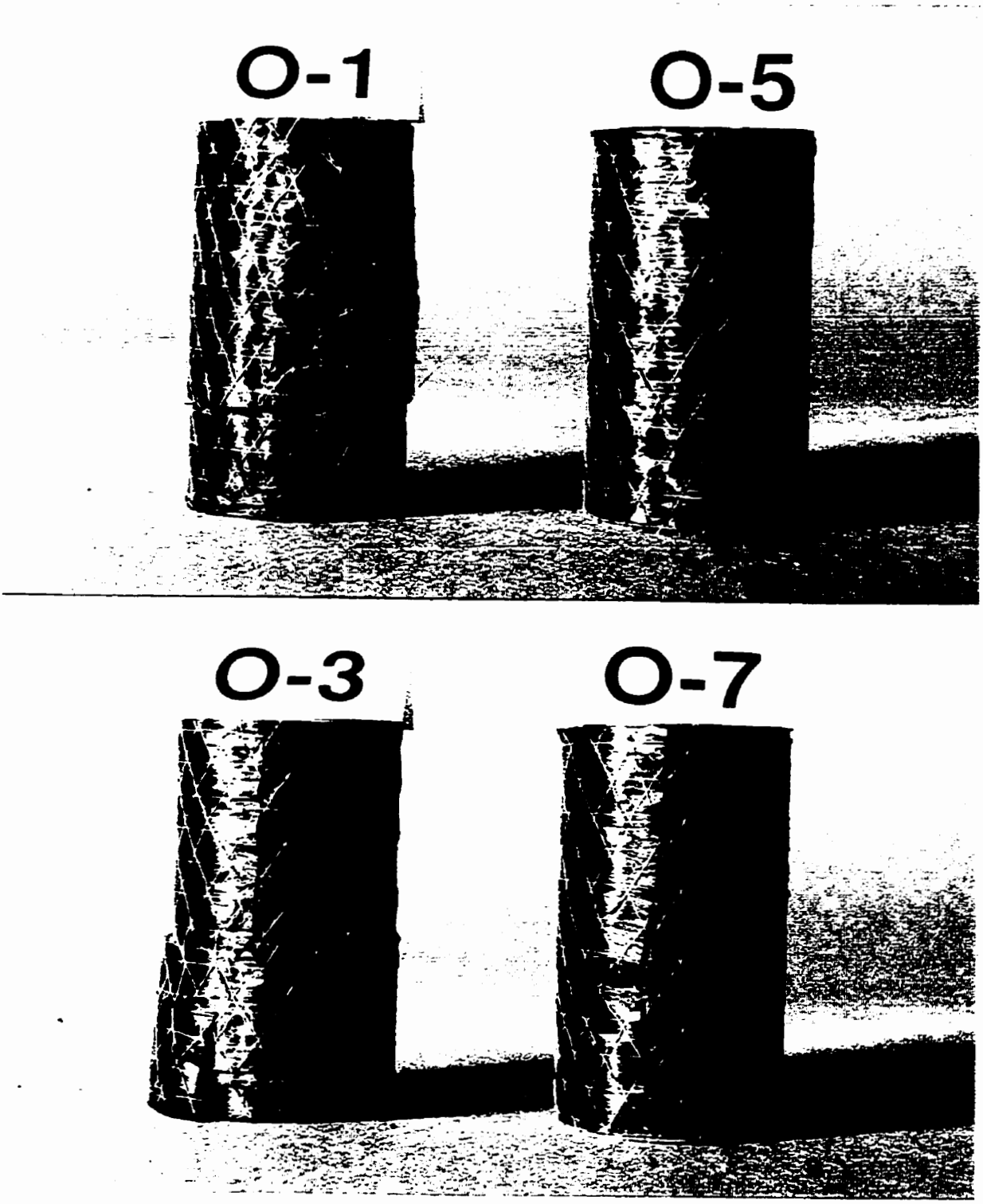

Figure 4-20: The 100×50 mm cylinders with 2 layers wrap

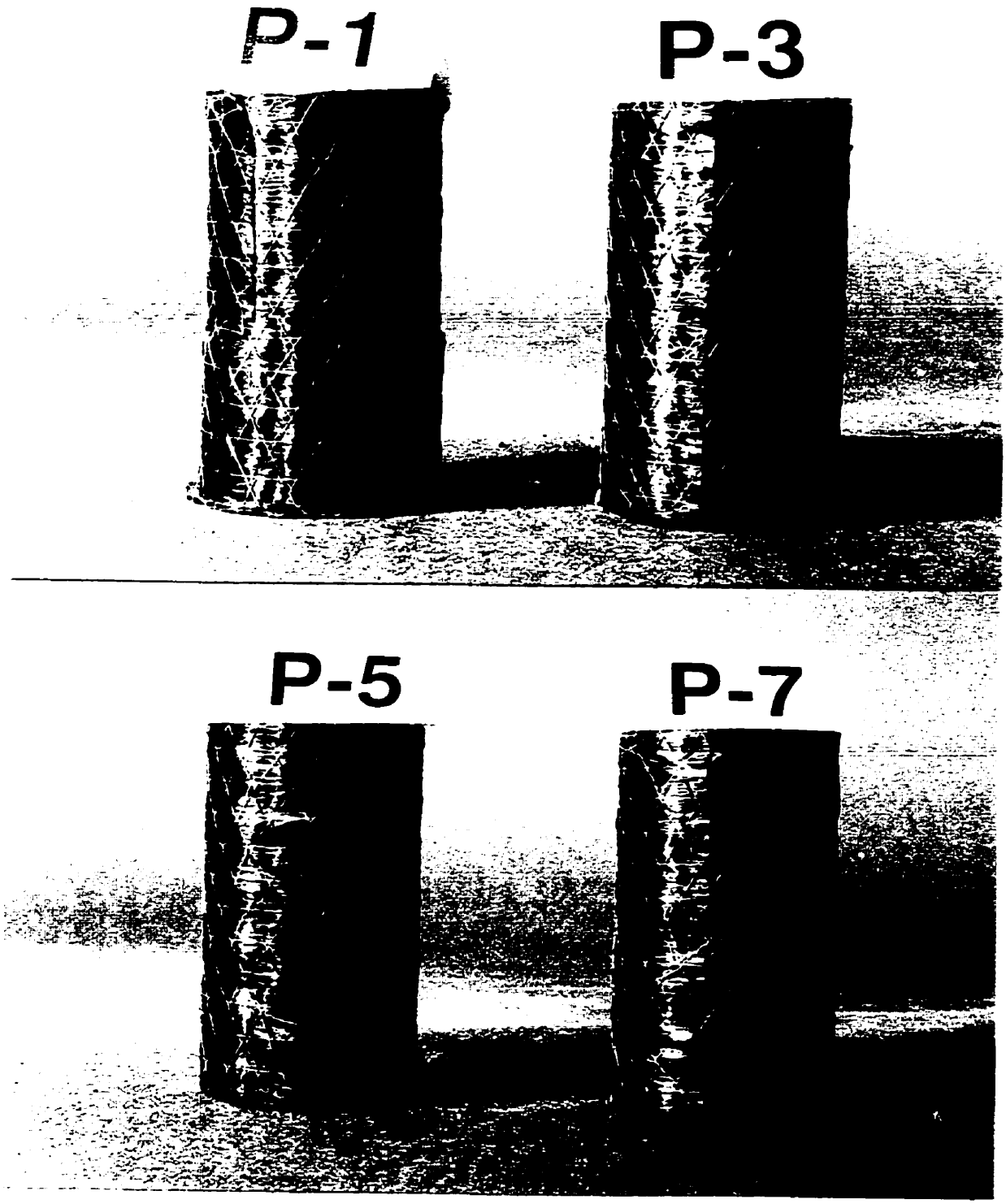

Figure 4-21: The 100×50 mm cylinders with 3 layers wrap

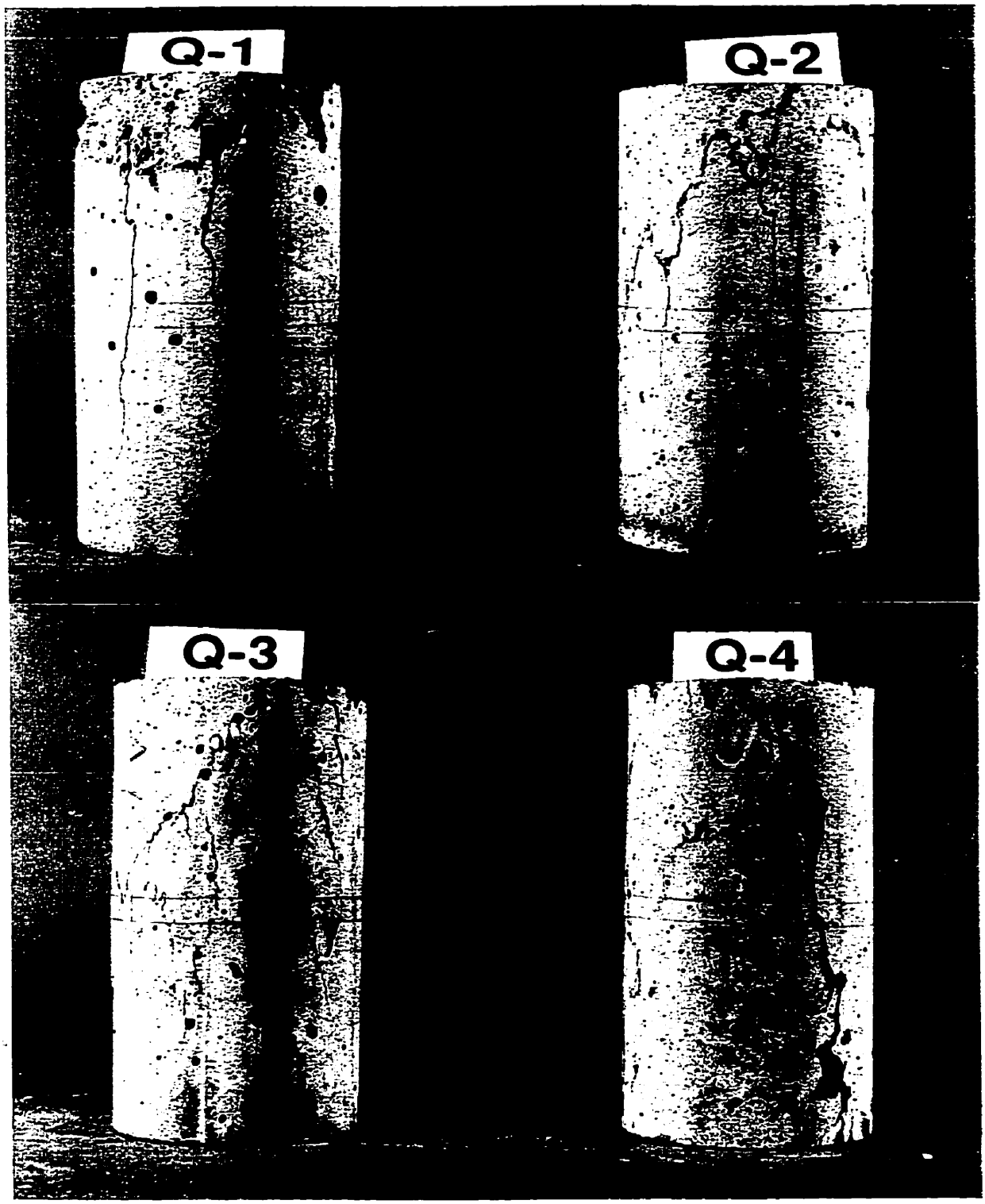

Figure 4-22: The 200×100 mm cylinders failed by uniaxial compression

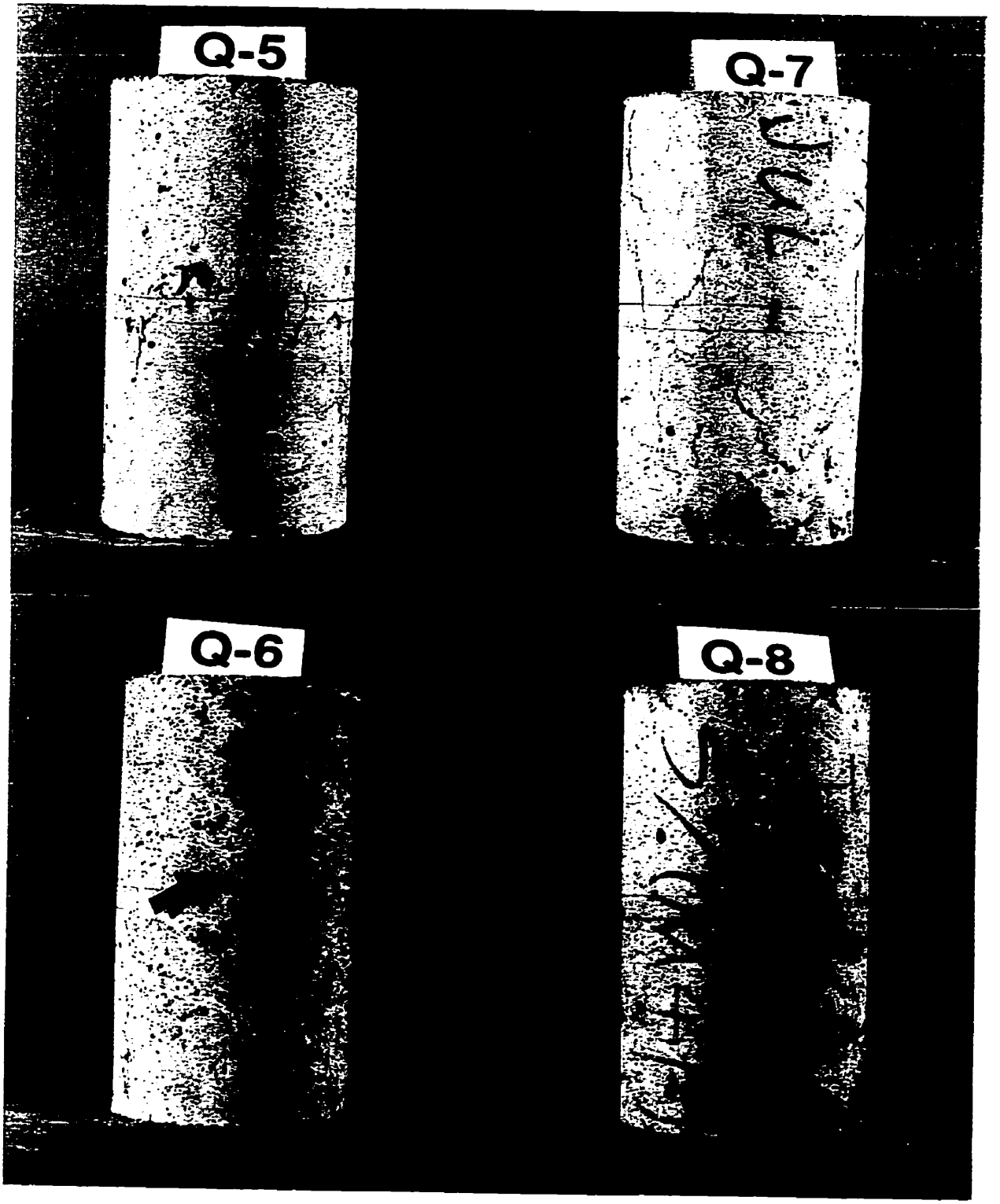

Figure 4-22: The 200×100 mm cylinders failed by uniaxial compression

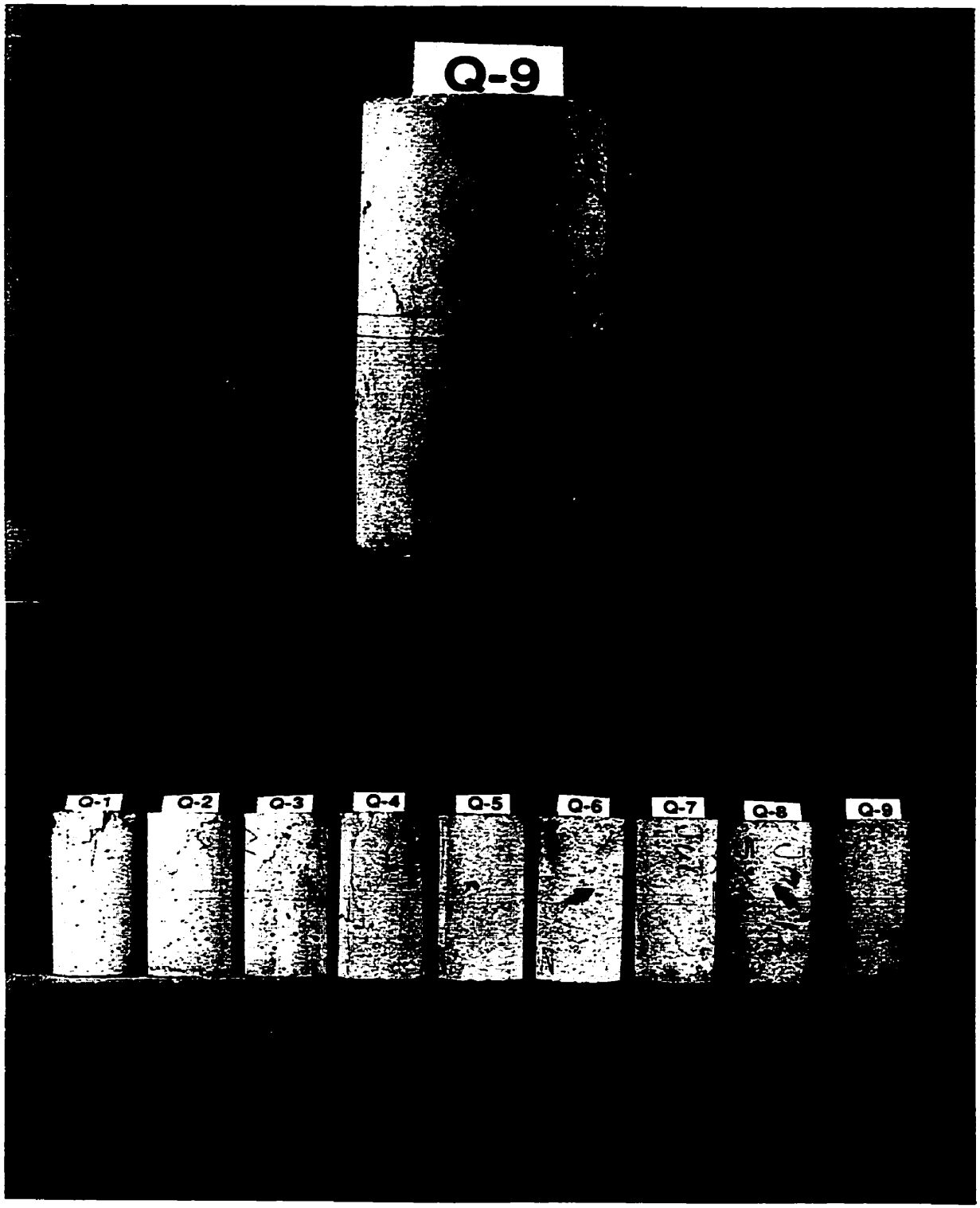

Figure 4-22: The 200×100 mm cylinders failed by uniaxial compression

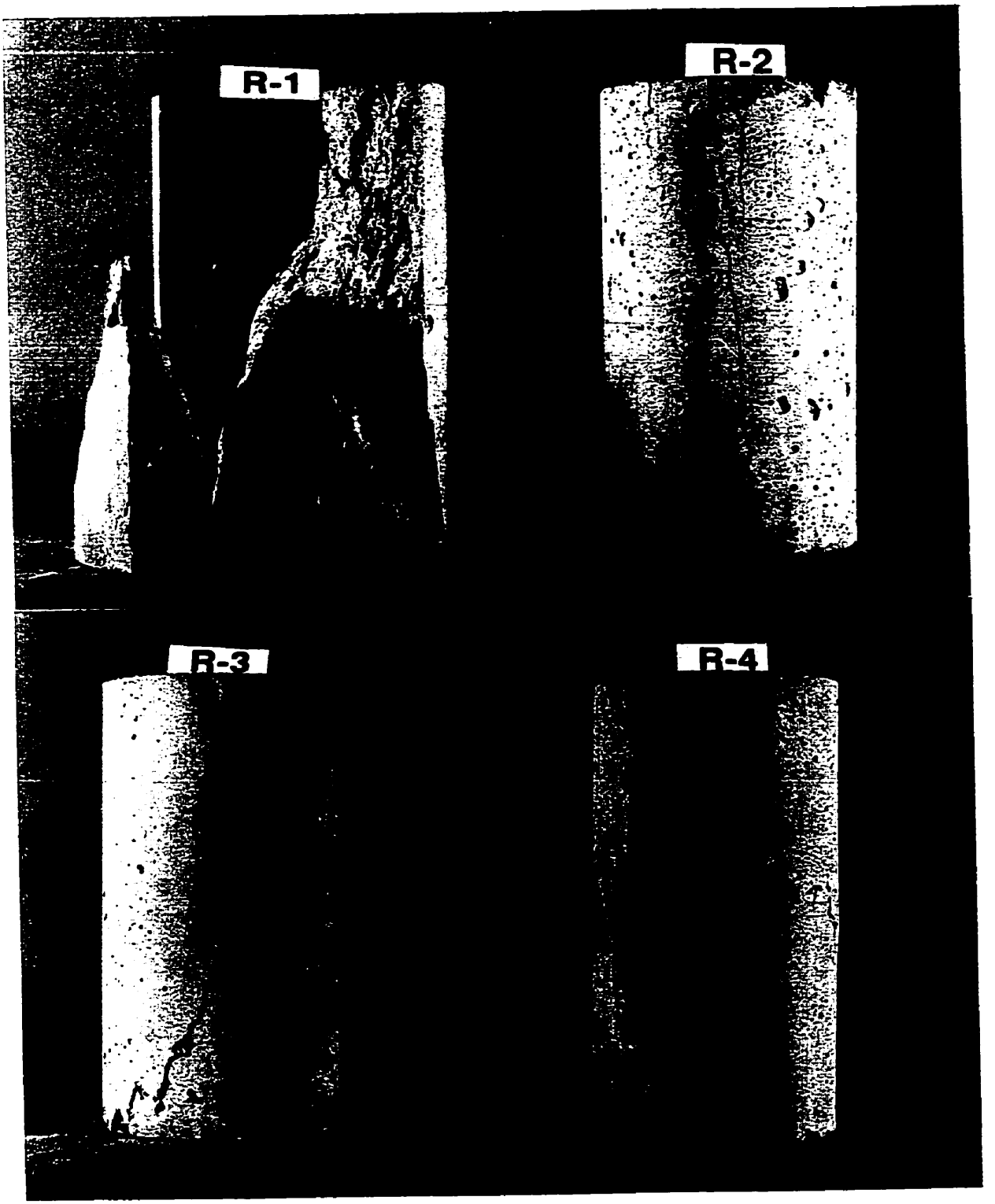

Figure 4-23: The 300×150 mm cylinders failed by uniaxial compression

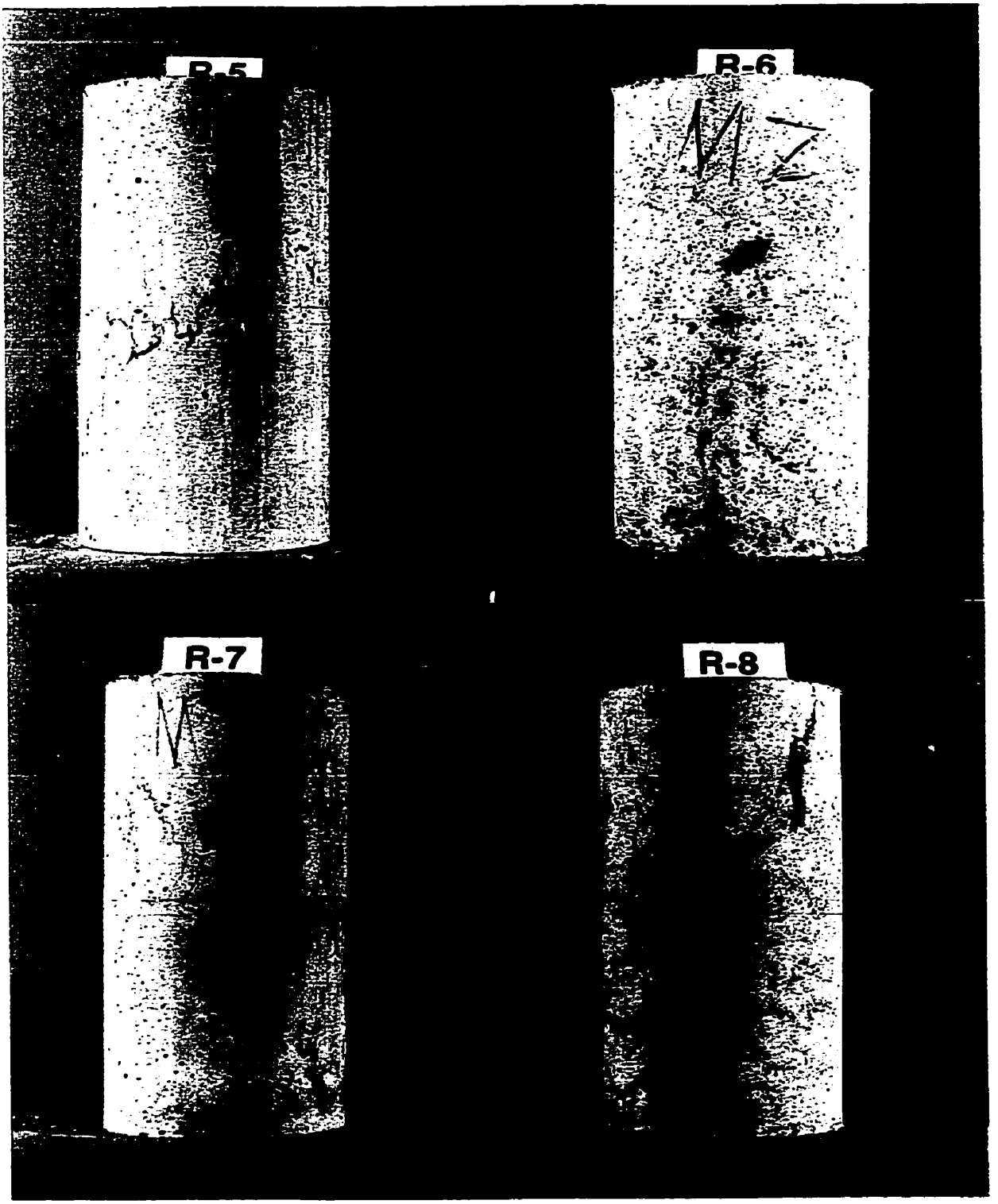

Figure 4-23: The 300×150 mm cylinders failed by uniaxial compression

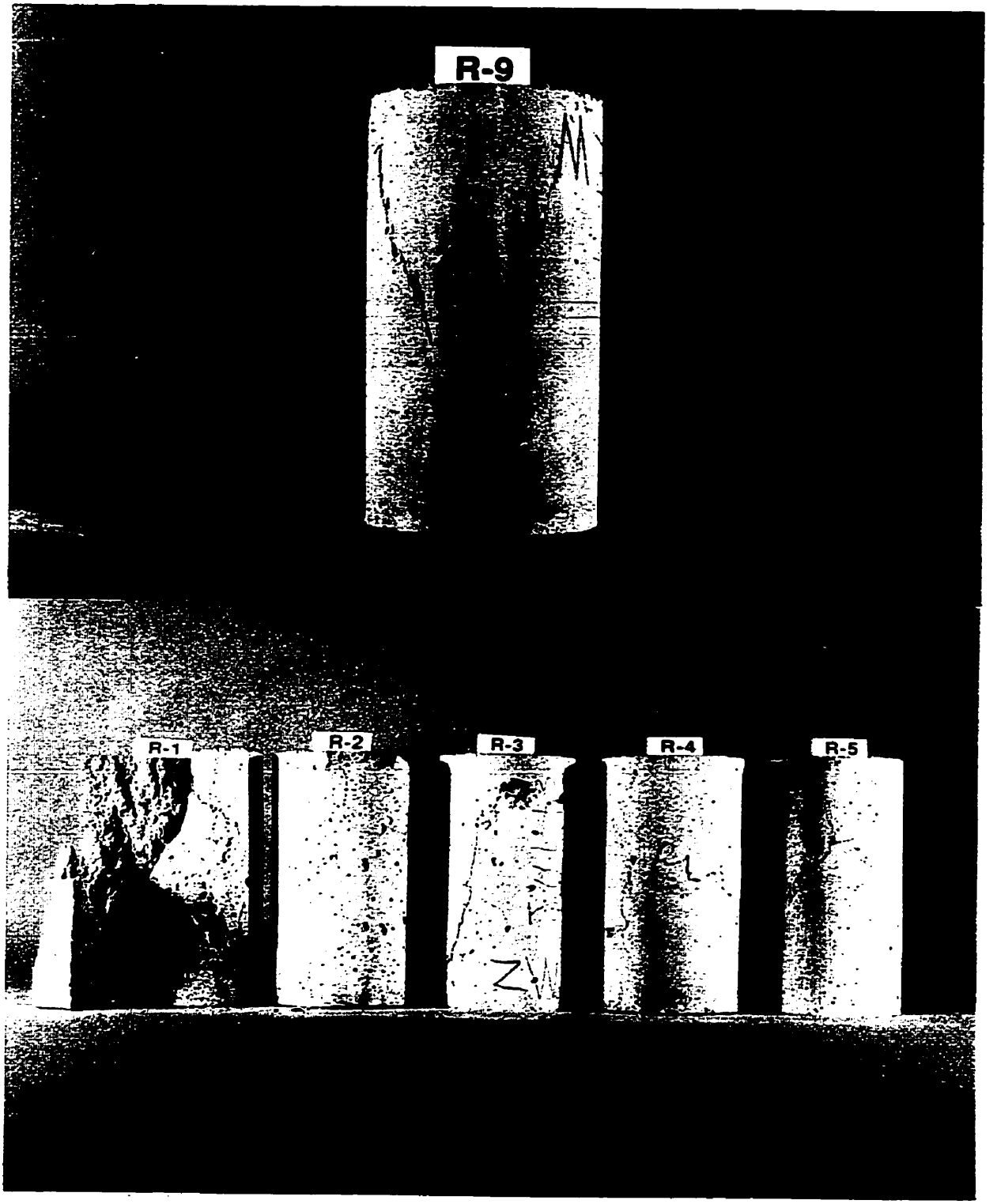

Figure 4-23: The 300×150 mm cylinders failed by uniaxial compression

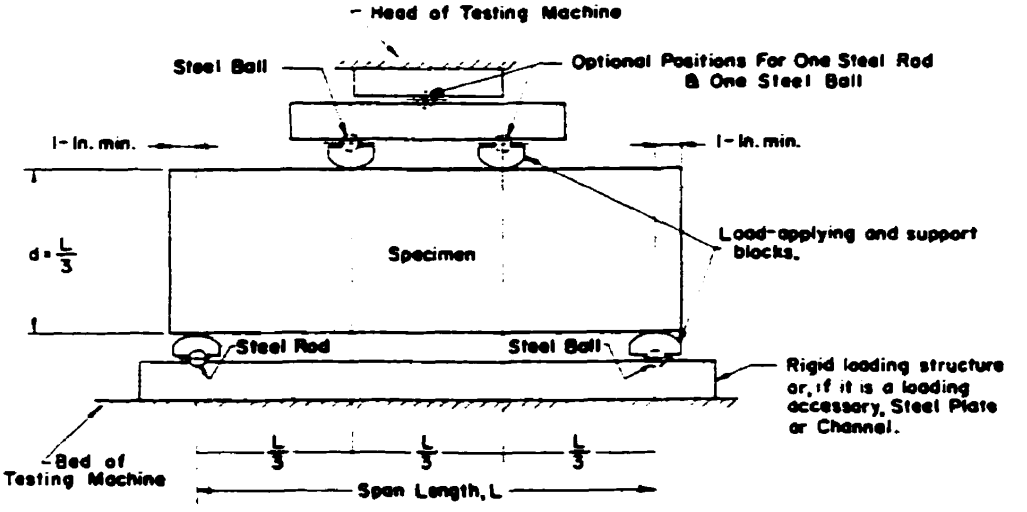

NOTE 1—This apparatus may be used inverted. If the testing machine applies force through a spherically seated head, the center pivot may be omitted, provided one load-applying block pivots on a rod and the other on a ball.
NOTE 2—1 in. = 25.4 mm.

Figure 4-24: Schematic four-point loading test
(taken from ASTM-C-78, 1994)

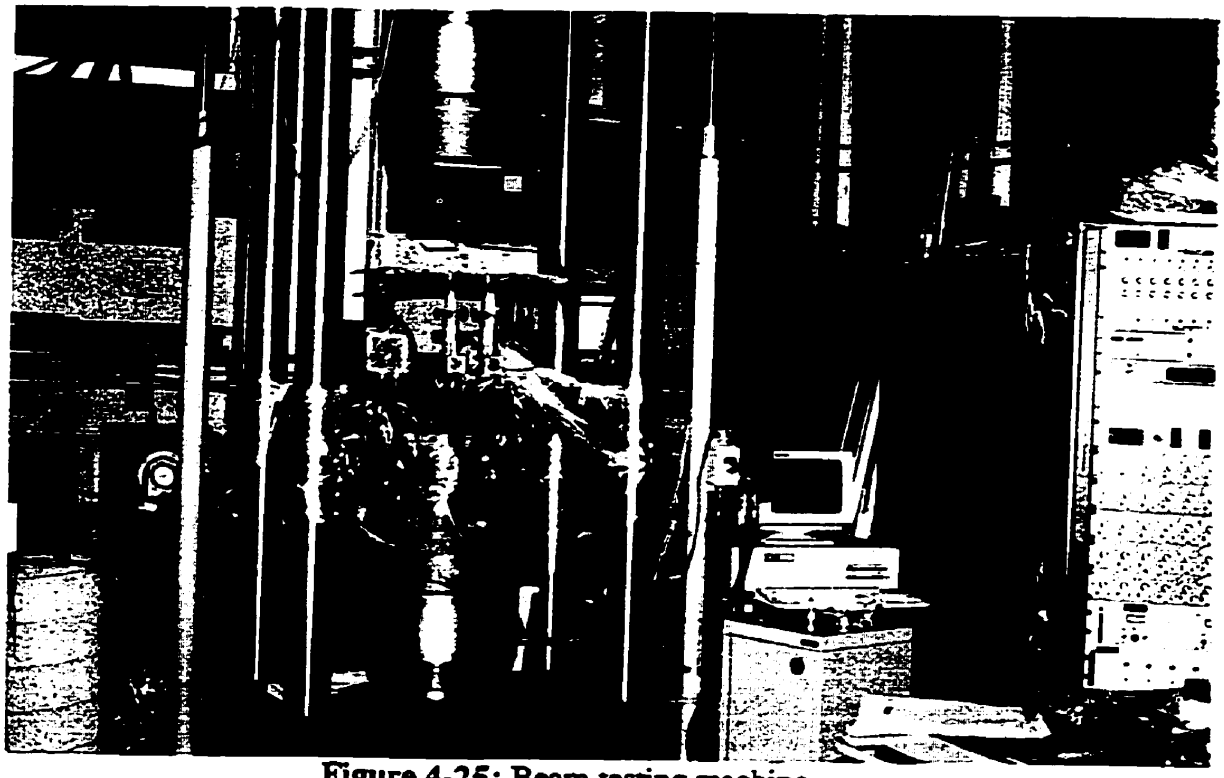

Figure 4-25: Beam testing machine

Figure 4-26: Beam loading system and LVDTs for measuring deformations

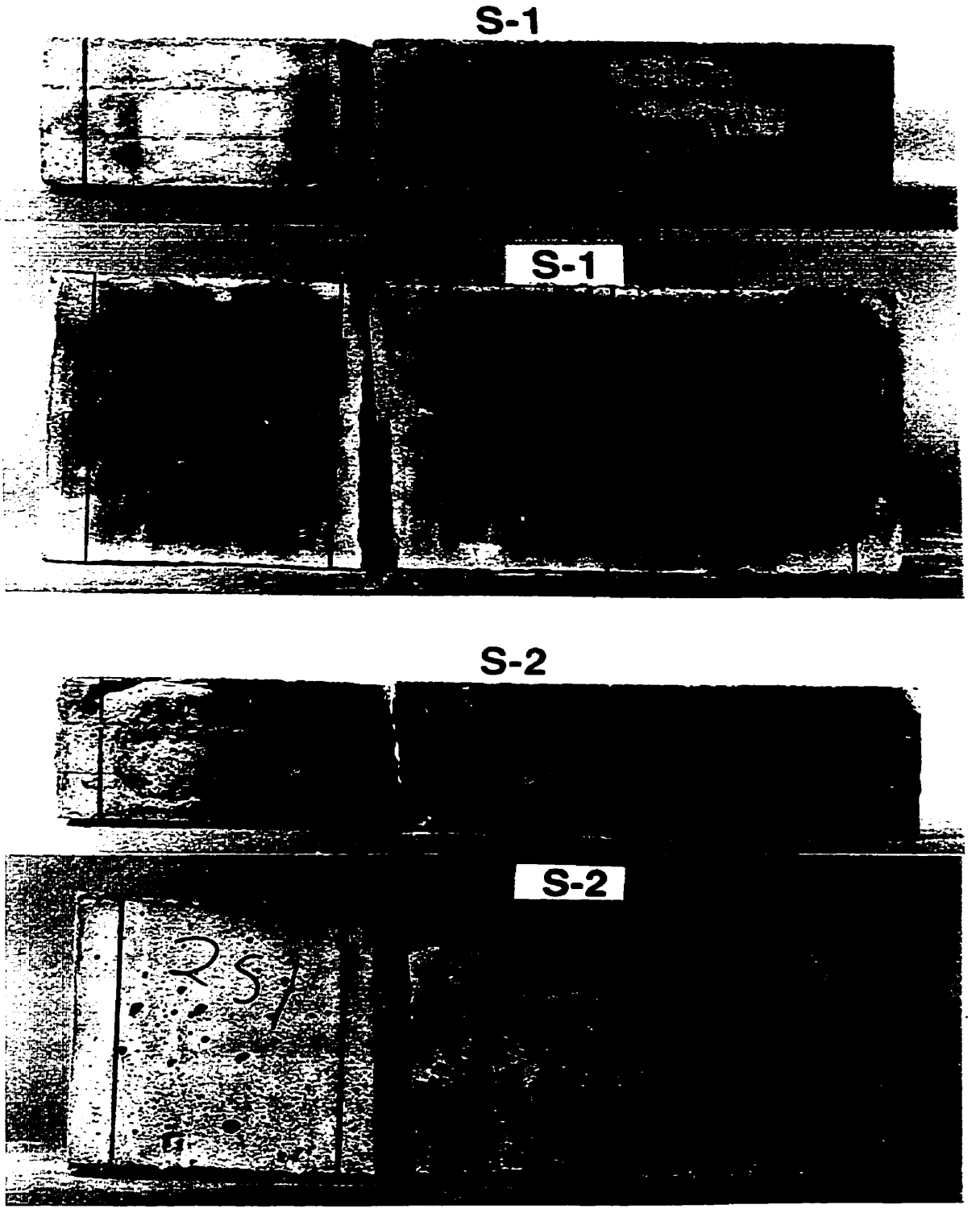

Figure 4-27: Beams after being tested
top: side view; bottom: bottom view

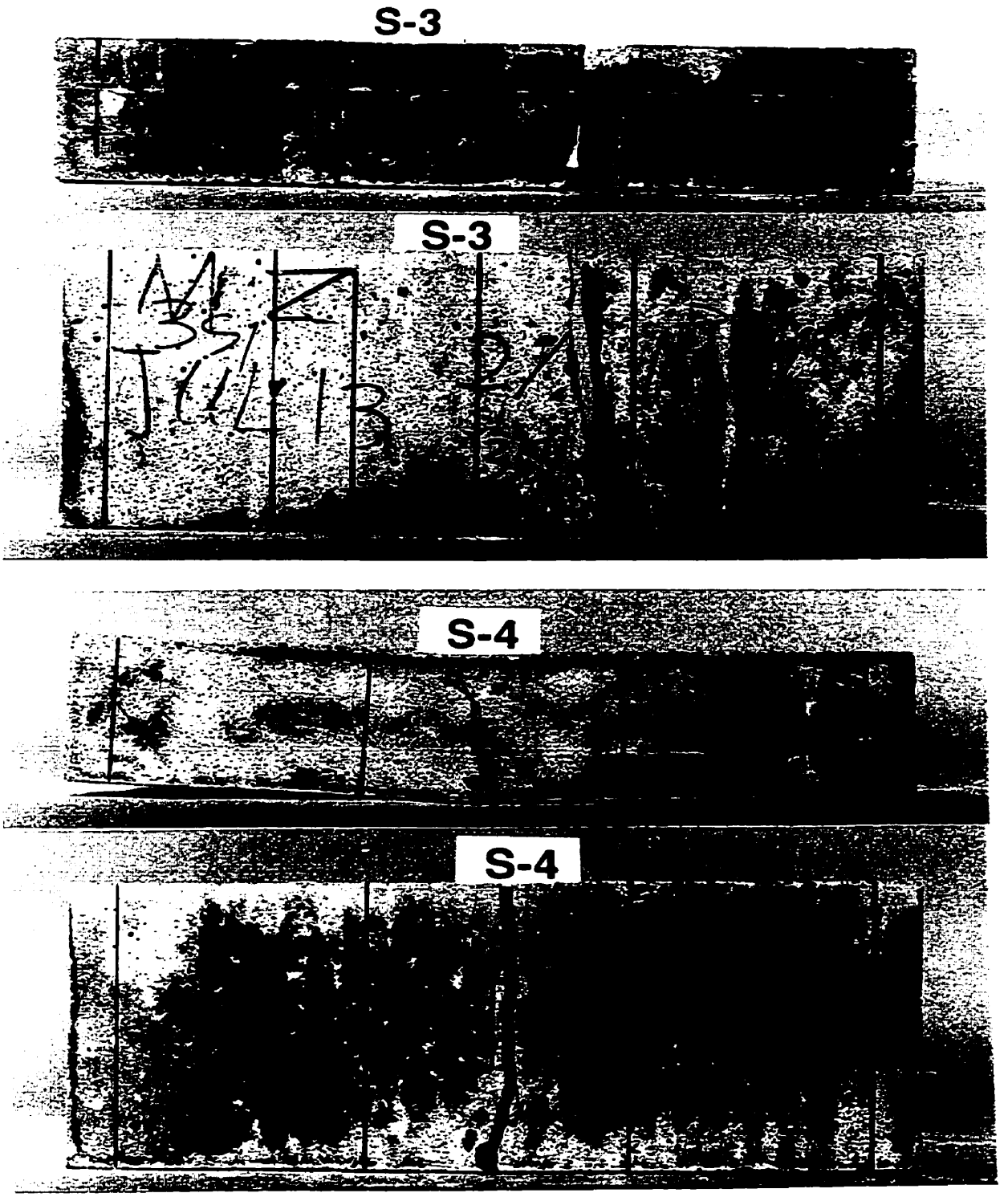

Figure 4-27: Beams after being tested
top: side view; bottom: bottom view

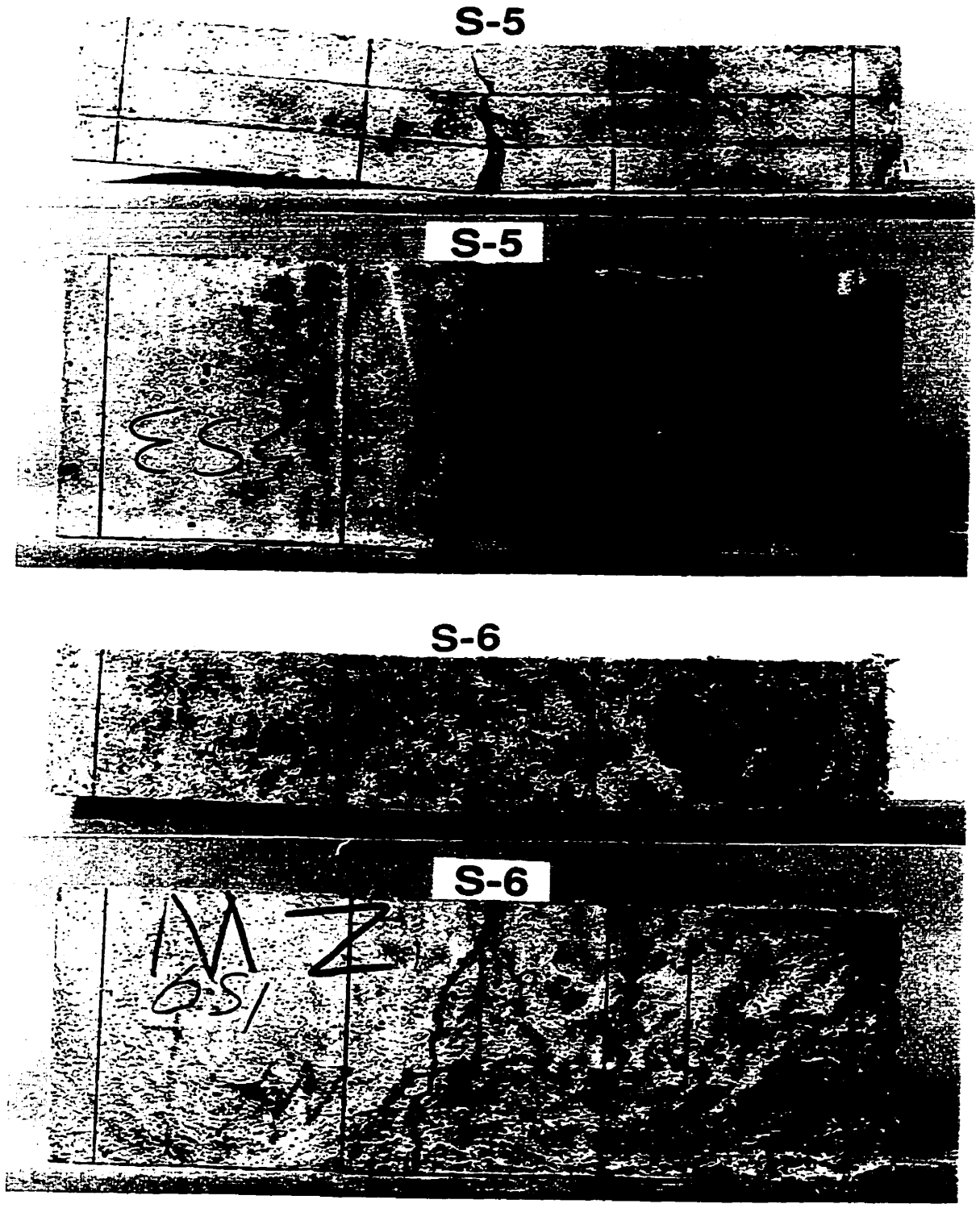

Figure 4-27: Beams after being tested
top: side view; bottom: bottom view

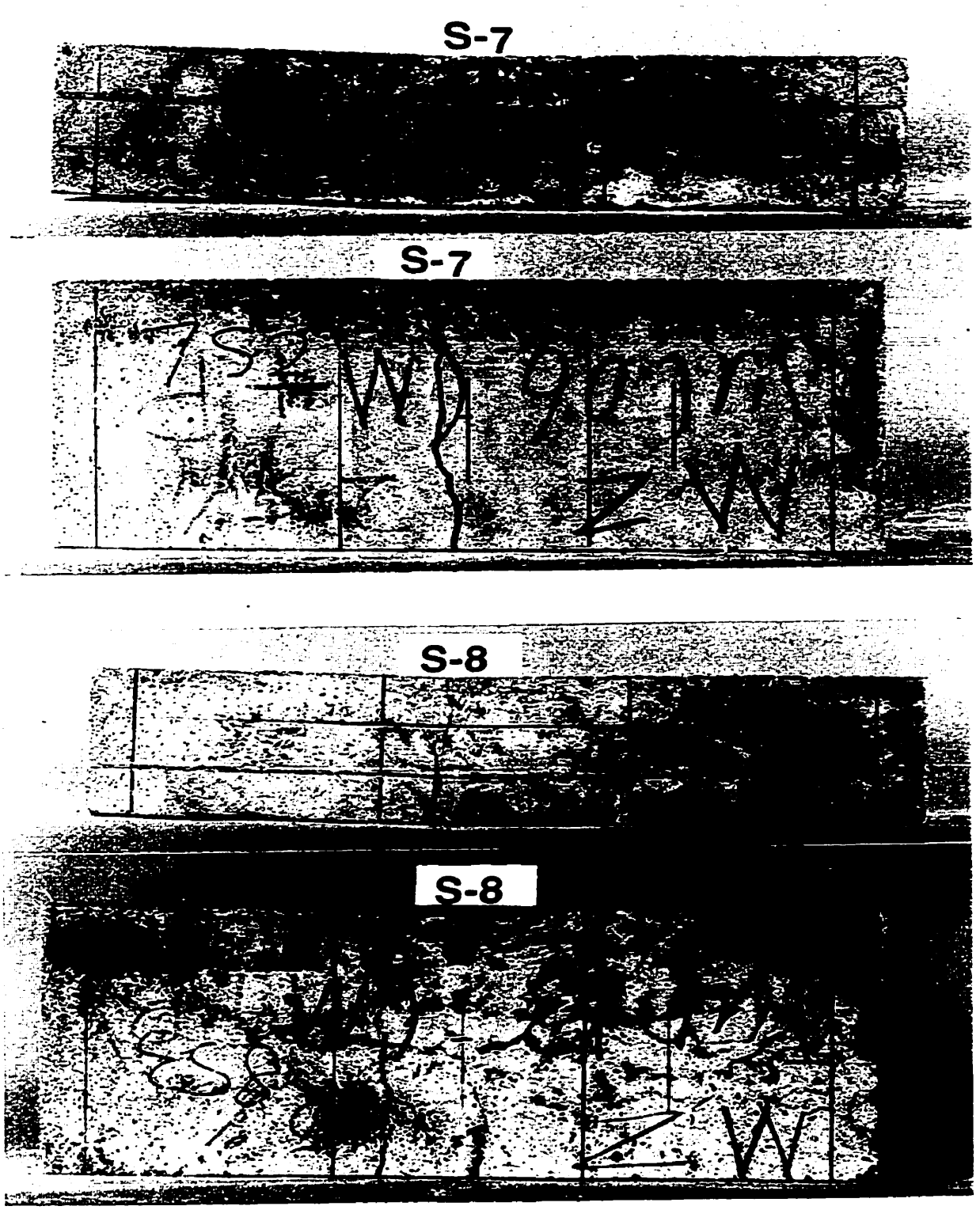

Figure 4-27: Beams after being tested
top: side view; bottom: bottom view

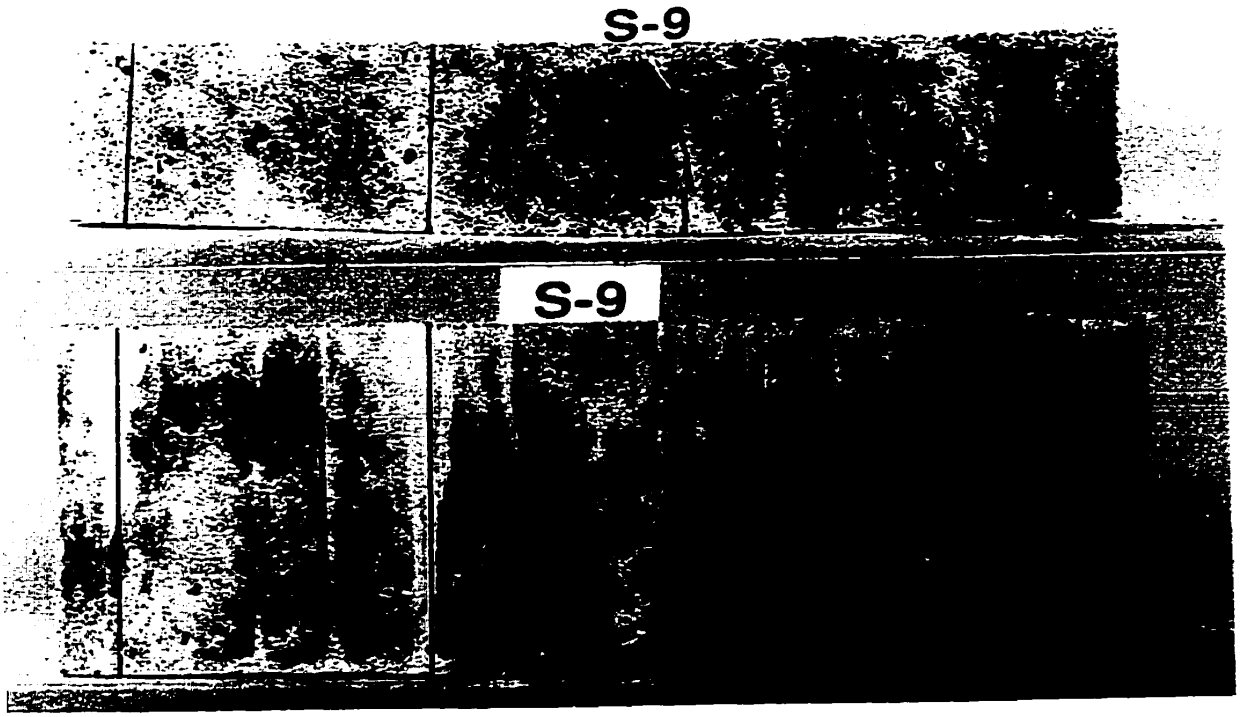

Figure 4-27: Beams after being tested
top: side view; bottom: bottom view

5. Discussion of Test Results

Addition of fibers to concrete alters its known behavior for any imposed stress condition. The purpose of this experimental study was to determine and quantify the response of fiber reinforced concrete, with respect to its fiber type and content, to a variety of loading conditions. The degree of internal damage, which was identified by volumetric strain, was assessed in order to establish the effects of these conditions on the internal structure, and the relationship between damage and response of various types of FRCs. A number of tests on a variety of FRCs (Table 3-1) were performed to illustrate each effect, and the test results are described and discussed in this chapter.

5.1. Porosity of The Internal Structure of FRC

Table 3-3 presents the unit weight of the batches which were used in this experiment. It can be seen that addition of fibers resulted in lower density than what was expected, which means an unintentional increase in porosity. This phenomenon was noted by Bayasi and Soroushian (1992), Rossi (1994), Raivio and Sarvaranta (1994), Tavakoli (1994), and Bayasi and Zeng (1994). The schematic model of Rossi (1994) (Figure 2-3) explains the formation of air pockets around the fibers, which was so called "wall effect", and BSE images (Raivio and Sarvaranta, 1994) have confirmed their existence.

In this experiment, the batches which contained steel micro-fibers and polypropylene fibers had the lowest relative unit weights. In the first group, big holes were formed which were not eliminated by different compaction methods. Hooton (1995) and Banthia (1995) suggested that, perhaps, organic impurities are mixed with the steel micro-fibers and due to chemical reaction with the cement produce gases which create holes in the concrete. Mixes which contained polypropylene fibers, particularly at high volume ratio, were stiff and very difficult to compact. The low relative unit weights of

these batches are caused mainly by this difficulty. However, the reasons which were just mentioned are additional to the "wall effect".

5.2. Effects of Type and Content of Fibers

A total of 9 batches were cast which contained the same concrete matrix, but different fiber types and contents. The results of test type A (Table 3-1), which is the uniaxial compression test on saturated 100×50 mm cylinders, have been used as reference in order to construct the comparative arguments of this section. Figures 5-1 and 5-2 show the response of one representetive specimen from each batch. Figure 5-1 presents the axial stress versus axial and circumferential strains, whereas Figure 5-2 illustrated the volumetric strain versus axial strain for those specimens.

- **Compressive Strength (f'_c):** The strength of different batches are presented in Figure 5-3. Additions of 1% micro and steel fibers (Batches 2 and 4) did not have considerable effects on the strength of concrete, but adding 2% of those fibers decreased the compressive strength (Batches 3 and 5). The increase in fiber content led to increase in void ratio (wall effect) which in turn weakened the strength of concrete. Addition of polypropylene fibers, which have low modulus of elasticity lowered the strength of concrete (Batches 6 to 9). As the fraction of polypropylene fibers increased, the strength decreased. The strength of high fiber content concrete (Batch 6) is about half that of plain concrete. Batch 9 had the highest strength among polypropylene fiber concretes. Batch 7, which had 1.5% polypropylene fibers (equal amount to that of Batch 9) and 1% micro-fibers (equal amount to that of Batch 2) had lower strength than either Batches 9 or 2.

- **Elastic Modulus (E):** Figure 5-4 shows the variation in the modulus of elasticity of the batches. Micro fibers had less weakening effect on E than steel fibers. The E

modulus of high content polypropylene fiber concrete (Batch 6) was about 70% of that of plain concrete, but the addition of 1.5% polypropylene fibers (Batch 9) caused a slight reduction in elastic modulus. The E value of batch 7 is between the respective values of Batches 2 and 9.

- **Poisson's Ratio (ν):** Figure 5-5 illustrates the ν value of all batches. In general the addition of fibers reduces the Poisson's ratio of concrete. Note that a high ν value indicates a high rate of increase of the lateral strain relative to the axial one, leading to higher area strain and a lower value of ε^* or a higher degree of internal damage. The fibers restrict the movements of concrete particles, and thereby lower the Poisson's ratio. However, the high content polypropylene fiber concrete (batch 6) has ν value higher than that of plain concrete. The dense network that the fibers had formed determined overwhelmingly the response of this fiber concrete. The increase of micro fiber content decreased the Poisson's Ratio slightly (batches 2 and 3). However, doubling the steel fiber content raised the ν value by 20% (batches 4 and 5). This can be explained by the wall effect and the increase in voids which leads to less effectiveness of steel fibers (in elastic region). However, more study in this area is required.

- **ε_c and ε^*:** Figure 5-6 illustrates the axial strain at peak load, ε_c, and the axial strain corresponding to zero volumetric change, ε^*. Addition of 1% micro and steel fibers resulted in slightly higher strain at peak load, but addition of 2% of these fibers decreased this strain. The polypropylene fibers at high volume (batches 6 and 8) increased the strain at peak about 25%, but these fibers at 1.5% volume decreased ε_c about 10%. The values of axial strain at zero volumetric change are higher than ε_c, and follow the same pattern for micro and steel fibers (batches 2 to 5). For concrete containing a high fraction of polypropylene fibers (batches 6 and 8), the ε^* value is

about 20% lower than the respective ε_c value, whereas for concrete with low fraction of this fiber type, ε^* is slightly higher. In general, it can be concluded that the internal structure of concrete containing high fraction of polypropylene fibers is severely damaged before it reaches its peak stress, where as for the other types of FRC severe damage (ε^*) occurs after bearing the peak stress.

- **Softening:** Softening, in this report, has been defined as the slope of the descending branch of stress-strain curve. Figure 5-7 represents the softening values based on three alternative computations of the softening parameter (S_{85}, S_{50}, and S'; ref. to Notation). The addition of certain fibers has caused reduction in the slope of descending branch. Steel fibers were more effective than micro (steel) fibers in this reduction, since they were anchored at the ends and could bridge macro-cracks in concrete. For batch 6 (4% polypropylene fibers) the values of S_{85} and S_{50} could not be obtained, since the descending branch remained close to a horizontal line. The concrete with low percentage of polypropylene fibers (batch 9) had similar response as that containing steel fibers. The other batches with polypropylene fiber mixed with micro-fibers (batches 7 and 8) had very low softening values.

- **Deformability:** In this report deformability has been defined by axial strain corresponding to 85% and 50% of the peak load on the descending branch of the stress-strain curve. Therefore, the ductility results are equivalent to the softening results. Figure 5-8 shows the deformability of different batches. The variation in ε_{50} is greater than that of ε_{85}. Batches 5 (2% micro and steel) and 8 (5% micro and polypropylene) show high values. The deformability of batch 6 (4% polypropylene) in the scale of Figure 5-8 is infinity.

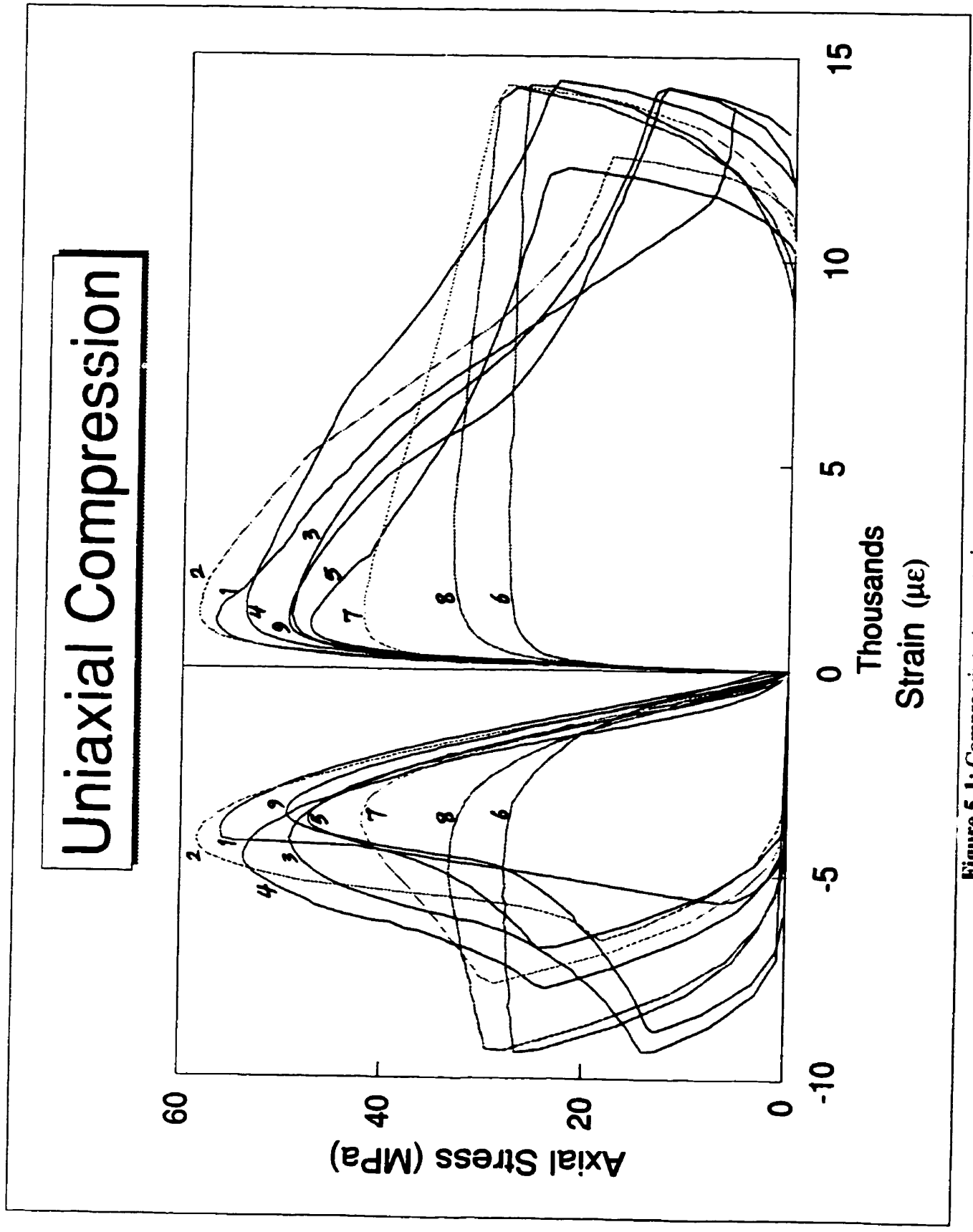

Figure 5-1: Compressive stress-strain curves
Left: axial; Right: circumferential

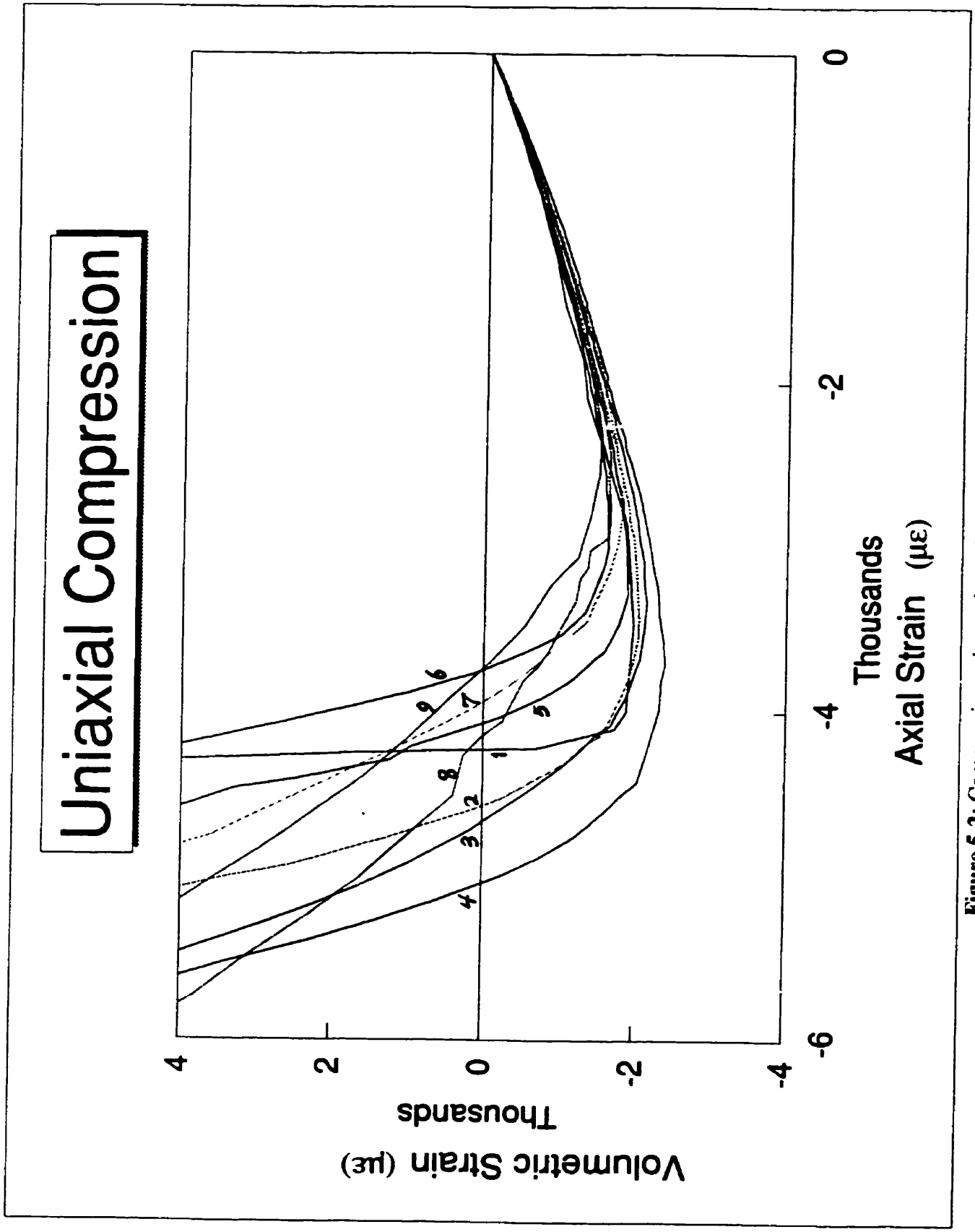

Figure 5-2: Compressive volumetric strain vs. axial strain curves

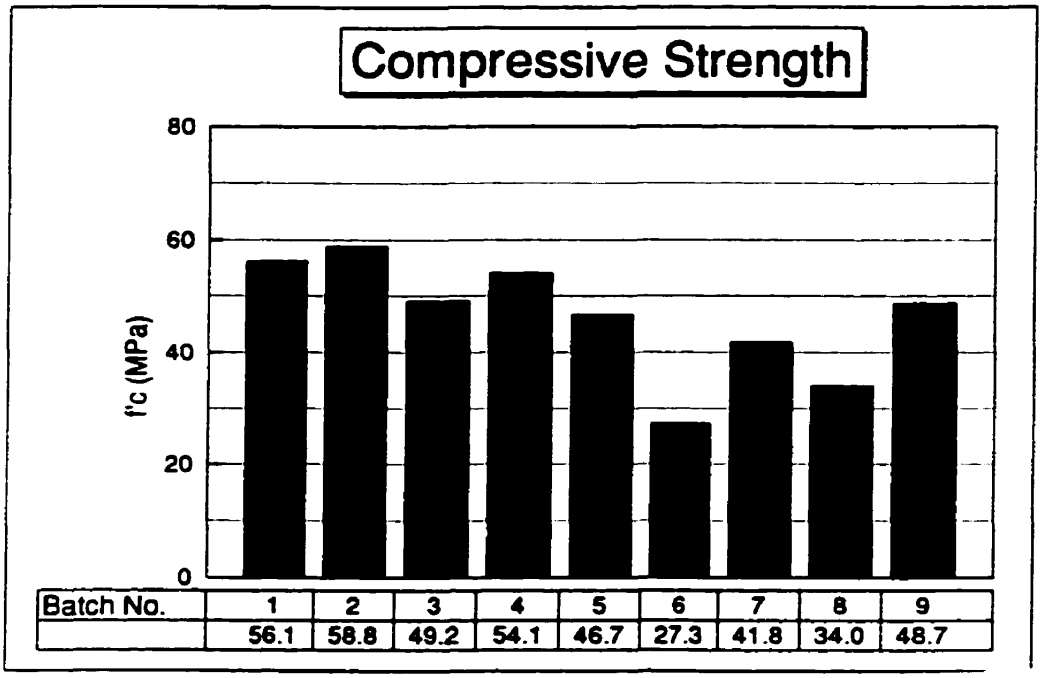

Figure 5-3; Compressive strength of the batches with various fiber types

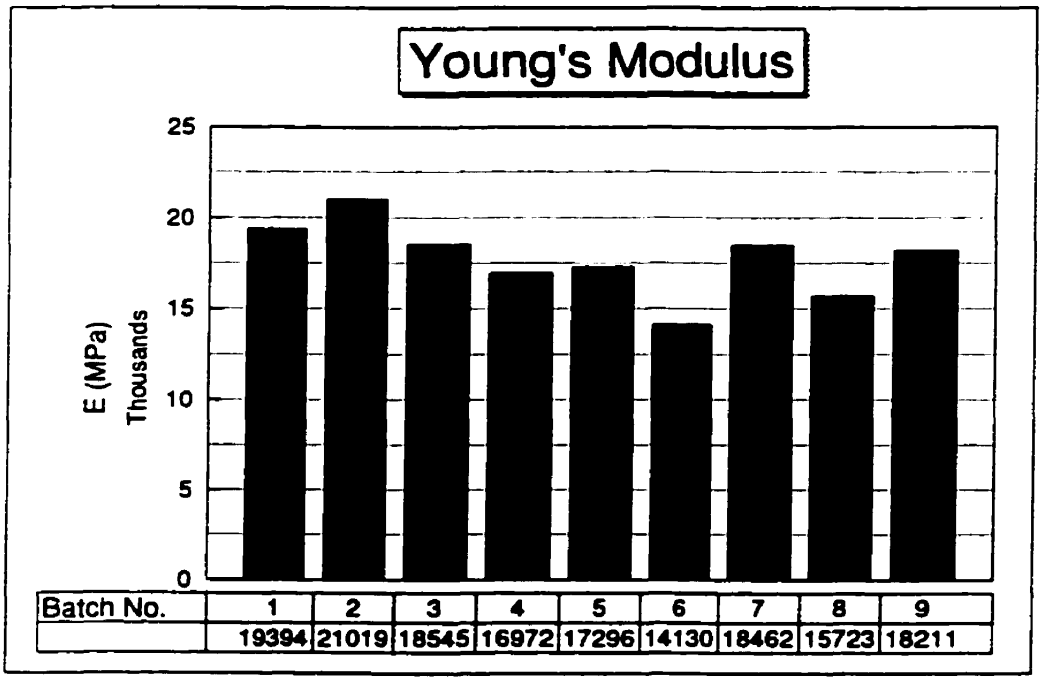

Figure 5-4; Young's Modulus of the batches with various fiber types

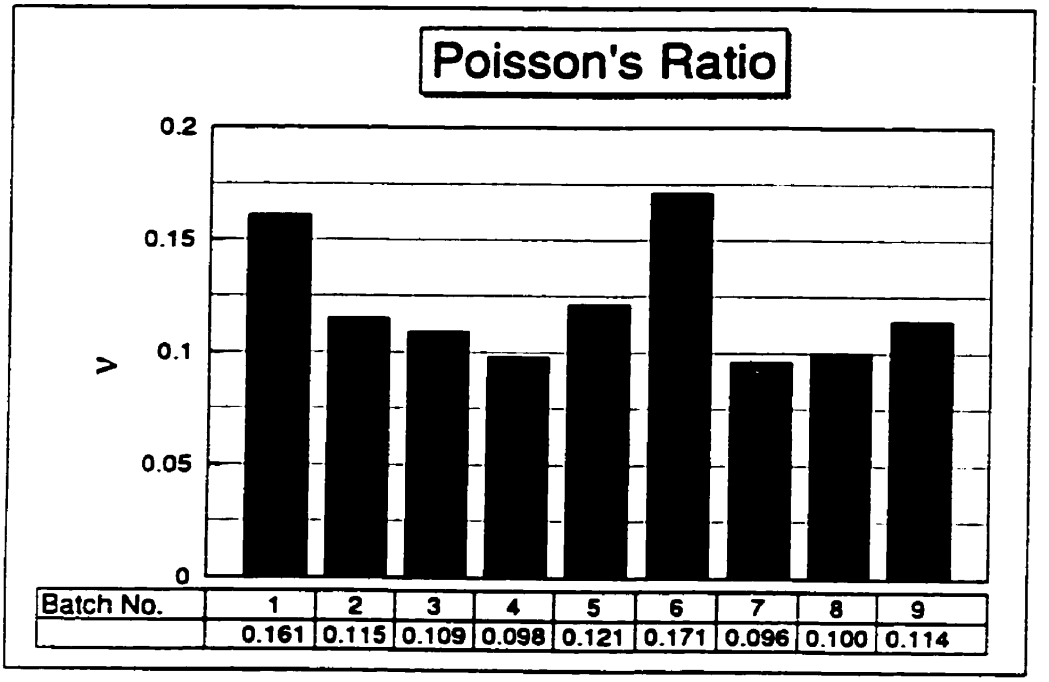

Figure 5-5; Poisson's Ratio of the batches with various fiber types

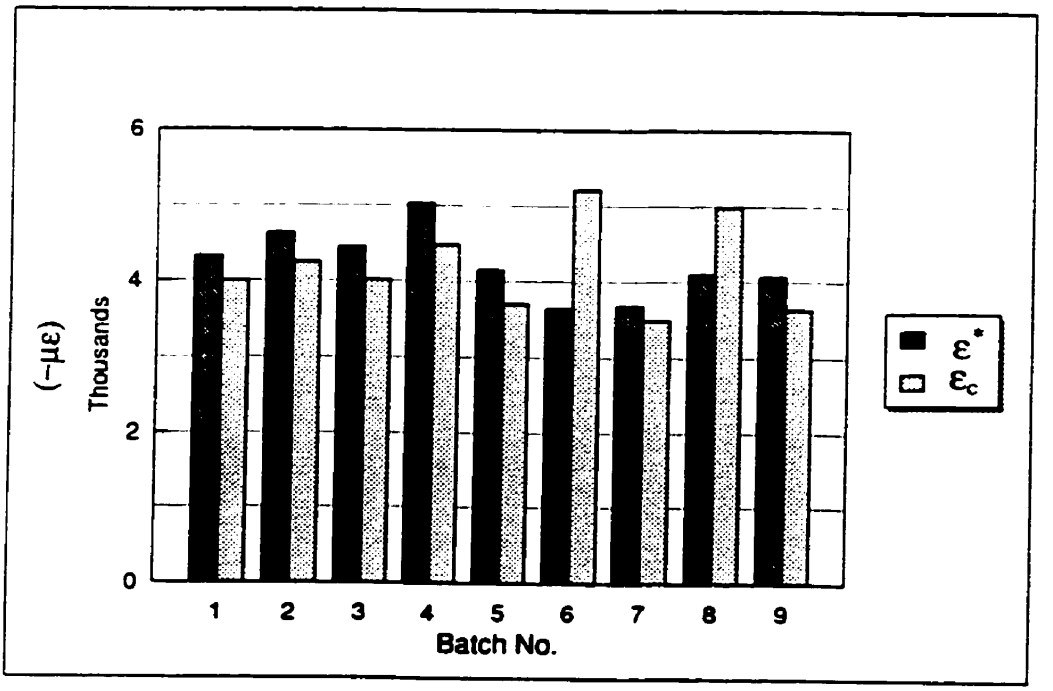

Figure 5-6; Values of ε^* and ε_c of the batches with various fiber types

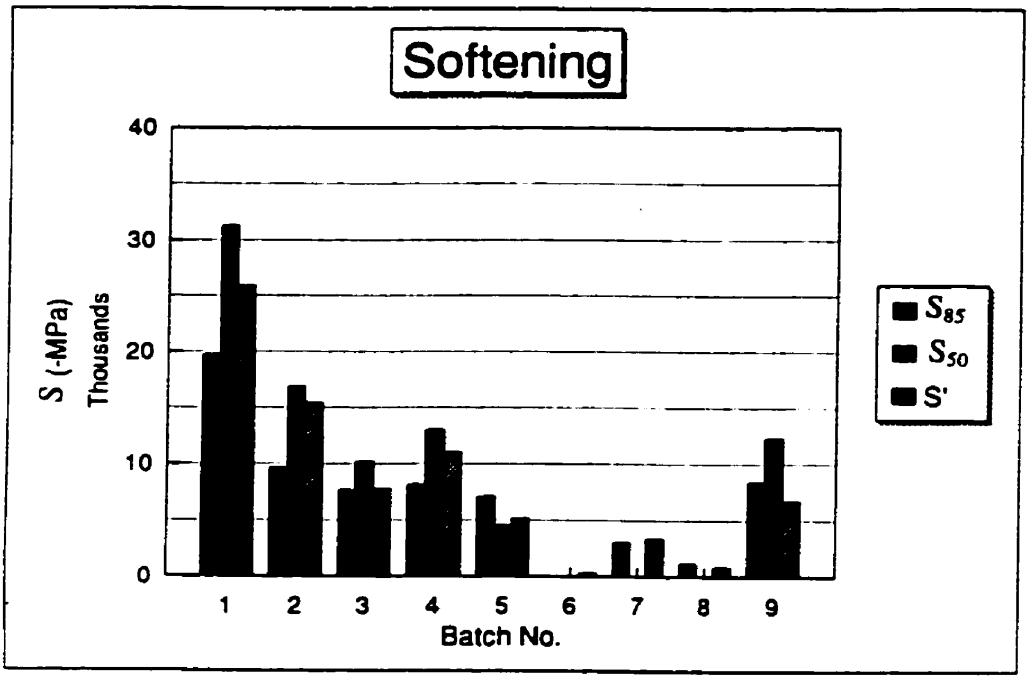

Figure 5-7; Softening values of the batches with various fiber types

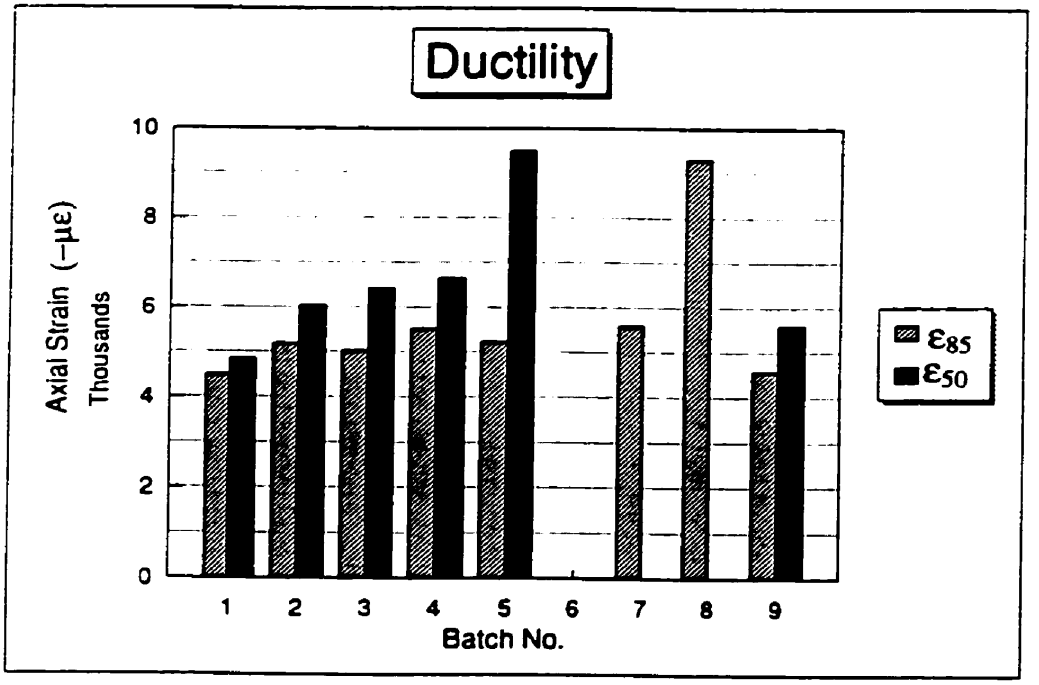

Figure 5-8; Ductility values of the batches with various fiber types

5.3. Effects of Confinement

The mechanical behavior of concrete shows load-path-independence with respect to strength, but not with respect to deformation (Imran and Pantazopoulou, 1995). Kinematic restraint, imposed by the boundary conditions, acts against volumetric expansion thereby delaying the onset of failure. Different damage processes which result from different rates of volumetric expansion lead to different concrete response. In this research, the effects of confinement on the mechanical properties of fiber concrete have been studied in active and passive confinement conditions. The test types, which are considered in this section, are listed in columns A to E of Table 3-1, for active confinement, and columns N to P of the same table, for passive confinement. Both series of tests have been performed on 100x50 mm saturated cylinders.

The effective lateral pressure, which was experienced by the saturated specimen during the confined tests, was actually less than the apparent pressure applied due to generated pore water pressure. Therefore, a corrective formula, which was proposed by Imran and Pantazopoulou (1995) to adjust the lateral stress values, has been used in this study to evaluate the effective circumferential stress:

$$\sigma'_{lat} = \sigma_{lat} - p\, v_{void} \qquad (5\text{-}1)$$

where, σ'_{lat} is the effective lateral stress, σ_{lat} is the applied lateral stress, v_{void} is the effective porosity of the concrete, and p is the pore pressure build up due to the initial volumetric contraction of the material. The pore water pressure p was taken equal to the applied lateral pressure. Then:

$$\sigma'_{lat} = \sigma_{lat}\ (1 - v_{void}) \qquad (5\text{-}2)$$

The values of v_{void} has been calculated in Chapter 4, and listed in Tables 4-5 and 4-6.

The mechanical properties of concrete batches under various degrees of confinement were determined from the recorded stress-strain response. The volumetric strain was assessed to study this properties of FRC through the state of internal damage. In the following discussions, the lateral pressure and the corresponding mechanical

properties are normalized to the respective values of test type A for each batch, in order to compare the results.

- **Maximum Strength:** The maximum strength of fiber concrete increases almost linearly with the degree of confinement (i.e. with lateral stress). Table 5-1 demonstrates these variations which are also plotted in Figure 5-9. Both passive and active confinements produce a similar pattern which can be approximated by a linear relationship. The effect of confinement is slightly less on Batch 5, which contains 2% micro plus steel fibers. Furthermore, note that some of the specimens subjected to passive confinement had two peak values on the stress-strain curve, which will be discussed in section 5.6 For these specimens the higher values have been considered in defining the entries of Table 5-1 and Figure 5-9.

- **Strains at Maximum Strength:** The values of axial strain corresponding to the maximum strength (defined in the previous section) are presented in Table 5-2 and Figure 5-10. These values show a non-linear increase with increasing lateral stress, and are more scattered than the relevant stresses. At high degrees of active confinement (60% and 80%) this strain is higher for Batch 7, which had 1% micro and 1.5% polypropylene fibers. The values of this strain are slightly higher for the case of passive confinement.

- **Zero Volumetric Strain (ε^*):** The axial strains at zero volumetric strain are shown in Table 5-3 and plotted in Figure 5-11. For many of the specimens, which were subjected to high confinement, theses values could not be obtained, because the dilative phase of the response was delayed past the limits of the testing system (measuring devices). In general the increase in confinement raised the value of ε^*, but the pattern of variation was not a regular relationship. From the comparison of Tables

5-2 and 5-3, it can be concluded that, by increasing confinement, ε^* increases faster than the axial strain corresponding to the maximum strength, i.e. the onset of severe internal damage occurs after the maximum strength is reached in many FRCs. This is the reason why the ε^* at higher degrees of confinement was not obtainable, and also the post peak softening response exhibited more ductility. The value of this strain was not obtained for Batch 7 at any degree of confinement, and for other batches at more than 40% confinement (except only one specimen). Batch 7 with total of 2.5% fibers is the only batch in this series of tests which contains polypropylene fibers.

- **Deformability (ε_{85}):** The values of axial strain corresponding to 85% of the peak stress (first peak for the wrapped cylinders) on the descending branch of stress-strain curve are presented in Table 5-4 and plotted in Figure 5-12. The specimens subjected to high degrees of active confinement, and many specimens subjected to various degrees of passive confinement did not experience 15% strength loss within the range of test. It appears that increase in confinement resulted in an almost exponential increase in the ε_{85} value. Furthermore the values of ε_{50} were hardly obtainable for confined FRC specimens. Batches 5 (2% micro and steel fibers) and 7 (2.5% micro and polypropylene fibers) did not reach to 85% of the peak value (on unloading branch) within the test range.

- **Elastic Modulus (E):** The values of the initial material stiffness obtained from stress-strain plots, E, are demonstrated in Table 5-5 and Figure 5-13. These values retain the same distribution pattern at different degrees of confinement. In general, increase in confining pressure raised the elastic modulus slightly (i.e. confinement raises the stiffness of structure).

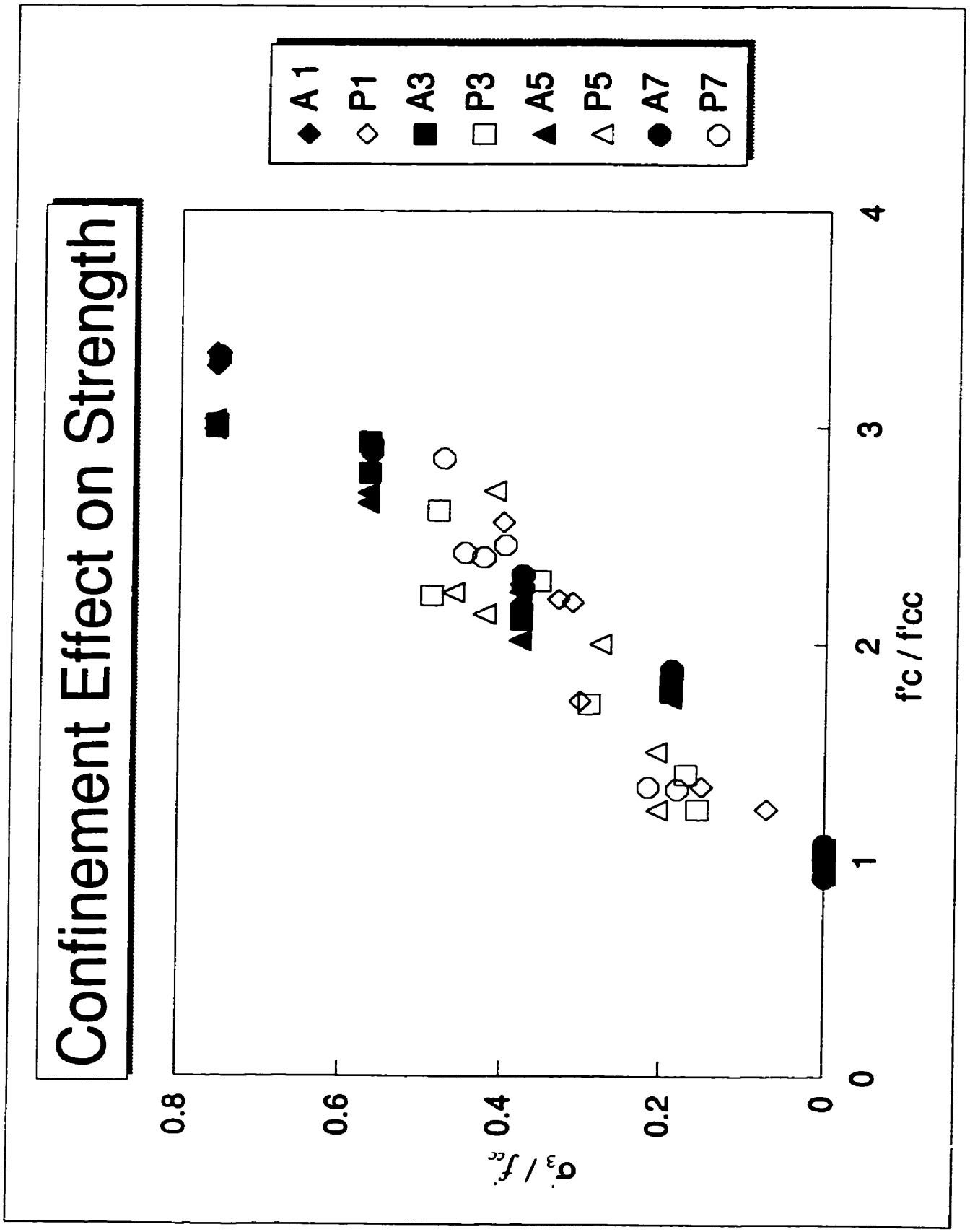

Figure 5-9: Effect of confinement on strength of FRC

A=active; P=passive

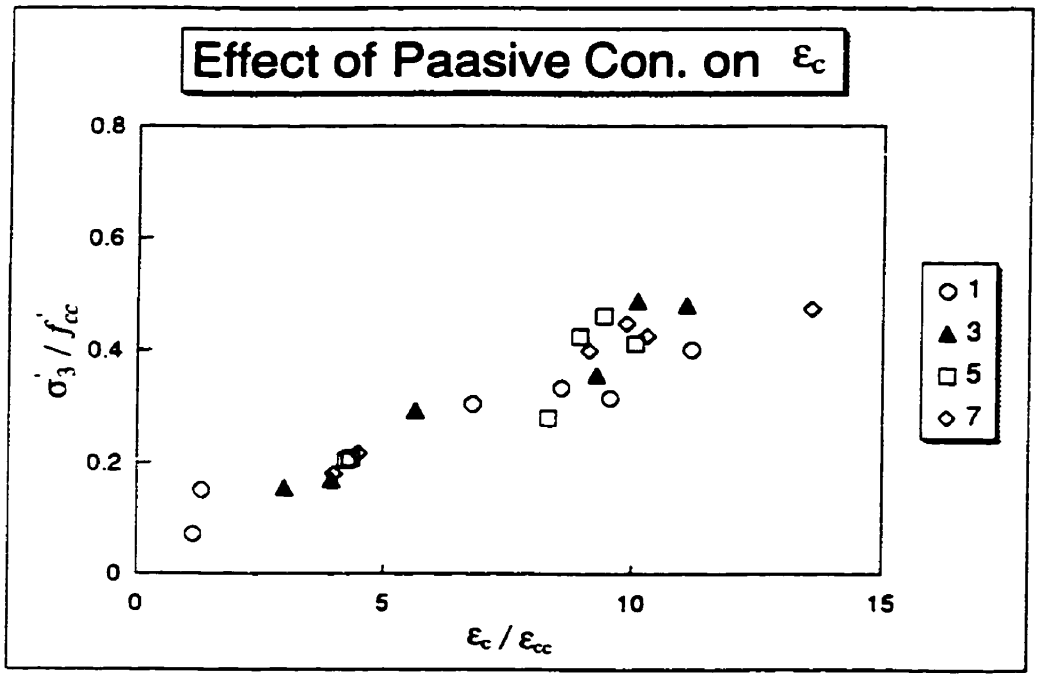

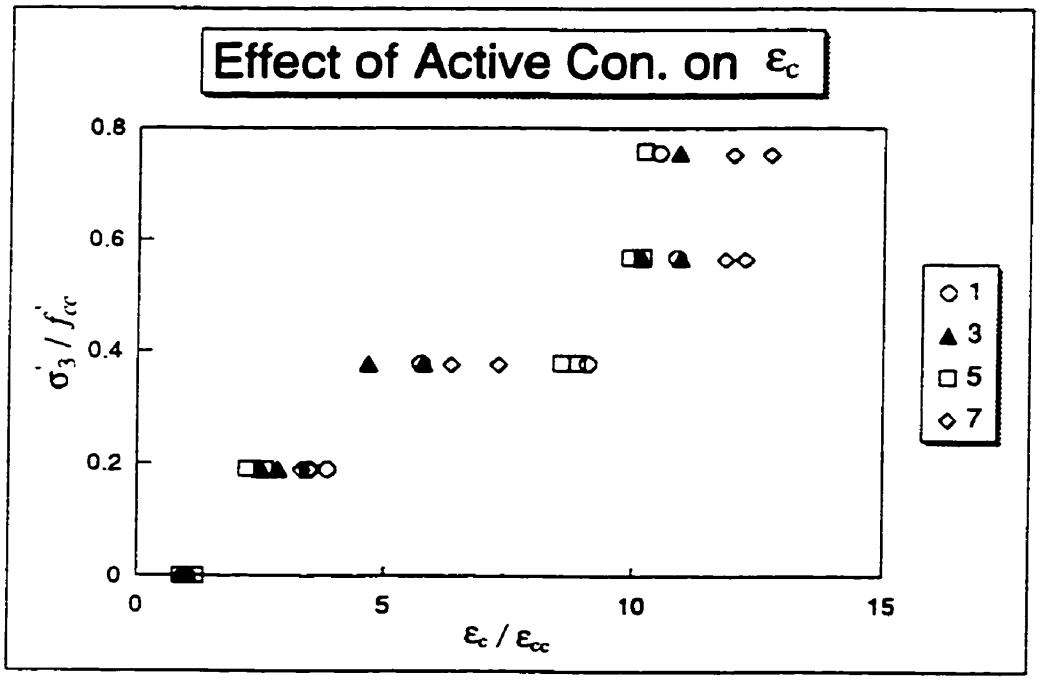

Figure 5-10: Effect of confinement on ε_c of FRC
active & passive separate

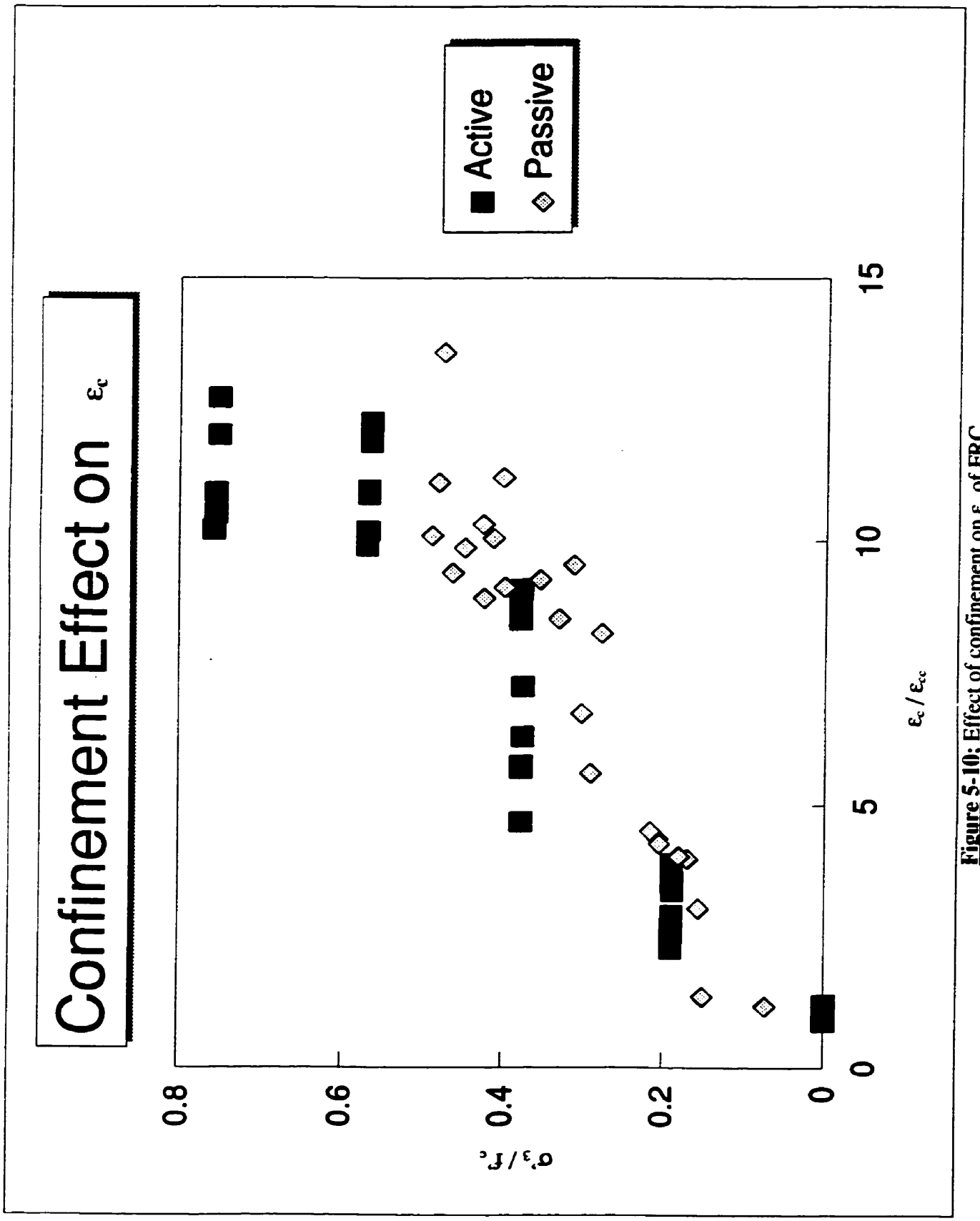

Figure 5-10: Effect of confinement on ε_c of FRC
active & passive combined

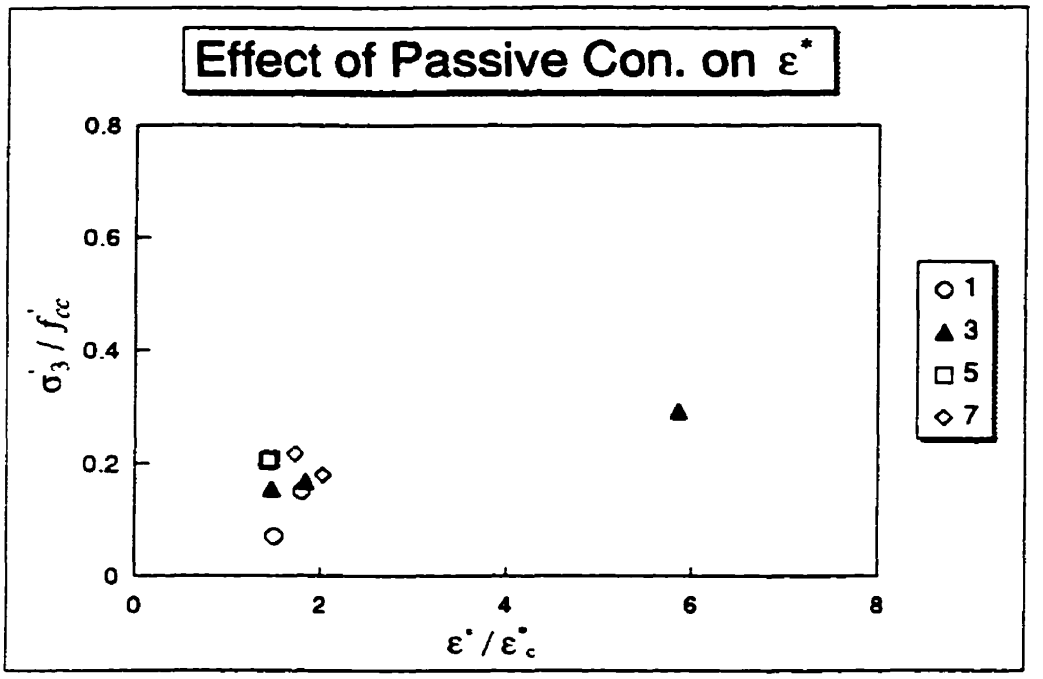

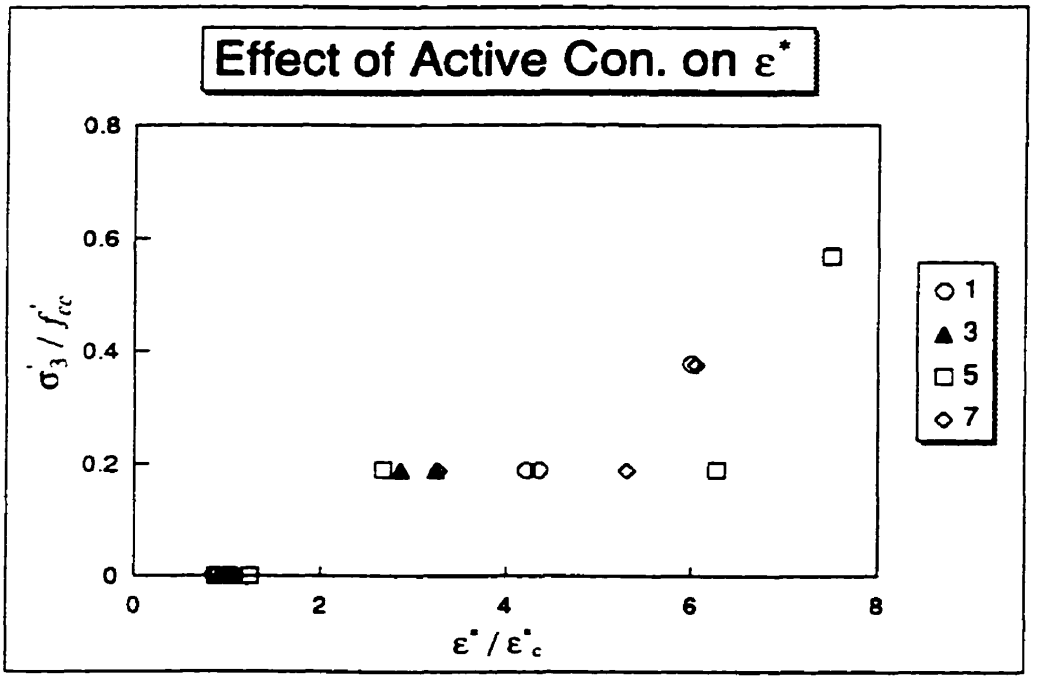

Figure 5-11: Effect of confinement on ε^* of FRC
active & passive separate

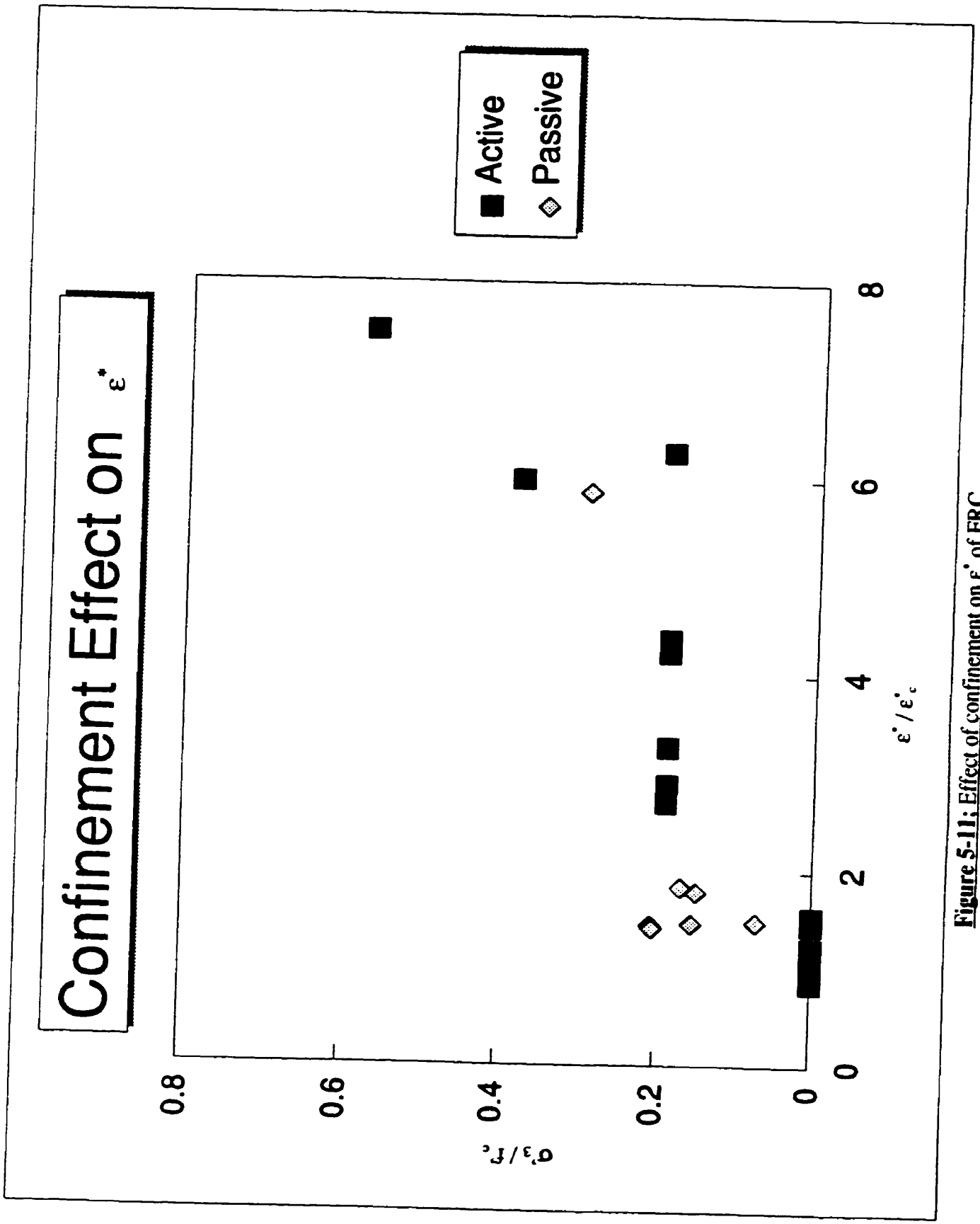

Figure 5-11: Effect of confinement on ε' of FRC
active & passive combined

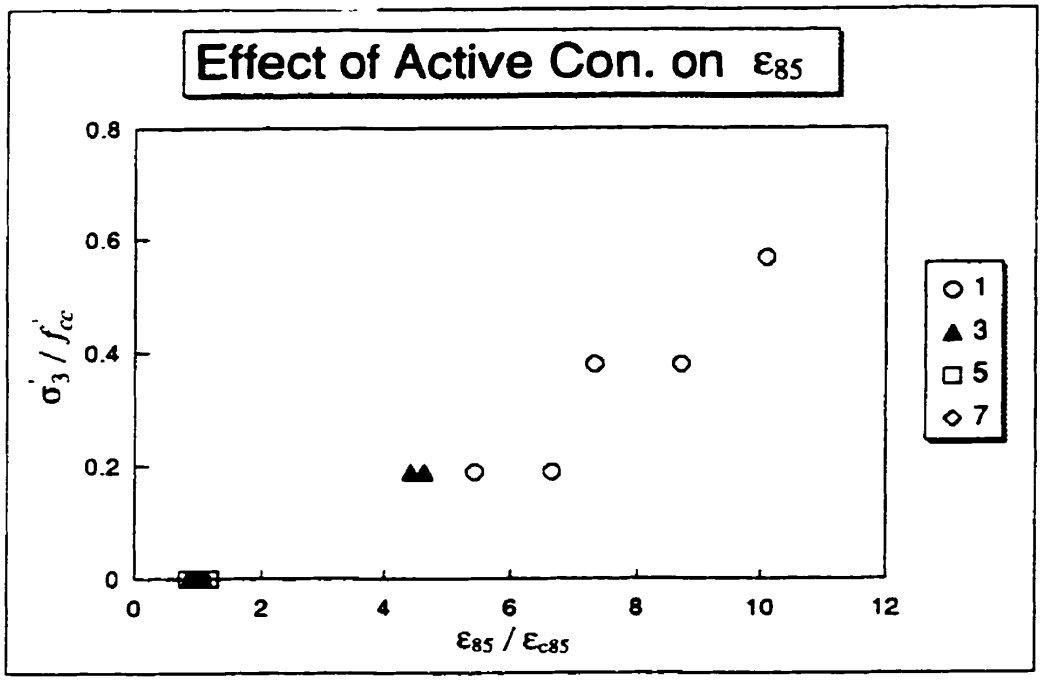

Figure 5-12: Effect of active confinement on ε_{85} of FRC (ductility)

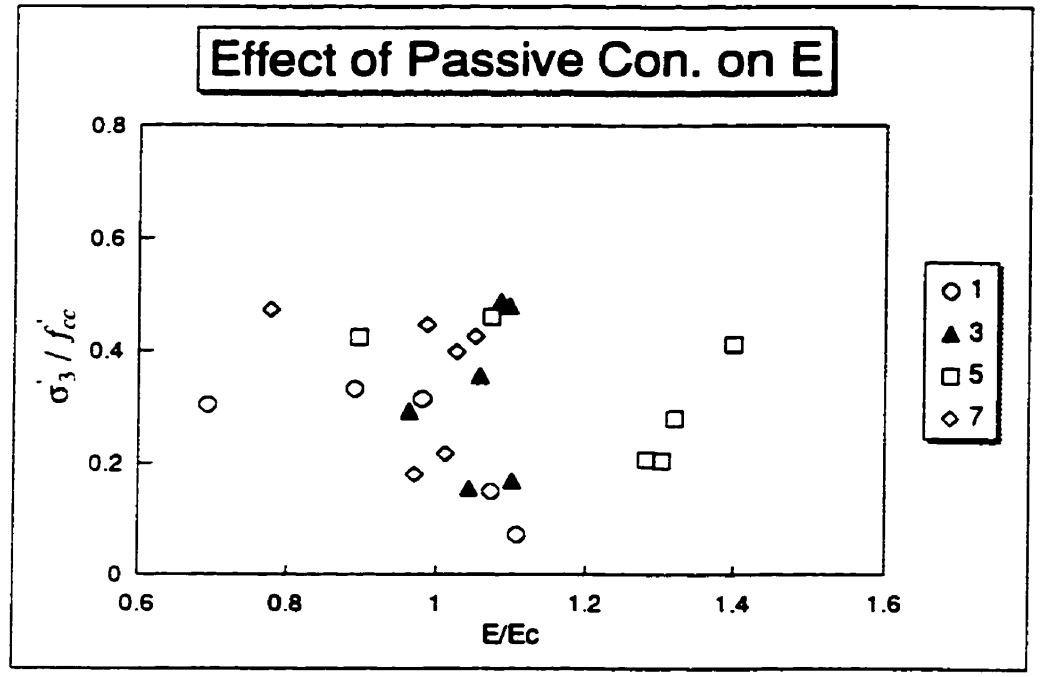

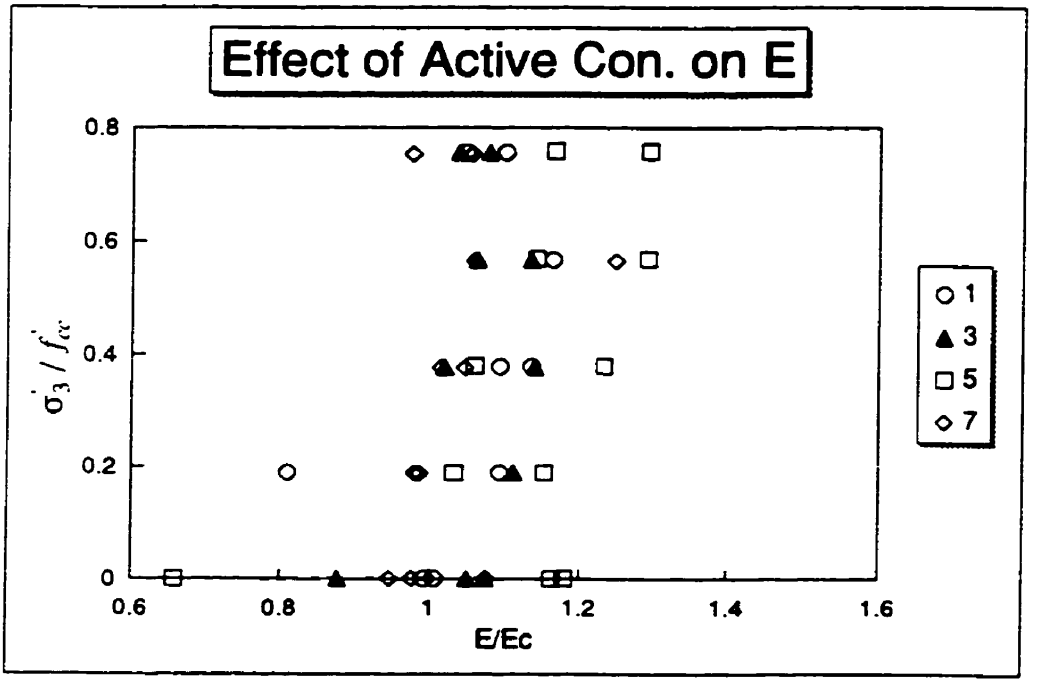

Figure 5-13: Effect of confinement on E values of FRC
active & passive separated

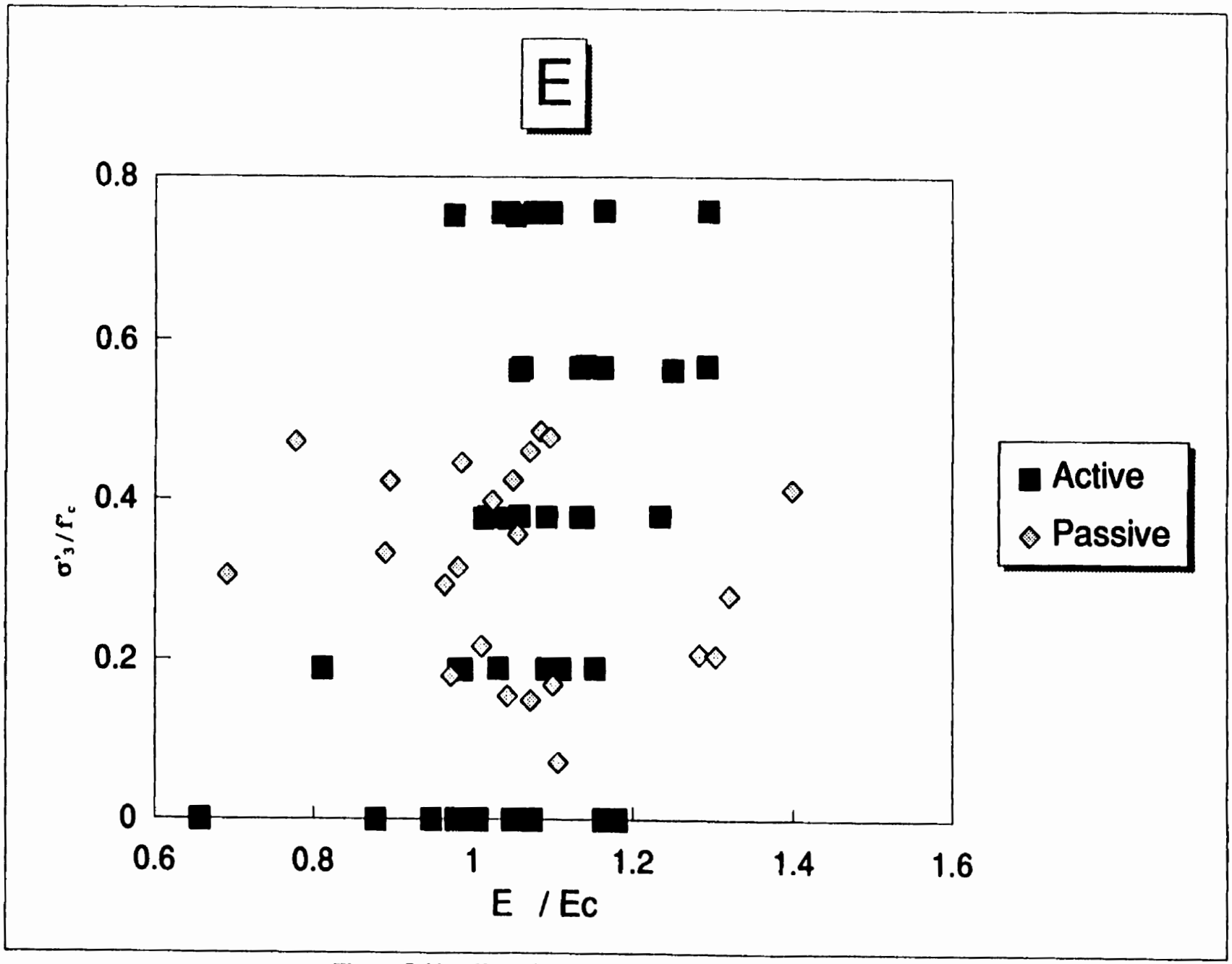

Figure 5-13: Effect of confinement on E values of FRC
active & passive combined

No.	f'_c / f'_{cc}	Active	Passive
1A1	1	0.00%	
1A2			
1A3	1	0.00%	
1B1	1.882353	18.90%	
1B2	1.849911	18.90%	
1C1	2.275936	37.79%	
1C2	2.182888	37.79%	
1D1			
1D2	2.887701	56.69%	
1E1	3.340463	75.58%	
1E2	3.279857	75.58%	
1N1	1.335116		15.00%
1N2	1.231729		7.12%
1O1	1.734403		30.38%
1O2	2.190731		31.44%
1P1	2.206774		33.21%
1P2	2.561497		40.01%
3A1	1.002712	0.00%	
3A2	1.000678	0.00%	
3A3	0.99661	0.00%	
3B1	1.777627	18.89%	
3B2	1.808136	18.89%	
3C1	2.131525	37.78%	
3C2	2.111186	37.78%	
3D1	2.786441	56.67%	
3D2	2.928814	56.67%	
3E1	2.997966	75.56%	
3E2	3.012203	75.56%	
3N1	1.39322		16.88%
3N2	1.230508		15.53%
3O1	1.720678		29.23%
3O2	2.290169		35.57%
3P1	2.223051		48.73%
3P2	2.613559		47.93%
5A1	1.049251	0.00%	
5A2	0.933619	0.00%	
5A3	1.017131	0.00%	
5B1	1.747323	18.96%	
5B2	1.798715	18.96%	
5C1	2.014989	37.92%	
5C2	2.239829	37.92%	
5D1	2.648822	56.87%	
5D2	2.69379	56.87%	
5E1	3.034261	75.83%	
5E2	2.989293	75.83%	
5N1	1.498929		20.70%
5N2	1.226981		20.48%
5O1	2.137045		42.32%
5O2	2		27.88%
5P1	2.237687		46.11%
5P2	2.704497		41.19%
7A1	1.069378	0.00%	
7A2	1.009569	0.00%	
7A3	0.921053	0.00%	
7B1	1.880383	18.80%	
7B2	1.849282	18.80%	
7C1	2.258373	37.60%	
7C2	2.318182	37.60%	
7D1	2.882775	56.41%	
7D2	2.923445	56.41%	
7E1	3.325359	75.21%	
7E2	3.313397	75.21%	
7N1	1.332536		21.68%
7N2	1.322967		17.99%
7O1	2.421053		44.66%
7O2	2.456938		39.78%
7P1	2.399522		42.44%
7P2	2.854067		47.32%

Table 5-1: Effective confinements and corresponding normalized strengths

No.	$\varepsilon_c / \varepsilon_{cc}$	Active	Passive
1A1	0.987019	0.00%	
1A2			
1A3	1.012981	0.00%	
1B1	3.515477	18.90%	
1B2	3.891163	18.90%	
1C1	9.080629	37.79%	
1C2	5.707688	37.79%	
1D1			
1D2	10.88268	56.69%	
1E1	10.51198	75.58%	
1E2		75.58%	
1N1	1.356216		15.00%
1N2	1.169995		7.12%
1O1	6.740639		30.38%
1O2	9.538692		31.44%
1P1	8.537693		33.21%
1P2	11.20494		40.01%
3A1	1.027974	0.00%	
3A2	0.915415	0.00%	
3A3	1.056612	0.00%	
3B1	2.570183	18.89%	
3B2	2.904624	18.89%	
3C1	5.759193	37.78%	
3C2	4.681913	37.78%	
3D1	10.17066	56.67%	
3D2	10.95733	56.67%	
3E1		75.56%	
3E2	10.91948	75.56%	
3N1	3.978667		16.88%
3N2	3.031128		15.53%
3O1	5.6043		29.23%
3O2	9.267452		35.57%
3P1	10.09944		48.73%
3P2	11.10326		47.93%
5A1	0.89461	0.00%	
5A2	1.207638	0.00%	
5A3	0.897752	0.00%	
5B1	2.271694	18.96%	
5B2	2.634759	18.96%	
5C1	8.5168	37.92%	
5C2	8.854	37.92%	
5D1	10.17597	56.87%	
5D2	9.912255	56.87%	
5E1	10.21006	75.83%	
5E2		75.83%	
5N1	4.361373		20.70%
5N2	4.267585		20.48%
5O1	8.922408		42.32%
5O2	8.266377		27.88%
5P1	9.402949		46.11%
5P2	10.04979		41.19%
7A1	1.044411	0.00%	
7A2	1.012675	0.00%	
7A3	0.942914	0.00%	
7B1	3.36167	18.80%	
7B2	3.556085	18.80%	
7C1	6.302773	37.60%	
7C2	7.25741	37.60%	
7D1	11.87334	56.41%	
7D2	12.25531	56.41%	
7E1	12.0223	75.21%	
7E2	12.72849	75.21%	
7N1	4.510436		21.68%
7N2	4.024969		17.99%
7O1	9.872582		44.66%
7O2	9.119794		39.78%
7P1	10.30516		42.44%
7P2	13.58506		47.32%

Table 5-2: Effective confinements and corresponding normalized ε_c

No.	$\varepsilon^* / \varepsilon^*_c$	Active	Passive
1A1	0.977013	0.00%	
1A2			
1A3	1.022987	0.00%	
1B1	4.226175	18.90%	
1B2	4.358323	18.90%	
1C1		37.79%	
1C2	5.999307	37.79%	
1D1			
1D2		56.69%	
1E1		75.58%	
1E2		75.58%	
1N1	1.789997		15.00%
1N2	1.485965		7.12%
1O1			30.38%
1O2			31.44%
1P1			33.21%
1P2			40.01%
3A1	1.046867	0.00%	
3A2	0.910983	0.00%	
3A3	1.04215	0.00%	
3B1	2.885229	18.89%	
3B2	3.264356	18.89%	
3C1		37.78%	
3C2		37.78%	
3D1		56.67%	
3D2		56.67%	
3E1		75.56%	
3E2		75.56%	
3N1	1.83679		16.88%
3N2	1.463278		15.53%
3O1	5.865913		29.23%
3O2			35.57%
3P1			48.73%
3P2			47.93%
5A1	0.901808	0.00%	
5A2	1.233392	0.00%	
5A3	0.8648	0.00%	
5B1	2.698192	18.96%	
5B2	6.280113	18.96%	
5C1		37.92%	
5C2		37.92%	
5D1	7.499043	56.87%	
5D2		56.87%	
5E1		75.83%	
5E2		75.83%	
5N1	1.449699		20.70%
5N2	1.42056		20.48%
5O1			42.32%
5O2			27.88%
5P1			46.11%
5P2			41.19%
7A1	1.085562	0.00%	
7A2	1.066859	0.00%	
7A3	0.847579	0.00%	
7B1	3.289483	18.80%	
7B2	5.289845	18.80%	
7C1		37.60%	
7C2	6.052584	37.60%	
7D1		56.41%	
7D2		56.41%	
7E1		75.21%	
7E2		75.21%	
7N1	1.715215		21.68%
7N2	2.028551		17.99%
7O1			44.66%
7O2			39.78%
7P1			42.44%
7P2			47.32%

Table 5-3: Effective confinements and corresponding normalized ε^*

No.	$\varepsilon_{85} / \varepsilon_{u85}$	Active	Passive
1A1	0.949288	0.00%	
1A2			
1A3	1.050712	0.00%	
1B1	5.447064	18.90%	
1B2	6.650356	18.90%	
1C1	8.696619	37.79%	
1C2	7.317616	37.79%	
1D1			
1D2	10.09786	56.69%	
1E1		75.58%	
1E2		75.58%	
1N1	1.572954		15.00%
1N2	1.291593		7.12%
1O1			30.38%
1O2			31.44%
1P1			33.21%
1P2			40.01%
3A1	1.086611	0.00%	
3A2	0.875646	0.00%	
3A3	1.037743	0.00%	
3B1	4.435439	18.89%	
3B2	4.64859	18.89%	
3C1		37.78%	
3C2		37.78%	
3D1		56.67%	
3D2		56.67%	
3E1		75.56%	
3E2		75.56%	
3N1			16.88%
3N2			15.53%
3O1			29.23%
3O2			35.57%
3P1			48.73%
3P2			47.93%
5A1	0.969372	0.00%	
5A2	1.19085	0.00%	
5A3	0.839778	0.00%	
5B1		18.96%	
5B2		18.96%	
5C1		37.92%	
5C2		37.92%	
5D1		56.87%	
5D2		56.87%	
5E1		75.83%	
5E2		75.83%	
5N1			20.70%
5N2			20.48%
5O1			42.32%
5O2			27.88%
5P1			46.11%
5P2			41.19%
7A1	1.01765	0.00%	
7A2	1.019259	0.00%	
7A3	0.963091	0.00%	
7B1		18.80%	
7B2		18.80%	
7C1		37.60%	
7C2		37.60%	
7D1		56.41%	
7D2		56.41%	
7E1		75.21%	
7E2		75.21%	
7N1			21.68%
7N2			17.99%
7O1			44.66%
7O2			39.78%
7P1			42.44%
7P2			47.32%

Table 5-4: Effective confinements and corresponding normalized ε_{85} (ductility)

No.	E / Ec	Active	Passive
1A1	1.006468	0.00%	
1A2			
1A3	0.993532	0.00%	
1B1	1.091359	18.90%	
1B2	0.810177	18.90%	
1C1	1.092109	37.79%	
1C2	1.133883	37.79%	
1D1			
1D2	1.161831	56.69%	
1E1	1.097864	75.58%	
1E2	1.04512	75.58%	
1N1	1.071355		15.00%
1N2	1.106476		7.12%
1O1	0.691502		30.38%
1O2	0.981205		31.44%
1P1	0.889989		33.21%
1P2			40.01%
3A1	1.048966	0.00%	
3A2	1.073018	0.00%	
3A3	0.878015	0.00%	
3B1		18.89%	
3B2	1.109681	18.89%	
3C1	1.018561	37.78%	
3C2	1.138256	37.78%	
3D1	1.060729	56.67%	
3D2	1.13301	56.67%	
3E1	1.076033	75.56%	
3E2	1.035869	75.56%	
3N1	1.099589		16.88%
3N2	1.042633		15.53%
3O1	0.964696		29.23%
3O2	1.055831		35.57%
3P1	1.083797		48.73%
3P2	1.095747		47.93%
5A1	1.179724	0.00%	
5A2	0.657698	0.00%	
5A3	1.162578	0.00%	
5B1	1.031492	18.96%	
5B2	1.151672	18.96%	
5C1	1.233624	37.92%	
5C2	1.058151	37.92%	
5D1	1.292096	56.87%	
5D2	1.140614	56.87%	
5E1	1.294049	75.83%	
5E2	1.164026	75.83%	
5N1	1.28228		20.70%
5N2	1.302988		20.48%
5O1	0.896111		42.32%
5O2	1.320514		27.88%
5P1	1.070709		46.11%
5P2	1.398857		41.19%
7A1	1.073946	0.00%	
7A2	0.978356	0.00%	
7A3	0.947698	0.00%	
7B1	0.98104	18.80%	
7B2	0.986209	18.80%	
7C1	1.01351	37.60%	
7C2	1.044542	37.60%	
7D1	1.24894	56.41%	
7D2	1.056791	56.41%	
7E1	1.052955	75.21%	
7E2	0.976428	75.21%	
7N1	1.010908		21.68%
7N2	0.972077		17.99%
7O1	0.986159		44.66%
7O2	1.024509		39.78%
7P1	1.049697		42.44%
7P2	0.776509		47.32%

Table 5-5: Effective confinements and corresponding normalized E values

5.4. Size Effects

One of the behavioral issues studied in this research was the effect of specimen size on the mechanical properties of fiber concrete. Size effects on concrete subjected to various stresses have been extensively studied in the literature. The part of literature which is concerned with the effects of size on the compression response of concrete is reviewed briefly, in the following section.

5.4.1. Literature Review

Scaling is the most fundamental aspect of every physical theory . In the classical theories of failure, the strength is determined by a constitutive law in terms of stresses or strains. However, rational analysis of failure must take into account the energy release caused by failure and its balance with the energy needed to produce fracture or damage zones (Bazant 1993). Bringing the energy release into consideration leads to the anticipation of size effect in the mechanical behavior of materials failing by fracture.

For a long time the size effect had been explained statistically by the fact that in a larger structure it is more likely to encounter a material point of smaller strength (Bazant et al 1994; Neville 1990). The variation of strength throughout concrete is random and independent of structure size . The stress gradient, on the other hand, varies inversely with the structure size, and the region of high stress becomes larger in a larger structure (Bazant 1984). Therefore, the possibility of encountering low strength in the peak stress region is higher in a larger structure, and hence the apparent strength necessarily declines with the structure size (Bazant 1984). In contrast, Bazant (1993) has brought three reasons for rejecting the statistical explanation:

- Quasibrittle materials are not elasto-plastic in compression, because the load-deflection diagram exhibits post-peak gradual softening instead of a long plastic plateau.
- The failure is a fracture process, in which the energy release matters.

- The coarse micro-structure of quasibrittle materials indicate that there must be a characteristic dimension (i.e. dimension is effective in the response of material).

The proper explanation of size effect is based on the release of strain energy due to fracture growth, producing damage localization instabilities (Bazant et al 1994). Prior to failure, distributed damage, consisting of microcracks, localizes into a narrow fracture process zone, which ultimately becomes the major crack (Bazant and Kwon 1994). This fracture process is driven by the release of stored strain energy from the structure (Bazant et al 1994). In a larger structure, the strain energy is released from a greater zone, and so the amount of energy released is larger for a unit crack (Bazant et al 1994; Bazant and Kwon 1994). However, the amount of energy which is required to extend a unit fracture is not dependent to the size of structure (Bazant and Kwon 1994). Therefore, the energy required must match the fracture formation, and the failure stress for a larger structure must be lower (Bazant et al 1994).

Fracture is considered to be caused by propagation of a crack band that has a fixed width at its front relative to the aggregate size (Bazant 1984; Fanella and Krajcinovic 1988; Mazars et al 1993). The linear (classical) form of fracture mechanics has been clearly shown to be inapplicable to concrete (Bazant 1984). However, it has been established that concrete does obey a proper non-linear form of fracture mechanics in which fracture front progress by the large size of the micro-cracked zone is taken into account (Bazant 1984).

The effect of size on the compression strength of concrete is not so remarkable as that on the tensile, flexural, and shearing strength . The compression strength for a full scale member is about 80 to 90% of that for common laboratory test specimens (Hatanaka et al 1994).

Compressive fracture is a complex problem which has been already intensely studied (Bazant 1993; Markeset and Hillerborg, 1995; Murakami et al 1993). However, despite many useful results, the mechanism of compressive failure has not been understood

and the size effect has not been determined (Bazant 1993). This type of failure always is accompanied by lateral deformation. The lateral deformation is related to longitudinal distributed splitting cracks, which form and expand during the failure process (Markeset and Hillerborg, 1995). In addition to the longitudinal splitting cracks, localized shear deformations may also occur . Hence, it is difficult to clarify the damage mechanism and to evaluate the distribution of damage density in the damage process zone as well as the magnitude of energy dissipated in the zone (Murakami and Hillerborg, 1993).

Morita et al (1993) showed that the size effect is not significant for cylinders larger than 50×100 mm, but Bazant and Kwon (1994) explained that this disappearance of size effect in compression was misinterpretation of the plots. On the other hand, Neville (1990) showed that the compressive strength of cylinders larger than 600 mm in diameter remain size insensitive.

5.4.2. Experiment Results

The results of test types A, Q, and R (Table 3-1) are considered in this section. All these tests were uniaxial compression and were performed on three different sizes of saturated cylinders with equal ratio of length/diameter. In order to compare the results, the considered mechanical properties are normalized to the respective values of test type A of the same batch.

- **Compression Strength (f'_c):** Figure 5-14 plots the strength of specimens of various sizes. It appears that as the size increases, the strength decreases, but the rate of this change also decreases. This indicates that there must be a limit for the strength of large size specimens. However, the effect of size variation is not equal on different batches. Batches 2 and 8 exhibit more sensitivity, whereas Batches 4 and 5 exhibit less sensitivity. The two latter batches contained steel fibers.

- **Strains at Peak (ε_c):** The axial strains corresponding to the peak load are illustrated in Figure 5-15. The variation of ε_c with the increase in size is similar to the changes in f'_c. The amount of this strain effects the magnitude of stored energy at failure. Hence, for larger specimens lower strain at peak is required. Batch 8 (2% micro plus 3% polypropylene) shows less sensitivity to size variation, whereas 2 and 6 show high sensitivity.

- **Axial Strain at Zero Volumetric Strain (ε^*):** The values of axial strain corresponding to zero volumetric strain are presented in Figure 5-16. The value of ε^* drops about 40% from the 50 to the 100 mm diameter specimens, and remains stable thereon for the 150 mm diameter specimens. This pattern of variation is in agreement with that of Poisson's ratio. Since for larger specimens the ratio of lateral strain to axial strain is higher, the volumetric contraction is less, and hence the magnitude of ε^* is lower. The amount of energy which is stored in larger specimens causes earlier onset of severe damage. Figure 5-16 indicates that the effect of size variation is higher for Batches 6 and 8, and lower for Batch 3.

- **Elastic Modulus (E):** Figure 5-17 shows the variation of E with size. The pattern of the variation is opposite to that of f'_c. The E value increases with size, but reaches to a limit. This indicates that the variation of f'_c is lower relative to ε_c for smaller sizes than that ratio in larger sizes. The modulus of elasticity shows an increase of 60% from 50 to 100 mm diameter, while it gains another 15% increase from the 100 to the 150 mm diameter specimens. Figure 5-17 also indicates that Batch 8 shows more variation, whereas Batch 4 exhibit less variation than other batches.

- **Poisson's Ratio (v):** Poisson's ratio increases with size, but approaches to a limiting value. Figure 5-18 illustrates these changes for different batches. This means that the

rate of lateral strain increase is lower in smaller specimens than larger ones. This behavior can be explained by the models of Markeset and Hillerborg (1995) and Taerwe (1995). Figure 5-19 shows how the longitudinal concrete bars develop along the loading direction, which eventually leads to vertical cracks. The cross sectional area of these bars are related to aggregate size. Therefore, in a larger specimen a higher number of them are formed, whose deformations result in a higher accumulated lateral strain. The ν value shows an increase of 80% from 50 to 100 mm diameter, and almost no change from 100 to 150 mm diameter. Figure 5-18 indicates that Batch 6 is less , and Batch 5 is more effected by size variation.

- **Deformability (ε_{85}):** Figure 5-20 indicates that for larger specimens the value of ε_{85} decreases. This means that the smaller specimens are more ductile than the larger ones. The reason is explained clearly by the concept of absorbed energy. Since larger structures store higher energy, after failure, they gain greater damage. Furthermore, the relative stiffness of the compression machine and the specimens is involved in this response. A 30% drop occurs for ε_{85} when the diameter increases from 50 to 100 mm, and an additional 10% drop occurs when the diameter increases to 150 mm. Batch 5 is more sensitive, and Batch 3 is less sensitive to size variation than other batches.

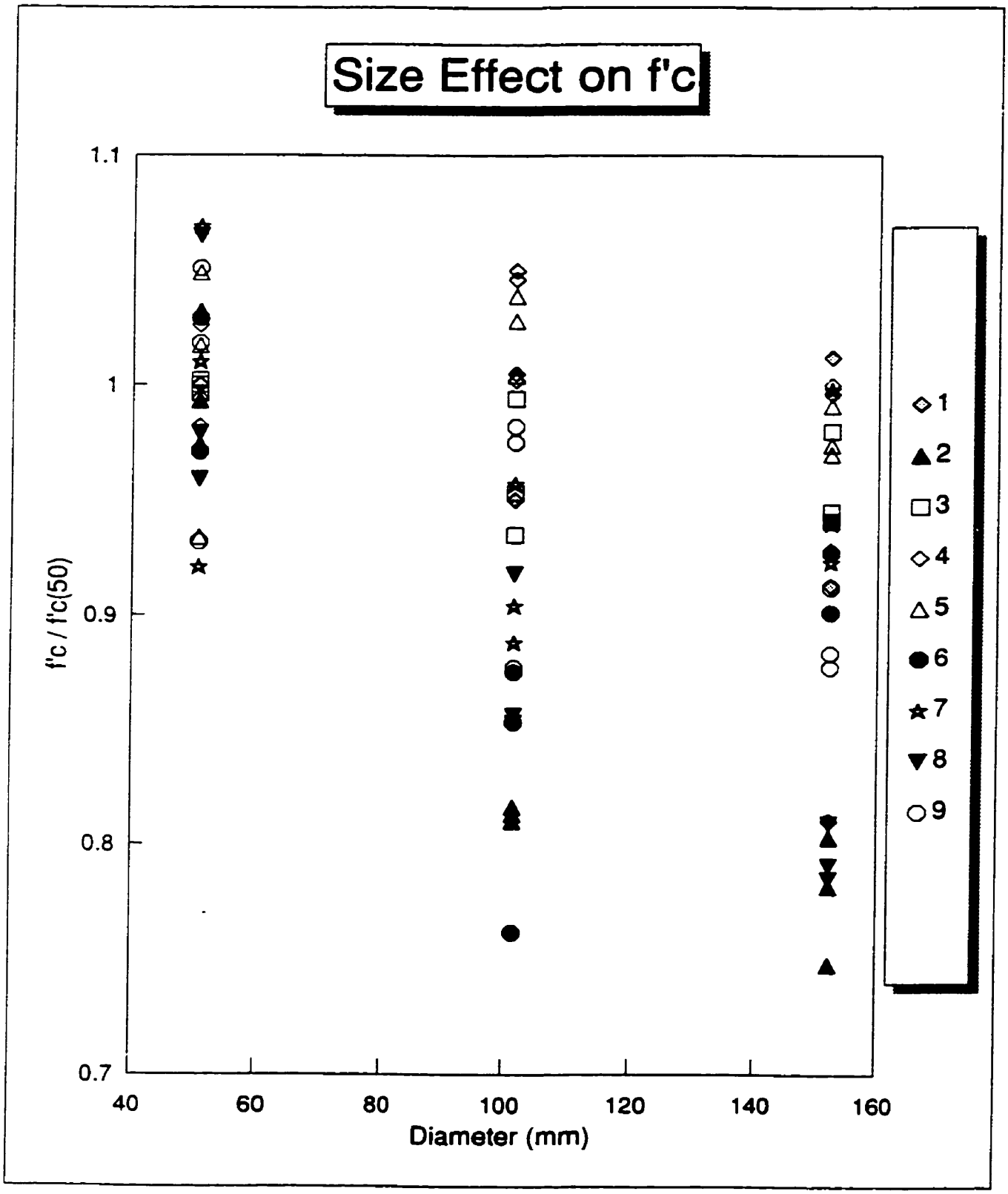

Figure 5-14: Effect of size on the compressive strength of FRC
all the specimens

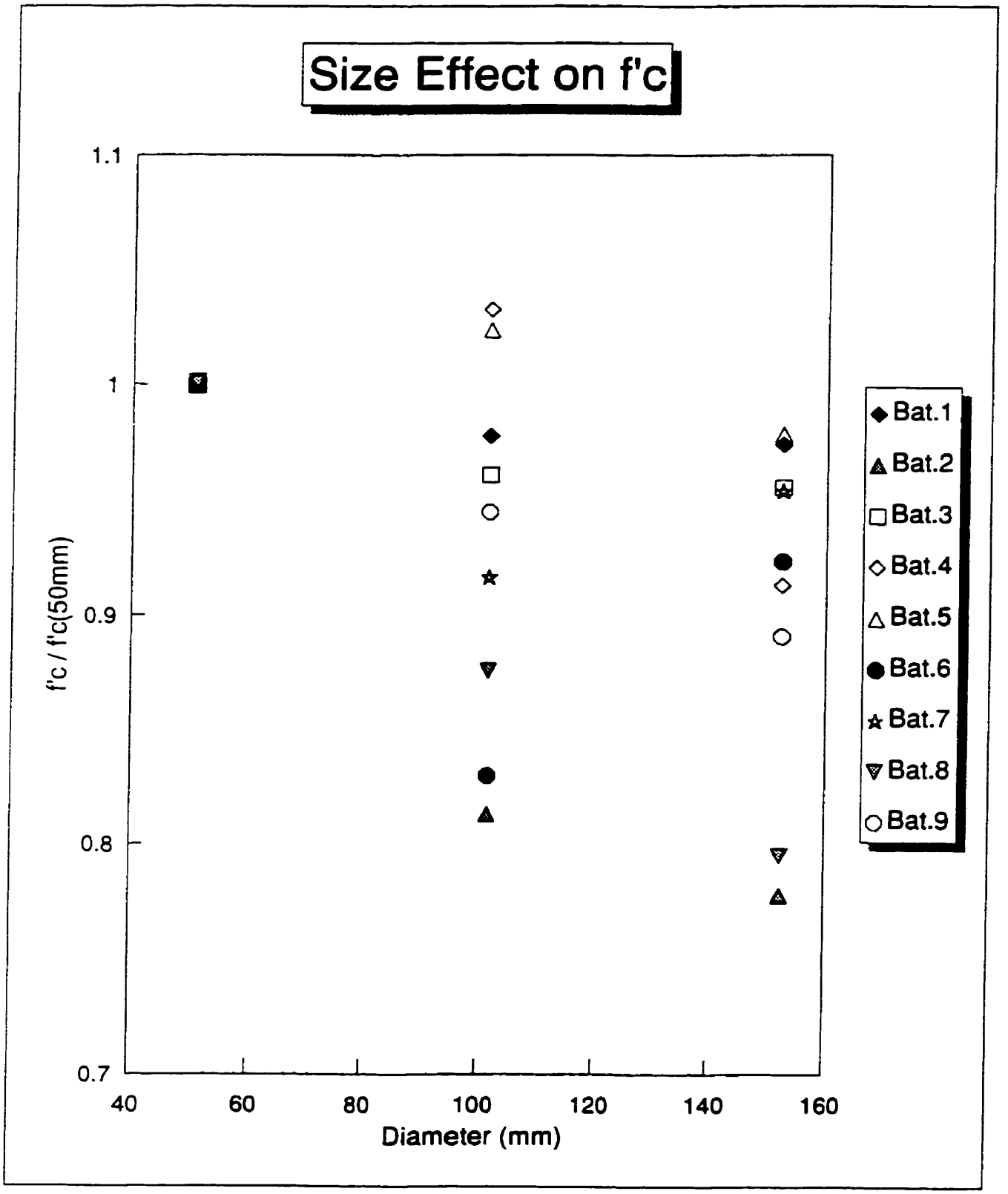

Figure 5-14: Effect of size on the compressive strength of FRC
mean values of each batch

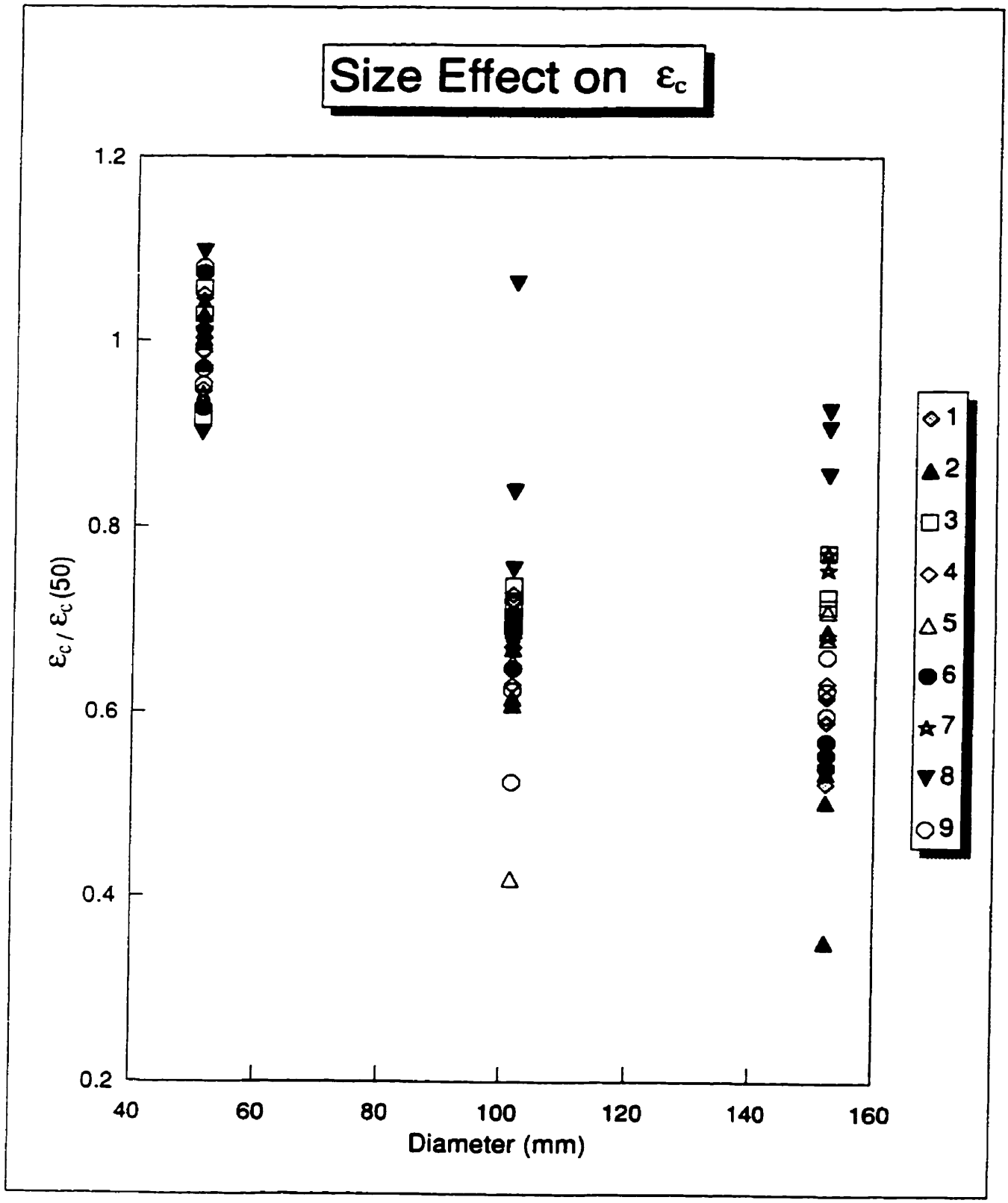

Figure 5-15: Effect of size on the ε_c value of FRC all the specimens

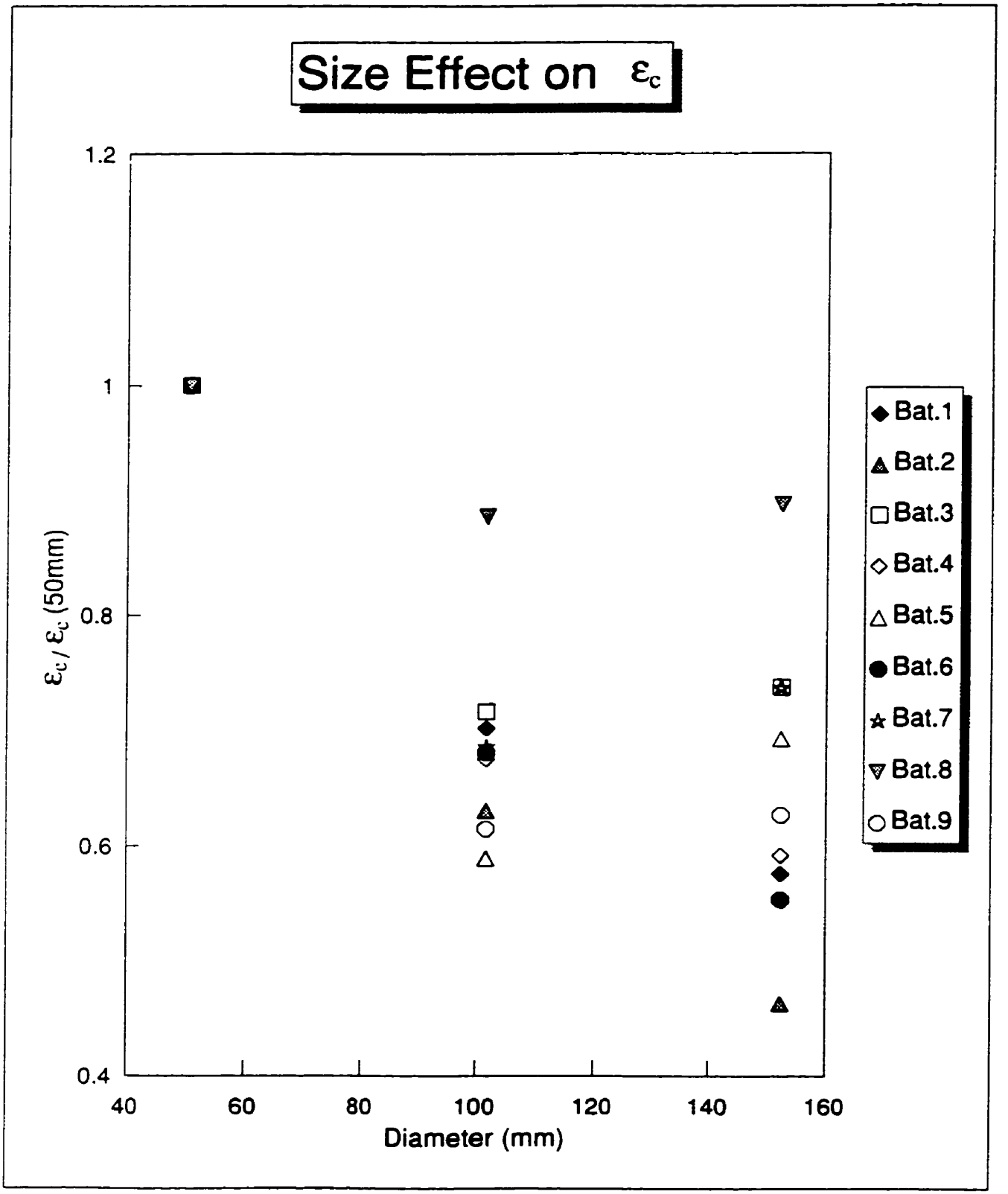

Figure 5-15: Effect of size on the ε_c value of FRC
mean values of each batch

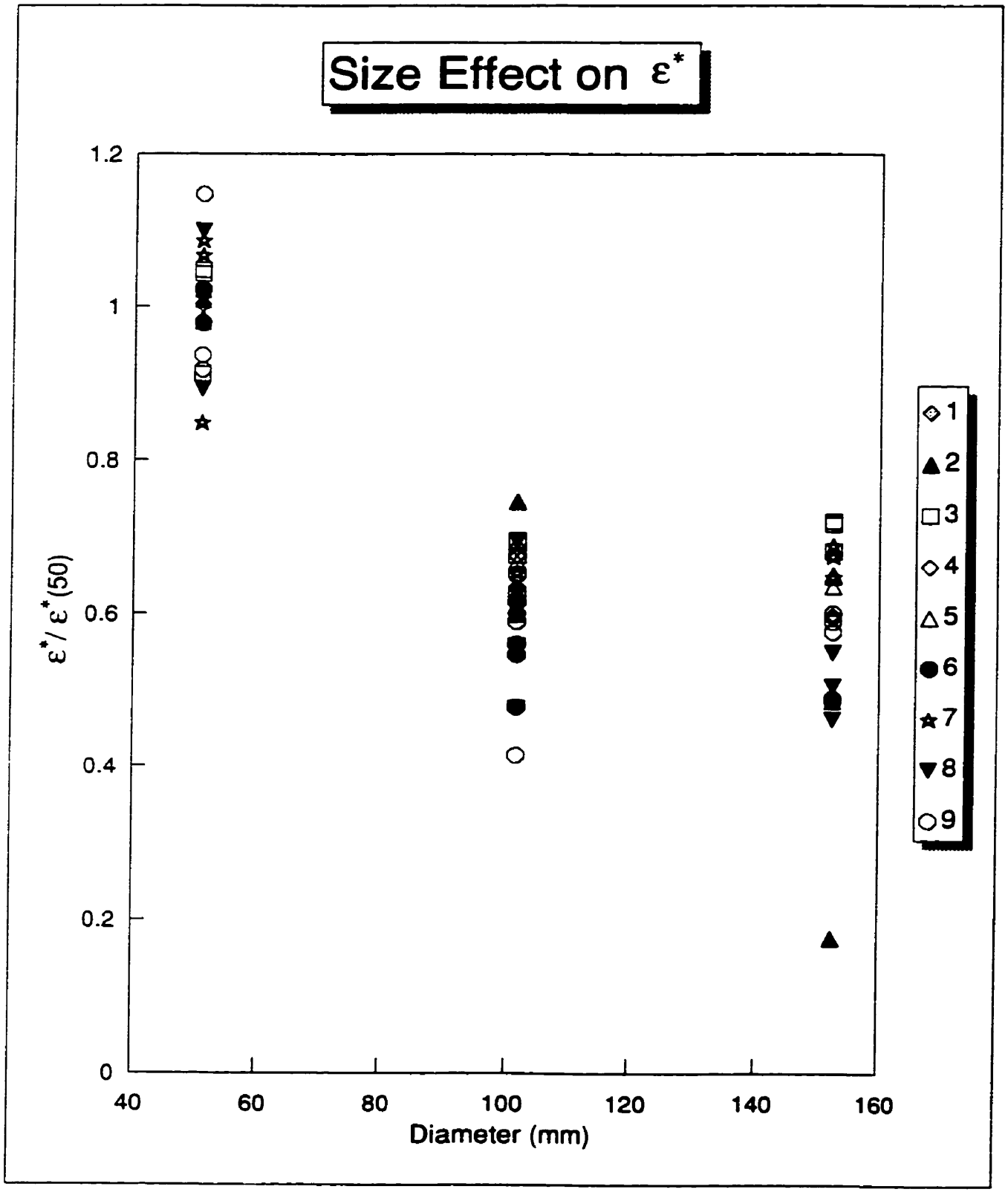

Figure 5-16; Effect of size on the ε^* value of FRC all the specimens

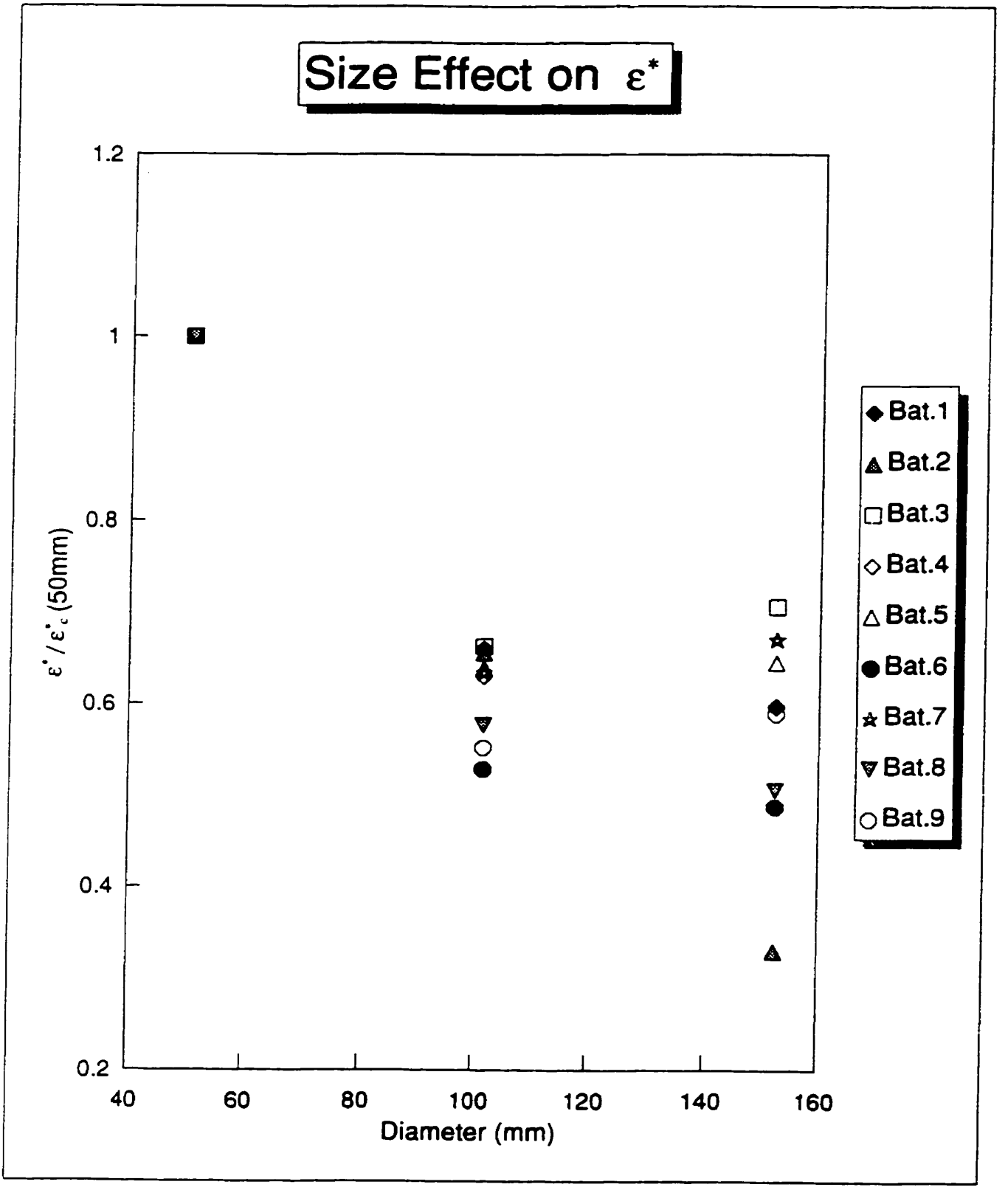

Figure 5-16; Effect of size on the ε^* value of FRC
mean values of each batch

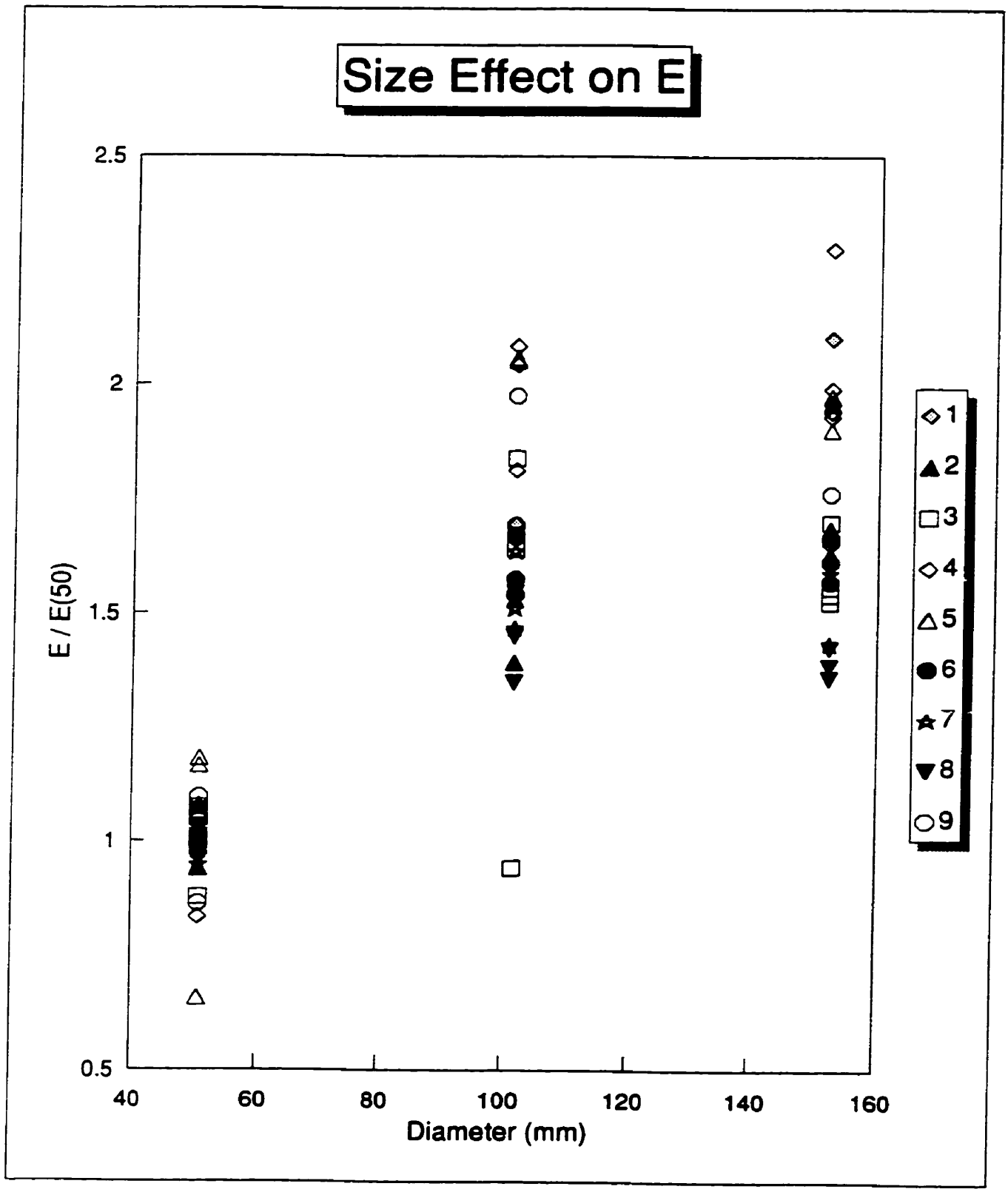

Figure 5-17: Effect of size on the E value of FRC
all the specimens

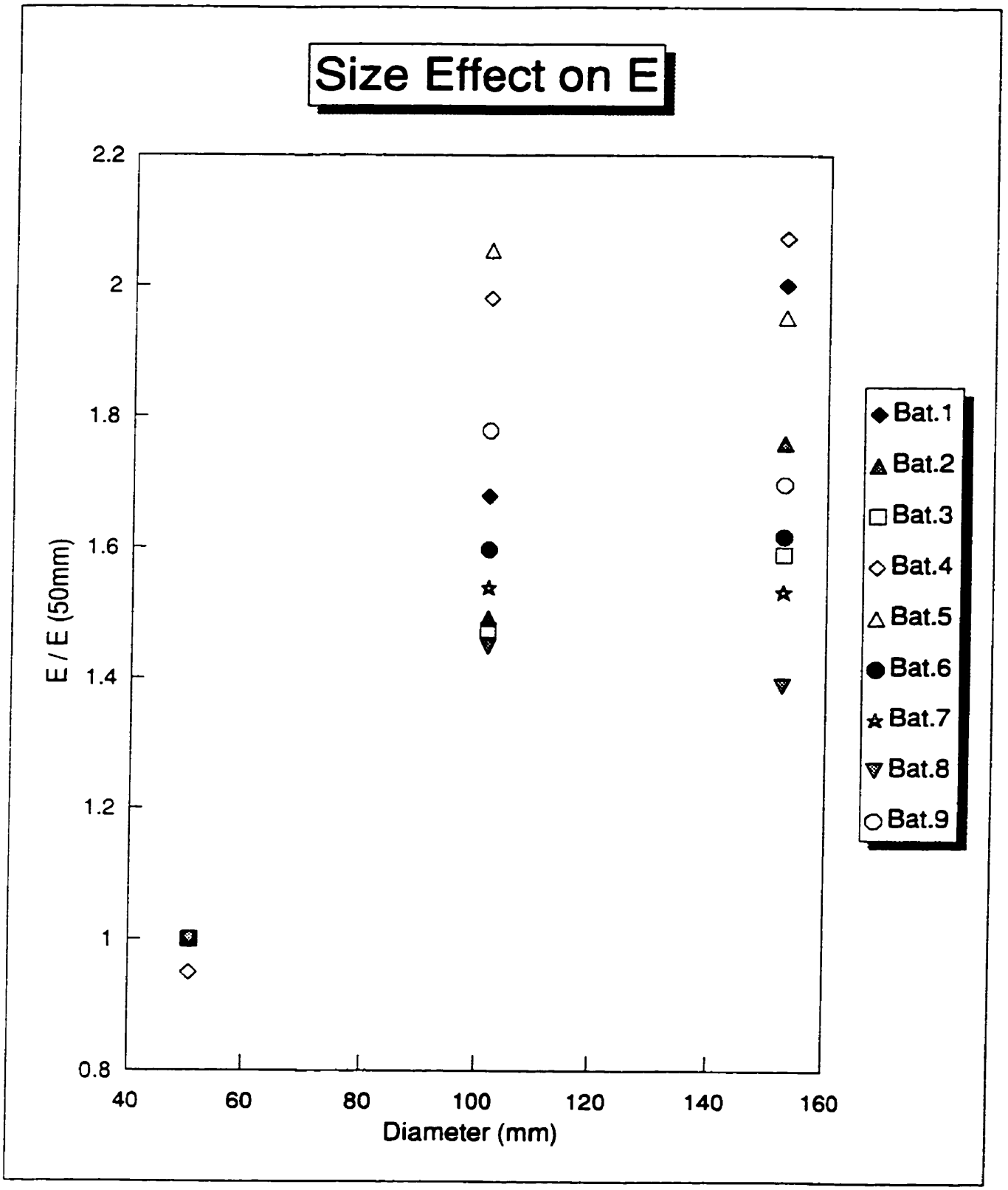

Figure 5-17: Effect of size on the E value of FRC
mean values of each batch

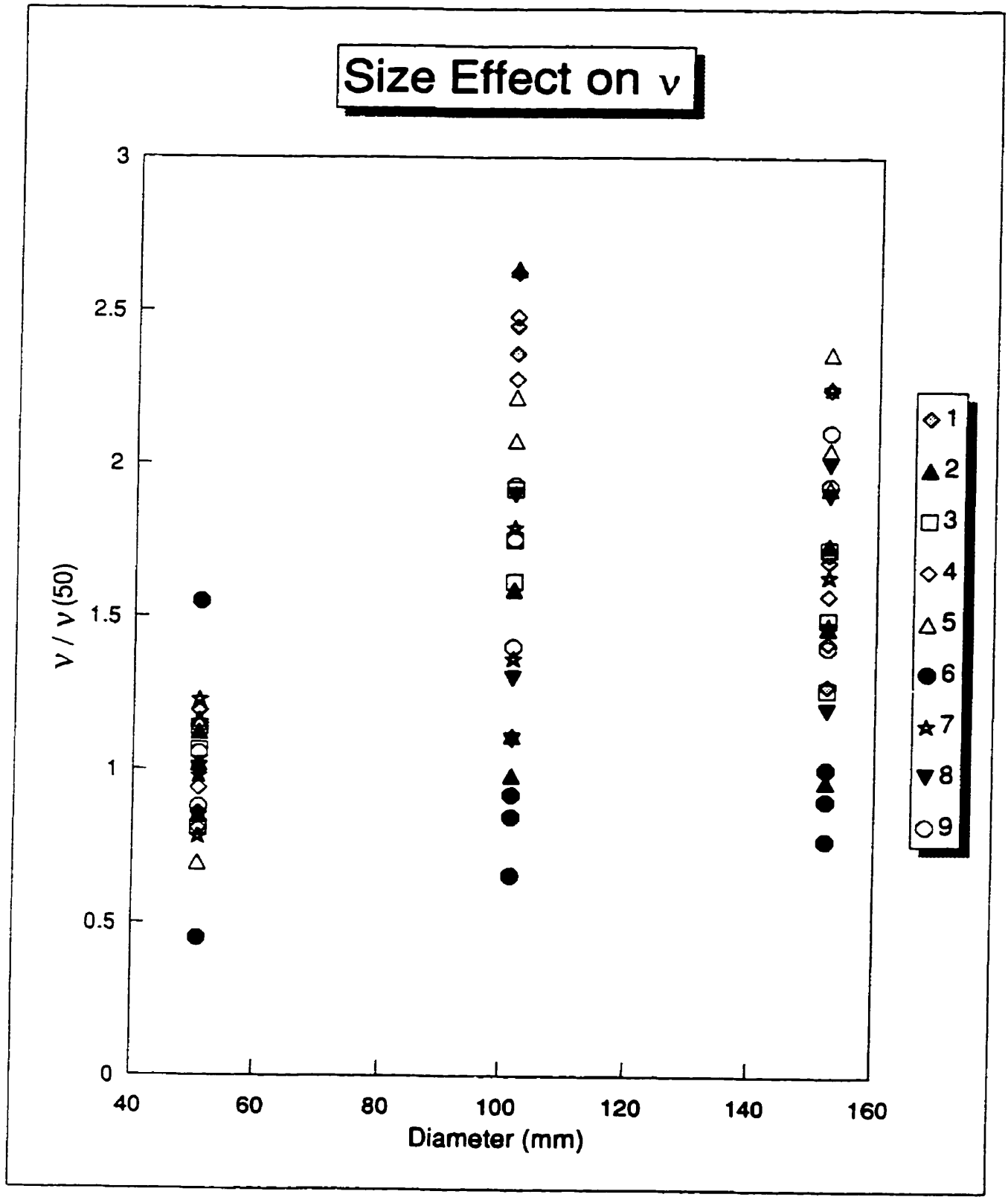

Figure 5-18: Effect of size on the ν value of FRC all the specimens

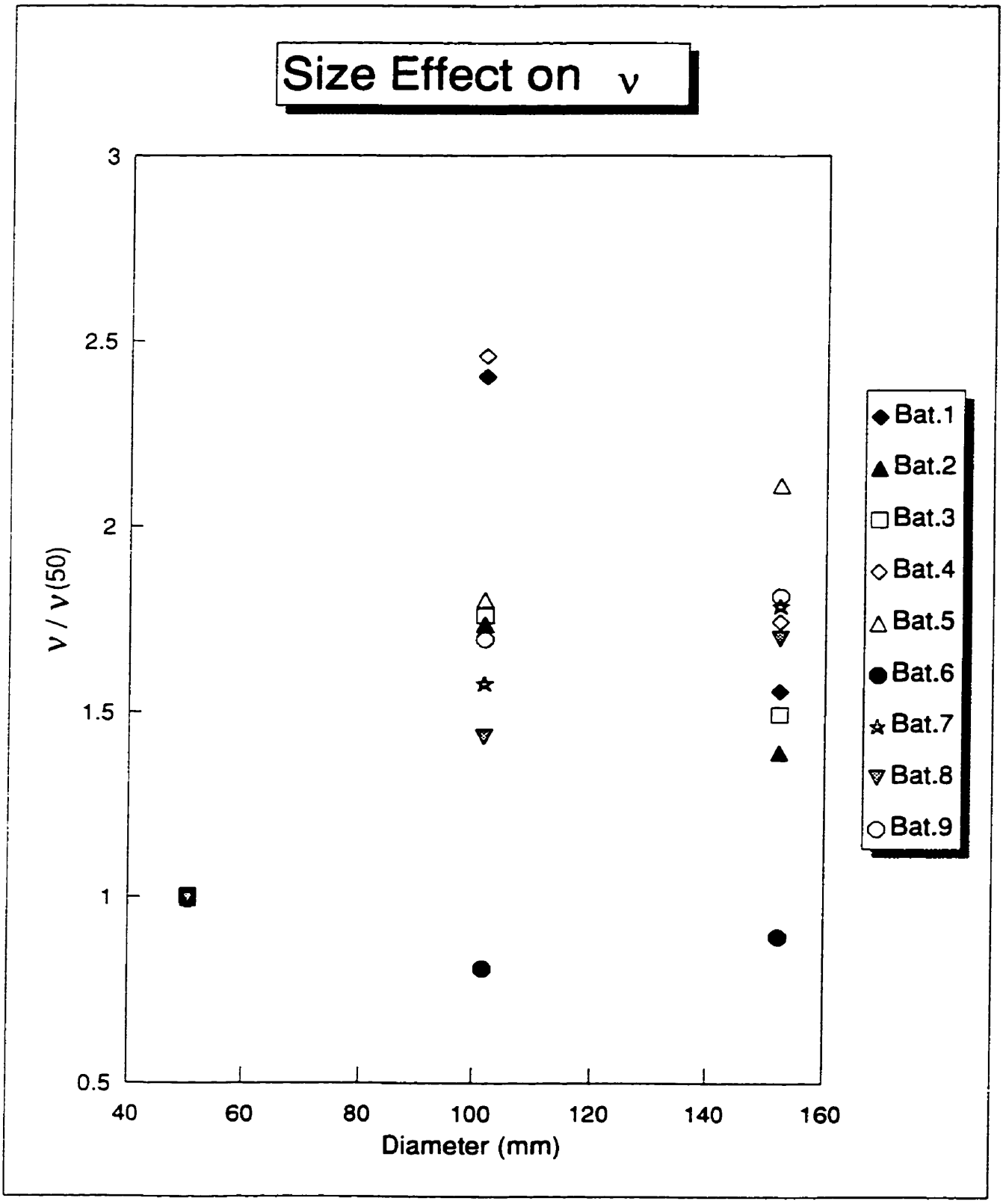

Figure 5-18: Effect of size on the ν value of FRC
mean values of each batch

(i)

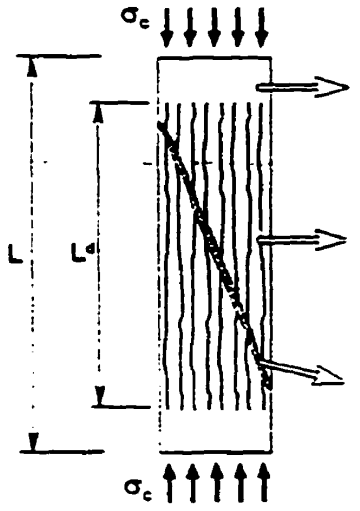

(ii)

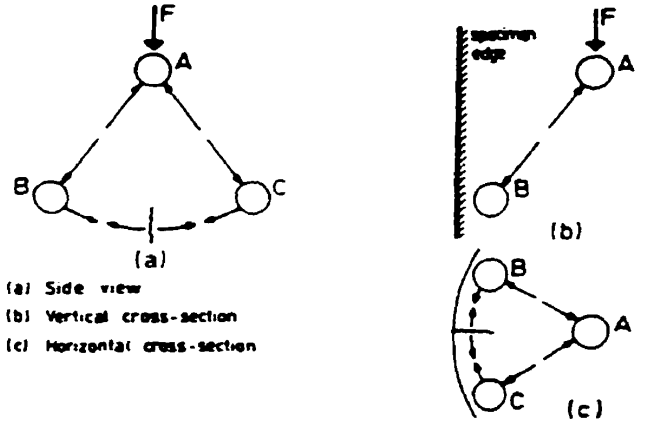

(a) Side view
(b) Vertical cross-section
(c) Horizontal cross-section

Side view; b) Vertical cross-section; and c) Horizontal cross-section

Figure 5-19; Mechanism of developing lateral expansion
(i) development of concrete bars due to compression (taken from Markeset and Hillerborg, 1995)
(ii) force transfer between aggregates causes lateral separation (taken from Taerwe, 1995)

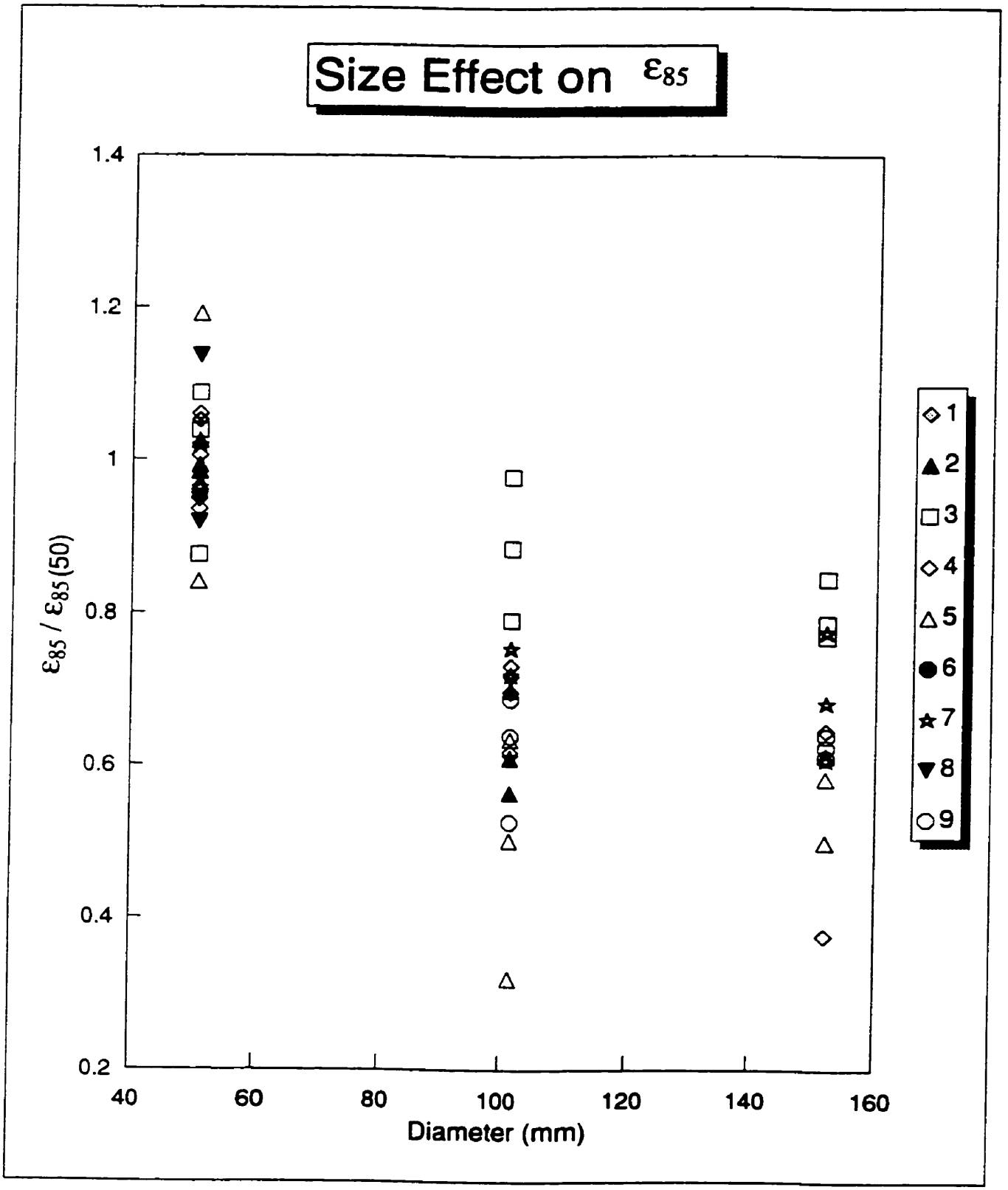

Figure 5-20: Effect of size on the ε_{85} value of FRC
all the specimens

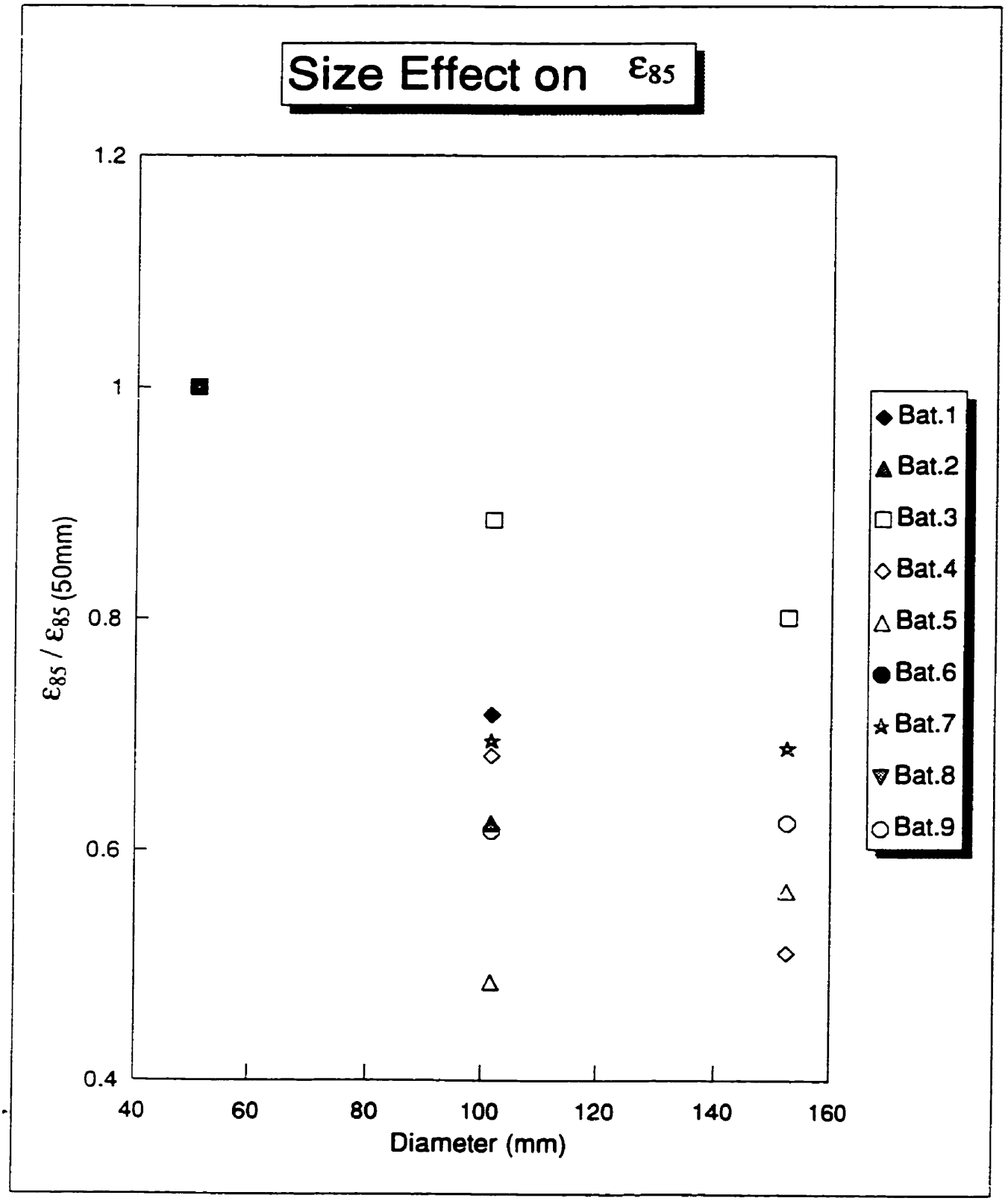

Figure 5-20; Effect of size on the ε_{85} value of FRC
mean values of each batch

5.5. Saturation Effects

In Section 5-3, the confining pressures were adjusted to account for the internal pore pressure. This step was taken in order to reflect, in particale terms, the adverse effect that saturation has on concrete strength. The effects of saturation on plain concrete have been studied extensively in the literature. In the following a brief review of scientific explanation for this phenomenon is presented, and then the important experimental variables of FRC, from this perspective, are discussed.

5.5.1. Literature Review

The compressive strength of concrete in wet condition is lower than that of dry concrete (Neville 1990; Imran and Pantazopoulou, 1995). Several theories have been proposed to explain the reason for this phenomenon. Mills (1960) suggested that absorbed water dilates the gel, and the force of cohesion of the solid particles decreases. Another theory indicated that the absorbed water creates a shielding effect and decreases the cohesive forces acting between opposite solid surfaces (Rehbinder et al 1948). On the other hand, microscopically, when the specimen is loaded, absorbed water develops pore pressure due to the volumetric contraction of specimen (Akroyd 1961), and this pore pressure generates tension in concrete and weakens its micro-structure. The absorbed water also develops a swelling pressure in the gel (Mills 1966) which has to be in equilibrium with the interparticle forces (Van der Waal's forces). This process reduces the cohesive bond of the concrete particles, and decreases the strength.

Robertson and Mills (1985) describe the effect of water on the cement paste in a slightly different way. When concrete dries, water molecules migrate away from the cement gel and Van der Wall's bonds between the solid particles are strengthened. Upon re-saturation the process is reversible except for new solid-solid bonds (due to the collapse of structure of hydrated cement paste) which are stronger than solid-water attraction. Robertson and Mills (1985) have mentioned that there are other factors which are

involved in the weakening of concrete by absorbed water, such as: chemical reactions with the water, and change in concrete surface energy which leads to propagation of Griffith cracks.

5.5.2. Experimental Results

The saturation effects are investigated in this research by studying the behavior of identical dry and wet specimens. In this regard, the test types A to D (Table 3-1) for saturated condition, and F to I for dry condition have been considered.

5.5.2.1. Uniaxial Compression

The mechanical properties of fiber concrete batches subjected to uniaxial compression are determined by considering test types A (wet) and F (dry). The results are presented in Figures 5-21 to 5-26. Each point on these plots represents a particular batch. The horizontal axis represents the value of a considered mechanical property in wet condition (average value of 3 specimens), and vertical axis indicates the same variable in dry condition (average value of 2 specimens). Therefore, the diagonal represents the equal value line.

The strength of fiber concrete in dry condition is higher than that of identical concrete in wet condition. This has been clearly explained in the literature. The internal pore pressure developed in the saturated specimens acts as negative confinement causing weakening of the concrete structure. Figure 5-21 presents the results of the experiments. All the points on the plot are closer to the dry axis, which means dry strength is higher than wet strength. The difference of the two values is related to the strength and porosity of the concrete.

Figure 5-22 illustrates the values of ε_c in wet and dry conditions. These values are much higher for dry concrete than wet one. Since the increase in ε_c is higher relative to f'_c

for dry fiber concrete, the E values which are presented in Figure 5-23 are higher for wet specimens.

Figure 5-24 indicates that the value of Poisson's ratio is higher for wet specimens. This means the rate of ε_3 increase is higher than that of ε_1, which leads to smaller ε^* for wet concrete, which is indicated by Figure 5-25. It can be concluded that wet fiber concrete suffers more damage than the dry one, since its volumetric strain increases at a faster rate. This result was expected considering that the internal pressure acts as tensile lateral stress on the concrete.

Figure 5-26 presents the values of ε_{85} for wet and dry conditions. Higher value of this strain indicates higher ductility. These values are higher for the dry specimens.

5.5.2.2. Triaxial Compression

Table 5-6 and related Figure 5-27 show the strength of dry and wet confined specimens. The strength of dry concrete is higher for all degrees of confinement. Table 5-7 and Figure 5-28 indicate that the values of ε_c for dry specimens are lower for higher degrees of confinement than those of wet specimens. Table 5-8 and Figure 5-29 show that the value of E slightly increases with the degree of confinement, but its changes are equal for dry and wet specimens.

The variations of ε^* for dry and wet concrete are presented by Table 5-9 and Figure 5-30. This value is slightly lower for dry concrete at higher confinement. Perhaps, dry fiber concrete suffers more damage at high degrees of confinement. A large amount of contraction occurs during the application of lateral pressure prior to loading the wet specimens, which causes compaction and delay in sever damage (Imran and Pantazopoulou, 1995). The values of ε_{85}, which are indications of ductility, are shown in Table 5-10 and Figure 5-31. These values are slightly lower for dry high confined specimens.

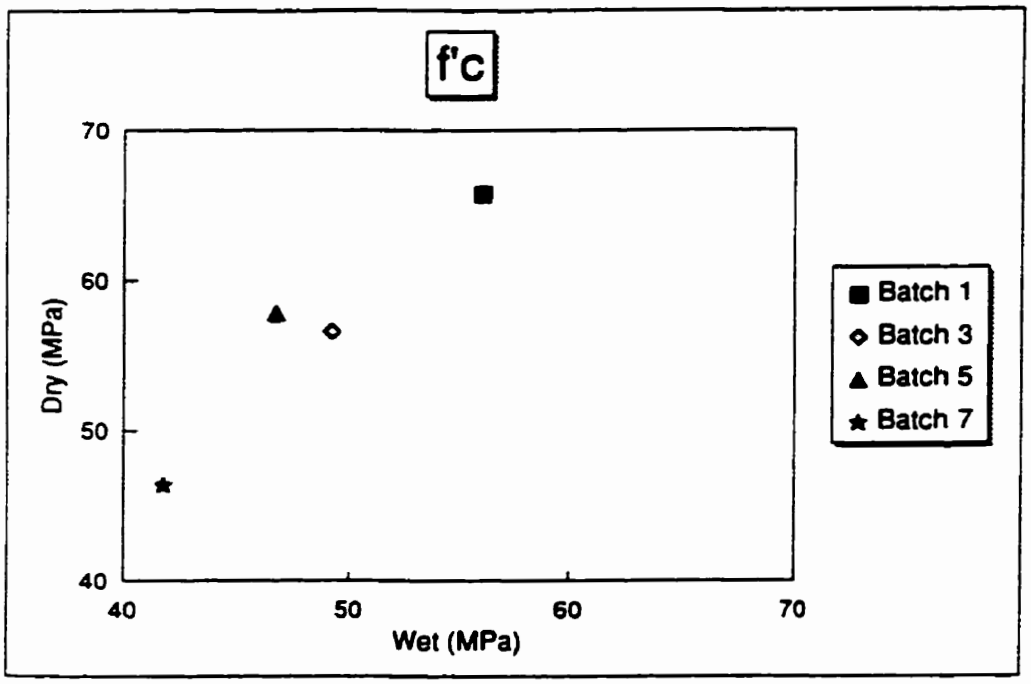

Figure 5-21: Effect of saturation on strength
(uniaxial)

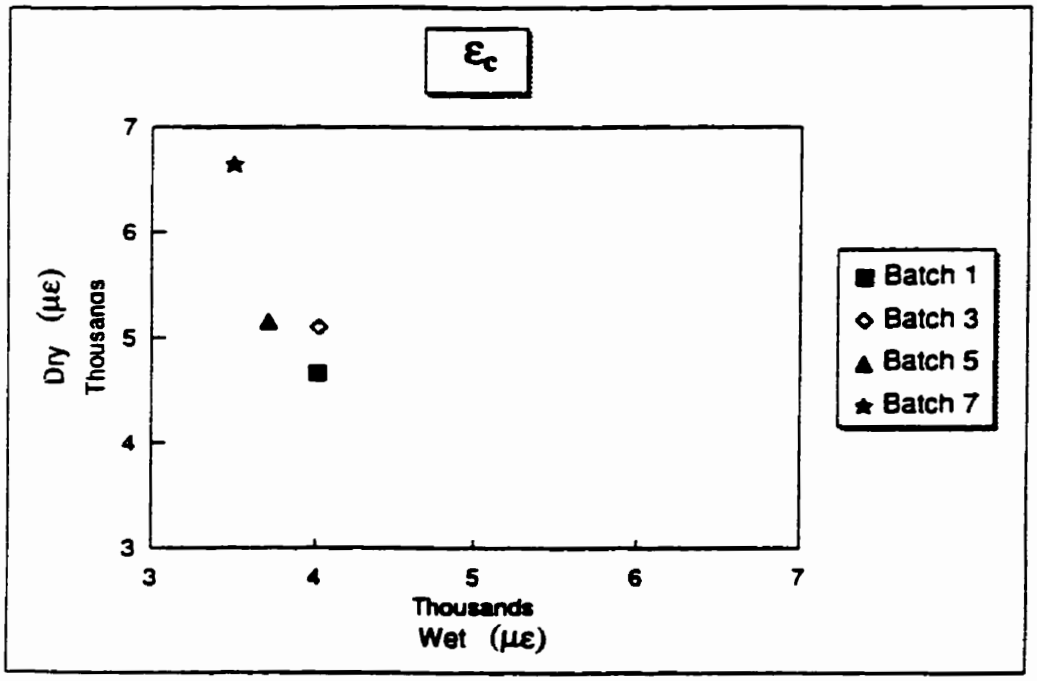

Figure 5-22: Effect of saturation on ε_c
(uniaxial)

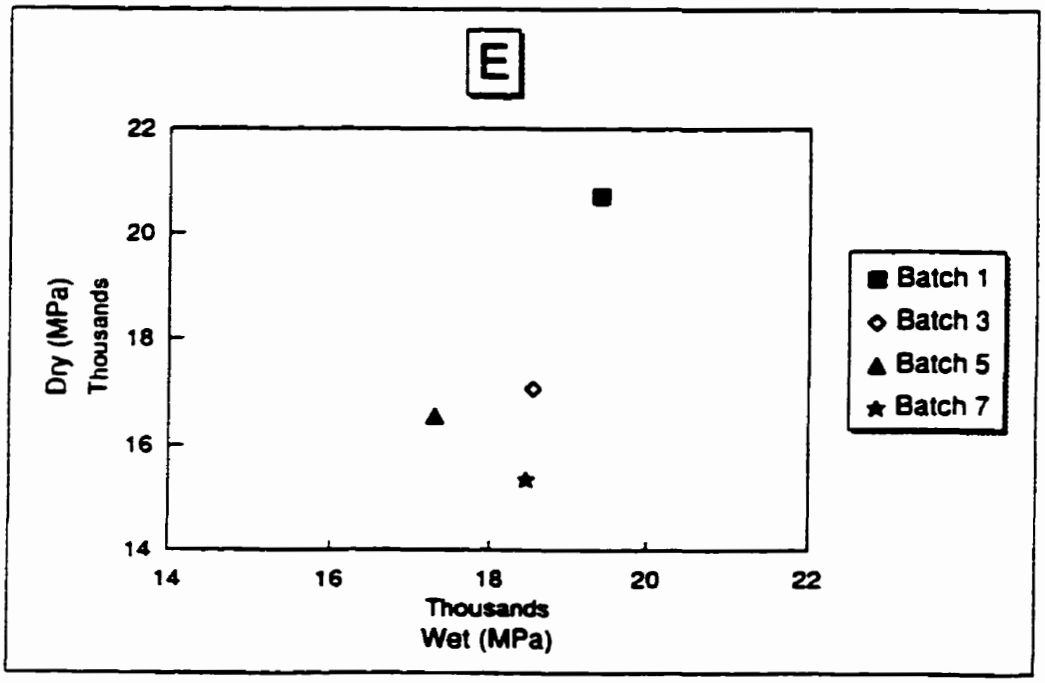

Figure 5-23: Effect of saturation on E value
(uniaxial)

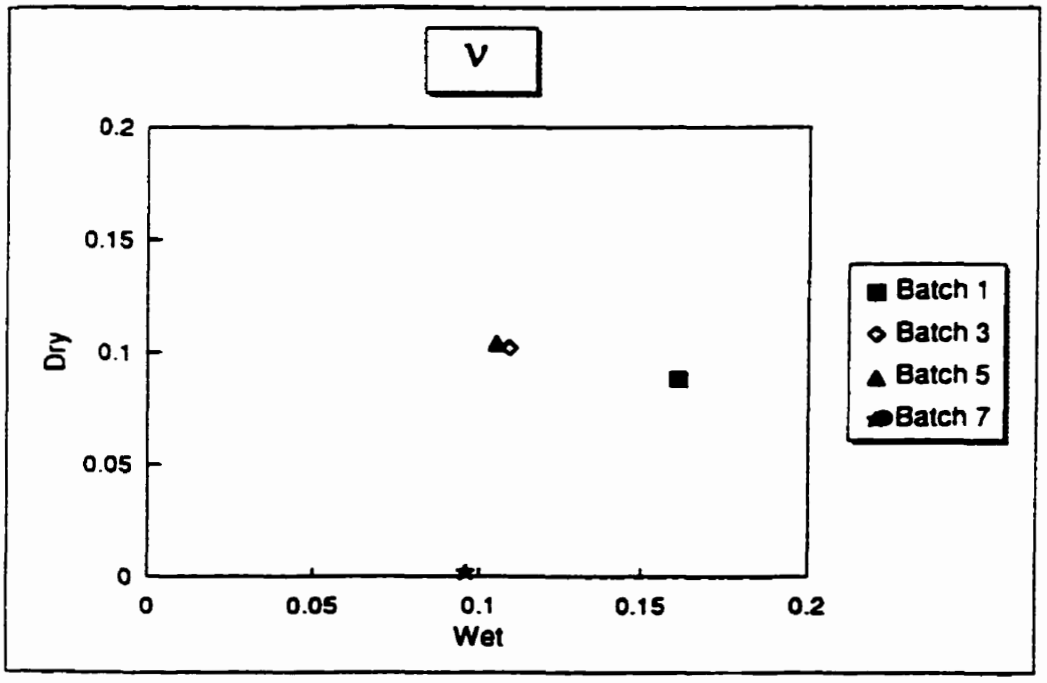

Figure 5-24: Effect of saturation on ν
(uniaxial)

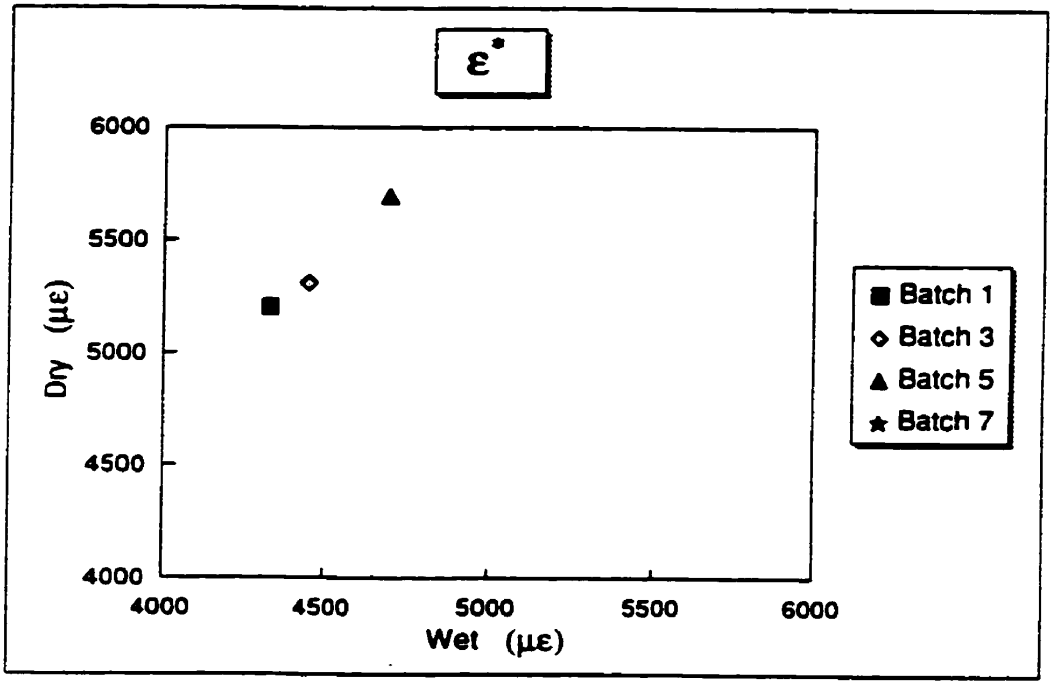

Figure 5-25: Effect of saturation on ε^*
(uniaxial)

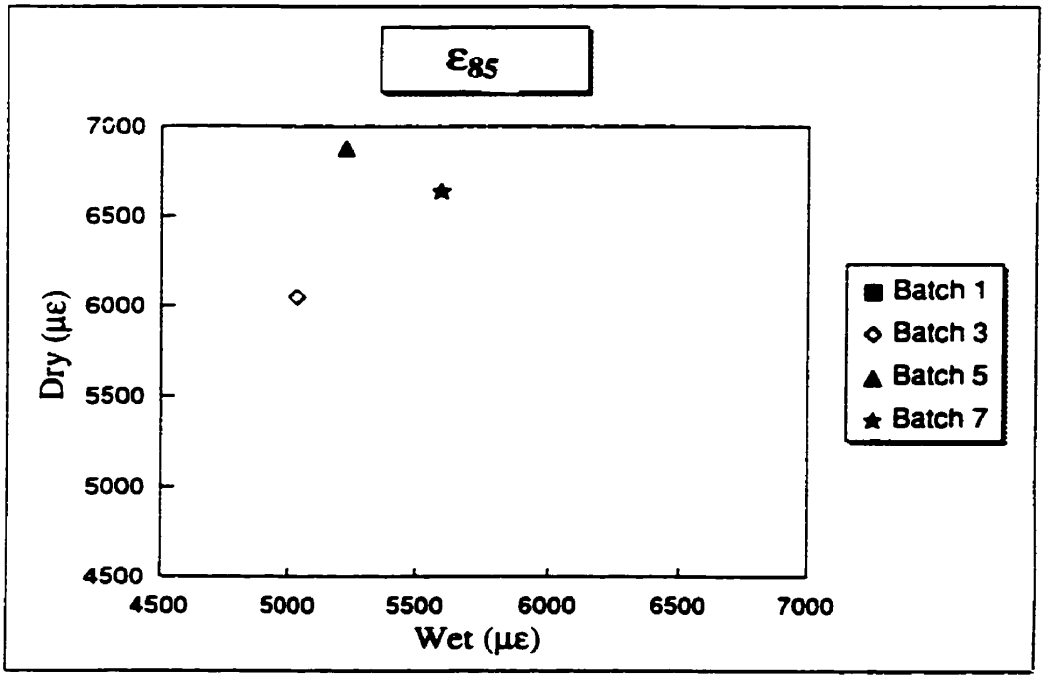

Figure 5-26: Effect of saturation on ε_{85}
(uniaxial)

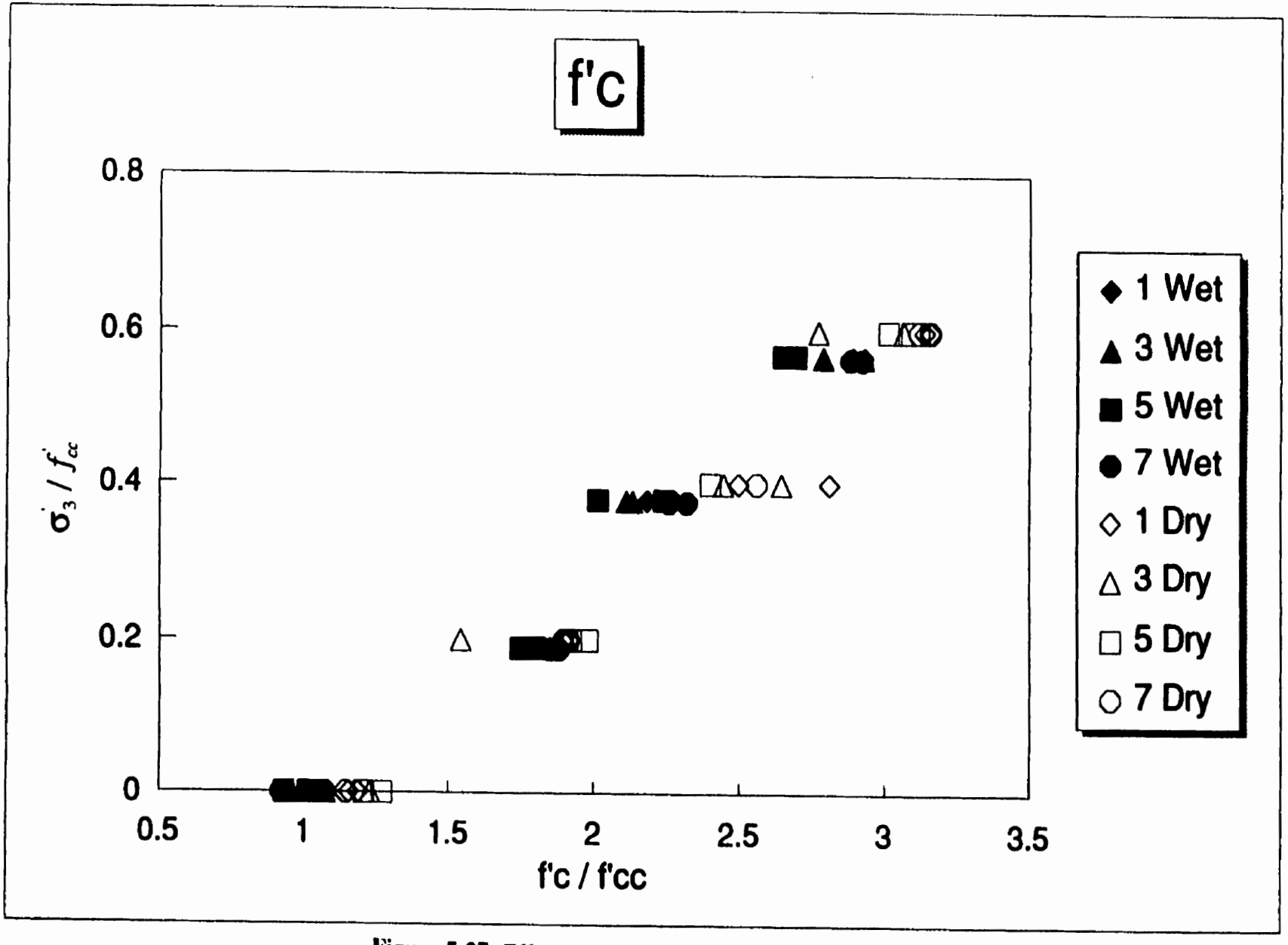

Figure 5-27; Effect of saturation on the confined strength

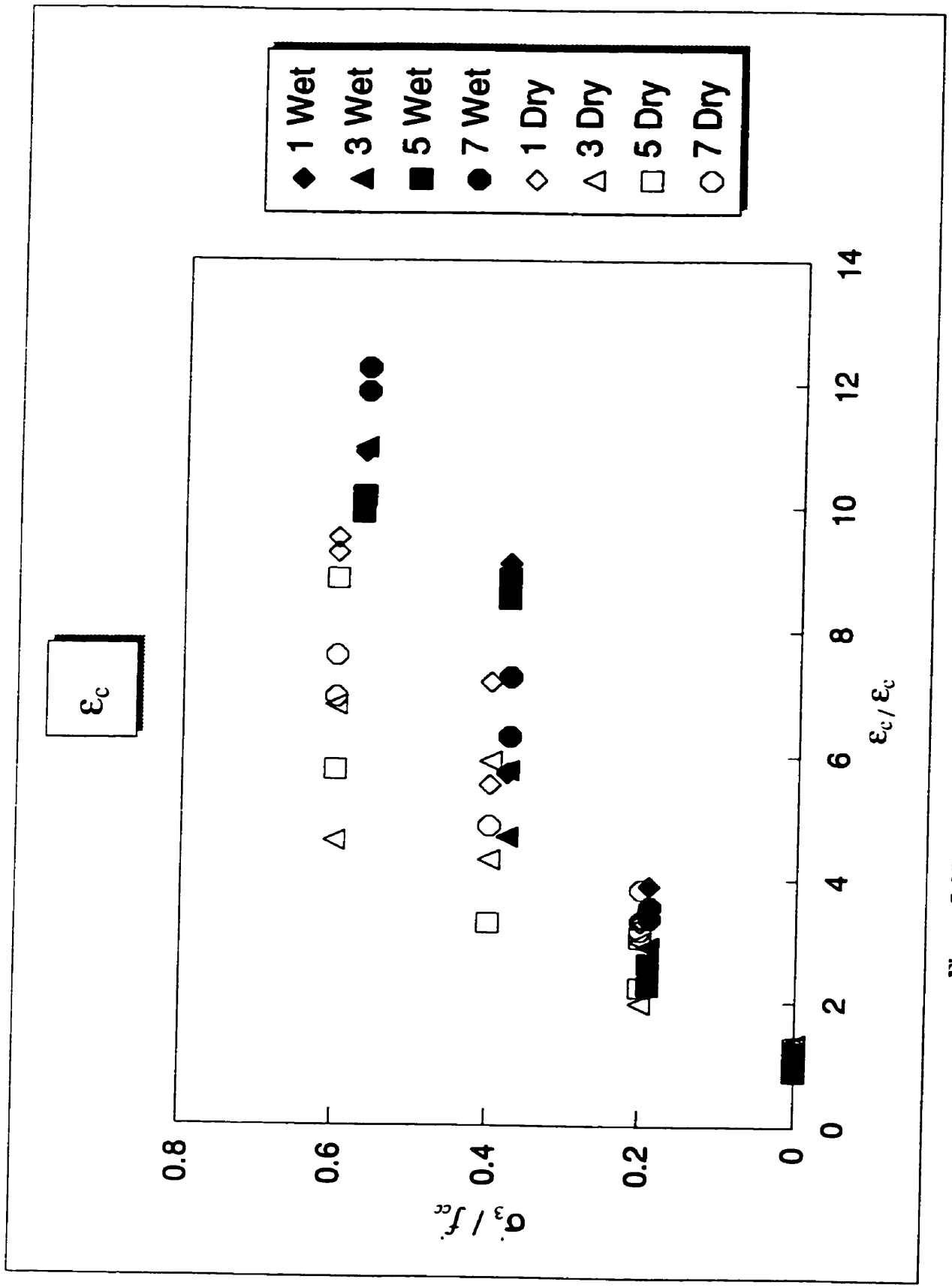

Figure 5-28: Effect of saturation on the ε_c value of confined FRC

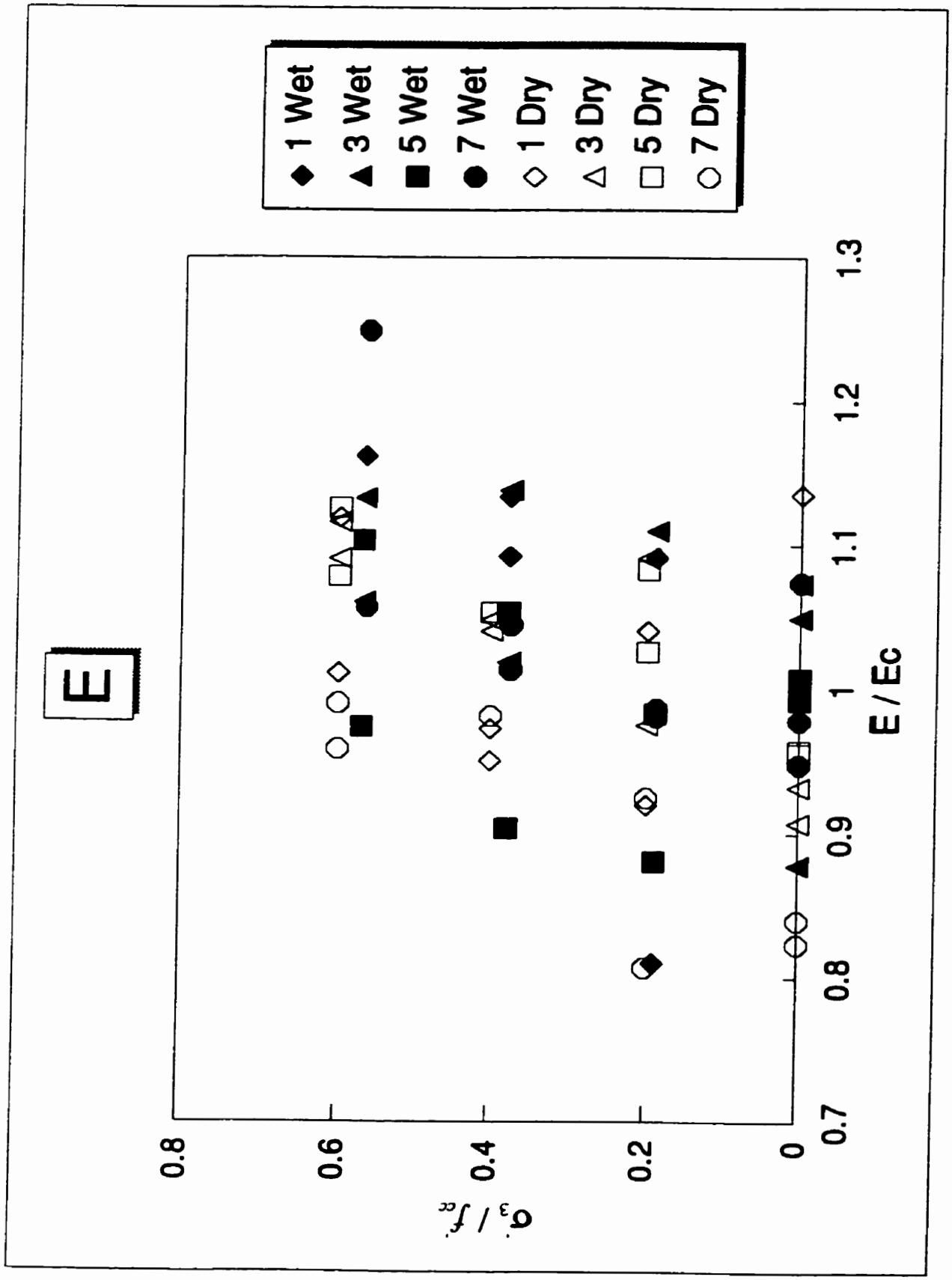

Figure 5-29: Effect of saturation on the E value of confined FRC

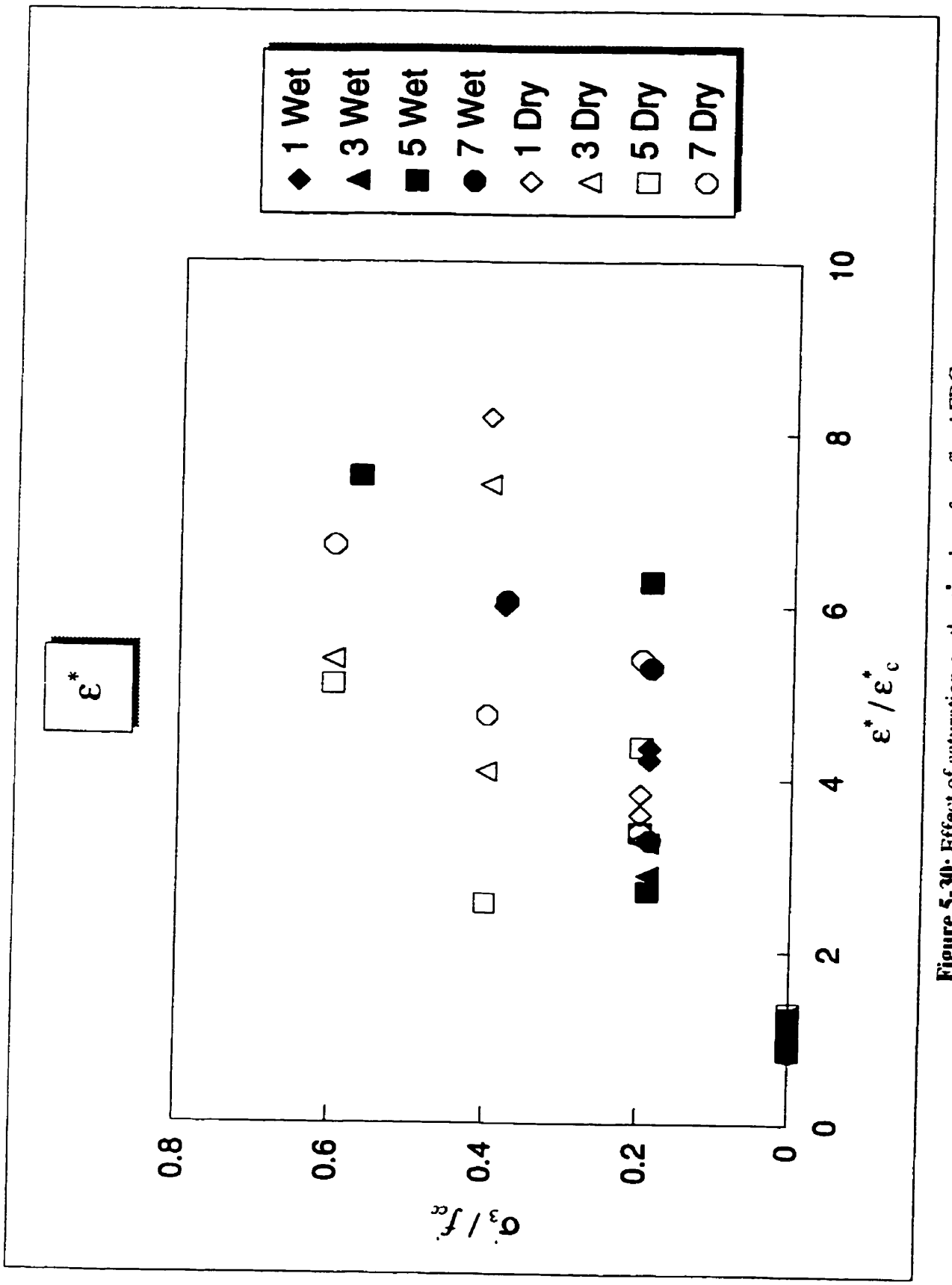

Figure 5-30: Effect of saturation on the ε* value of confined FRC

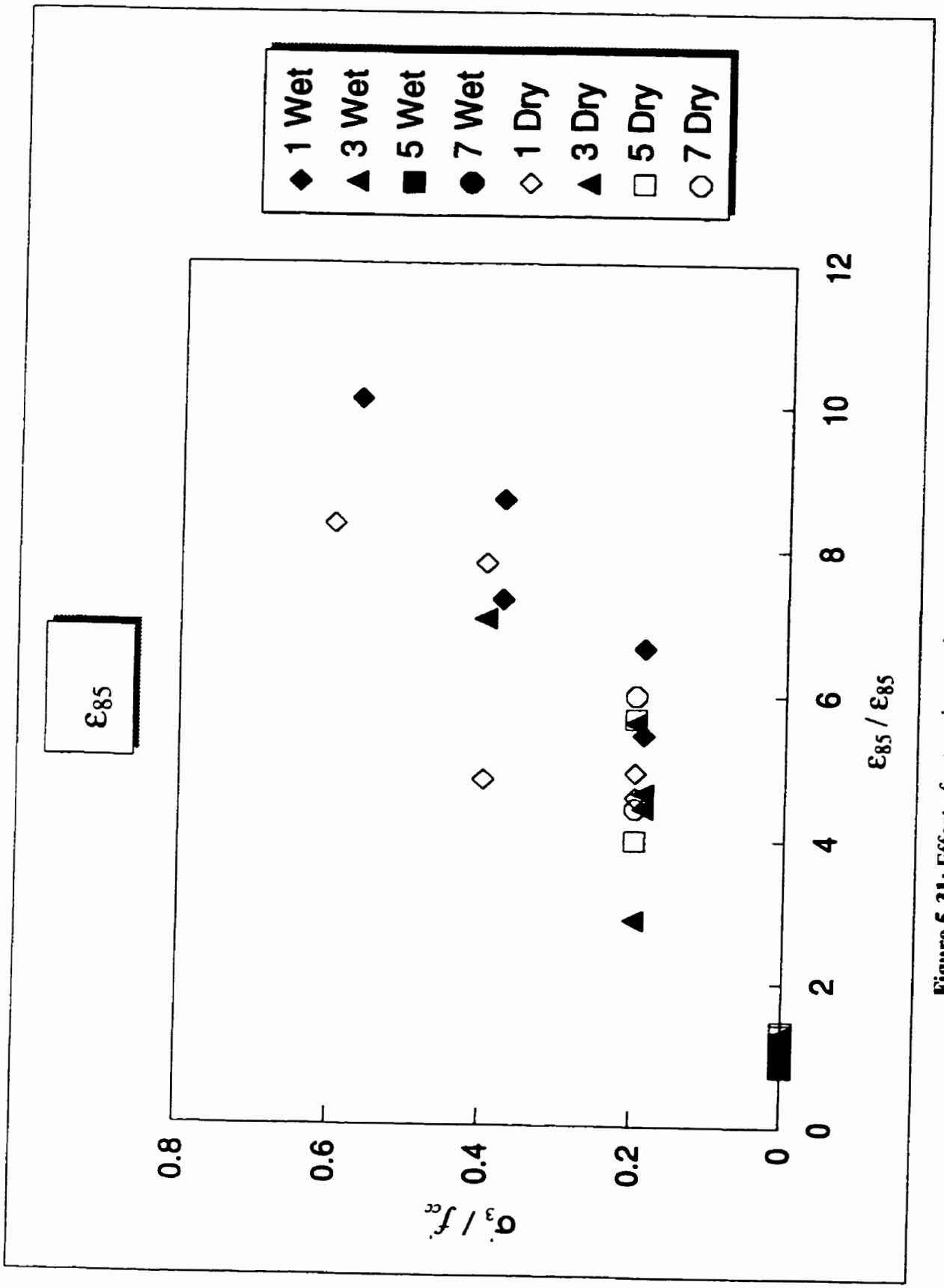

Figure 5-31: Effect of saturation on the ε_{85} value of confined FRC

No.	fc / fcc	Wet	Dry
1A1	1	0.00%	
1A2			
1A3	1	0.00%	
1B1	1.882353	18.90%	
1B2	1.849911	18.90%	
1C1	2.275936	37.79%	
1C2	2.182888	37.79%	
1D1			
1D2	2.887701	56.69%	
1F1	1.188948		0.00%
1F2	1.15508		0.00%
1G1	1.893048		20.00%
1G2	1.914439		20.00%
1H1	2.809269		40.00%
1H2	2.497326		40.00%
1I1	3.137255		60.00%
1I2	3.160428		60.00%
3A1	1.002712	0.00%	
3A2	1.000678	0.00%	
3A3	0.99661	0.00%	
3B1	1.777627	18.89%	
3B2	1.808136	18.89%	
3C1	2.131525	37.78%	
3C2	2.111186	37.78%	
3D1	2.786441	56.67%	
3D2	2.928814	56.67%	
3F1	1.228475		0.00%
3F2	1.075932		0.00%
3G1	1.905763		20.00%
3G2	1.541695		20.00%
3H1	2.444746		40.00%
3H2	2.644068		40.00%
3I1	2.770169		60.00%
3I2	3.065085		60.00%
5A1	1.049251	0.00%	
5A2	0.933619	0.00%	
5A3	1.017131	0.00%	
5B1	1.747323	18.96%	
5B2	1.798715	18.96%	
5C1	2.014989	37.92%	
5C2	2.239829	37.92%	
5D1	2.648822	56.87%	
5D2	2.69379	56.87%	
5F1	1.207709		0.00%
5F2	1.269807		0.00%
5G1	1.978587		20.00%
5G2	1.920771		20.00%
5H1	0		40.00%
5H2	2.398287		40.00%
5I1	3.092077		60.00%
5I2	3.012848		60.00%
7A1	1.069378	0.00%	
7A2	1.009569	0.00%	
7A3	0.921053	0.00%	
7B1	1.880383	18.80%	
7B2	1.849282	18.80%	
7C1	2.258373	37.60%	
7C2	2.318182	37.60%	
7D1	2.882775	56.41%	
7D2	2.923445	56.41%	
7F1	1.074163		0.00%
7F2	1.145933		0.00%
7G1	1.894737		20.00%
7G2	1.913876		20.00%
7H1	2.559809		40.00%
7H2	0		40.00%
7I1	3.119617		60.00%
7I2	3.157895		60.00%

Table 5-6: Effect of saturation on the confined strength

No.	$\varepsilon_c / \varepsilon_{cc}$	Wet	Dry
1A1	0.987019	0.00%	
1A2			
1A3	1.012981	0.00%	
1B1	3.515477	18.90%	
1B2	3.891163	18.90%	
1C1	9.080629	37.79%	
1C2	5.707688	37.79%	
1D1			
1D2	10.88268	56.69%	
1F1	1.171243		0.00%
1F2	1.156765		0.00%
1G1	3.296555		20.00%
1G2	3.351722		20.00%
1H1	5.527958		40.00%
1H2	7.171493		40.00%
1I1	9.259611		60.00%
1I2	9.494508		60.00%
3A1	1.027974	0.00%	
3A2	0.915415	0.00%	
3A3	1.056612	0.00%	
3B1	2.570183	18.89%	
3B2	2.904624	18.89%	
3C1	5.759193	37.78%	
3C2	4.681913	37.78%	
3D1	10.17066	56.67%	
3D2	10.95733	56.67%	
3F1	1.340749		0.00%
3F2	1.200548		0.00%
3G1	2.988545		20.00%
3G2	1.975264		20.00%
3H1	4.310368		40.00%
3H2	5.90811		40.00%
3I1	4.619158		60.00%
3I2	6.805595		60.00%
5A1	0.89461	0.00%	
5A2	1.207638	0.00%	
5A3	0.897752	0.00%	
5B1	2.271694	18.96%	
5B2	2.634759	18.96%	
5C1	8.5168	37.92%	
5C2	8.854	37.92%	
5D1	10.17597	56.87%	
5D2	9.912255	56.87%	
5F1	1.21344		0.00%
5F2	1.280155		0.00%
5G1	3.04496		20.00%
5G2	2.231327		20.00%
5H1			40.00%
5H2	3.281363		40.00%
5I1	8.840222		60.00%
5I2	5.773507		60.00%
7A1	1.044411	0.00%	
7A2	1.012675	0.00%	
7A3	0.942914	0.00%	
7B1	3.36167	18.80%	
7B2	3.556085	18.80%	
7C1	6.302773	37.60%	
7C2	7.25741	37.60%	
7D1	11.87334	56.41%	
7D2	12.25531	56.41%	
7F1	1.205661		0.00%
7F2	1.284857		0.00%
7G1	3.831126		20.00%
7G2	3.163252		20.00%
7H1	4.857238		40.00%
7H2			40.00%
7I1	6.937768		60.00%
7I2	7.602211		60.00%

Table 5-7: Effect of saturation on the ε_c value of confined FRC

No.	E / Ec	Wet	Dry
1A1	1.006468	0.00%	
1A2			
1A3	0.993532	0.00%	
1B1	1.091359	18.90%	
1B2	0.810177	18.90%	
1C1	1.092109	37.79%	
1C2	1.133883	37.79%	
1D1			
1D2	1.161831	56.69%	
1F1	0.999765		0.00%
1F2	1.13518		0.00%
1G1	1.040179		20.00%
1G2	0.91979		20.00%
1H1	0.95063		40.00%
1H2	0.972641		40.00%
1I1	1.011153		60.00%
1I2	1.119212		60.00%
3A1	1.048966	0.00%	
3A2	1.073018	0.00%	
3A3	0.878015	0.00%	
3B1		18.89%	
3B2	1.109681	18.89%	
3C1	1.018561	37.78%	
3C2	1.138256	37.78%	
3D1	1.060729	56.67%	
3D2	1.13301	56.67%	
3F1	0.932219		0.00%
3F2	0.907254		0.00%
3G1	1.090784		20.00%
3G2	0.975057		20.00%
3H1	1.040109		40.00%
3H2	1.048232		40.00%
3I1	1.090465		60.00%
3I2	1.115973		60.00%
5A1	1.179724	0.00%	
5A2		0.00%	
5A3	1.162578	0.00%	
5B1	1.031492	18.96%	
5B2	1.151672	18.96%	
5C1	1.233624	37.92%	
5C2	1.058151	37.92%	
5D1	1.292096	56.87%	
5D2	1.140614	56.87%	
5F1	1.121316		0.00%
5F2	1.118676		0.00%
5G1	1.201488		20.00%
5G2	1.267993		20.00%
5H1			40.00%
5H2	1.233631		40.00%
5I1	1.318657		60.00%
5I2	1.262546		60.00%
7A1	1.073946	0.00%	
7A2	0.978356	0.00%	
7A3	0.947698	0.00%	
7B1	0.98104	18.80%	
7B2	0.986209	18.80%	
7C1	1.01351	37.60%	
7C2	1.044542	37.60%	
7D1	1.24894	56.41%	
7D2	1.056791	56.41%	
7F1	0.839619		0.00%
7F2	0.823437		0.00%
7G1	0.924541		20.00%
7G2	0.806728		20.00%
7H1	0.981485		40.00%
7H2			40.00%
7I1	0.990225		60.00%
7I2	0.958358		60.00%

Table 5-8: Effect of saturation on the E value of confined FRC

No.	$\varepsilon^* / \varepsilon^*_c$	Wet	Dry
1A1	0.977013	0.00%	
1A2			
1A3	1.022987	0.00%	
1B1	4.226175	18.90%	
1B2	4.358323	18.90%	
1C1		37.79%	
1C2	5.999307	37.79%	
1D1			
1D2		56.69%	
1F1	1.166455		0.00%
1F2	1.162296		0.00%
1G1	3.830195		20.00%
1G2	3.59501		20.00%
1H1			40.00%
1H2	8.184591		40.00%
1I1			60.00%
1I2			60.00%
3A1	1.046867	0.00%	
3A2	0.910983	0.00%	
3A3	1.04215	0.00%	
3B1	2.885229	18.89%	
3B2	3.264356	18.89%	
3C1		37.78%	
3C2		37.78%	
3D1		56.67%	
3D2		56.67%	
3F1	1.268099		0.00%
3F2	1.117392		0.00%
3G1	3.299169		20.00%
3G2			20.00%
3H1	7.401962		40.00%
3H2	4.086172		40.00%
3I1	5.381448		60.00%
3I2			60.00%
5A1	0.901808	0.00%	
5A2	1.233392	0.00%	
5A3	0.8648	0.00%	
5B1	2.698192	18.96%	
5B2	6.280113	18.96%	
5C1		37.92%	
5C2		37.92%	
5D1	7.499043	56.87%	
5D2		56.87%	
5F1	1.132364		0.00%
5F2	1.290181		0.00%
5G1	3.381141		20.00%
5G2	4.371854		20.00%
5H1			40.00%
5H2	2.553137		40.00%
5I1	5.096065		60.00%
5I2			60.00%
7A1	1.085562	0.00%	
7A2	1.066859	0.00%	
7A3	0.847579	0.00%	
7B1	3.289483	18.80%	
7B2	5.289645	18.80%	
7C1		37.60%	
7C2	6.052584	37.60%	
7D1		56.41%	
7D2		56.41%	
7F1			0.00%
7F2			0.00%
7G1	3.395464		20.00%
7G2	5.387152		20.00%
7H1	4.738797		40.00%
7H2			40.00%
7I1			60.00%
7I2	6.69335		60.00%

Table 5-9: Effect of saturation on the ε^* value of confined FRC

No.	ε_{as} / ε_{cs}	Wet	Dry
1A1	0.949288	0.00%	
1A2			
1A3	1.050712	0.00%	
1B1	5.447064	18.90%	
1B2	6.650356	18.90%	
1C1	8.696619	37.79%	
1C2	7.317616	37.79%	
1D1			
1D2	10.09786	56.69%	
1F1			0.00%
1F2			0.00%
1G1	4.587856		20.00%
1G2	4.925267		20.00%
1H1	4.81895		40.00%
1H2	7.81161		40.00%
1I1	8.346753		60.00%
1I2			60.00%
3A1	1.086611	0.00%	
3A2	0.875646	0.00%	
3A3	1.037743	0.00%	
3B1	4.435439	18.89%	
3B2	4.64859	18.89%	
3C1		37.78%	
3C2		37.78%	
3D1		56.67%	
3D2		56.67%	
3F1	1.288041		0.00%
3F2	1.115812		0.00%
3G1	5.619587		20.00%
3G2	2.868494		20.00%
3H1	7.045491		40.00%
3H2			40.00%
3I1			60.00%
3I2			60.00%
5A1	0.969372	0.00%	
5A2	1.19085	0.00%	
5A3	0.839778	0.00%	
5B1		18.96%	
5B2		18.96%	
5C1		37.92%	
5C2		37.92%	
5D1		56.87%	
5D2		56.87%	
5F1	1.294793		0.00%
5F2	1.338055		0.00%
5G1	5.671899		20.00%
5G2	3.980475		20.00%
5H1			40.00%
5H2			40.00%
5I1			60.00%
5I2			60.00%
7A1	1.01765	0.00%	
7A2	1.019259	0.00%	
7A3	0.963091	0.00%	
7B1		18.80%	
7B2		18.80%	
7C1		37.60%	
7C2		37.60%	
7D1		56.41%	
7D2		56.41%	
7F1	1.179536		0.00%
7F2	1.197245		0.00%
7G1	5.99195		20.00%
7G2	4.426212		20.00%
7H1			40.00%
7H2			40.00%
7I1			60.00%
7I2			60.00%

Table 5-10: Effect of saturation on the ε_{as} value of confined FRC

5.6. Effects of Wrapping

Various degrees of passive confinement was applied to the cylindrical specimens by layers of carbon fiber wrap, and the compressive responses of various types of fiber reinforced concrete were assessed under these circumstances. The test types K to P (Table 3-1) are related to this part of the research, where K to M are 200×100 mm and N to P are 100×50 mm cylinders. All the specimens were tested in saturated condition. The number of wraps varied from 1 to 3 individual layers.

When a specimen is loaded, it develops lateral deformation, which generates longitudinal strain in the wrap, and after the collapse of internal structure of concrete the confining mechanism is fully mobolised. It has been shown by energy balance consideration that at that stage, any increment of axial strain in concrete, requires two components of external work input, one to compress the concrete mass, and one to stretch by the necessary amount the confining system (Pantazopoulou, 1995). Therefore, the more layers the confining system possesses the stiffer the overall system, and hence, the greater the required load to produce a given amount of axial strain. This explains the observed post-peak stiffening of the stress-strain curves of the wrapped cylindrical specimens. The second peak which marks the end of life of the composite specimen corresponds to the occurance of catastrophic failure, either in the concrete-wrap interface propagating to the seam, or directly on the seam if the overlapping provided is inadequate for development of the wrap strength.

The wrap which was used in this experiment was carbon fiber. Therefore, the strain at failure of the carbon fibers determines the ultimate deformation (or strength) capacity of the composite. The ultimate elongation for carbon fiber type C1-20 is 1.5% (Forca catalogue, Appendix B). Figures 5-32 to 5-40 show that the lateral strains at failure (wrap breakage) have values between 0.5% to 1.5%. The low values of ε_3 could be caused by premature failure in the wrap seam or by imperfections in the wrap installation. The axial strain at failure for a wrapped specimen (wrap breakage) is more

than that for an unwrapped specimen. Hence, when the wrap breaks, the concrete can not withstand the existing axial strain and explosive failure occurs. Furthermore, the circumferential strain is the highest at the mid-height of the cylinders, and wrap breakage begins from this region and moves to the ends. This movement is very rapid, but produces a short distinguishable steep unloading part on the stress-strain curves.

5.6.1. The Effects of Various Number of Layers

In this section test types K to M (200×100 mm cylinders) have been considered, which include all the batches. Figures 5-32 to 5-40 illustrate the behavior of the batches with various numbers of layers. These figures plot the variation of stress with axial and circumferential strains (on the top), and that of axial strain versus volumetric strain (on the bottom). In these plots the behavior of the specimen which was more representetive (from two identical specimens) have been used for each batch. The specifice characteristics of the responses of wrapped specimens are discussed in greater detail in the following sections.

5.6.1.1. Maximum Strength

The study of Figures 5-32 to 5-40 indicates that the general shape of stress-strain curves for wrapped cylinders are of bi-linear type with a kink-point in between the two parts. The kink-point is at the end of the elastic behavior of specimens. Up to this point, the circumferential strain increases at a low rate, and the resistance is mainly resulting from the concrete structure. After the kink-point the circumferential strain increases rapidly, and the passive confinement becomes entirely effective. The figures show that applying the first layer of wrap increases the strength of concrete by about 20%, and additional layers do not effect that strength (location of the kink-point) considerably. A number of specimens show consistently two peaks on the stress-strain curves: the first one

at the end of the elastic part of the curve, and the second one at the point of failure of the wrap. The general pattern of these peaks can be defined as follows:

- The peaks are sharper for plain concrete (batch 1) and concrete with low volume of micro and steel fibers (batches 2 and 4), and smoother for higher volume of micro and steel fibers (batches 3 and 5) and for any volume of polypropylene fibers. The first peak vanishes as the volume of fibers go higher (batches 6 to 8), and converts to a kink point. In other words, the more ductile the concrete is, the smoother the curve becomes (e.g. Figures 5-32 and 5-36).
- By increasing the number of layers (increasing confinement) the second peak goes higher, providing a smoother transition between the two peaks.
- The location of the first peak (kink-point) does not vary considerably.

The explanation for the existence of two peaks requires more study. However, a closer look at the interaction of concrete cylinder and wrap may explain this behavior to some extend. Note that the fiber wraps were oriented perpendicular to the loading direction, and therefore, they do not carry any axial load. When the specimen is loaded, the concrete cylinder bears the entire axial load, and therefore develops lateral strain which brings the passive confinement into action. The rate of lateral strain production is given by the difference of the ε_v - ε_l curve and a line inclined at 45° to the two axis (Figure 4-1).

The second part of the stress-strain curves are related to the fully mobilised confining system. The specimens need a considerable amount of deformation to be able to reach to this stage. This exsesive deformation associates with the collapse of internal structure of fiber concrete. Those batches which exhibited gradual failure (high content fiber concrete) illustrated a smooth transition from the first peak to the second one. Whereas, those batches which had sudden failure (plain and low fiber content concrete) resulted in a rapid expansion,which caused damage in the confining system leading to a drop after the first peak in the stress-strain curve.

It should be mentioned that in this experiment, the fiber wraps were individual layers, perpendicular to the axis of loading. Labossière (1996) used combinations of layers at different angles and found similar shape of the two peaks. He suggested that the first peak occurs when the layer which bears a greater share of the load (due to its angle) breaks. However, further research may be required for a better judgment.

Figure 5-41 presents the effect of various number of layers on the maximum strength (the highest peak). In this plot, the strengths are normalized to the average strength of uniaxial compression 200×100 mm cylinders (test type Q) of each batch. In general, the strength of fiber concrete increases by adding layers of wrap. This effect is more pronounced for high fiber content concrete (batches 6 and 8) than for low fiber content concrete (batches 1, 2 and 4). It should be mentioned that the strengths of the batches 6 and 8 were low. Therefore, it may be concluded that the wrapping system does not increase the strength of high strength concrete as effectively as in the case of lower strength concrete.

5.6.1.2. Strain at Maximum Strength

Figure 5-42 shows the normalized axial strains (to ε_c of test type Q) at the maximum strength of various specimens. The addition of wraps increases this strain, but it is more effective for high fiber content concrete batches. The lateral restraint prevents dramatic increase in area strain, and specimens can bear far greater axial deformation.

5.6.1.3. Elastic Modulus (E)

Figure 5-43 shows the normalized values of modulus of elasticity (to E obtained of test type Q) which are effected by the number of wraps. In general, the addition of layers increases the elastic modulus due to the stiffening action provided by the confining mechanism. However, as the number of layers increases the values of E are more scattered.

5.6.1.4. Strain at Zero Volumetric Strain (ε^*)

Figures 5-32 to 5-40 indicate that adding layers of wraps increases the value of ε^*, i.e. delays the onset of expansive response in the concrete structure. It was discussed in the proceeding that confinement acts against the lateral deformation, and lowers the rate of increase of ε_3, hence, slowing the rate of ε^*. The figures show that for half of the batches the rate of increase of ε_v is greater for specimens wrapped with three layers than that of specimens wrapped with two layers. Figure 5-44 shows the values of ε^* which are normalized to the similar value of test type Q, which leads to the same conclusion. Aaddition of layers of wrap appears to cause scattering in the results.

5.6.2. Size Effect Due to Wrapping

Size effects also have been studied in the wrapped cylinders. The specimens for test types K to M are 200×100 mm, and N to P are 100×50 mm cylinders. Figure 5-45 shows the effects of number of layers on the maximum strength of the concrete batches. In this plot, the average strength of each small cylinder is normalized to that of the large cylinder from the same batch. With one layer of wrap, the strength of the two sizes are equal, but adding more layers increases the strength of the small specimens relative to that of the large ones. The rate of increase is lower from 2 to 3 layers than from 1 to 2 layers. The results become more scattered as the number of layers goes higher.

Figure 5-46 illustrates the effects of number of layers on the normalized strain corresponding to the maximum strength of specimens with different sizes. The vertical axis shows the ratio of the strain of smaller cylinders to that of larger cylinders of the same batch. One layer of wrap increases this strain by 50%. Adding second layer increases this value by considerable amount. The addition of third layer does not have considerable effect.

Figure 5-47 shows the normalized values of the elastic modulus for the two sizes of specimens. The vertical axis indicates the ratio of this value of smaller cylinders to that of the larger cylinders. One layer of wrap decreases this value by 35% (i.e. larger wrapped cylinders are stiffer). The addition of the second layer causes an additional reduction of 10%, and the third layer has about 5% decreasing effect. These changes are more pronounced for the plain concrete (batch 1). Decreasing the value of E leads to a more flexible structure.

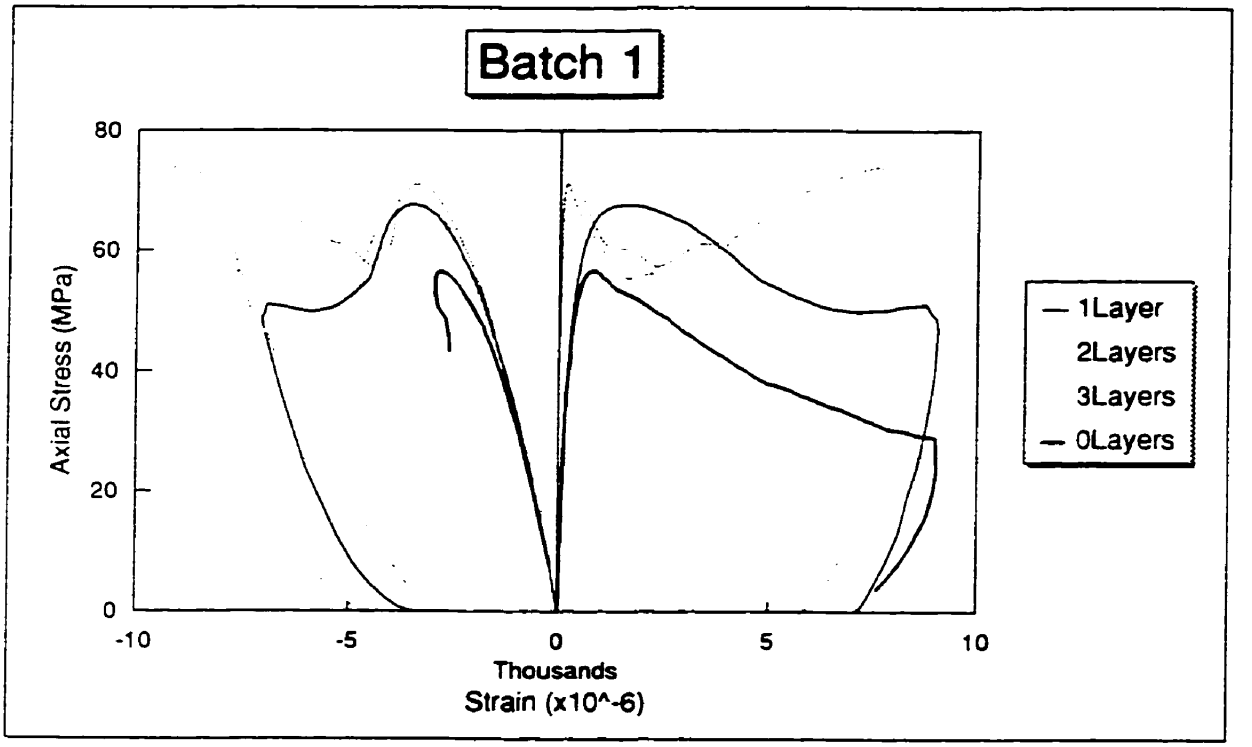

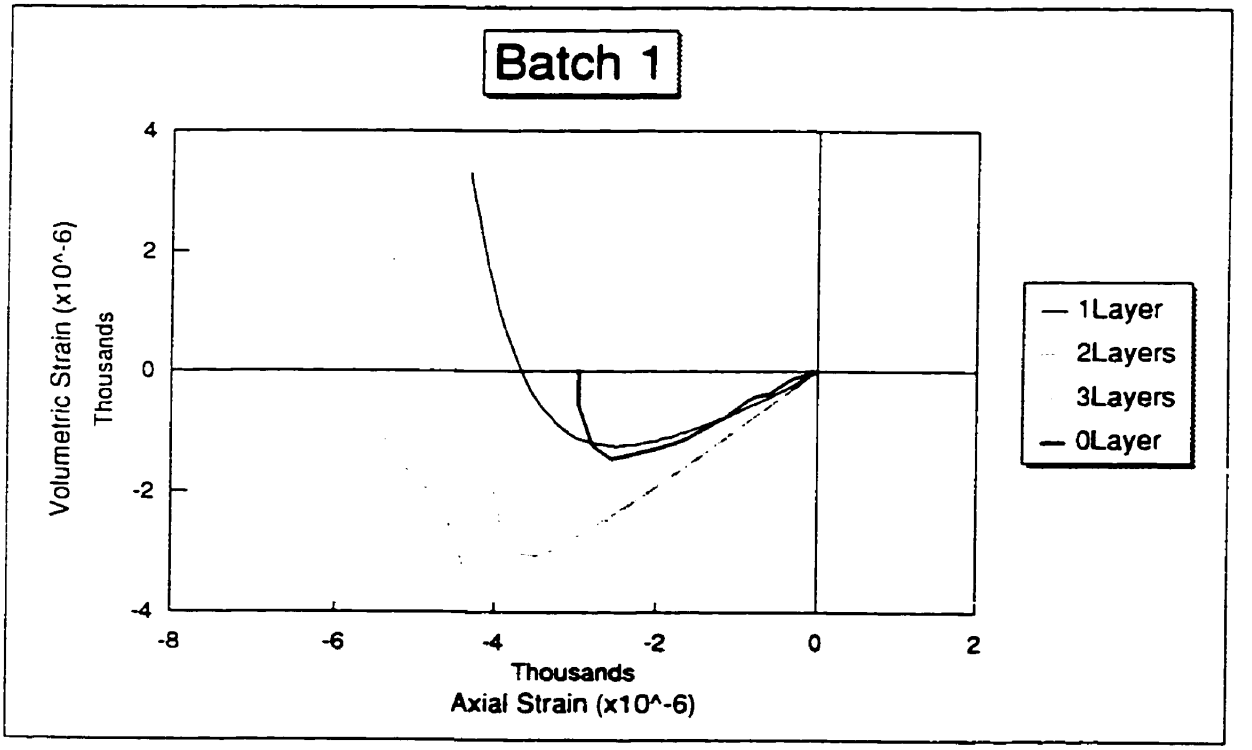

Figure 5-32: Compressive response of wrapped cylinders Batch 1(plain)
Top: axial (left) and circumferential (right) strains versus axial stress
Bottom: volumetric strain versus axial strain

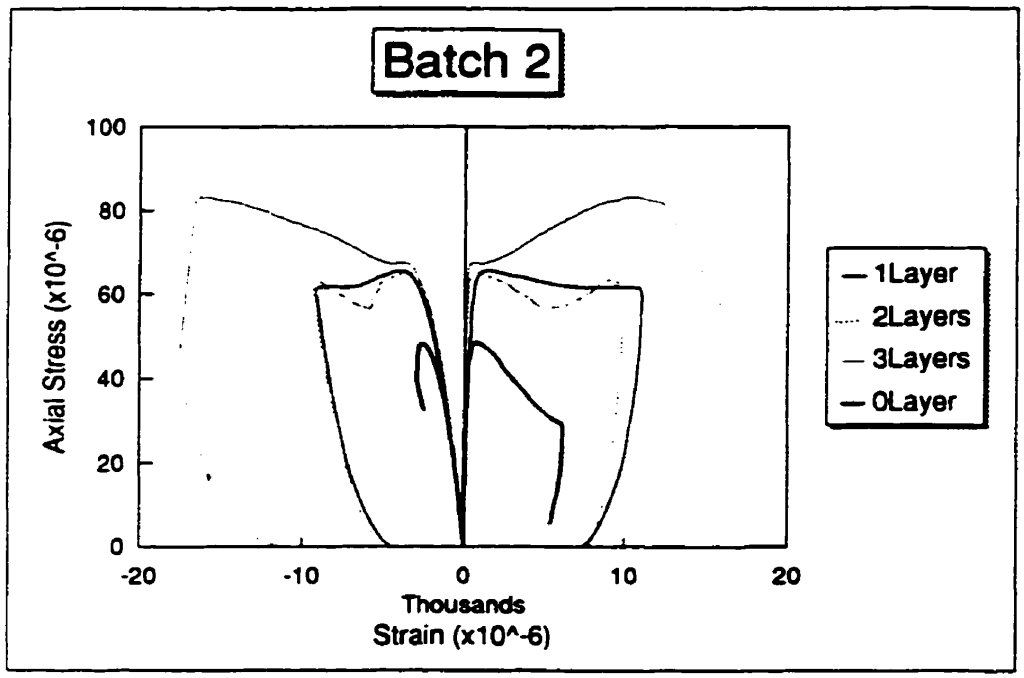

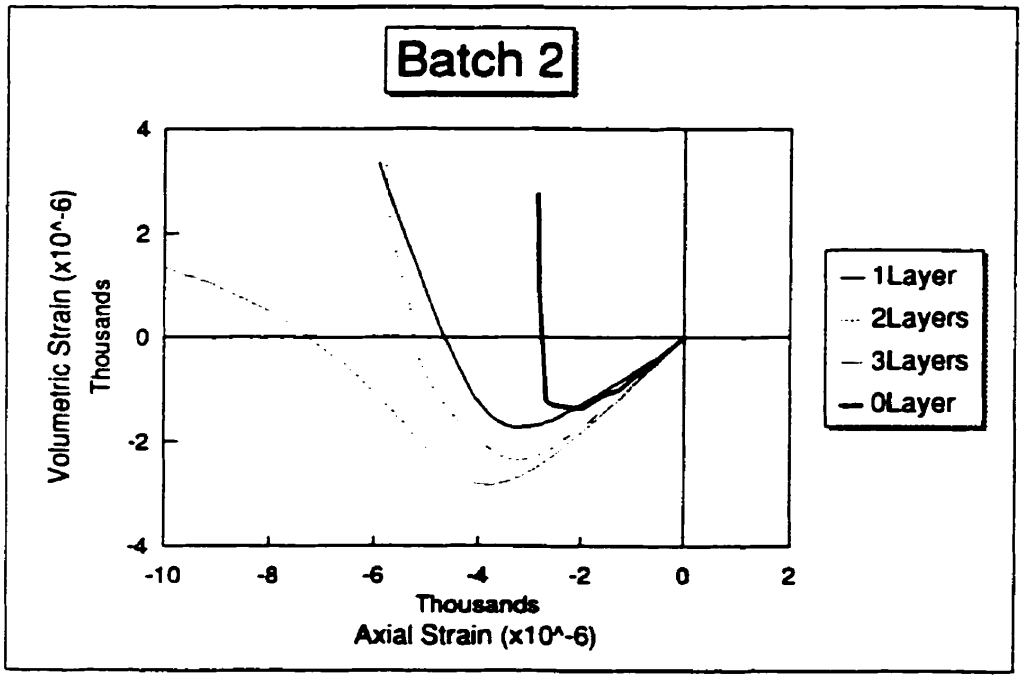

Figure 5-33: Compressive response of wrapped cylinders Batch 2 (1% M)
Top: axial (left) and circumferential (right) strains versus axial stress
Bottom: volumetric strain versus axial strain

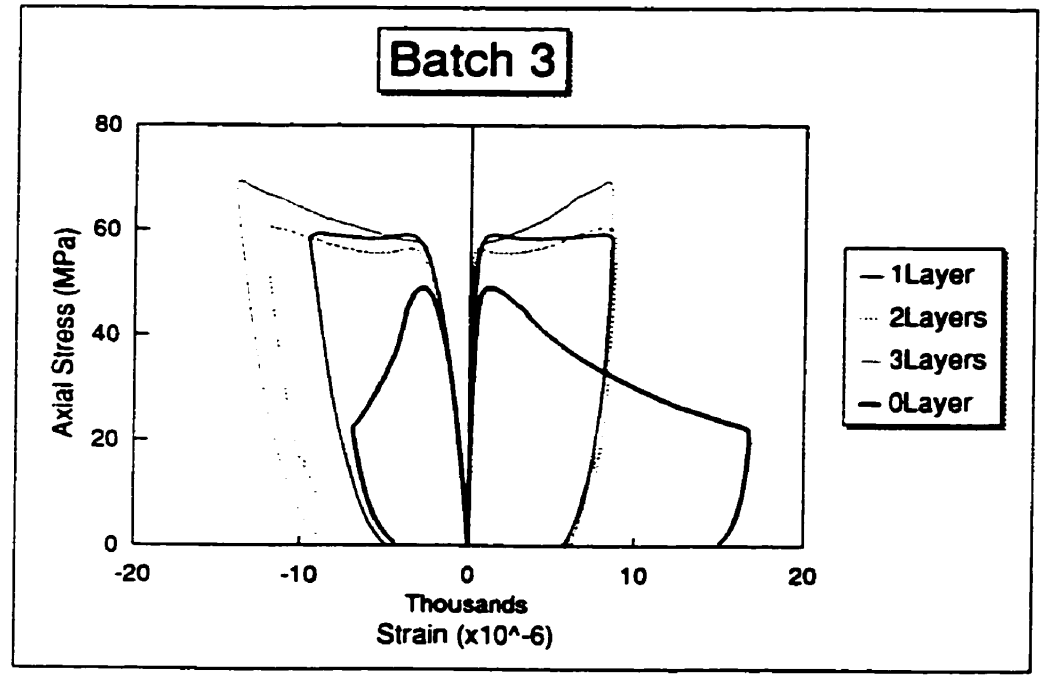

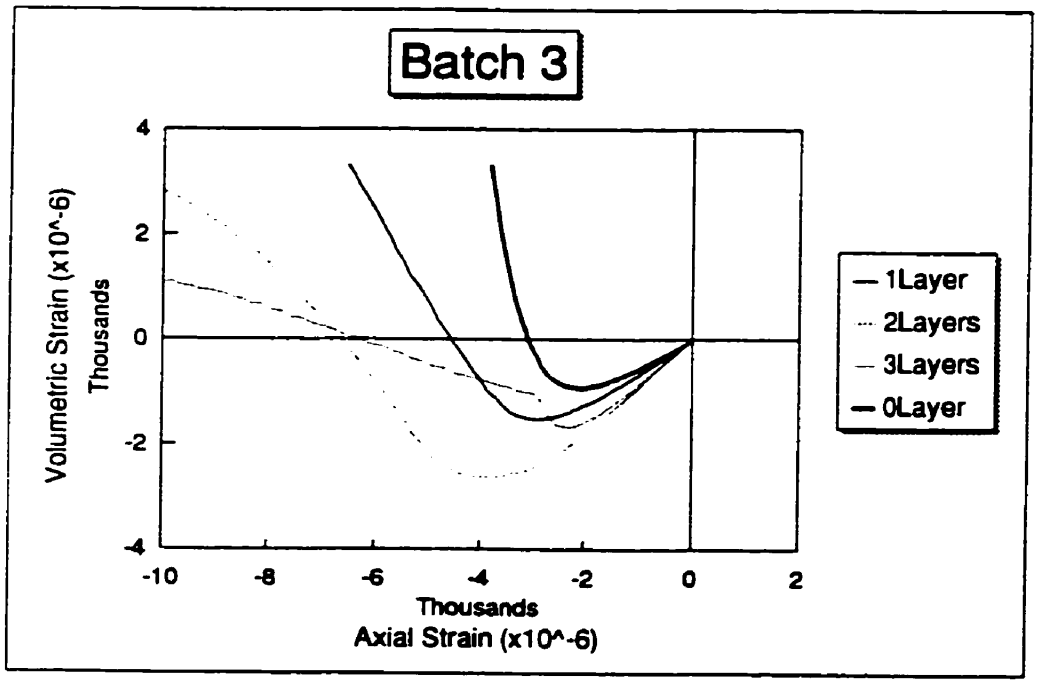

Figure 5-34: Compressive response of wrapped cylinders Batch 3 (2% M)
Top: axial (left) and circumferential (right) strains versus axial stress
Bottom: volumetric strain versus axial strain

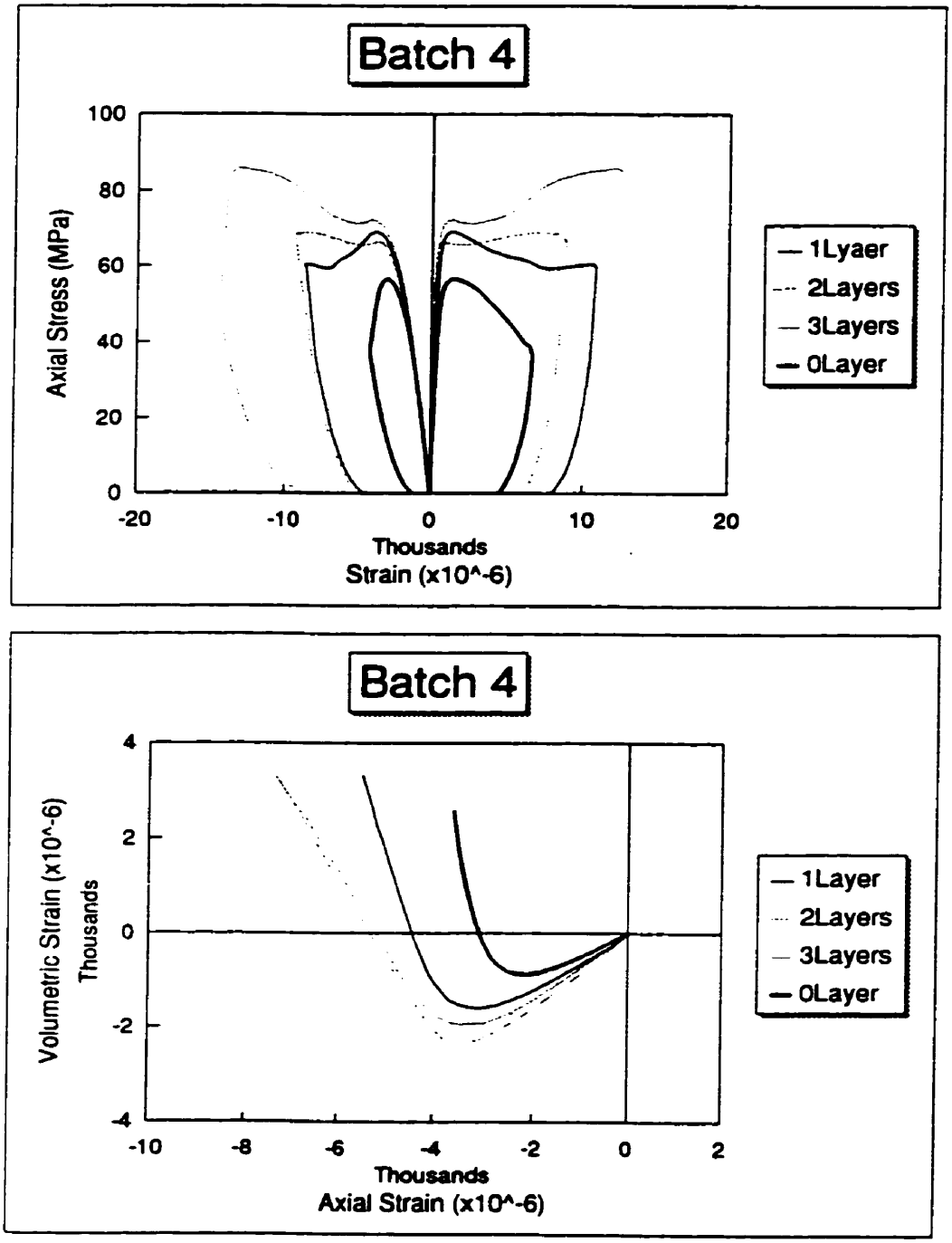

Figure 5-35: Compressive response of wrapped cylinders Batch 4 (1% S+M)
Top: axial (left) and circumferential (right) strains versus axial stress
Bottom: volumetric strain versus axial strain

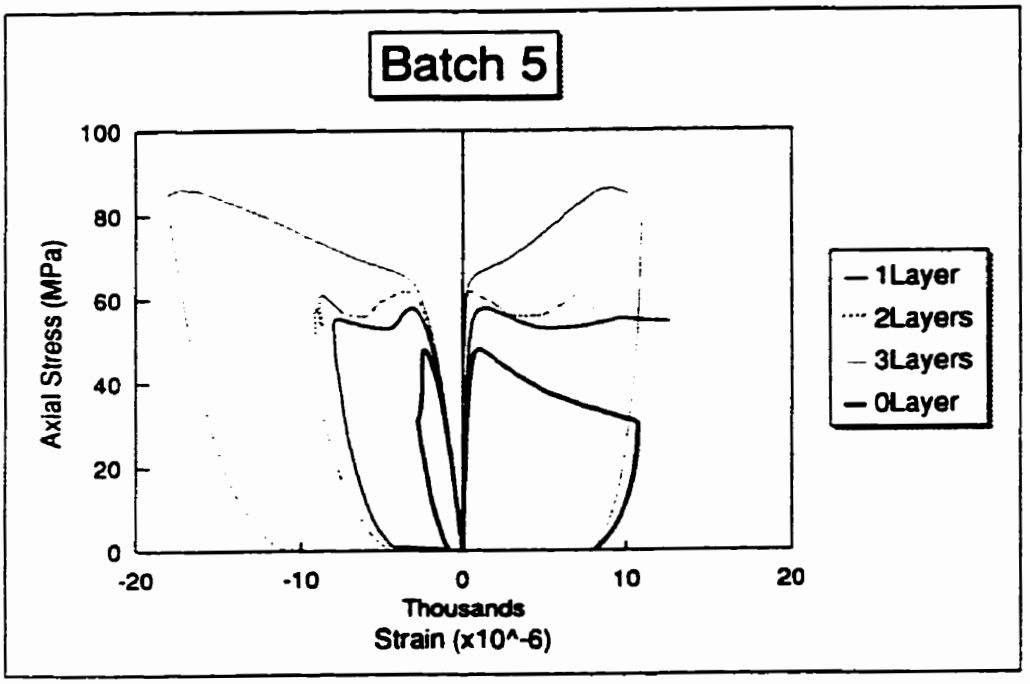

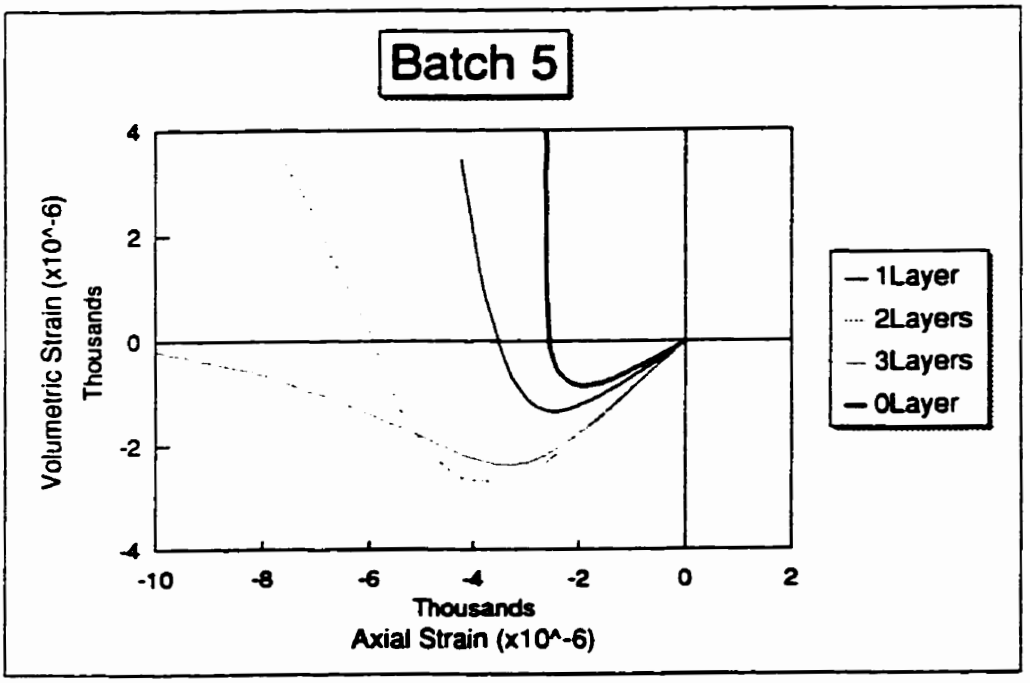

Figure 5-36: Compressive response of wrapped cylinders Batch 5 (2% S+M)
Top: axial (left) and circumferential (right) strains versus axial stress
Bottom: volumetric strain versus axial strain

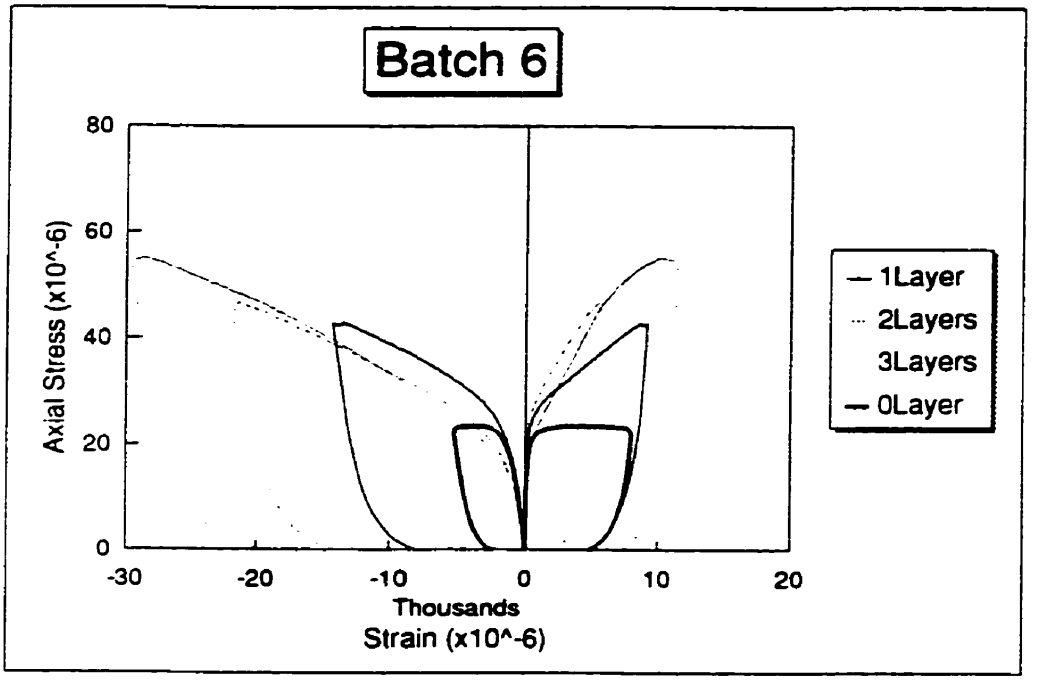

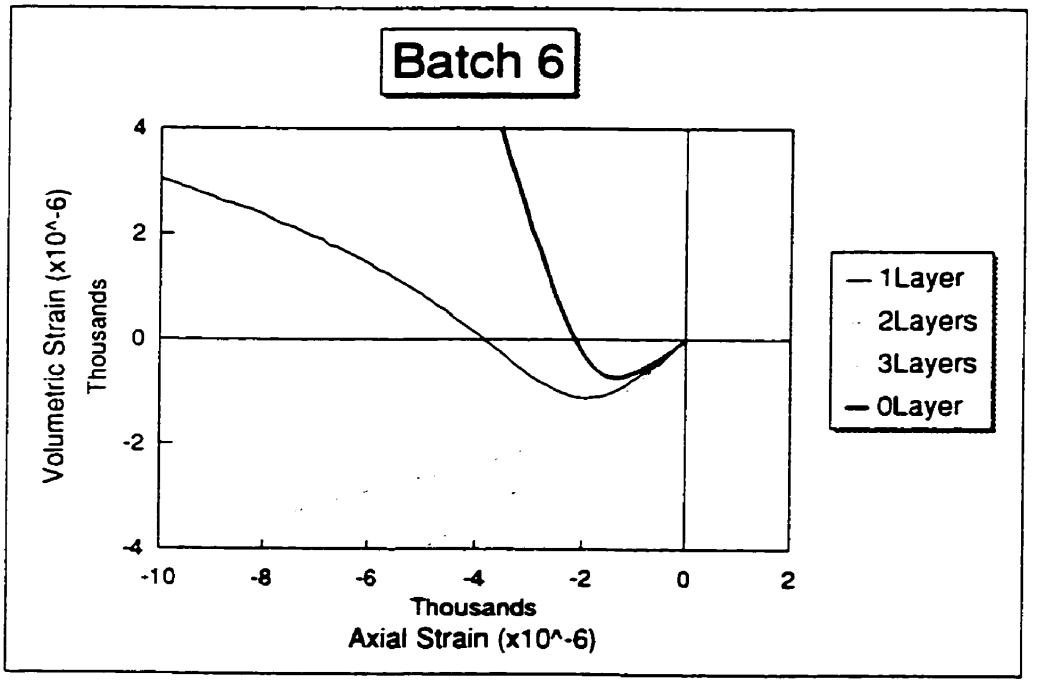

Figure 5-37: Compressive response of wrapped cylinders Batch 6 (4% P)
Top: axial (left) and circumferential (right) strains versus axial stress
Bottom: volumetric strain versus axial strain

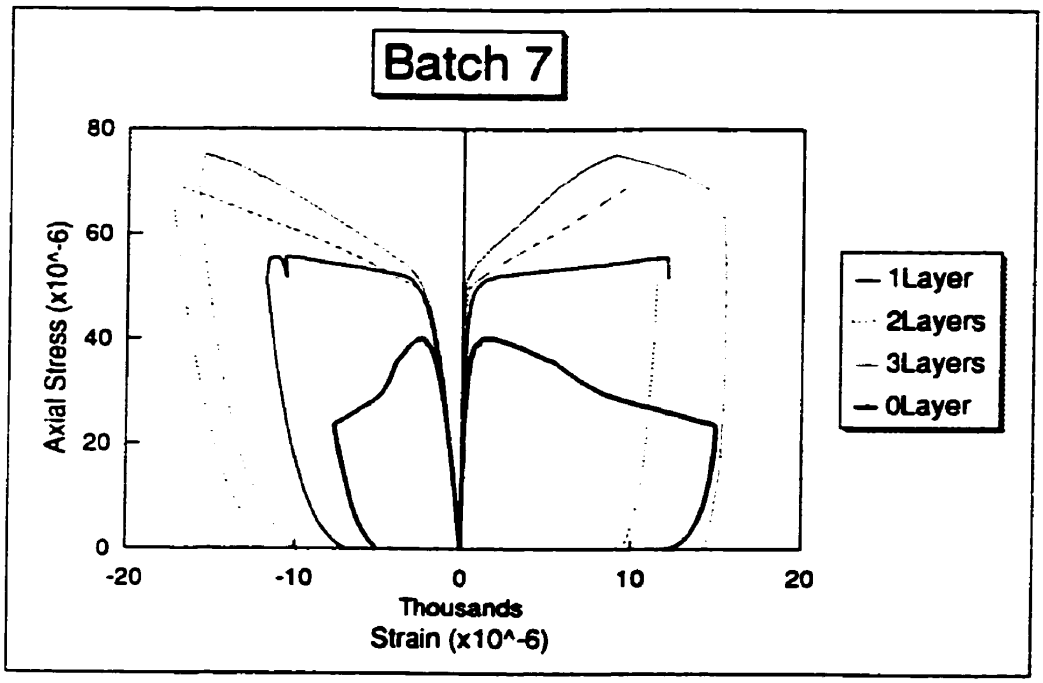

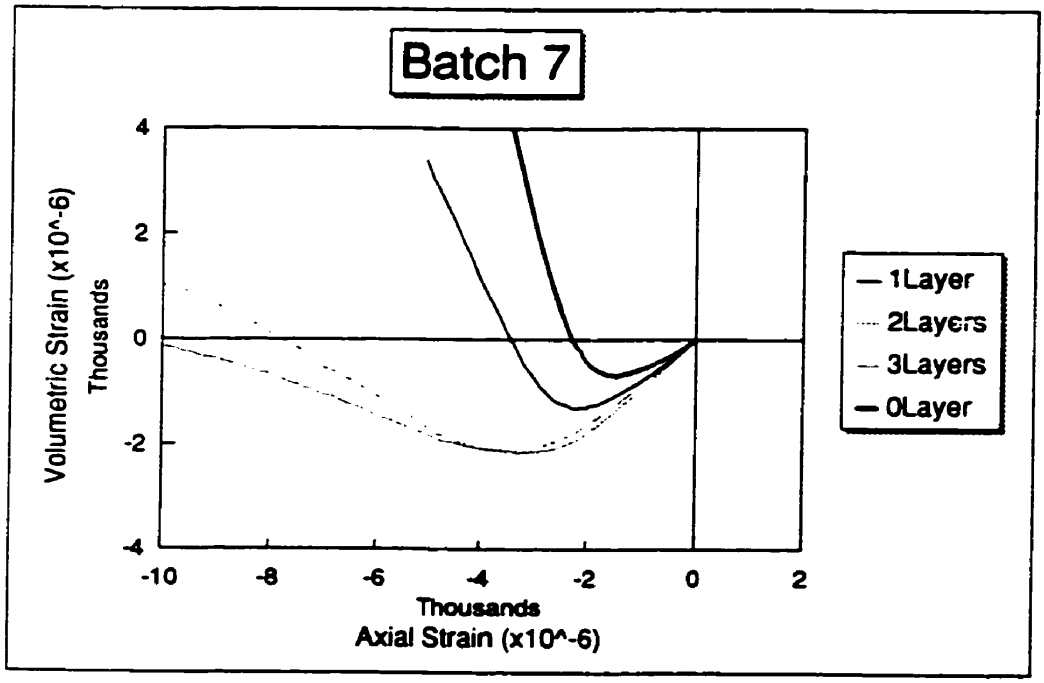

Figure 5-38: Compressive response of wrapped cylinders Batch 7 (2.5% P+M)
Top: axial (left) and circumferential (right) strains versus axial stress
Bottom: volumetric strain versus axial strain

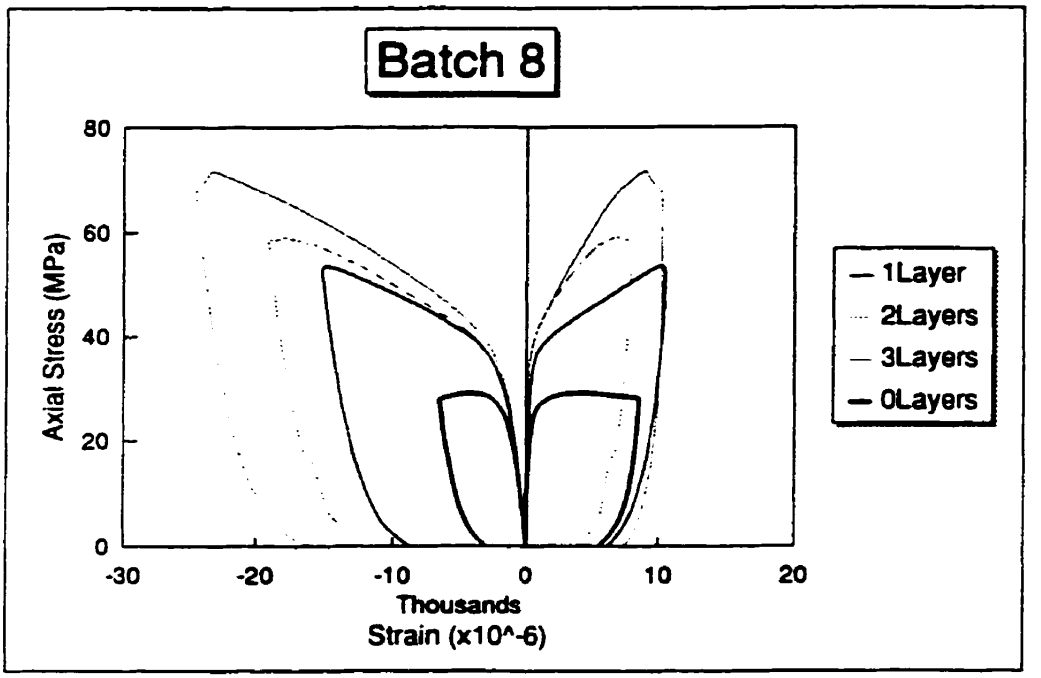

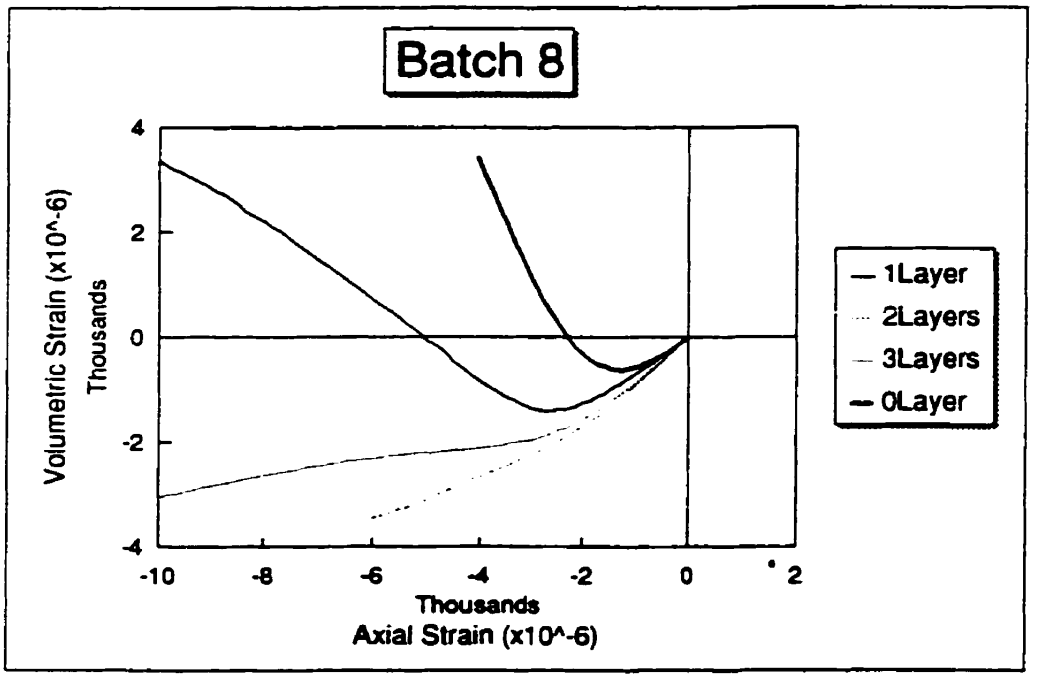

Figure 5-39; Compressive response of wrapped cylinders Batch 8 (5% P+M)
Top: axial (left) and circumferential (right) strains versus axial stress
Bottom: volumetric strain versus axial strain

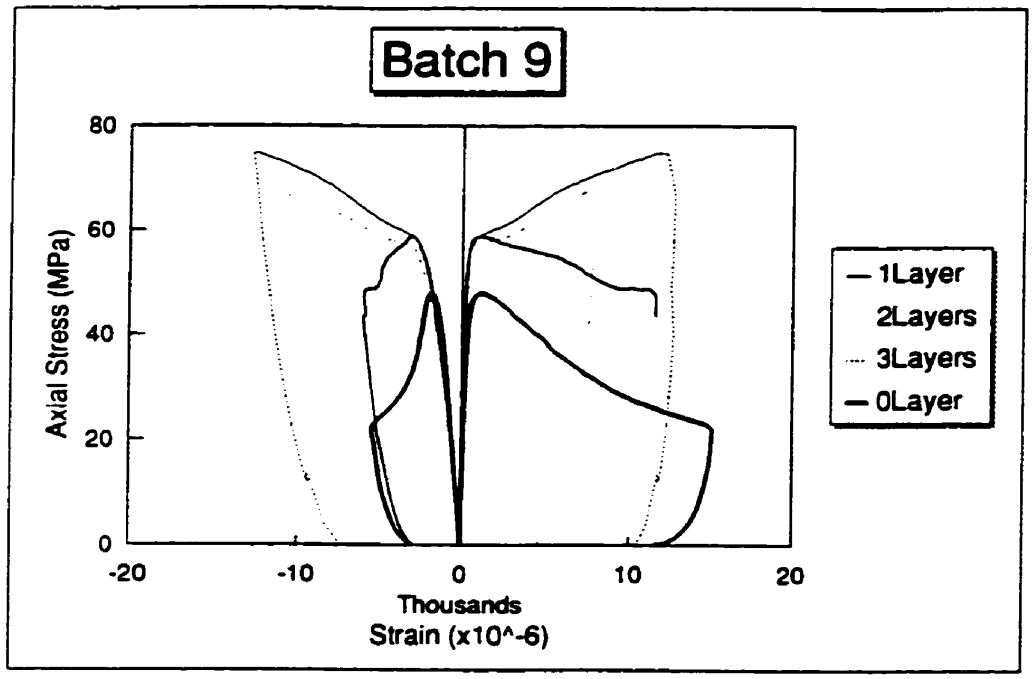

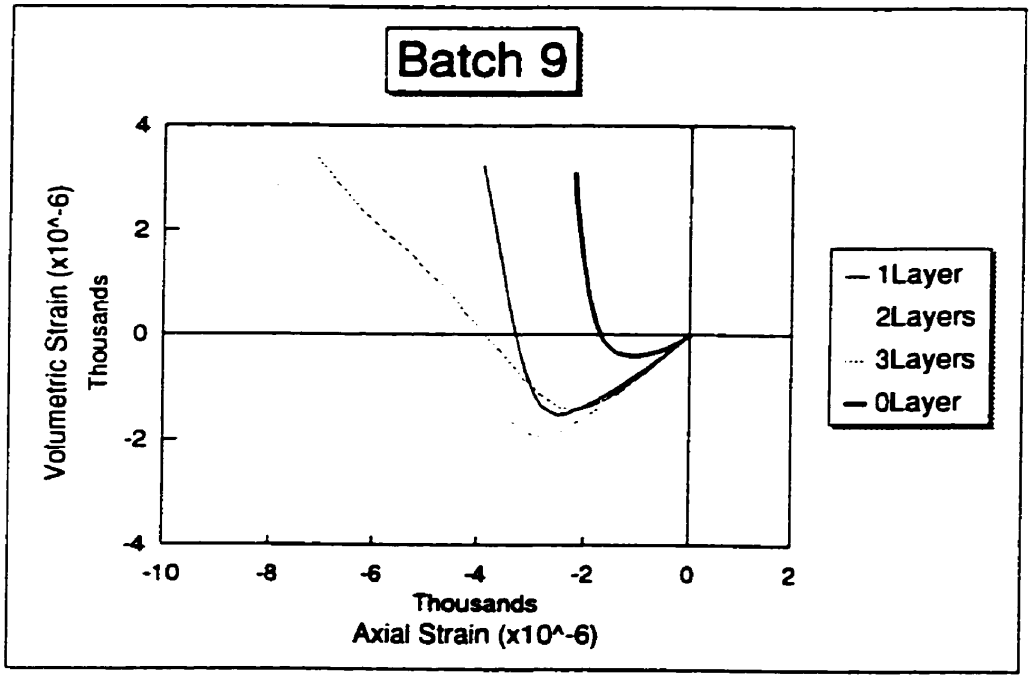

Figure 5-40; Compressive response of wrapped cylinders Batch 9 (1.5% P)
Top: axial (left) and circumferential (right) strains versus axial stress
Bottom: volumetric strain versus axial strain

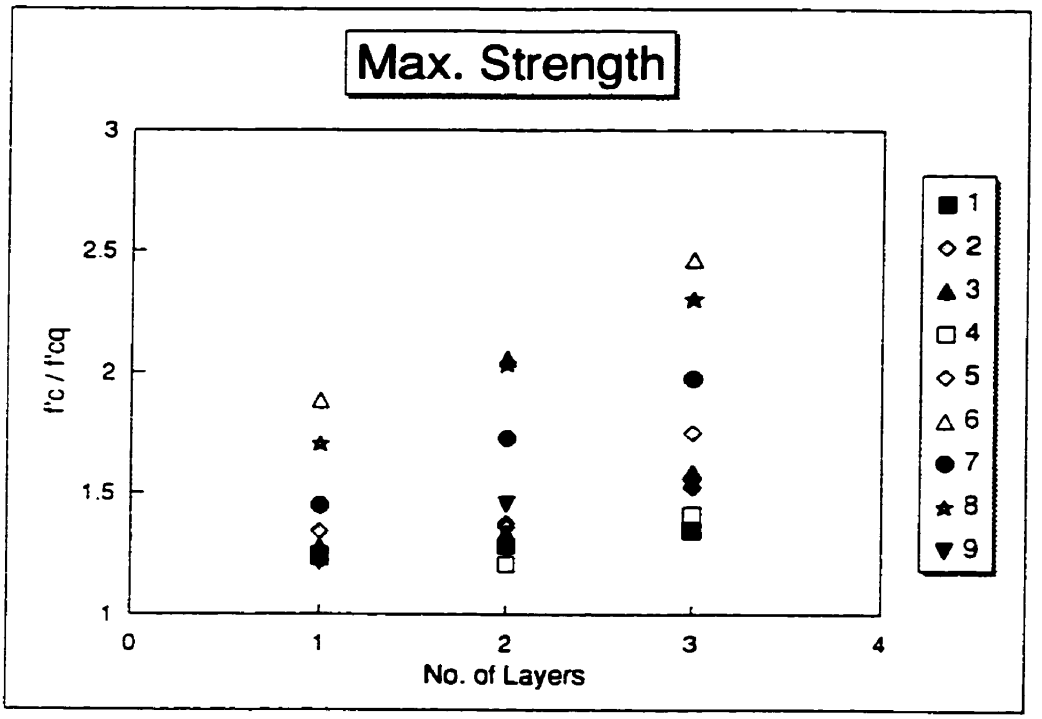

Figure 5-41; Effect of number of layers of wrap on the maximum strength

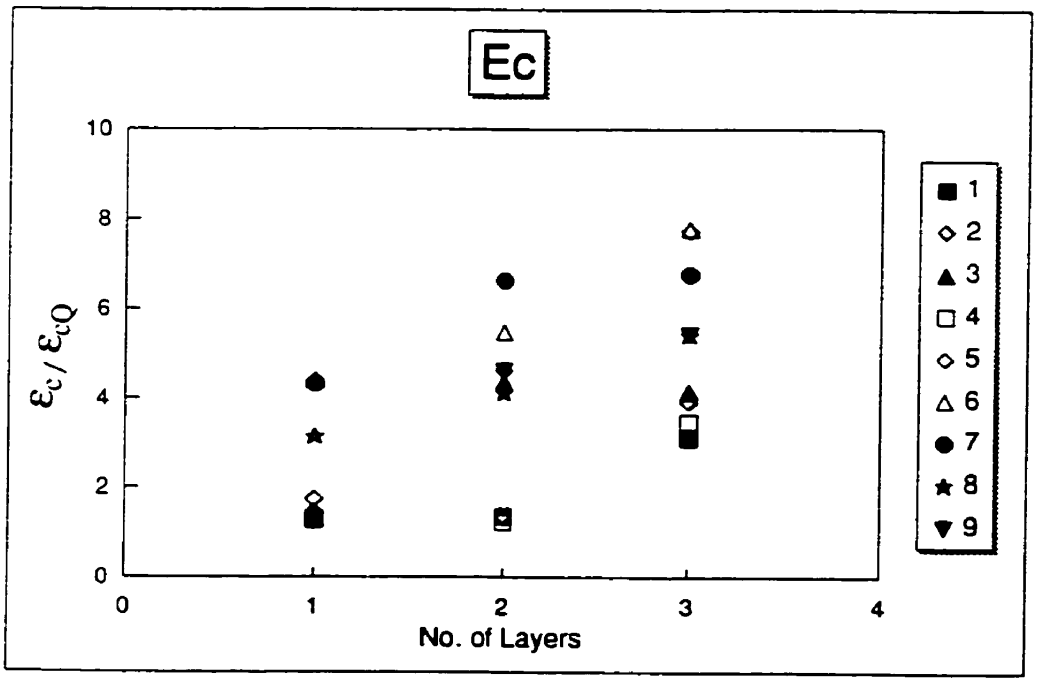

Figure 5-42; Effect of number of layers of wrap on the ε_c

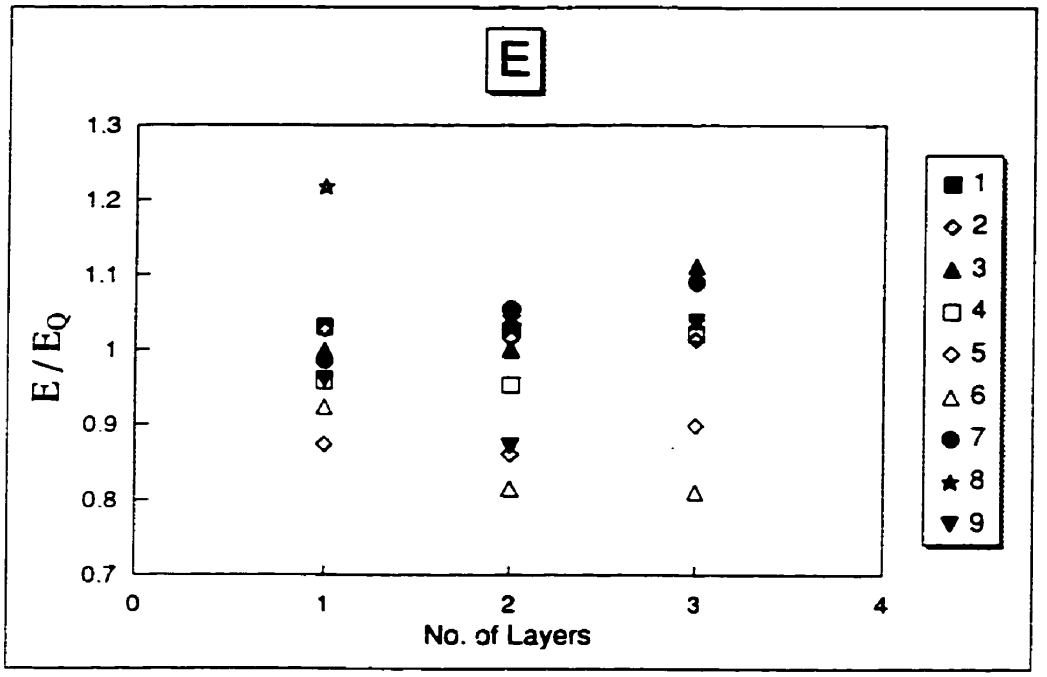

Figure 5-43: Effect of number of layers of wrap on the stiffness

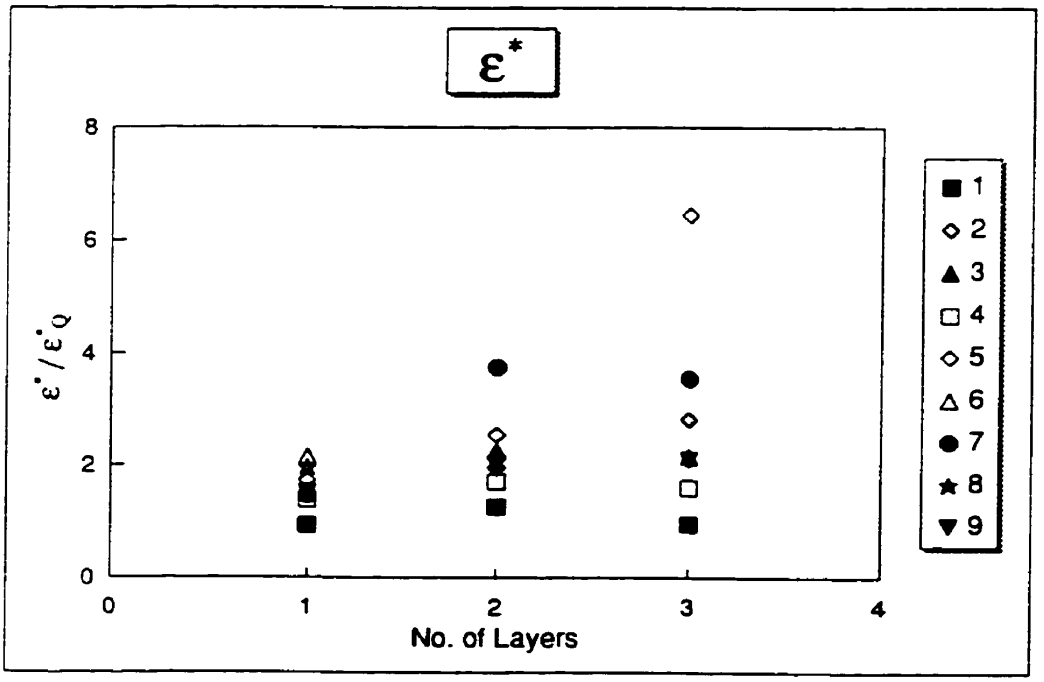

Figure 5-44: Effect of number of layers of wrap on the ε^*

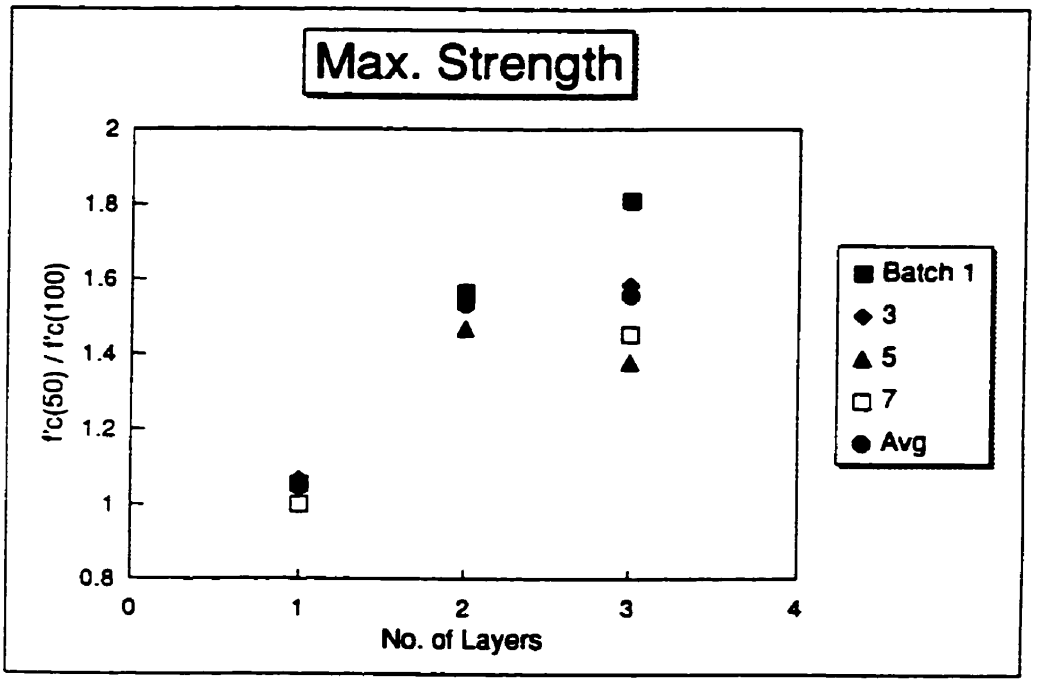

Figure 5-45: Effect of size on the maximum strength of wrapped specimens

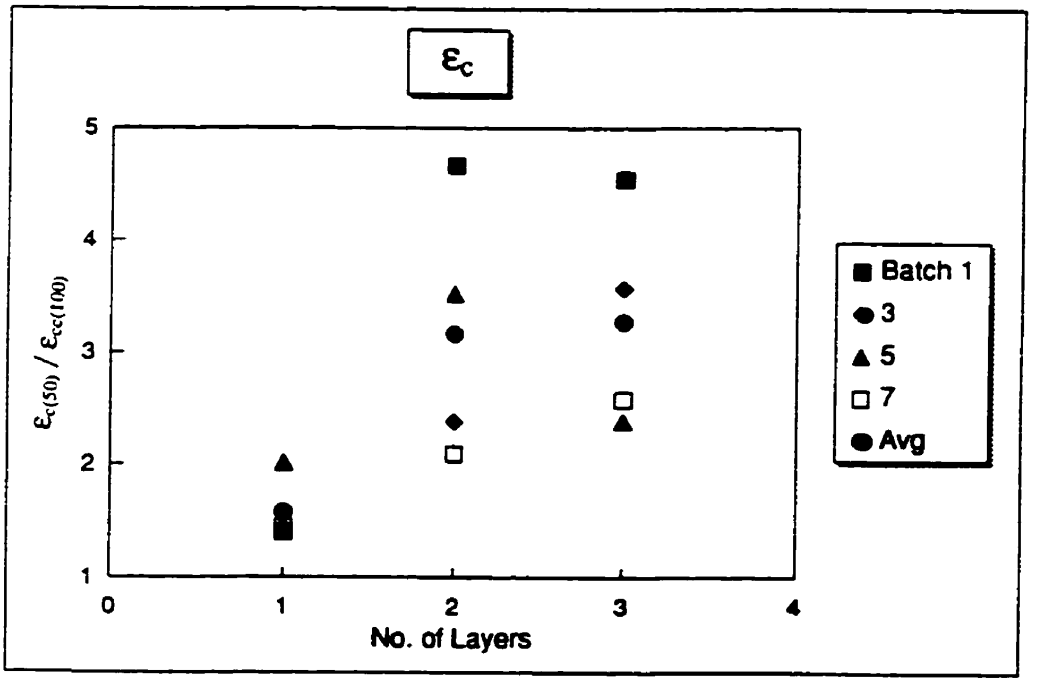

Figure 5-46: Effect of size on the strain at max. strength of wrapped specimens

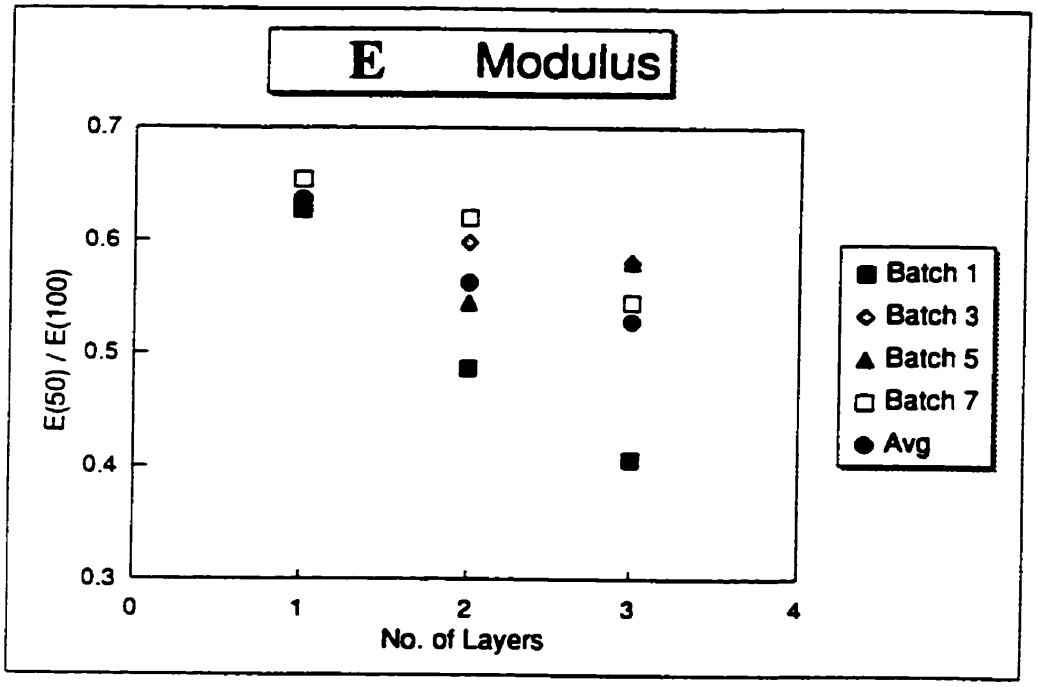

Figure 5-47: Effect of size on the stiffness of wrapped specimens

5.7. Toothpaste Response

The effect of lateral pressure on the behavior of axially unrestrained fiber concrete was a narrow section of this research. Test type J in Table 3-1 is related to this part of the study. From the total of 8 specimens from 4 batches, 4 specimens (one of each batch) were destroyed due to complexity in practically implementing the test. Drawing conclusions based on the remaining samples is difficult, and in a stric statistically sence unjustified.

Figures 5-48 to 5-51 present the responses of the batches under only lateral pressure, and with no simultaneously axial restraint. The top plots show the lateral stress versus axial strain (positive) and circumferential strain (negative), and the bottom plots show axial strain versus volumetric strain. The overall shapes of these plots reveal the following points:

- The shapes of the stress-strain curves are similar to regular stress-strain curves with a sudden breakage.
- The growth rate of ε_1 is greater than ε_3.
- The shape of the axial strain versus volumetric strain is comparable with that of compression tests, only the sign of ε_1 is opposite.
- Addition of fibers do not have considerable influense on these curves.

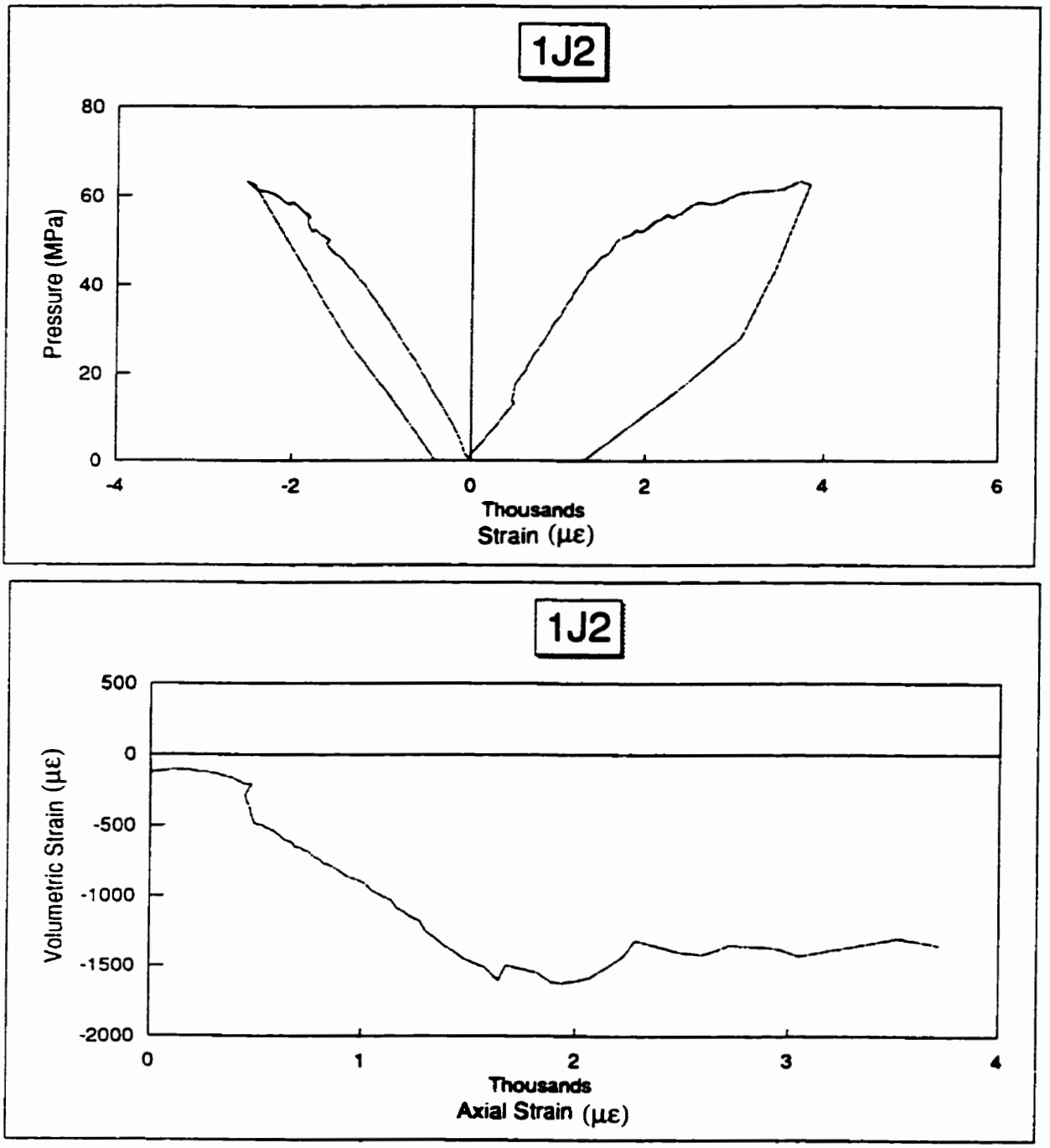

Figure 5-48; Response of specimen subjected to "Toothpaste" test, Batch 1 (plain)
Top: axial (left) and circumferential (right) strains versus axial stress
Bottom: volumetric strain versus axial strain

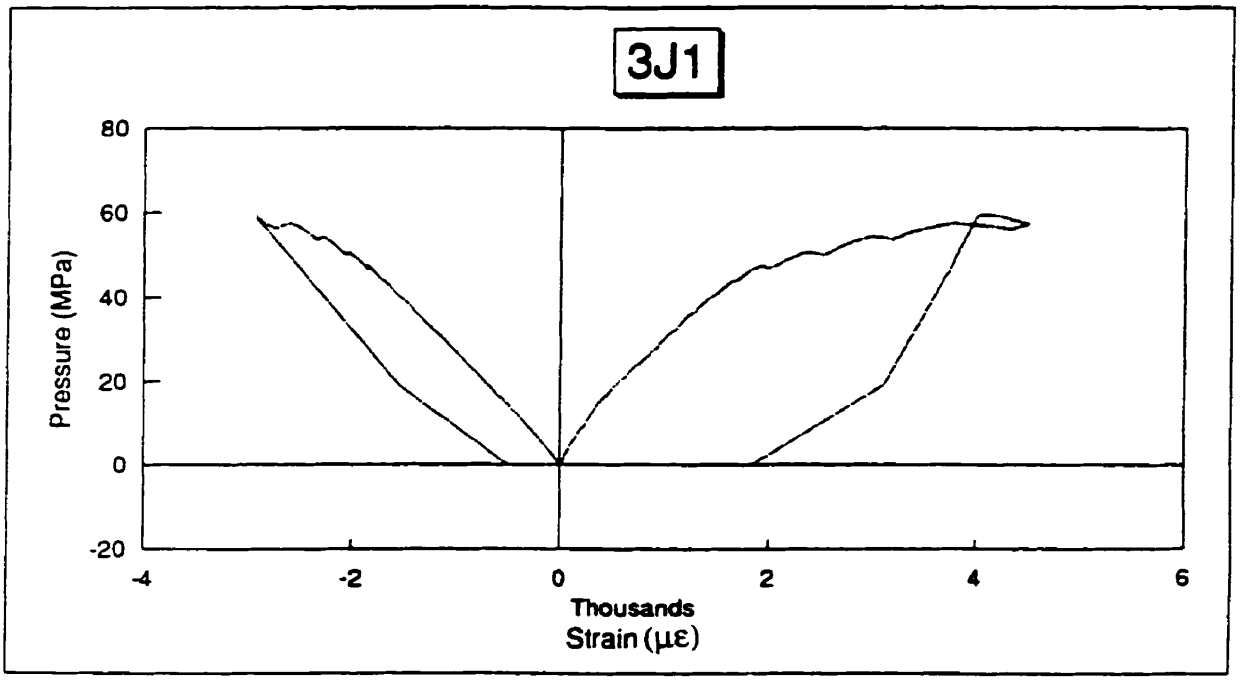

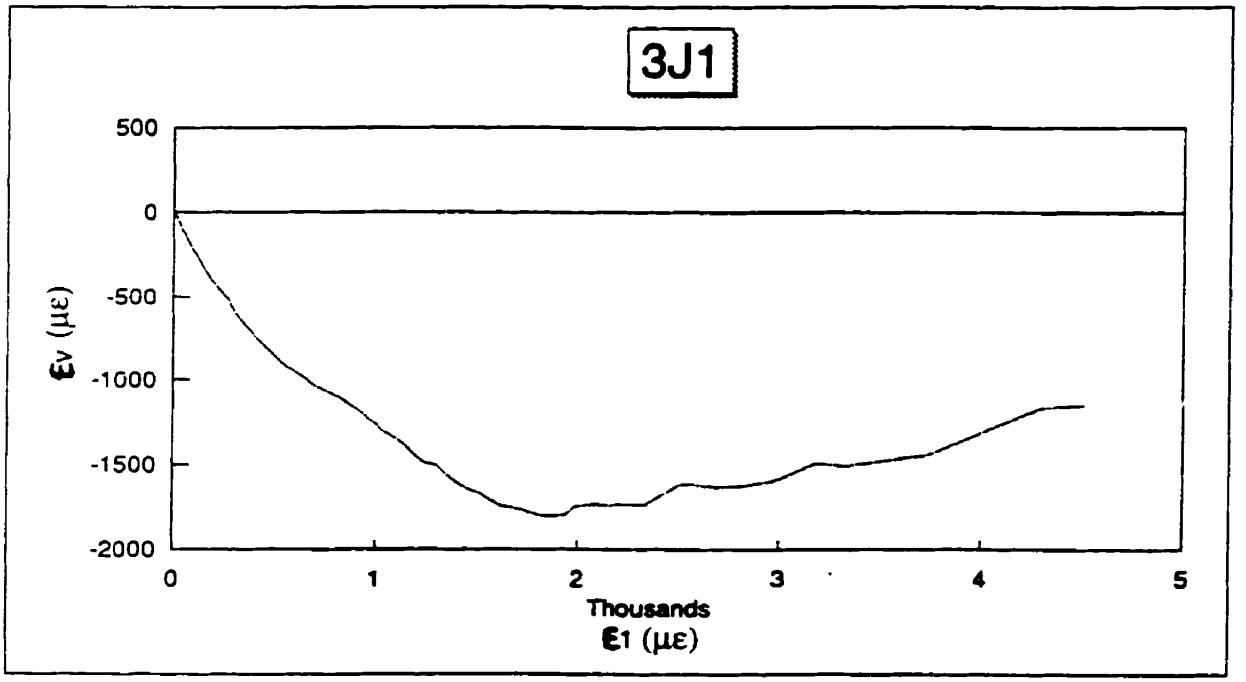

Figure 5-49; Response of specimen subjected to "Toothpaste" test, Batch 3 (2% M)
Top: axial (left) and circumferential (right) strains versus axial stress
Bottom: volumetric strain versus axial strain

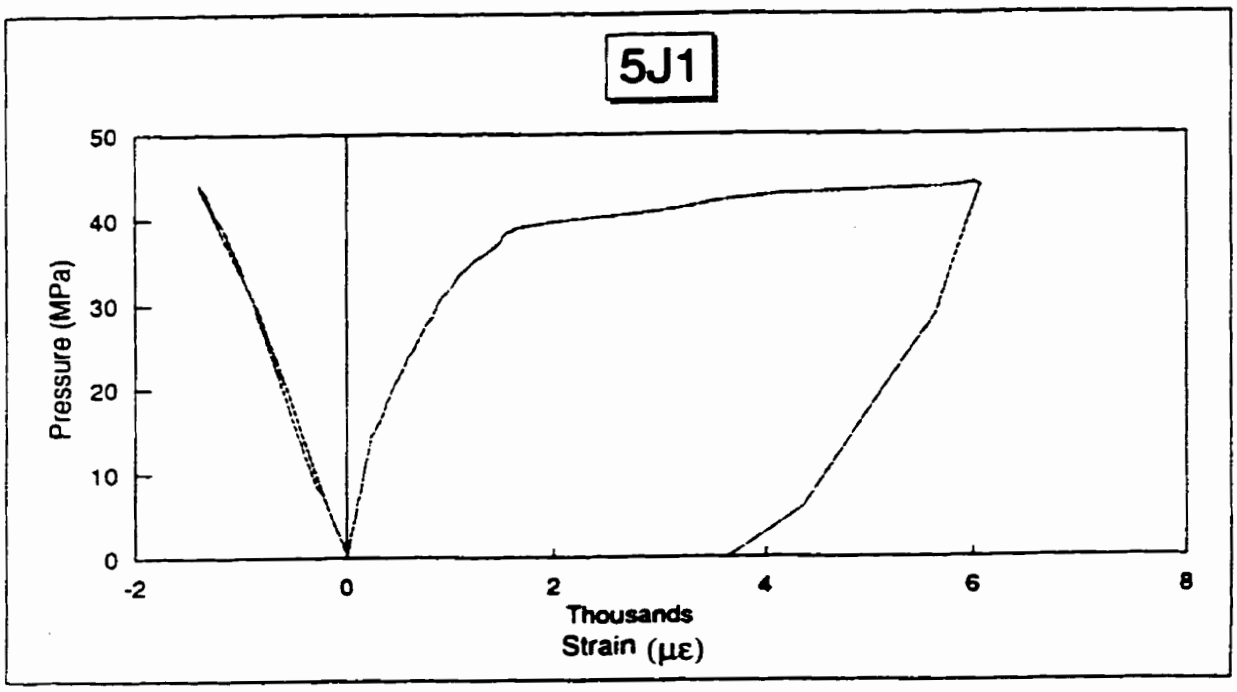

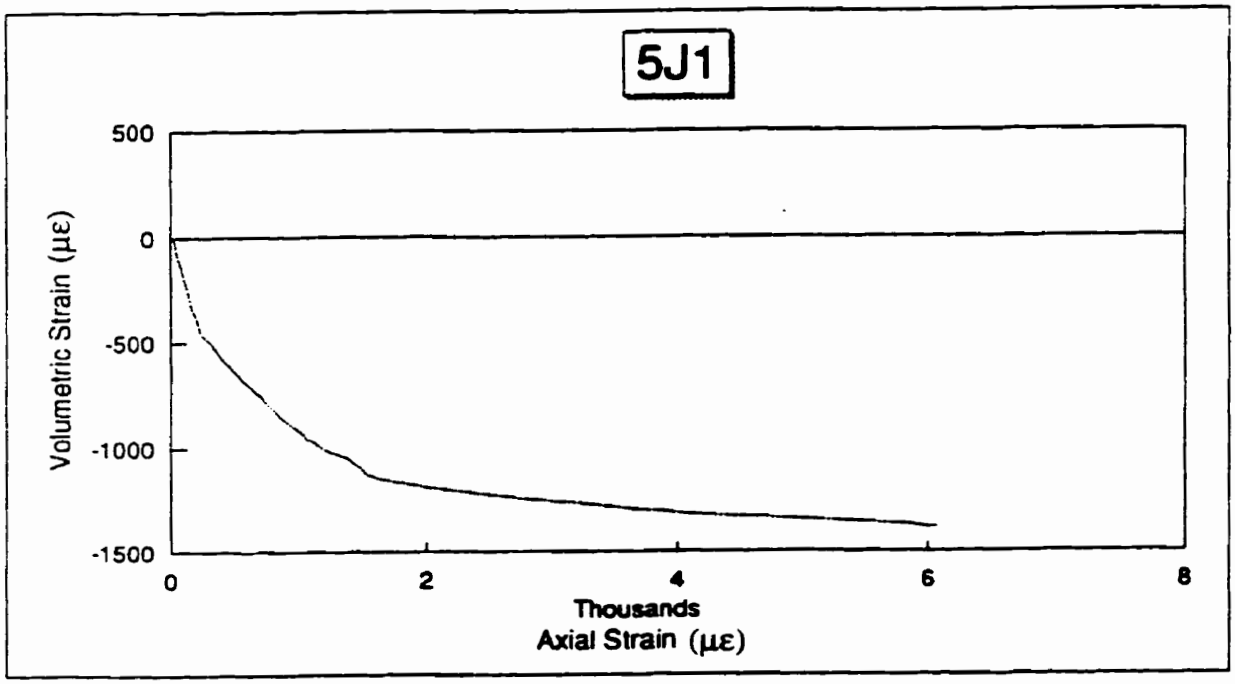

Figure 5-50; Response of specimen subjected to "Toothpaste" test, Batch 5 (2% S+M)
Top: axial (left) and circumferential (right) strains versus axial stress
Bottom: volumetric strain versus axial strain

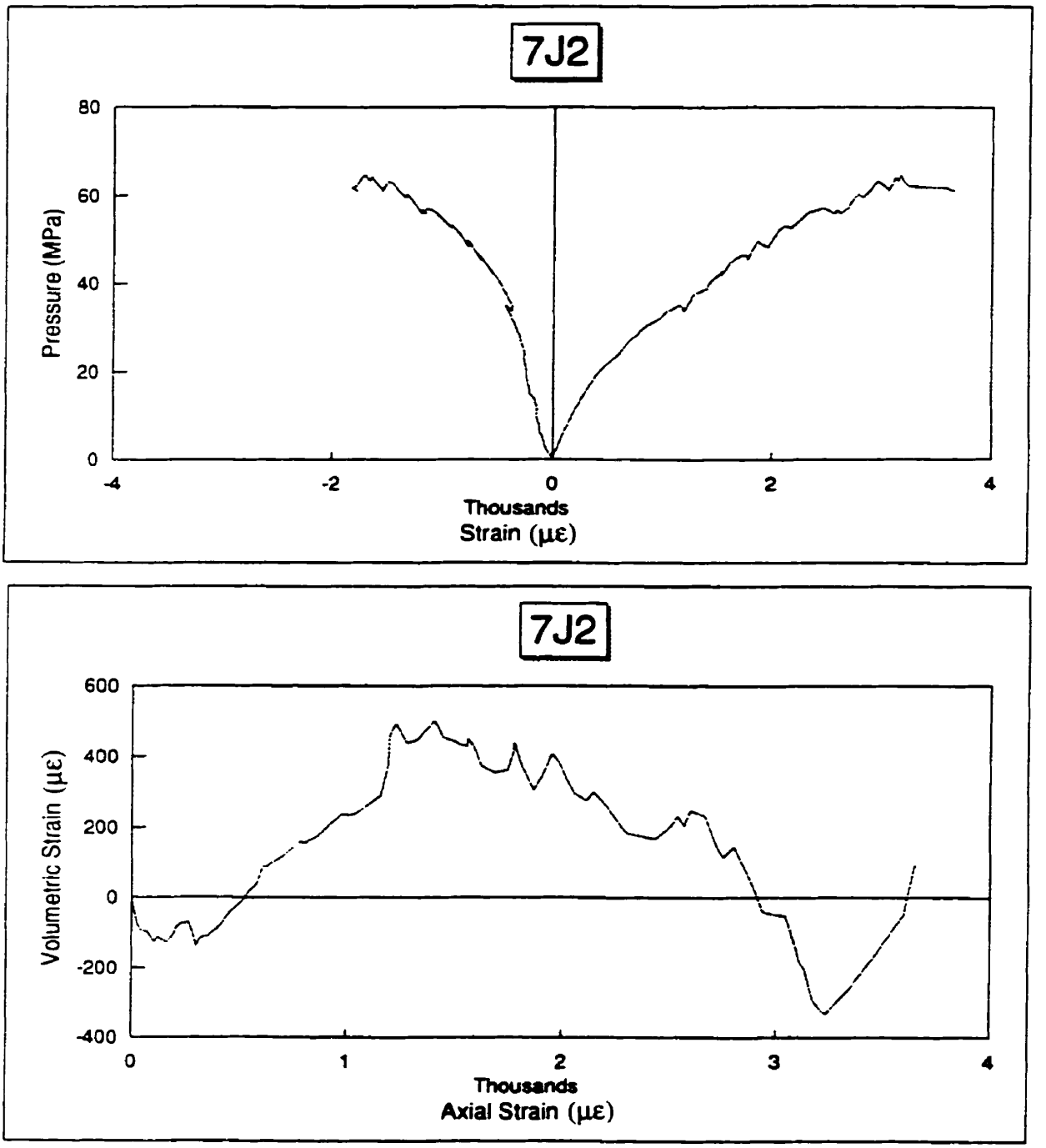

Figure 5-51: Response of specimen subjected to "Toothpaste" test, Batch 7 (2.5% P+M)
Top: axial (left) and circumferential (right) strains versus axial stress
Bottom: volumetric strain versus axial strain

5.8. Bending Behavior

Figure 5-52 presents the load-deflection curves of one representetive specimen from each batch (out of three identical ones). Figure 5-53 plots the modulus of rupture for different batches, and Figure 5-54 shows their means and variations. Addition of steel fibers and steel micro fibers increased the tensile strength of concrete. The strength of concrete with 2% micro-fibers (Batch 3) is the highest. The strength of concrete with 2% of steel and micro fiber mix (Batch 5) is less than that of concrete reinforced with 1% of the same type of fiber mix (Batch 4). The tensile strength of Batch 7, which containes steel micro fibers equal to the volumetric fraction of Batch 2, is equal to that of the plain concrete. Batch 8, which has 2% steel micro-fibers plus polypropylene fibers, exhibit more strength than plain concrete. The batches with only polypropylene fibers (Batch 6 with 4%, and Batch 9 with 1.5%) show equal reduction in strength.

Figure 5-55 presents the tensile strains at peak stress, and Figure 5-56 shows their means and variations. Addition of 1% and 2% (Batches 2 and 3) micro-fibers alone did not cause an increase for this concrete strain. The value of this strain remained unchanged by adding 1% micro and steel fibers (Batch 4), but Batch 5 which had 2% of the same fiber types showed an increase of about 25% in this value. Batch 8 which had highest amount of fibers (5%) exhibited the highest strain at peak stress. This strain for Batch 9 with 1.5% polypropylene is the lowest, but for batch 6 with 4% of this fiber is equal to that of plain concrete. The strength of Batch 7 with 2.5% micro and polypropylene fibers is slightly higher than that of plain concrete.

Various types of fibers exhibit different tensile post peak response (Figure 5-52). The batches with 1% and 2% steel micro-fibers (Batches 2 and 3) had similar failure mode as plain concrete (Batch 1). A crack was formed at the maximum moment region, and propagated immediately, leading to a sudden failure and complete separation of the two parts. The loading deflection curves of other specimens (Batches 4 to 9) had a general post peak form of: a linear drop in load, a hardening part, and a softening or unloading

section. These responses can be explained as follows: the energy which has been stored in the beams at the peak is suddenly released upon formation of a crack in the concrete prism, which causes a rapid unloading (very steep unloading), then the fibers start to pick up the tensile force up to their pull out (breakage for polypropylene nets) resistance which is manifested by the concave curve, and after this point fibers start to release the tensile force leading to the softening part of the curves.

The post-peak response is mainly influenced by the amount of fibers. Batch 9 with 1.5% polypropylene fibers had the highest drop after the peak, where as Batch 6 with 4% of these fibers had the lowest drop and, then, it hardened to a strength more than that of the peak. Batch 7 with 1% micro and 1.5% polypropylene fibers had a drop less than that of Batch 9. Batch 8 with 2% micro and 3% polypropylene had small drop and considerable amount of hardening. The post-peak curve of Batch 5 with 0.8% micro and 1.2% steel fibers (twice of the fibers of Batch 4) is higher than that of Batch 4.

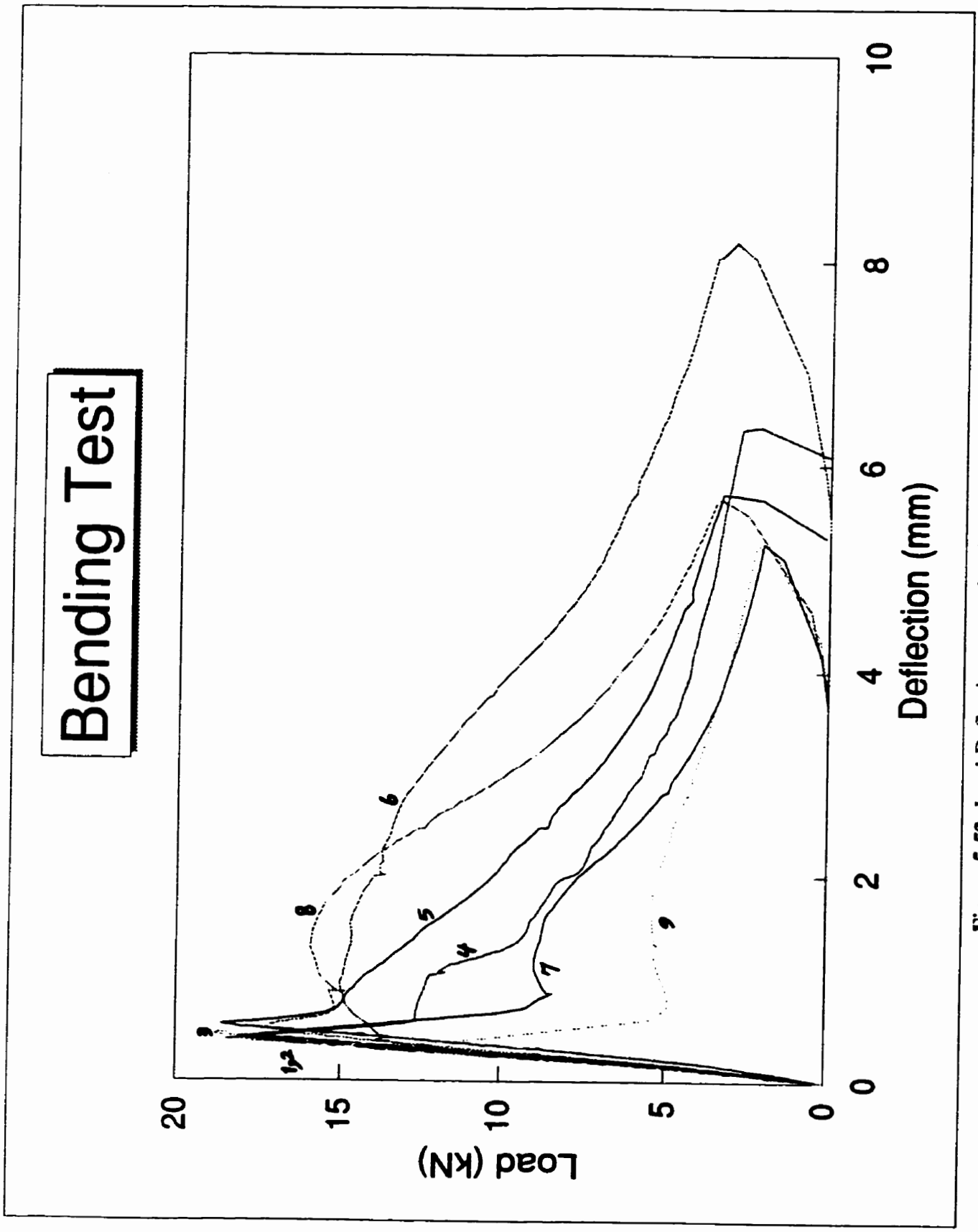

Figure 5-52: Load-Deflection curves for all the batches

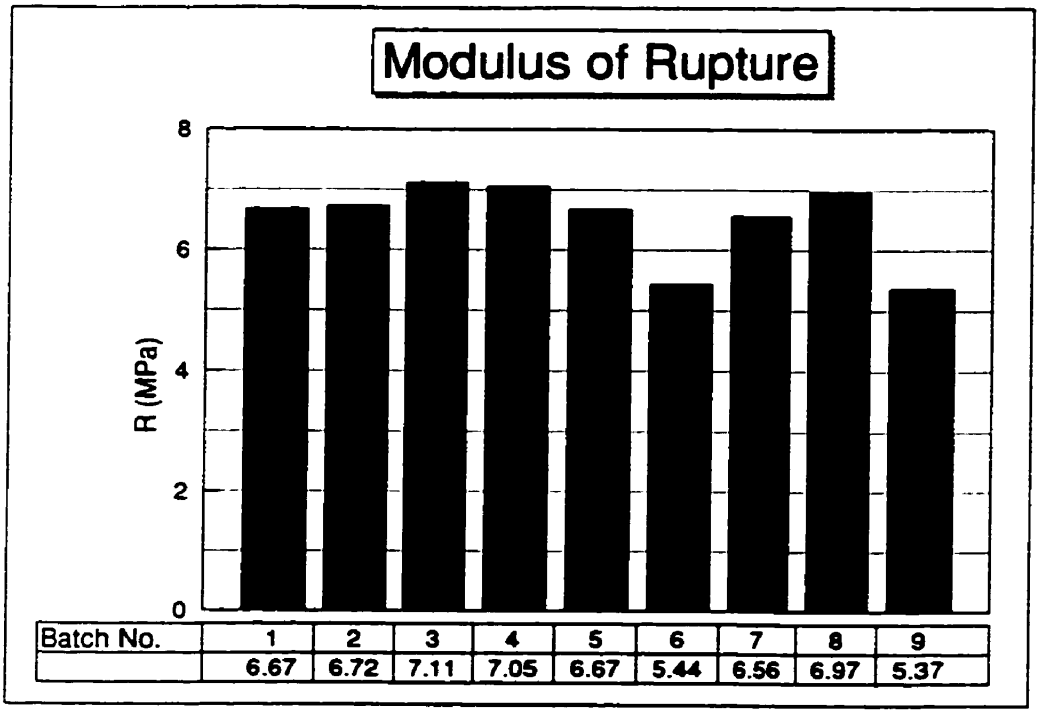

Figure 5-53; Values of Modulus of Rupture for all the batches

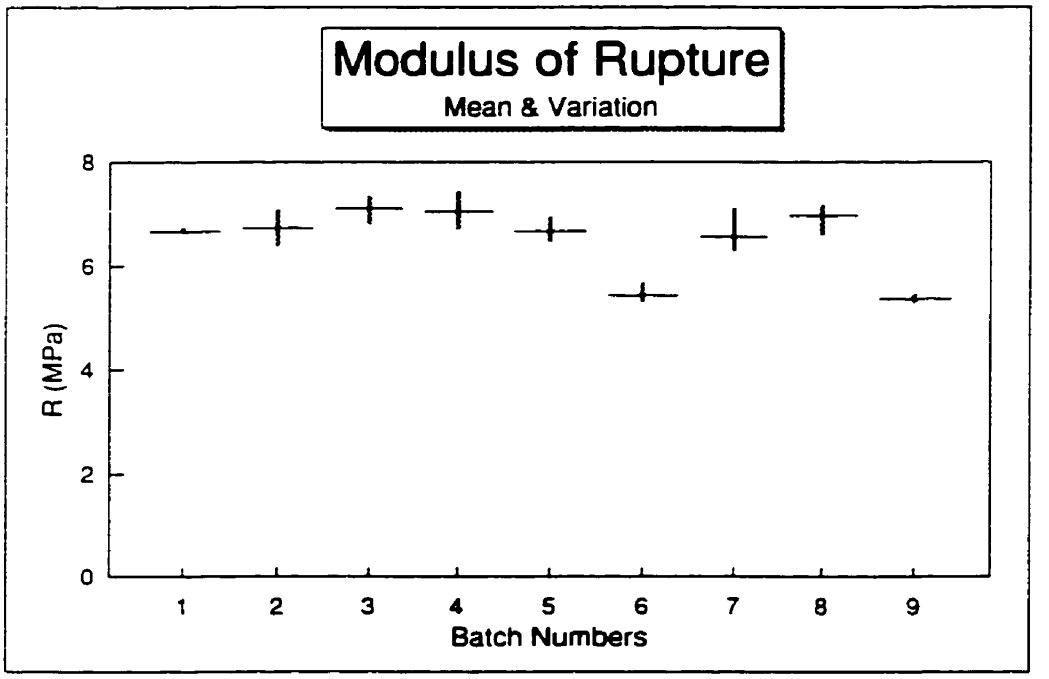

Figure 5-54; Modulus of Rupture; means and variations

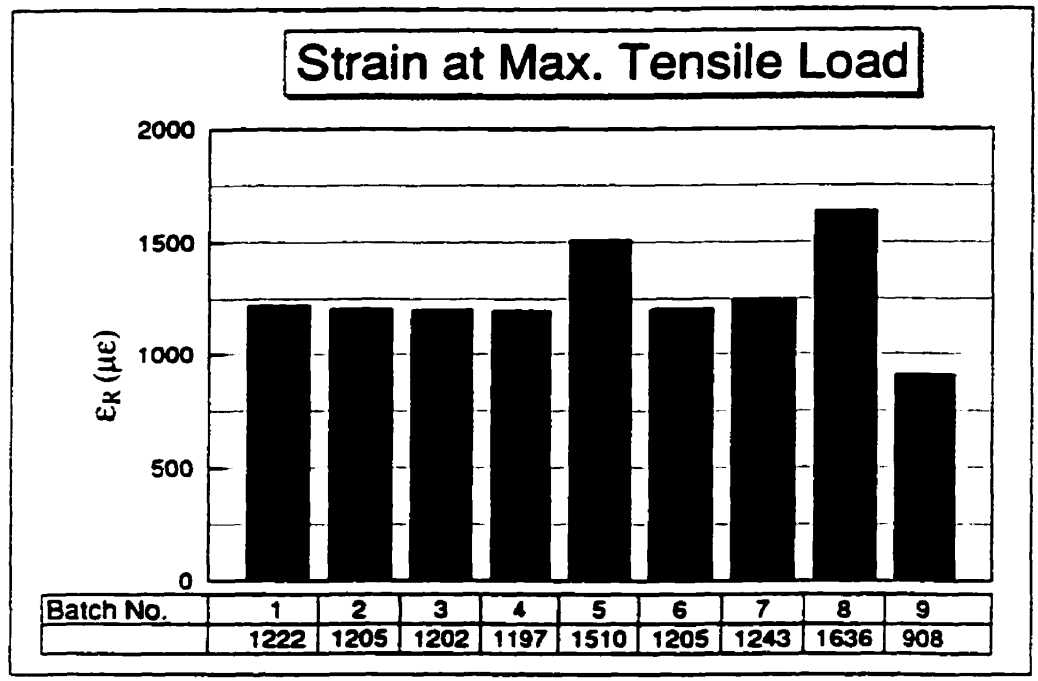

Figure 5-55: Tensile strains at peak loads for the prism test

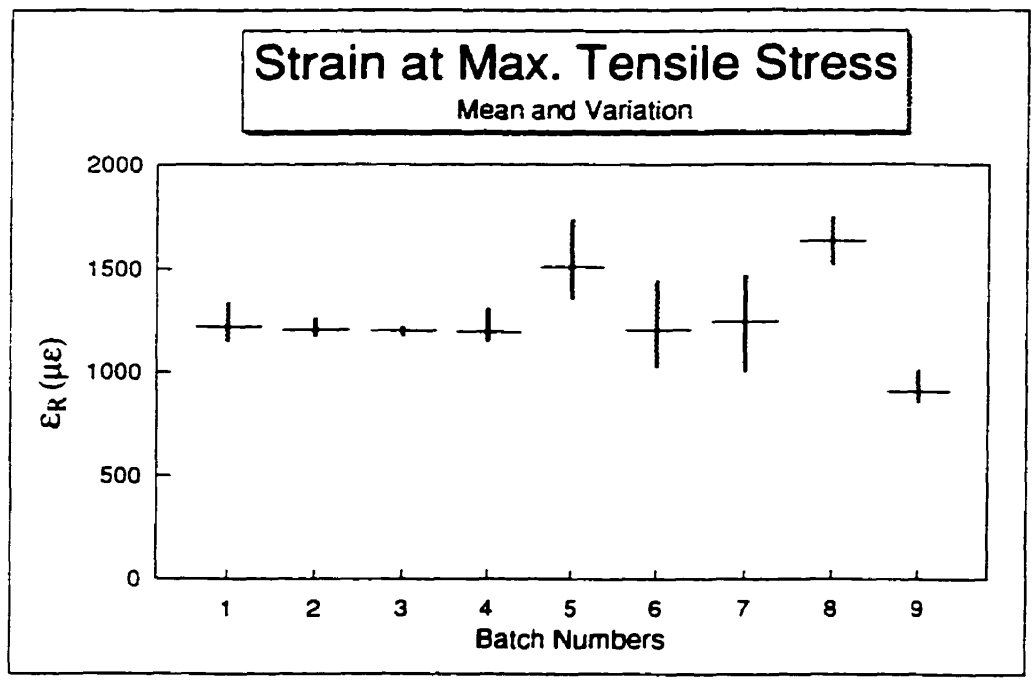

Figure 5-56: Strain at peak load; means and variations

6. Summary and Conclusions

6.1. Experiment Summary

An extensive experimental study on 256 specimens was performed to determine the mechanical properties of fiber concrete under various conditions. A total of 8 fiber concrete batches (Table 3-1), and a plain high strength concrete matrix were examined. The batches contained the same concrete matrix, and these variations of fibers:

- Fiber types; steel micro-fiber, steel fiber, polypropylene fiber
- Fiber content; from 1% to 5% by the total volume
- Combinations of fiber types; micro with steel, and micro with polypropylene with constant ratio of 40% to 60% respectively

The concrete batches were cast into 4 sizes which were required for the various test types of this research:

- 300×150 mm nominal size cylinders
- 200×100 mm nominal size cylinders
- 420×150×80 mm prisms
- 420×420×150 mm blocks; cored samples, with 100×50 mm nominal size, were extracted from these blocks

Each specimen was prepared for the certain test type and the measurement readings associated with the test. A variety of physical conditions were applied to the specimens by these test types (Table 3-1), which are:

- Various sizes; 150, 100 and 50 mm diameter cylinders
- Active confinement; 0%, 20%, 40%, 60% and 80% lateral pressure
- Dry and wet; at 0%, 20%, 40% and 60% confinement
- Passive confinement; 1, 2 and 3 layers of carbon fiber wrap
- Variation of size in passive confinement; 100 mm and 50 mm diameter cylinders

- Lateral pressure only; 100×50 mm cylinders subjected to toothpaste like squeeze
- Bending; loading the prisms in bending

The experiment produced an extensive database to study the mechanical properties of fiber reinforced concrete. In addition, a number of articles, which were concerned with various aspects of this study, have been reviewed. The literature review was of great importance in providing guidance to conduct this experimental study, and draw the conclusions.

6.2. Conclusions

Addition of fibers to concrete alters its mechanical properties, and enhances its tensile strength. This experimental study showed that behavior of FRC is depended on the interaction of fibers with the concrete matrix, the reaction of pores, and imposed boundary conditions. The imposed boundary conditions, which can be provided by either active or passive confinement, lead to different responses. The effects of these variations have been quantified through a large number of tests.

6.2.1. Effects of Fiber Type and Content

The fibers which were used in this study consisted of different shapes and materials. The fibers were made of steel with high modulus of elasticity and polypropylene with low modulus of elasticity. The steel micro-fibers were straight and rounded, and the steel fibers were rounded with anchored ends. The polypropylene fibers were collated fibers which formed a net after opening in the mix, and in the case of high fiber fraction these nets could attach to each other and form a network. The bond adhesion of this network to the matrix is low, hence, concrete with high fraction of polypropylene fibers demonstrates different response than typical fiber concrete. The

shape and modulus of elasticity of fibers determined the level of tensile force which could be developed in them.

6.2.1.1. Air Content

Addition of fibers to concrete increases its porosity. The walls of fibers prevent the natural compaction of concrete grains, and trap air pockets. Low workability (flow ability) increases the air content, additionally. The impurities mixed with fibers can react with cement and generate gases which results in more porosity. Therefore, increase in fiber volume fraction raises the amount of air content of FRC. The polypropylene fibers had the lowest workability and steel micro-fibers contained some impurities.

6.2.1.2. Strength

Adding fibers to concrete improves some of its mechanical properties. The main role of fibers in concrete is crack arresting, which distributes the internal deformations over a greater region of concrete. This action causes improvement in tensile strength and ductility of concrete member. Besides, the mechanical properties of the fiber itself contributes to the overall response of fiber concrete structure. Thus the behavior of fiber reinforced concrete differs from that of plain concrete. The extend of this variation depends on the fiber material, fiber fraction, and its interaction with the matrix. The latter issue relates to the shape and aspect ratio (length/thickness) of the fiber. On the other hand, it was stated that addition of fibers increases the air content in concrete which weakens the concrete internal structure.

Addition of small amount of fibers (up to 1%) with high modulus of elasticity (steel) does not influence the compressive strength of concrete, but higher amount of these fibers (2%) results in a reduction in the strength due to the increase in air content (wall effect). Adding fibers with low modulus of elasticity (polypropylene) to concrete

decreases its strength, and this decrease relates to the amount of fibers. For concrete with 4% polypropylene fibers, the compressive strength drops to half.

The bending tests on the specimens revealed that addition of high modulus of elasticity fibers increased the modulus of rupture slightly, but addition of fibers with low modulus of elasticity causes a decrease by 20%. When a specimen is loaded in bending, tensile strains develop in the tension zone of the beam. Therefore, the fibers with higher modulus of elasticity than concrete pick up more stress which increases the overall tensile strength of concrete, whereas fibers with low elasticity pick up less stress than concrete which leads to less overall strength.

6.2.1.3. Axial Strain at Peak Strength

High percentage of polypropylene fibers increases ε_c considerably (by 25%), but low percentage of them demonstrate reduction in this value (about 10%). In concrete with high content of these fibers, the dense fiber network dominates the overall response of the specimen, whereas in concrete with low content of these fibers the individual fiber nets (with low modulus of elasticity) allow lateral expansion which leads to early onset of severe damage and lower ε_c. For steel fibers the effects on ε_c are opposite with narrower range of variation, since their high modulus of elasticity attribute to restriction of lateral expansion and a higher fiber fraction applies higher restriction. This strain is higher for steel fibers due to the additional restriction imposed by anchored ends. However, increase in fiber volume is associated with increase in air content and weakening of the internal structure.

Addition of low fraction of fibers with high modulus of elasticity does not change the strain corresponding to the maximum tensile strength (modulus of rupture), whereas addition of low fraction of fibers with low elasticity reduces the value of this strain by 25%. Addition of high fraction of steel fibers increased this strain due to the anchored

ends of these fibers. High percentage of polypropylene fibers had ε_R equal to that of plain concrete due to the dense network system of the fibers.

6.2.1.4. Elastic Modulus

Except for low percentage of micro fibers which shows slight increase, addition of fibers decreases the modulus of elasticity. The steel micro fibers are distributed more evenly in the matrix, hence they have better control over the structure of pores. High fraction of this fibers creates more porosity which has adverse effect and lowers the value of E. The space between steel fibers is wider and they have less control over the structure of pores, hence steel fiber concrete exhibits smaller apparent stiffness. However, increase of these fibers (which has high modulus of elasticity) increases the overall E of the specimen.

The value of E is higher for low fraction of low elasticity fibers than that of concrete with steel and micro fibers, since they do not create air content as much as micro-fibers do. However, increase in these fibers decreases the E value rapidly. This value for concrete with 4% polypropylene fibers is about 75% of that of plain concrete.

6.2.1.5. Poisson's Ratio (ν)

The fibers decrease the value of Poisson's ratio dramatically, since they restrict the movement of particles in the material. However, this value for the batch with high content polypropylene is slightly higher, since the dense network that these fibers formed controlled overwhelmingly the response of the specimens. Increase in micro-fibers decreases the ν value since they stiffen the micro-structure by bridging the pores. Low percentage of steel fibers decreases the Poisson's ratio more than micro-fibers since their longer length allow them to even bridge over large size pores. However, higher amount of these fibers causes an increase in the apparent ν value, which may be explained by the "wall effect". Steel fibers have wider walls compared with steel micro-fibers which results

in less compaction of concrete. Increase in the fraction of polypropylene fibers raises the v value. For high fiber volume fraction, response of the concrete is dominated by the properties of the resulting fiber-network.

6.2.1.6. Strain at Zero Volumetric Strain (ε^*)

The values of ε^* are higher for concretes with fibers having a high modulus of elasticity (micro and steel) than those of batches with low elasticity fibers. Fibers with high modulus of elasticity restrict the lateral expansion of specimens, whereas fibers with low modulus of elasticity are not able to apply this restriction. Steel fibers are more effective than micro-steel fibers in increasing the value of ε^*, since they bridge larger size pores and cracks, due to their longer length and anchored ends. Increase in the amount of fibers with low modulus of elasticity decreases the value of ε^*, since they do not contribute additional restriction over lateral expansion, but nevertheless they cause a more porous structure (larger size pores) due to the low workability of those concrete mixes.

6.2.1.7. Post-Peak Response

In compression, the failure of plain concrete (particularly HSC) is associated with extensive opening of macro cracks and crushing into pieces. Fibers, at failure, act as bridges along the crack width, and hold pieces of material attached. Therefore, they can attribute post-peak response to concrete. The extension of post-peak curve depends on type of fibers and their volume ratio. The softening rate, in the post peak region, is the lowest for polypropylene fibers, is higher for steel fibers, and is even higher for steel micro-fibers. It should be noted that the shape of the fibers have important role in this response, since it determines the amount of tensile force that they can develop.

After failure, fibers pick up tensile force up to the limit of their pull out force capacity. This tensile capacity depends on the aspect ratio and shape of the fibers. The anchorage of steel fibers allowed them to develop more tensile stress before pulling out of

the matrix, whereas the network system of polypropylene fibers caused the fibers to accommodate all the deformation within the test ranges without any pull out. Perhaps, if the deformation in the tests was extended even further, this type of polypropylene fibers would fail in fracture rather than pulling out. It is important that based on the stored energy in the fibers (depending on their tensile capacity) the failed FRC can recover its initial shape to some extend. The end part of the curves in Figures 5-1 and 5-52, which relate to removing the load from the specimens, indicates that FRC with polypropylene fibers can recover more deformation. Therefore, after removing the load, the cracks on these specimens partially close back, and they are less visible on the failed samples (Figures 4-6, 4-22, 4-23, and 4-27).

In bending (indirect tension), a rapid drop was observed in load-deflection curves after the peak. The energy which was stored in the FRC beams was released upon formation of a major crack in the matrix. This swift release of energy caused a sudden damage (crack opening) in the material. Micro-fibers did not exhibit any post-peak response, since they are not able to bridge over macro-cracks, due to their short length. In general, increase in fiber amount lessens the drop on the load-deflection curves. Concretes with steel fibers exhibited smaller strength loss than concrete with polypropylene fibers, due to their higher modulus of elasticity.

After the rapid drop in load, the fibers began to pick up more tensile force and increase the loading capacity of the beams. Polypropylene fibers were more effective in this increase, due to their net shape. In case of the high fraction of this fiber type, the curve could reach to a peak higher than the first peak, due to the network system of the fibers. High fraction of steel and polypropylene fibers smoothens the post-peak curve, and for high fraction of steel fibers the second rise in the loading-deflection curve is hardly visible.

After the second rise in the load-deflection of FRC beams, load drops gradually. The slope of this part is steeper for high fiber content specimens. In addition,

polypropylene fibers exhibit lower rate of unloading, due to their lower modulus of elasticity.

6.2.2. Wrapping Effects

The wraps were individual layers of carbon fibers with zero degree angle of orientation (i.e. perpendicular to the loading direction). The tensile strength of these fibers was 383 kN per one meter width of the sheet, their ultimate elongation was 1.5%, and their modulus of elasticity was 25400 kN/m.

6.2.2.1. Failure Mode

Upon loading specimens, lateral expansion develops in the cylinders. This expansion is greater at the mid-height of the specimen, since loading plates apply high amount of confinement to its ends due to the interface friction. The lateral expansion remains very low up to the point that micro cracks have well developed in the internal structure of concrete. After this point, which can be related to ε^*, the bearing concrete struts begin to separate, area strain increases dramatically, and lateral expansion occurs at an increasing rate. This expansion applies tensile force to the FRP, which increases as the expansion advances. The limit of the tensile force that the FRP sleeve can bear is determined by its strength (at ultimate elongation). The stress-strain curve for carbon fibers is a linear elastic response which ends at a brittle failure.

As the axial strain (loading) proceeds, the lateral expansion increases and the fibers of the wrap approach their ultimate strength. At this point, the concrete cylinder has gone through extensive amount of strain which is far beyond its unwrapped capacity. The fibers of wrap first break at the mid-height of cylinder. Since the concrete can no longer bear the load by itself at this region, it suddenly expands more, and applies more stress to the fiber wraps in that neighborhood. Therefore, the breakage of fiber wraps initiates at the

mid-height and propagates rapidly to the ends. Besides, at this stage concrete is well crushed and does not carry any load. Hence, by ignoring the very short time of breakage propagation, it can be concluded that failure of wrapped cylinders is associated with extensive amount of deformation, terminated by an explosive failure.

6.2.2.2. Maximum Strength

The stress-strain curves of wrapped cylinders can be divided into two parts: from the origin to the kink-point (first peak), and from the kink-point to the complete failure (second peak). The kink-point is at the end of elastic part of the curve, whereas the complete failure occurs at the wrapping breakage. At the first part of curve, the lateral strain is low and the load is mainly carried by the concrete. After the first peak the lateral strain increases rapidly which causes a growing degree of confinement by the wrap in response to the applied circumferential strain.

The peaks on the stress-strain curves are sharper for fiber concretes which are more brittle, and smoother for more ductile ones. By adding layers, the second peak moves higher, and smoothens the part of curve between the peaks. Addition of the first layer of wrap increases the stress of the first peak (kink-point) significantly, but by adding more layers of wrap the location of the kink-point does not vary considerably.

For those specimens for which the un-wrapped response were less ductile, the second part of curve demonstrates irregular shape (a drop between the peaks). Perhaps, the sudden failure of the internal structure of concrete cylinder causes the formation of the drop after the first peak. This sudden partial failure causes some damage to the whole system, and leads to a lower increase of the second peak. Imperfect wrap installation can be an additional cause of the irregular shape of the second part of curves.

The maximum strength is defined as the stress at the higher peak. FRCs show higher sensitivity to addition of wrap layers than plain concrete. Concrete with high fraction of polypropylene fibers exhibit the most, and concrete with low fraction of steel

fibers exhibit the least sensitivity to the addition of fibers wraps. It should be noted that wrap layers are more effective in raising the second peak of the curves. The maximum strength of plain concrete and concrete with low fraction of steel fibers were determined by the first peaks which were higher. Therefore, their maximum strength (first peak) was not significantly increased.

6.2.2.3. Strain at Maximum Strength

The addition of wraps increases the axial strain at maximum strength. This effect is more pronounced for concrete with high content of polypropylene fibers, and less evident for plain concrete and concrete with low fraction of steel fibers. The maximum strength for the latter batches occur at the first peak, which its corresponding strain does not vary significantly by addition of wrap layers. The generated confinement delays failure of the specimens, leading to higher value of strain at maximum stress.

6.2.2.4. Modulus of Elasticity

The elastic modulus is not affected greatly by wrapping. The first part of the stress-strain curve, which exhibit the elastic behavior, is mainly the response of the concrete cylinder. At this stage the lateral expansion is very low, and confinement effect remains insignificant.

6.2.2.5. Strain at Zero Volumetric Strain

The axial strain corresponding to zero volumetric strain increases with increasing the number of wrapping layers. However, plain concrete and concrete with low fraction of steel fibers did not show any sensitivity, since the drop after the first peak caused extensive damage in the micro-structure of concrete. The value of ε^* for concrete with high fraction of steel fibers increased dramatically with addition of wrap layers. The

wrapping system could improve the immediate strength loss after the first peak, and eliminate the associated sudden damage.

6.2.3. Confinement Effects

Confinement acts against the increase in area strain, and delays volumetric expansion, which causes enhancement in mechanical behavior of concrete. Applying lateral pressure to saturated concrete causes development of pore water pressure, which reduces the effective confinement. Applying lateral pressure to dry concrete squeezes the empty pores and causes partial alteration (damage) in its micro-structure. In the case of active confinement, the pores are affected before applying the load, whereas in the case of passive confinement the effects occur as loading proceeds. Furthermore, the values of lateral pressures were corrected to find the actual confinements for wet specimens.

6.2.3.1. Maximum Strength

The maximum strength of fiber concrete increases with raising the degree of confinement. The specimens subjected to both passive and active confinement exhibit the same variations, which is a linear relationship. Concretes containing micro and steel fibers are slightly less influenced by variation in confinement, due to stiffer restraint that these fibers apply.

6.2.3.2. Axial Strain at Maximum Strength

The values of axial strain corresponding to maximum strength show a nonlinear increase with higher degree of confinement. This strain is slightly higher for the case of passive confinement than that of active confinement. In the case of active confinement, the lateral pressure which is applied first causes partial contraction of the pores and

stiffens the system, thereby requiring a greater amount of external work input to achieve a given increment of axial contraction. Whereas in the case of passive confinement, axial load can compress the micro-structure earlier and develop more axial strain. At high degrees of active confinement, the relative value of strain corresponding to maximum strength of concrete with polypropylene fibers is higher than that of plain concrete. This indicates that the micro-structure of this FRC has better flow ability, due to lower modulus of elasticity of these fibers and their net shape.

6.2.3.3. Apparent Elasticity Modulus

Confinement has a slight increasing effect on the apparent modulus of elasticity. This effect is higher for concrete with steel fibers and lower for plain concrete and concrete with micro fibers. Note that micro-fibers have better distribution in the matrix than regular (macro) fibers.

The variation of modulus of elasticity is greater under passive confinement. It should be noted that in the elastic region, the lateral expansion of cylinders is very low, and the FRP sleeves do not imply considerable confinement. However, concrete with steel fibers which exhibited more expansion was more affected. Other batches, more or less, exhibited the modulus of elasticity of un-wrapped specimens.

6.2.3.4. Strain at Zero Volumetric Strain

Increase in confinement raised the value of ε^*, since it imposed restriction against the increase in area strain and delayed the onset of dramatic damage. At high degrees of confinement this value was not obtained (within the range of tests). For more than 20% f'_c passive confinement the value of ε^* was hardly obtainable, whereas in active confinement this value was assessed for a few specimens. The range of variation in passive confinement is narrow, whereas is active confinement it is very broad. Note that in active confinement a constant lateral pressure is applied to the specimen, whereas in passive

confinement the expansion of specimen causes increase in the lateral pressure, hence the severity of expansion is more controlled.

6.2.3.5. Ductility

Ductility increases with confinement. In passive confinement, except for plain concrete at low degree of confinement, the second part of the stress-strain curve has positive slope. In active confinement, the value of ε_{85} which was obtained for plain concrete shows six times increase for 20% f'_c confinement, and lower increase for higher degrees of confinement. This value was not obtained for plain concrete at 80% f'_c confinement, due to limitations of the testing equipments. In FRC specimens, only for concrete with micro-fibers the ε_{85} value at 20% confinement could be obtained, since confinement increases the ductility of FRCs even more. Micro-fibers have better distribution (i. e. less fiber spacing), and perhaps can control the pore structure better, and cause the matrix to be less effected by lateral pressure.

6.2.4. Size Effects

The mechanical properties of concrete change with increasing the size of the member, but these variations approach to limiting values for large size specimens. The most likely explanation for this phenomenon is that large structures can store more energy at a certain strain. At the failure the magnitude of released energy which is greater for large size structures causes more damage and crack propagation.

6.2.4.1. Compressive Strength

Size variation has inverse effect on the compressive strength, which is compatible with the theory of energy release. This variation is more manifest in concrete with low content of micro-fibers, and less evident in concrete with steel fibers. The hooked ends of steel fibers enable them to have better control over the stored energy release. Higher fractions of micro-fibers provides smaller fiber spacing (denser distribution) which also leads to better control over the stored energy.

6.2.4.2. Strain at Peak Strength

Increase in size decreases the value of ε_c, since lower strain is required for large structures to produce the necessary failure energy. This effect is the most for low content micro-fibers, and the least for high content of this fiber type. Micro-fibers produced additional porosity, which reduced the amount of energy required for fracture. However, high fraction of these fibers can control better the stored energy release, due to their denser spacing.

6.2.4.3. Modulus of Elasticity

The elasticity modulus increases with size, which indicates the relative decreasing rate of f'_c is higher than that of ε_c as the size increases. Larger cylinders are stiffer than smaller ones, because the core of the cylinder is confined by the outer part, leading to overall stiffer response. Concrete containing steel fibers exhibit more sensitivity to size variation than concrete reinforced with other fiber types. This response can be explained by the fact that in larger structures fibers are more randomly scattered (walls of the molds orient the fibers in their neighborhood, and in the case of cored specimens fibers are cut at the side of cylinders).

6.2.4.4. Poisson's Ratio

Poisson's ratio increases with size. This means that the relative circumferential strain is lower for smaller specimens than larger ones. The cross sectional area of longitudinal concrete bars, which develop along the loading direction (leading to vertical cracks), are related to the aggregate size. Hence, in a larger specimen a higher number of these bars are formed, and their deformations result in a higher accumulated lateral strain.

With respect to the magnitude of ν, concrete with high content of polypropylene fibers exhibit low sensitivity, and concrete with steel fibers exhibit high sensitivity to variation in size. The network system of polypropylene fibers attach the concrete fragments, and causes less accumulated deformation, whereas steel fibers act individually, and impose less restraint against separation of these concrete fragments.

6.2.4.5. Strain at Zero Volumetric Strain

As the result of higher circumferential strain for larger specimens, the value of ε^* decreases with increase in specimen size. Larger structures store higher energy which causes earlier onset of severe damage. Concrete with a high fraction of polypropylene fibers is more affected, whereas concrete with high content of micro-fibers is less affected by size variation. Polypropylene fibers have low modulus of elasticity, and impose lower restriction against increase in area strain. Hence, lower amount of energy (which is dependent on axial strain) is required to create severe damage. Whereas high content of steel micro-fibers (high elasticity and dense fiber spacing) demands higher amount of energy to cause severe damage in concrete.

6.2.4.6. Ductility

Larger structures store higher energy, which causes higher damage after failure. Hence, smaller specimens exhibit more ductility than larger ones. The value of ε_{85} is

affected more for concrete with high content of steel fibers, and less for concrete with high content of micro-fibers.

6.2.4.7. Size Effects in Wrapped Specimens

Adding layers of wrap increases the compressive strength of smaller cylinders faster than that of larger ones. A layer of wrap can hold certain amount of energy. On the other hand, the amount of energy that larger structures produce is higher than that of smaller ones at a certain strain. Therefore, a layer of wrap on the larger specimens fails earlier than that on smaller ones. By increasing the number of layers, the accumulated difference in the strength of the two sizes increases, but approaches to a limit. Plain concrete is more sensitive to these variations, since release of energy is rapid after the first peak.

The axial strain corresponding to the maximum strength increases faster for smaller cylinders by addition of wrap layers. The theory of energy release explains this variation, as was mentioned in the preceding paragraphs. However, this rate of increase also approaches a limiting value. The variation in this strain is higher for plain concrete, as was explained in the previous paragraph.

The relative modulus of elasticity of smaller wrapped cylinder to that of larger ones shows reduction as the number of layers increases.

6.2.5. Saturation effects

When a saturated concrete member is loaded under compression, pore water pressure develops which then acts against the internal structure of concrete. Hence, the applied confinement to a saturated specimen must be corrected to evaluate the effects of true lateral pressure.

6.2.5.1. Maximum Strength

Dry specimens show higher strength for all degrees of confinement. However, the difference between these values at dry and wet conditions remain almost constant at any level of lateral pressure. Although the influence of pore pressure is eliminated by the correction in applied confinement, the other phenomena such as dilation of the gel, shielding effect, swelling pressure in the gel, and solid-water bonds still are in effect. It is believed that because these phenomena are not affected by the presence of confinement, the difference of the maximum strength of wet and dry specimens at a certain degree of confinement is a constant value.

6.2.5.2. Strain at Peak Strength

The value of ε_c is much higher for dry concrete than wet one at zero confinement, particularly for concrete with polypropylene fibers. Perhaps, the effect of solid-solid bond, which occurs in dry concrete with polypropylene fibers, is highly significant. This bond provides more interaction between fiber and matrix, leading to enhancement of the ε_c value. Besides, the pore pressure produced by axial load causes damage in wet specimens.

At higher levels of confinement, the value of ε_c increases at a slower rate for dry FRCs. Since the pore pressure is zero in dry concrete, the lateral pressure (which is applied prior to the loading) causes contraction and partial collapse of the pores. The extend of this damage depends on the level of lateral pressure. Therefore, at higher degrees of confinement, the damage is higher, and the value of ε_c is lower.

6.2.5.3. Modulus of Elasticity

The modulus of elasticity is slightly higher for wet FRC at zero confinement, particularly for concrete with polypropylene fibers. Pore distribution is deferent in FRC than that of plain concrete, since air pockets form at the sides of fibers. Perhaps, when water molecules migrate away from the concrete (upon drying) some damage occurs in the material micro-structure, which affect the apparent E value. Besides, upon migration

of water, solid-solid bonds are formed in concrete. In FRC, possibly the bond of concrete-polypropylene has lower strength than the bond of concrete-steel, leading to lower E value for dry polypropylene FRC.

At higher level of confinement, the value of apparent E increases for both dry and wet specimens. The difference of stiffness in dry and wet conditions remains unchanged for various level of confinement.

6.2.5.4. Poisson's Ratio

At zero confinement, the Poisson's ratio is slightly higher for wet plain concrete and slightly lower for wet concrete with steel and micro-fibers. The concrete with the mix of micro and polypropylene fibers exhibit a dramatic drop in the value of ν at dry condition. Both micro-fibers and polypropylene fibers create high amount of porosity, which make the concrete micro-structure susceptible to higher drying damage.

6.2.5.5. Strain at Zero Volumetric Strain

The value of ε^* is higher for dry specimens at zero confinement. The negative pore pressure which is developed in the material causes early damage in the internal structure. In addition, the solid-solid bonds, which are formed in the drying stage, are stronger than solid-water bond. These strong bonds work against the increase in area strain, and delay the onset of severe damage. Furthermore, the ε^* value was not obtained for concrete with polypropylene plus micro fibers, because these fibers provided a significant degree of restraint against volumetric growth.

The ε^* value of wet specimens is higher at higher degrees of confinement. Upon application of axial load on wet specimen, the generated pore pressure acts against the internal structure of concrete at zero confinement (reducing ε^*), and partially cancels out the lateral pressure at higher confinements (increasing ε^*). In dry case, at high lateral

pressure the pores collapse earlier which leads to a lower ε^* value. At high levels of confinement, most of wet specimens did not provide ε^* value within the test range.

6.2.5.6. Ductility

Ductility is presented by the value of ε_{85}. This value for dry concrete is higher at zero confinement stress. The strong solid-solid bonds which are formed in dry concrete slow down the unloading rate on the descending branch of stress-strain curve.

The value of ε_{85} of dry specimens is slightly lower at higher degrees of confinement. The damage that lateral pressure produces in empty pores (dry concrete) causes less ductility for dry confined specimens. At high levels of confinement the ε_{85} value was not obtained for FRCs, due to their high deformation capacity.

6.2.6. Effects of Mixing Fiber Types

Various fiber types alter the mechanical properties of concrete differently. Mixing different fiber types can tailor these properties to desired values. The interaction of fiber types has great significant in this respect. The fraction of each fiber type in the mix determines its influence on the overall response of FRC. In this experimental study, the volumetric ratio of mixed fiber types was maintained at 40% steel micro-fibers and 60% steel or polypropylene fibers, but the total volume fraction of fibers was a variable.

6.2.6.1. Unconfined Response

Concrete containing steel and micro-fibers reached a slightly lower strength than concrete containing only micro-fibers with the same fiber fraction. Steel fibers have broader spacing, and less control over the micro-structure of concrete. Combining micro-fibers and polypropylene fibers resulted in lower compressive strength than using them individually, since micro-fibers produce porosity and polypropylene fibers have low

elasticity. The tensile strength of concrete with combined steel and micro fibers does not differ than that of concrete containing either of those fiber types, since both have the same modulus of elasticity. When combining polypropylene with micro fibers, steel micro fibers dominate the tensile strength of FRC, due to the high elasticity of steel.

In compression, addition of steel fibers in low fraction raised ε_c, and in high fraction lowered ε_c slightly. Combining polypropylene and micro fibers resulted in lower ε_c for low fraction fibers, and higher ε_c for high fraction fibers (than using them individually). In tension, only high fraction of combined fibers (micro with steel, or polypropylene) caused an increase of more than 20% in the ε_R value.

In compression, addition of steel fibers to a concrete containing micro-fibers lowered its E value, due to their less control over the pore structure. Addition of polypropylene fibers to the same concrete had similar effect, due to their low modulus of elasticity. Addition of either steel or polypropylene fibers at low fraction to concrete containing micro-fibers decreased the value of ν, and at high fraction had the reverse effect. The fiber network which is formed at high fraction of polypropylene fibers changes the influence of this fiber type. Addition of low fraction of polypropylene fibers to concrete with micro-fibers reduced its ε^* value, whereas addition of high fraction of these fibers had reverse effect.

In compression, steel fibers increase the ductility, however the most dramatically increase was seen in concrete containing mixed polypropylene and micro-fibers. In bending, addition of steel fibers reduced the brittleness of the post-peak response of concrete with micro-fibers. Combination of micro-fibers with polypropylene fibers produced higher residual strength in the post-peak response, but similar shape to the post-peak response of polypropylene fiber concrete.

6.2.6.2. Size Effect

Combining high fraction of polypropylene and micro fibers result in high sensitivity of compressive strength to size variation, but concrete with low fraction of these fiber types show insignificant size effects. Both fiber types create high porosity when used at high volume ratio. The high porosity leads to less control over the release of stored energy, which results in lower ultimate stress for large specimens. Besides, the individual polypropylene fiber nets form fiber network at high fiber fraction, which changes the influence of this fiber type.

Concretes with high content of polypropylene or micro-fibers showed low sensitivity of E value to size increase. The rate of increase in the modulus of elasticity of concrete with high content of mixed polypropylene and micro fibers is slightly lower than that of the individual batches, meaning even less sensitivity to size effect.

When combined with polypropylene fibers, micro fibers dominate in determining the size effect on Poisson's ratio of FRC. Both high and low content of this combination exhibit similar sensitivity to size variation as plain concrete.

Concrete with high content polypropylene and micro fibers exhibit high sensitivity to size variation in the strain corresponding to zero volumetric strain. This sensitivity is equal to that of concrete with high content polypropylene fibers, hence, this fiber type dominates in determining the size effect on $\varepsilon^{\bullet}$.

The sensitivity in ductility to size increase of the concrete with low content of polypropylene and micro fibers is lower than that of concretes which contain individual types of these fibers. The ductility of concrete containing high content of these fiber types was not evaluated, since ε_{85} was not obtainable within the test range for this batch.

6.2.6.3. Wrapping Effects

Increase in the number of wrapping layers increases significantly the maximum strength of concrete containing high fraction of polypropylene and micro fibers. Polypropylene fibers dominate in determining this effect. The variation in the value of

strain corresponding to maximum stress is higher for concrete containing low content of polypropylene and micro fibers. This response also is determined by polypropylene fibers. Variation of modulus of elasticity with increase in number of wrapped layers is high for concrete containing low fraction of polypropylene and micro fibers, where as it has slight increase for concrete containing high fraction of these fiber types. Addition of wrapping layers doubles the value of ε^* for concrete containing polypropylene and micro fibers.

6.2.7. Toothpaste Effects

Because of the difficulties involved in conducting the related test, only limited information was obtained in this area. However, four tests (one of each batch) were accomplished, which illustrate the possibie sensitivity of the behavior of fiber concrete subjected to lateral squeeze. The shape of the stress-strain curves obtained from this experiment are similar to the ones obtained from compression test, but the signs of strains are opposite and the growth rate of ε_1 is greater than that of ε_3. The shape of the axial strain versus volumetric strain curve is, also, comparable with that of compression test, only the sign of ε_1 is opposite. Except concrete with mixed polypropylene and micro fibers, the strength at failure was within the compressive strength.

6.3. Empirical Results

The empirical formulas which were established by this experimental study are important from the design respective. These equation were developed for confinement and size effect on the compressive strength of cylindrical specimens.

6.3.1. Confinement Effect

A familiar empirical relation of the effect of lateral pressure on the strength of concrete was proposed by Richart et al (1928):

$$f'_{cc} = f'_c + 4.1\ \sigma_{lat} \tag{6-1}$$

where f'_{cc} is the axial compressive strength of concrete subjected to the lateral pressure σ_{lat}, and f'_c is the uniaxial compressive strength of concrete. Imran and Pantazopoulou (1995) found that Equation 6-1 was satisfactory for low strength concrete, and it overestimated the values for high strength concrete. They reasoned that the original database used in deriving Equation 6-1 only contained triaxial test data of dry concrete specimens with low uniaxial compressive strength (i.e, f'_c in the range of 5 to 25 MPa).

Figure 6-1 shows the relation between strength and confinement on all the batches used in this study under active and passive confinement. The data are organized along a linear pattern. The slope of the drawn line is 3.1, and hence Equation 6-1 is modified to:

$$f'_{cc} = f'_c + 3.1\ \sigma_{lat} \tag{6-2}$$

The uniaxial compressive strength of the concrete matrix in this experiment was 58 MPa. The high strength of concrete, fiber content, high cement content, modern cement product, and perhaps different aggregate material may be the cause of deduction in the coefficient of σ_{lat} in Equation 6-2.

6.3.2. Size Effect

The compressive strength of concrete reduces with size increase. Bazant (1984) proposed the following equation to describe size effect on the tensile strength of concrete:

$$\sigma_N = B f_u (1+\beta)^{-1/2} \tag{6-3}$$

where σ_N is the tensile strength of size d, f_u is tensile strength of size d_o, and

$$\beta = d / d_o \tag{6-4}$$

6.4. Summary of Conclusions

Maximum Strength

Increase in porosity due to addition of fiber to concrete leads to decrease in compressive strength. Addition of fibers with lower modulus of elasticity has more decreasing effect. Adding fibers with low elasticity decreases the bending (tensile) strength of concrete. Concrete has lower strength in wet condition that dry condition, mainly because of the developed pore water pressure. Confinement increases the compressive strength of concrete. When effective lateral pressure is considered, active and passive confinements produce similar results which is a linear relationship. Larger specimens exhibit lower strength, which is explained by the theory of "energy release".

Strain at Maximum Strength

In bending, high fraction of steel fibers and mixed polypropylene and micro fibers increase the strain at peak strength. In compression, low fraction of polypropylene fibers decreases strain at maximum strength, whereas high fraction of this fiber type has inverse effect. This strain is higher for dry concrete at zero lateral pressure, but is lower at higher degrees of confinement. Confinement increases the value of this strain. Passive confinement is more effective in this respect. Larger specimens exhibit lower strain at peak; which is explained by the stored energy.

Modulus of Elasticity

Addition of fibers to high strength concrete decreases its modulus of elasticity, due to increase in porosity. Fibers which have low elasticity lower this value even further. Saturation effect on this modulus is insignificant, however concrete containing polypropylene has slightly higher elasticity in wet condition. Confinement has slight increasing effect on the value of E, which is equal for active and passive cases. Larger specimens illustrate higher value for elasticity modulus.

Apparent Poisson's Ratio

Except high content of polypropylene fibers, addition of fibers decreases the value of ν. At high content this fiber type forms a fiber network system which has low adhesive bond to the matrix, which changes its effect as individual fiber nets. Wet concrete containing polypropylene fibers has higher Poisson's ratio. Larger specimens demonstrate higher value of ν.

Strain at Zero Volumetric Strain

Fibers with high modulus of elasticity increase this strain. Dry concrete has higher value of ε^* at zero lateral stress, and lower value of this strain at higher degrees of confinement. Confinement has high increasing effect on ε^*, and passive condition is more effective than active condition. Larger specimens exhibit lower value of this strain.

Ductility

Addition of fibers provides ductility for high strength concrete. Polypropylene fibers have higher effect. Ductility increases with increase in fiber content. Dry concrete is more ductile at zero lateral stress and less ductile at higher degrees of confinement. Confinement, particularly passive increases this value rapidly.

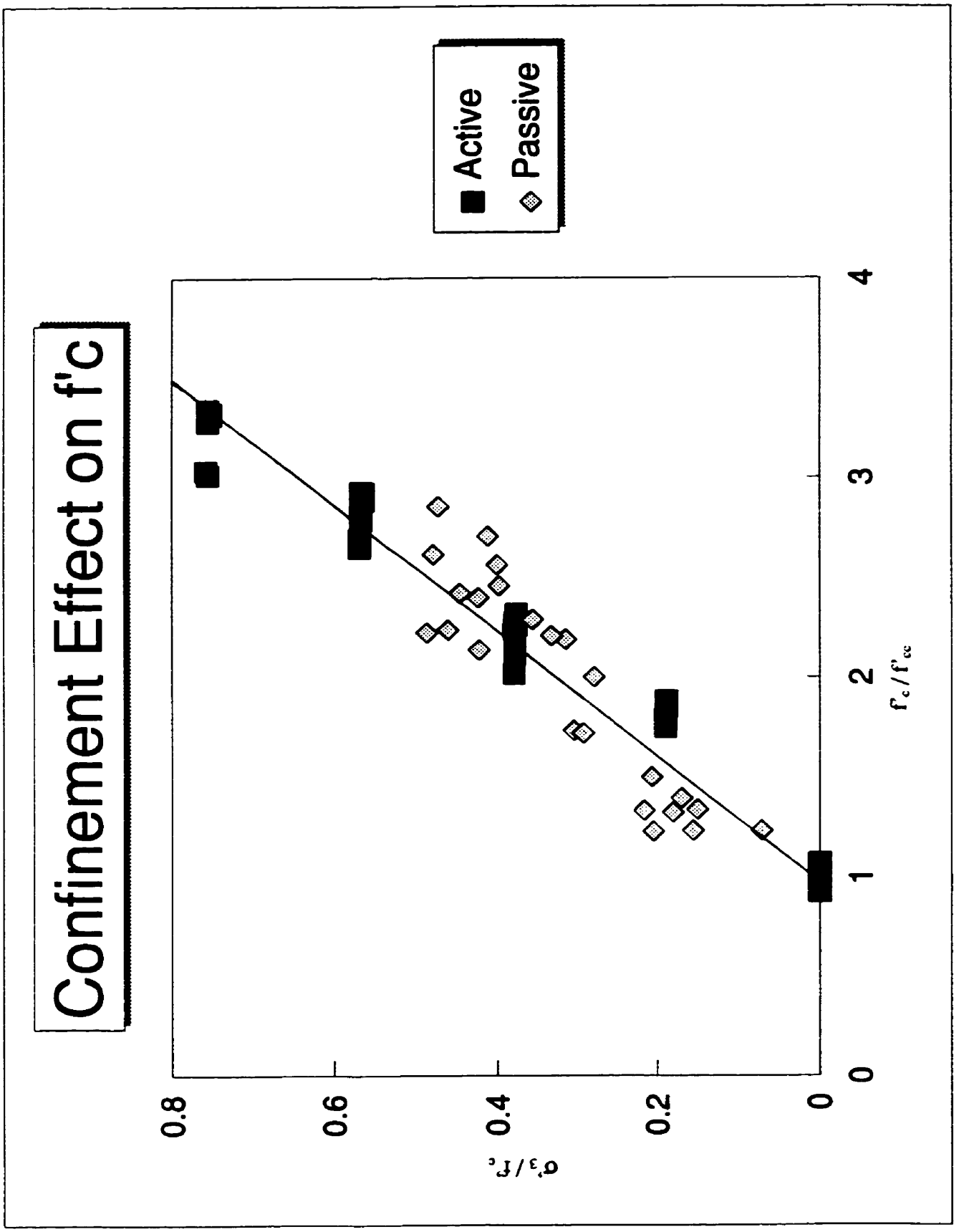

Figure 6-1: The relationship of confinement and strength

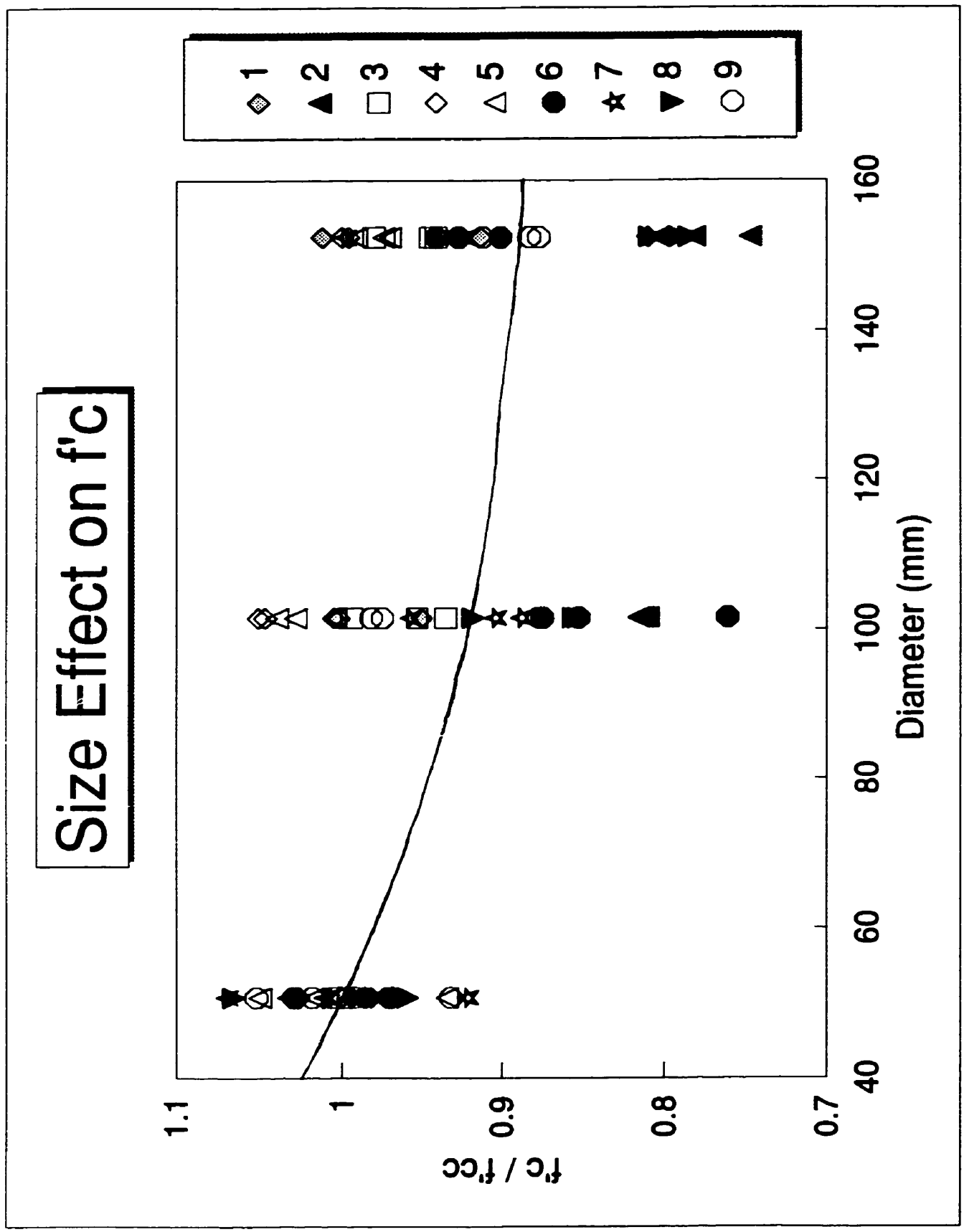

Figure 6-2: The relationship of size and strength

References

1. ACI Committee 544 (1993) "Guide for Specifying, Proportioning, Mixing, Placing, and Finishing Steel Fiber Reinforced Concrete", *ACI Material journal*, V. 90, No. 1, January-February , pp 94-101.

2. ACI Committee Report (1988) "Design Considerations for Steel Fiber Reinforced Concrete", *ACI Structural Journal*, September-October, pp 563-80.

3. Akroyd T.N.W. (1961) "Concrete under Triaxial Stress", *Magazine of Concrete Research*, V. 15, No. 39, pp 111-118.

4. ASTM C 78 (1994) "Standard Test Method for Flexural Strength of Concrete (Using Simple Beam with Third-Point Loading", p 30-32.

5. Ballinger C.A. (1992) "Development of Fiber-Reinforced Plastic Products for the Construction Market- how has and can it be done", 1st International Conference Advanced Composite Materials in Bridges and Structures, ACMBS (edited by Neale K.W. and Labossiere P.), Sherbrooke, Montreal, pp 3-13.

6. Banthia N. (1995), professor of University of British Colombia, private communications.

7. Banthia N., Moncef A., Chokri K., and Sheng J. (1995) "Uniaxial Tensile Response of Microfiber Reinforced Cement Composites", *Materials and Structures*, V. 28, N 183, November, pp 507-17.

8. Banthia N. and Sheng J. (1995) "Micro-Fiber Reinforced Cement Composites, II. Flexural Response and Fracture Studies", *Canadian Journal of Civil Engineering*, V. 22, N. 4, August, pp 668-82.

9. Bayasi M.Z. and Soroushian P. (1992) "Effect of Steel Fiber Reinforcement on Fresh Mix Properties of Concrete", *ACI Material Journal*, V. 89, No. 4, July- August, pp 369-374.

10. Bayasi Z. and Zeng J. (1993) "Properties of Polypropylene Fiber Reinforced Concrete", *ACI Material Journal*, V. 90, No. 6, November-December, pp 605-610.

11. Bazant Z.P. (1984) "Size Effect in Blunt Fracture: Concrete, Rock, Metal", *Journal of Engineering Mechanics*, V. 110, No. 4, April, pp 518-535.

12. Bazant Z.P. (1993) "Size Effect in Tensile and Compression Quasibrittle Failure", Proceeding of the Japan Concrete Institute International Workshop, October-November, "Size Effect in Concrete Structure" (edited by Mihashi H., Okamura H. and Bazant Z.P.), pp 161-180.

13. Bazant Z.P. and Kwon Y.W. (1994) "Failure of Slender and Stocky Reinforced Concrete Columns: tests of size effect", *Materials and Structures*, V. 27, No. 166, March, pp 79-90.

14. Bazant Z.P., Ozbolt J. and Eligehausen R. (1994) "Fracture Size Effect: Review of Evidence for Concrete Structure", *Journal of Structural Engineering*, ASCE, V. 120, No. 8, August, pp 2377-98.

15. Collins M.P. (1995), Structural professor of The Civil Engineering Department of The University of Toronto, private communication.

16. Erki M.A. and Agarwal A.C. (1995) "Strengthening of Reinforced Concrete Axial Members Using Fiber Composite Material-A Survey", Annual Conference of the Canadian Society for Civil Engineering, pp 565-574.

17. Fanella D. and Krajcinovic D. (1988) "Size Effect in Concrete", *Journal of Engineering Mechanics*, V. 114, No. 4, April, pp 704-715.

18. Forca Catalog (1994), The Manufacturer Manual for Carbon Fiber Tow Sheet, presented in the Appendix B of this report.

19. Hatanaka S., Mizuno E., Koike S. and Tanigawa Y. (1993) "Experimental Study on Size Effect in Constitutive Relationship of Compressive Concrete", Proceeding of the Japan Concrete Institute International Workshop, October-November, "Size Effect in Concrete Structure" (edited by Mihashi H., Okamura H. and Bazant Z.P.), pp 129-140.

20. Hannant D.J. (1995) "Fiber Reinforcement in the Cement and Concrete Industry", *Material Science and Technology*, V. 11, September, pp 853-61.

21. Hoek E. and Franklin J.A. (1968) "Simple Triaxial Cell for Field or Laboratory Testing of Rock", *Institute of Mining and Metallurgy*, V. 77, pp A22-A26.

22. Hooton R.D. (1995), Material Proffesor of The Civil Engineering Department of The University of Toronto, private communication.

23. Howie I. and Karbhari V.M. (1995) "Effect of Tow Sheet Composite Wrap Architecture on Strengthening of Concrete Due to Confinement: I-Experimental Studies", *Journal of Reinforced Plastics and Composites*, V. 14, No. 9, September, pp 1008-1030.

24. Hsu C.T.T. and Hsu L.S. (1994) "Stress-Strain Behavior of Steel-Fiber high-Strength Concrete under Compression", *ACI Structural Journal*, V.91, No. 4, July-August, pp 448-457.

25. Intertechnology (1995), The Company Supplying the Strain-Gauges and their Accessories, The Catalogue of 1995.

26. Imran I. and Pantazopoulou S.J. (1995) "Experimental Study of Plain Concrete Under Triaxial Stress", paper accepted for publication in The ACI Material Journal, 1996.

27. Karbhari V.M. and Eckel D.A. (1995) "Effects of Short-Term Environmental Exposure on Axial Strengthening *Capacity of Composite Jacketed Concrete", Journal of Composites Technology and Research*, V 17, No. 2, April, pp 99-106.

28. Kosa K. and Naaman A.E. (1990) "Corrosion of Steel Fiber Reinforced Concrete", *ACI Material Journal*, V. 87, No. 1, January-February, pp 27-37.

29. Kuilman C. (1988) "The Fiber Concrete Advantage", *Plant Engineering*, V. 42, October 27-1988, pp 52-53.

30. Labossière P.(1996), Professor of The University of Sherbrook, a presentation at The university of Toronto.

31. Lee S.L., Lim T.Y. and Paramasivam P. (1987) "Analytical Model for Tensile Behavior of Steel-fiber Concrete", *ACI Material Journal*, July-August, pp 286-298.

32. Loock L.V. (1988) "Bending Tests on Steel Fiber Concrete", *Civil Engineering*, October, pp61-65; and December-January, pp36-40.

33. Mandel J.A., Wei S. and Said S. (1987) "Studies of the Properties of the Fiber-Matrix Interface in Steel Fiber Reinforced Mortar", *ACI Material Journal*, V. 84, March-April, pp 101-109.

34. Markeset G. and Hillerborg A. (1995) "Softening of Concrete in Compression Localization and Size Effect", *Cement and Concrete Research*, V. 25, No. 4, March, pp 702-708.

35. Mazars.J, Perdikaris P. and Pijaudier-Cabot G. (1993) "Size Effect Prediction with Damage Modeling", Proceeding of the Japan Concrete Institute International Workshop, October-November, "Size Effect in Concrete Structure" (edited by Mihashi H., Okamura H. and Bazant Z.P.), pp 207-220.

36. Mills R.H. (1960) "Strength-Maturity Relationship for Concrete which is Allowed to Dry", RILEM International Symposium on Concrete and Reinforced Concrete in Hot Countries (Haifa).

37. Mills R.H. (1966) "Effects of Sorbed Water on Dimensions, Compressive Strength and Swelling Pressure Of Hardened Cement Paste", Special Report, No. 90, Highway Research Board, pp 84-111.

38. Mindess S. (1996) "Fiber Reinforced Concrete: Challenges and Prospects", The Second University-Industry Workshop on Fiber Reinforced Concrete and Other Advanced Composites, held in Canada, March 26 to 29, "Fiber Reinforced Concrete; Modern Developments" (edited by Banthia N. and Mindess S.).

39. Morita S., Fujii S. and Kondo G. (1993) "Experimental Study on Size Effect in Concrete Structure", Proceeding of the Japan Concrete Institute International Workshop, October-November, "Size Effect in Concrete Structure" (edited by Mihashi H., Okamura H. and Bazant Z.P.), pp 27-46.

40. Murakami M., Ishida K., Nishino K., Kubota T. and Ohtani Y. (1993) "Influence of Aggregate Size on Damaged Zone in Compression" Proceeding of the Japan Concrete

Institute International Workshop, October-November, "Size Effect in Concrete Structure" (edited by Mihashi H., Okamura H. and Bazant Z.P.), pp57-66.

41. Murugappan K., Tan K.H. and Paramasivam P. (1994) "Finite Element Formulation for the Analysis of Reinforced Fibrous Concrete Beam", *Finite Elements in Analysis and Design*, V. 18, No. 1-3, December, pp 67-74.

42. Namman A.E. and Najm H. (1991) "Bond-Slip Mechanisms of Steel Fiber in Concrete", *ACI Material Journal*, V. 88, No. 2, March-April, pp 135-145.

43. Naaman A.E. and Otter D.E. (1988) "Properties of Steel Fiber Reinforced Concrete under Cyclic Loading", *ACI Material Journal*, July-August, pp 254-261.

44. Neville A.M. (1990) "Properties of Concrete" third edition, 779 p.

45. Pantazopoulou S.J. (1995) "Role of Expansion on Mechanical Behavior of Concrete", ASCE, *Journal of Structural Engineering*, V. 121, No. 12, December, pp 1795-1805.

46. Pantazopoulou S.J. and Mills R.H. (1995) "Microstructural Aspects of the Mechanical Response of Plain Concrete", *ACI Material Journal*, V. 92, No. 6, November-December, pp 605-16.

47. Picher F. and Labossière P. (1995) "Confinement De Cylindres En Béton Avec Des Matériaux Composites", Annual Conference of The Canadian Society for Civil Engineering, pp 575-583.

48. Raivio P. and Sarvaranta L. (1994) "Microstructure of Fiber Mortar Composites under Fire Impact- Effect of Polypropylene and Polyacrylonitrile Fibers", *Cement and Concrete Research*, V. 24, No. 5, May, pp 896-906.

49. Ramakrishnan V. (1988) "Materials and Properties of Fiber Reinforced Concrete", *Civil Engineering*, April, pp 29-40.

50. Rehbinder P.A., Schreiner L.A. and Zhigach K.F. (1948) "Hardness Reducers in Drilling", Colloids-Electrochemical Institute, Acadamy of Science, USSR, pp 1-39.

51. Richart F.E., Brandtzaeg A. and Brown R.L. (1928) "A Study of the Failure of Concrete under Combined Compressive Stresses", Engineering Experiment Station Bulletin, No. 185, University of Illinois, Urbana.

52. Robertson B. and Mills R.H. (1985) "Influence of Sorbed Fluids on Compressive Strength of Cement Paste", *Cement and Concrete Research*, V. 15, pp 225-232.

53. Rossi P. (1994) "Steel Fiber Reinforced Concrete (SFRC): An Example of French Research", *ACI Material Journal*, V. 91, No. 3, May-June, pp 273-279.

54. Sheikh S., Pantazopoulou S., Bonacci J., Thomas M., Hearn N. (1996) "Repair of Delaminated Circular Pier Columns by ACM", Ontario Joint Transportation Research Report, MTO Reference number 31902.

55. Slattery K.T. and Harmon T.G. (1992) "Advanced Composite Confinement of Concrete", 1st International Conference Advanced Composite Materials in Bridges and Structures, ACMBS (edited by Neale K.W. and Labossiere P.), Sherbrooke, Montreal, pp 299-306.

56. Soroushian P. and Bayasi Z. (1991) "Fiber-Type Effects on the Performance of Steel Fiber Reinforced Concrete", *ACI Material Journal*, V. 88, No. 2, March-April, pp 129-134.

57. Soroushian P. and Lee C.D. (1990) "Distribution and Orientation of Fibers in Steel Fiber Reinforced Concrete", *ACI Marerial Journal*, V. 87, No. 5, September-October, pp 433-439.

58. Sugama T., Carciello N. and Kukacka L.E. (1992) "Interface Between Zinc Phosphate-Deposited Steel Fibers and Cement Paste", *Journal of Materials Science*, V. 27, June 1-1992, pp 2863-72.

59. Taerwe L.R. (1995) "Fracture and Internal Cracking of High-Strength Concrete under Axial Compression", *ACI SP-156:* Interface and Bond (edited by Bayukozturk O. and Wecharatana M.), American Concrete Institute, Detroit, pp 25-44.

60. Taerwe L.R. (1992) "Influence of Steel Fibers on Strain-Softening of High-Strength Concrete", *ACI Structural Journal*, V. 88, No. 6, January-February, pp 54-60.

61. Tavakoli M. (1994) "Tensile and Compressive Strength of Polypropylene Fiber Reinforced Concrete", *ACI SP-142:* Fiber Reinforced Concrete Developments and Innovations (edited by Daniel J.I. and Shah S.P.).

62. Yin W. and Hsu T.T.C. (1995) "Fatigue Behavior of Steel Fiber Reinforced Concrete in Uniaxial and Biaxial Compression", *ACI Material Journal*, V. 92, No. 1, January-February, pp 71-81.

Appendices

Appendix A

The computer disks containing all the processed testing data in spread-sheet form.

Appendix B

Forca catelogue; copies of the pages which are relevant to the application of cabon fiber wraps on the cylinderical specimens.

Appendix B

PROPERTIES OF FORCA TOW SHEET

TYPE	CARBON FIBER TOW SHEET			GLASS FIBER TOW SHEET	
GRADE	FTS-C1-20	FTS-C1-30	FTS-C5-30	FTS-GE-30	FTS-GT-30
FIBER	HIGH TENSILE CF	HIGH TENSILE CF	HIGH MODULUS CF	E-GLASS	T-GLASS
FIBER DENSITY, g/cm3	1.82	1.82	1.82	2.55	2.50
FIBER AREAL WEIGHT, g/m2	200	300	300	300	300
TOW SHEET WIDTH, cm	50	50	50	50	50
TENSILE STRENGTH					
kg /cm-sheet width	390	590	500	180	330
k-lb / inch-sheet width	2.2	3.3	2.8	1.0	1.8
TENSILE MODULUS					
kg / cm-sheet width	25,900	38,800	62,700	8,700	10,300
k-lb / inch-sheet width	145	220	350	49	57
DESIGN THICKNESS					
mm / ply *1	0.110	0.165	0.165	0.118	0.120
inch / ply *1	0.00433	0.00650	0.00650	0.00465	0.00472
TENSILE STRENGTH FOR DESIGN *2					
kg / cm2	35,500	35,500	30,000	15,500	27,500
ksi	505	505	427	220	391
TENSILE MODULUS FOR DESIGN *2					
kg / cm2	2.35E+06	2.35E+06	3.80E+06	0.74E+06	0.86E+06
Msi	33	33	54	10	12
ULTIMATE ELONGATION, %	1.5	1.5	0.8	2.1	3.2

NOTE *1 The design thickness is defined as the calculated total cross sectional area of fibers per single ply and is used for design purposes. Refer to " Design Procedure " in this technical note. From experience, the actual cured thickness of Tow Sheet on average is 0.024 to 0.039 inch (0.6 to 1.0 mm).

NOTE *2 The tensile strength and modulus for design are derived from the tensile strength and modulus divided by the design thickness. Refer to " Design Procedure " in this technical note.

Appendix B

4-4. Application of primer coat

* No primer coat should be applied if ambient temperature is lower than 5 °C (41 °F), or if rainfall or dew condensation is anticipated. Temperature and degree of dampness of the concrete to be prepared must be confirmed in order to select type of primer which is best suited.

1) FP primer must be thoroughly mixed with hardener at the specified ratio in the mixing pot until it is uniformly mixed (about 2 minutes). Agitation shall be by means of electric hand mixer. Volume of primer to be prepared at one time must be such that it can be applied within its batch life. A mixed primer batch which has exceeded its batch life must not be used. (Life of mixed primer batch is shown in Attach-3. The batch life may vary subject to ambient temperature or volume of the mixed primer batch and care must be taken accordingly.)
2) The mixed primer must be applied using a roller brush. If necessary, a second coat shall be applied after first coat has penetrated into the concrete. Volume of primer to be applied may vary depending on direction or coarseness of concrete surface to be prepared.
3) Applied primer coat must be cured for 3 hours to a half day until tack-free by finger.
4) Surface irregularity caused by primer coating must be ground and removed using disc sander, etc. If any minor protrusions on the concrete surface still remains, such surface defects may be corrected again using epoxy resin putty as needed.

* Work site must be thoroughly ventilated.
Use of fire is strictly prohibited. Because permeable type primer (FP-S) contains organic solvent, care must be taken to prevent inhalation of organic solvent fumes. Protective gear such as masks, goggles, rubber gloves, etc. must be used without fail whenever primer is applied.

4-5. Adhesion of Tow Sheet

* No Tow Sheet will not be applied whenever ambient temperature is lower than 5 °C (41 °F), or whenever rainfall or dew condensation is anticipated. Temperature and dampness of the concrete surface to which Tow Sheet is to be adhered must be confirmed in order to select the proper type of resin to be used.

1) Tow Sheet must be cut beforehand into prescribed sizes using scissors and cutter. The size of Tow Sheet to be cut is preferably less than 2m in length. The number of Tow Sheets to be cut shall be limited to the number to be adhered within the day
2) It must be confirmed that the primer coat applied onto the concrete surface is thoroughly cured. When the primer coat has been left unattended for more than one week after the application, surface of the primer coat must be roughened using sand paper.

Appendix B

3) FR resin must be mixed with hardener at the specified ratio in the mixing pot until uniformly mixed (about two minutes). Agitation is preferably by means of an electric hand mixer. Volume of mixed resin batch must be such that it can be applied within its batch life. A mixed resin batch which has exceeded its batch life must not be used. (Life of a mixed resin batch is shown in Attach-4. The life may vary subject to ambient temperature and volume of mixed resin batch and care must be taken accordingly.)

5) The mixed resin batch must be uniformly applied to the concrete surface using a roller brush (Primary coat). Volume to be applied may vary depending on direction and roughness of the concrete surface. More resin mix must be applied into internal angles than for flat concrete surfaces.

6) Tow Sheet is placed fiber side down onto concrete surface on which resin mix coat has been applied and surface paper is peeled away. Surface of adhered Tow Sheet must be squeezed rather strongly two to three times in fiber longitudinal direction using defoaming roller and rubber spatula in order to impregnate resin into Tow Sheet and to defoam the resin coat. For joining strips of Tow Sheet, a 10 mm overlapping must be maintained in fiber longitudinal direction. No lapping is required in the fiber lateral direction.

7) Tow Sheet so adhered must be left alone for at least 30 minutes. Any lifting or dislocation which may occur during this period must be corrected by pressing down Tow Sheet using a roller or spatula.

8) Mixed resin must then be applied onto the surface of the Tow Sheet (secondary coat). The surface onto which resin has been applied must be squeezed rather strongly two to three times in fiber longitudinal direction, in order to impregnate and replenish resin into the Tow Sheet, using defoaming roller and spatula in the same manner as detailed in item 6) above.

9) In case more than two layers of Tow Sheet must be laminated, the processes as detailed in items 5) through 8) must be repeated.

* Work site must be thoroughly ventilated. Use of fire is strictly prohibited.
  Care must be taken to prevent inhalation of resin fumes.
  Protective gear such as masks, goggles and rubber gloves must be used without fail during adhesion of Tow Sheet.

4-6. Protection

* In the case of outdoor application, the work must be protected from rain, sand, dust, etc. by using protective sheeting or other barriers.

1) After completion of Tow Sheet adhesion step, the work must be protected against rainfall using

Appendix B

PVC sheets in order to autocatalitically cure the adhered Tow Sheet. Care must be taken so that the protective sheets do not come into contact with the surface of the adhered Tow Sheet.

2) Curing of adhered Tow Sheet must be for no less than 24 hours.

3) The following curing time is required in order to achieve full design strength.

Two weeks curing time @ Average ambient temperature of 10 °C (50 °F)

One week curing time @ Average ambient temperature of 20 °C (68 °F)

4.7 Finish coat

* Finish coat shall be applied to the surface of adhered Tow Sheet as necessary.

1) Carbon fiber (CF) Tow Sheet, by virtue of the carbon fiber itself, is capable of preventing deterioration of resin by interrupting the ultraviolet rays. However, it is preferable to apply a weather resistant paint coat (urethane system paint, fluorine system paint, etc.) in cases where the concrete surface onto which Tow Sheet has been adhered will be exposed to direct sun light.

2) Application of the paint coat must be carried out after completion of the initial resin curing step, as determined when a nail mark can no longer be left on the surface.

3) Application of finish coat shall be in compliance with the standard application process specific to each type of paint.